Engineering Approaches to Control Activity and Selectivity of Enzymes for Multi-Step Catalysis

Walaa K. Abdallah

Submitted in partial fulfillment of the
requirements for the degree of
Doctor of Philosophy
in the Graduate School of Arts and Sciences

COLUMBIA UNIVERSITY

2019

ABSTRACT

Engineering Approaches to Control Activity and Selectivity of Enzymes for Multi-Step Catalysis

Walaa K. Abdallah

Enzymes are desirable catalysts as they may exhibit high activity, high selectivity, and may be easily engineered. Additionally, enzymes can be mass-produced recombinantly making them a potentially less expensive option than their organic or inorganic counterparts. As a result, they are being used more in industrial applications making their relevance ubiquitous. In this work, various engineering approaches were developed to control the activity and selectivity of enzymes for multi-step catalysis. Unlike nature, many industrial processes require multiple steps to produce the desired product, which is both timely and expensive. Through the use of enzymes, biosynthesis can be used to develop efficient multi-step catalytic cascades.

The majority of this work focused on engineering a hyperthermophilic enzyme from the aldo-keto reductase (AKR) superfamily, alcohol dehydrogenase D (AdhD) from *Pyrococcus furiosus*, to develop approaches to control activity and selectivity. As the AKR superfamily contains many unifying characteristics, such as a conserved catalytic tetrad, $(\alpha/\beta)_8$-barrel quaternary fold, conserved cofactor binding pocket, and varying substrate loops, the approaches developed here can be applied to many enzymes. AKR members participate in a broad range of redox reactions, such as those involving aldehydes, hydrocarbons, xenobiotics, and many more, and are necessary in physiological processes in all living systems, making these enzymes industrially relevant. AdhD in particular can oxidize alcohols or reduce aldehydes/ketones in the presence of NAD(P)(H). Furthermore, the tools utilized here are modular and can be used to

develop pathways with enzymes from different superfamilies' to expand their current capabilities.

In our initial engineering efforts, AdhD cofactor selectivity was broadened or reversed through site directed mutations or insertions in substrate loop B, on the back side of the cofactor binding pocket. To further examine how substrate loops affect cofactor selectivity, allosteric control was added to AdhD through the insertion of a calcium-dependent repeat-in-toxin domain from *Bordetella pertussis*. Through the chimeric protein, β-AdhD, we demonstrated that the addition of calcium shifts cofactor selectivity in real-time, reminiscent of a protein dimmer. Our next focus shifted towards unnatural amino acid incorporation to add an extra level of selectivity to AdhD. This was done by merging the properties of AdhD and an organic catalyst, TEMPO, for selective alcohol oxidation. We also demonstrated the ability to impart enzymatic selectivity onto an organic catalyst. This was done both in solution and in AdhD hydrogels for added functionality. The next study focused on increasing catalytic efficiency while retaining AdhD structure by engineering the microenvironment of AdhD with supercharged superfolder GFP (sfGFP). The complex interplay between salt, pH, and protein charge was studied and it was determined that catalysis is a function of protein charge, which can affect apparent local ionic strength. The final study focused on utilizing the previous tools examined to engineer substrate channeling in a multi-step cascade with hexokinase II (HK2), sfGFP, and glucose-6-phosphate dehydrogenase (G6PD).

In conclusion, we have utilized a myriad of tools to develop engineering approaches to regulate AdhD activity and selectivity. These tools were then extended to engineer substrate channeling in a three-enzyme system. These approaches are modular and provide a foundation for the development of multi-step catalytic cascades.

TABLE OF CONTENTS

LIST OF FIGURES

LIST OF TABLES

ACKNOWLEDGEMENTS

I would like to begin by thanking my committee members, Professor Banta, Professor Esposito, Professor Hess, Professor Ju, and Professor Obermeyer for their time. I would also like to give a special thanks to Professor Banta, thank you for your mentoring, patience, and guidance over the past couple of years.

I would also like to thank two special people – Kusum and Indrani. You both helped me inside of lab and out and allowed me to grow as an individual. I hope our friendship continues to last and you are by my side for future milestones.

Next, I would like to thank my siblings. Thank you, Ala, Ubadah, and Noor, you guys have stuck with me since the beginning.

Finally, a special thanks to my parents and my husband. Thank you, mom and dad, for everything. You have been my foundation throughout my entire education and I would not be where I am today if it weren't for you. Thank you Asem, you have put up with more than most can handle and have listened to your fair share of tirades where my anxiety blew things out of proportion. I will be forever indebted to you three and hope you accept my sincerest thanks.

P.S.: A very special thanks to my mom. Mom, thank you for everything! You know what you have done (the list would be too long, so I won't bother), but your support means the world to me.

CHAPTER 1

INTRODUCTION

Paraphrased versions of the AdhD section in this chapter are from "Extreme makeover: engineering the activity of a thermostable alcohol dehydrogenase (AdhD) from Pyrococcus furiosus" published in Biotechnology Journal in 2016 in volume 11, issue 12, pages 1483-1497.

1.1 Protein Engineering for Biomimetic Catalytic Cascades

DNA is the basis of life and is a preliminary component in protein production where DNA is converted to RNA, which is then converted to protein. Proteins are involved in cell production and, second to water, are the most abundant component in cells. Proteins with function, enzymes, are found in almost every biochemical reaction needed to sustain life [1]. These include redox reactions for energy conversion, biosynthesis of metabolites, transcription and translation in genes, and transport of molecules, among others [1]. Protein engineering broadly defines the engineering of proteins to yield novel properties that were previously not present, primarily through changing their structure [1, 2]. This is commonly approached by altering enzyme kinetics through active site engineering making these proteins relevant in both industrial and biomedical processes.

However, a new trend has emerged allowing for the merger between conventional engineering approaches, such as internal mutagenesis, and new engineering techniques involving microenvironment engineering. This new engineering approach involves changes in an enzymes local chemical or physical environment or active site resulting in a difference from the bulk environment [1]. Combining these two approaches can result in increasing catalytic rates, substrate selectivity, ability of enzymes to work in extreme conditions, and dynamic control allowing enzymes to respond to external stimuli [1].

The advancement of protein engineering techniques and their unique properties has resulted in the emergence of enzymes in all aspects of life such as in household products, pharmaceutical production, and energy production [3]. The ability to mass produce recombinant proteins and the optimization of related processes has made proteins extremely valuable molecules that are worth billions of dollars [4, 5]. In 2014, enzymes were worth $4.2 billion, and their worth is expected to increase seven percent from 2015 to 2020 [3]. Since structure and function go hand

in hand, we must study enzyme structure to understand what is happening on the molecular scale to enhance the development of industrially relevant proteins.

Enzymes, which are biological catalysts, have several advantages over inorganic catalysts (metals and metal alloy nanoparticles) and organic catalysts. Although metals can be shaped, can be controlled using temperature and pressure, and can be used both homogenously and heterogeneously, they may lack selectivity [6]. Organic catalysts may work in extreme conditions and, like metals, can be used homogeneously or heterogeneously, however some may lack substrate specificity [7]. Biological catalysts have the ability to be chemoselective, enantioselective, and have substrate and site selectivity [1, 8]. Also their turnover rates (per site) can exceed homogenous and heterogenous catalysts [1]. Additionally, systems that solely use metals may require extra steps in industrial processes [9]. Overall enzymes have many advantages compared to their inorganic and organic counterparts, and their activity, selectivity, and ability to be easily engineered has made them desirable industrial catalysts [1].

By engineering proteins and utilizing different classes of catalysts we can develop novel biocatalysts and through biomimetics, we can use these catalysts to develop multi-step cascades. Nature or biosynthesis involves the conversion of reactant A to product D without halting the process to remove intermediates [10]. Reactions can proceed with low concentrations of all reagents, which decreases the chance of side reactions and unwanted products, resulting in maximum selectivity. The products are also recovered *in situ*, which allows for the recycling of energy and redox carriers such as ATP and NAD^+, which again increases the throughput of the system. The success of these systems results from the inherent selectivity found in nature [10]. To mimic nature, we need man-made or organic synthesis that covers two key components: compatibility and compartmentalization. This requires the combination of various classes of

catalysts, selectivity, ability to work in a standard set of conditions, *in situ* product removal, techniques to screen products, and flexibility [10].

To develop these systems, we generated a toolbox of engineering approaches to alter enzymatic structure and function. This was done through site-directed mutagenesis to retain protein structure, domain insertion which allowed for dynamic external control, the addition of unnatural amino acids to introduce new functionality and develop biological and organic catalytic hybrids, and the modification of enzyme microenvironments to alter activity and enable substrate channeling.

The model enzyme we chose to generate a toolbox for developing multi-step cascades was thermostable alcohol dehydrogenase D (AdhD) from deep thermal sea vent archaea *Pyrococcus furiosus*. AdhD is monomeric, extremely thermostable, can withstand most chemical denaturation, and catalyzes many redox reactions [11]. It is also able to catalyze reactions in a wide pH range and is enantioselective. The Banta Lab has extensively engineered AdhD for over a decade making it a well-characterized enzyme while its ease of expression and purification makes it a great potential candidate for industrial applications.

In this thesis work, we altered the cofactor selectivity of AdhD through site-directed mutagenesis (chapter 2) and allowed for external regulation of this selectivity via domain insertion with an intrinsically disordered protein (chapter 3). We also developed biological-organic catalytic hybrids with AdhD and TEMPO to selectively oxidize alcohols and impart enzyme selectivity onto an organic catalyst both in solution and in hydrogels (chapter 4). Furthermore, we altered the microenvironment of AdhD using a superfolder green fluorescent protein scaffold (sfGFP) (chapter 5). We used the tools we learned from chapters 2-5 to engineer substrate channeling in a

three-enzyme system with hexokinase II, glucose-6-phosphate-dehydrogenase, and a sfGFP scaffold (chapter 6).

1.2 Alcohol Dehydrogenase D (AdhD)

Alcohol dehydrogenase D (AdhD) is a thermostable protein from *Pyrococcus furiosus* (archaea from deep thermal sea vents). Its physiological role is unknown, but its gene is located next to the wor4 gene in *P. furiosus*. Wor4 is an aldehyde reductase, so it is presumed that AdhD is involved in the consumption or production of aldehydes/ketones from wor4 [12]. AdhD is a member of the aldo-keto reductase (AKR) superfamily, which catalyzes redox reactions. This superfamily has broad substrate specificity, which is used to participate in the detoxification of drugs and xenobiotics. This family of enzymes can synthesize and degrade intermediate metabolites including aldehydes, ketones, hydroxysteroids, prostaglandins, biotoxins, and glycosylated products [13]. Shared properties in this superfamily include the $(\alpha/\beta)_8$-barrel, which consists of eight beta sheets surrounded by eight alpha helices, a conserved cofactor binding pocket, conserved catalytic tetrad, and three substrate binding loops with different lengths and composition. This superfamily is subdivided into 14 families based on their amino acid sequences, with alcohol dehydrogenases in the ninth class [13]. Alcohol dehydrogenases can be further subdivided based on their cofactor specificity. These groups include enzymes that are dependent on: NAD(P); pyrrolo-quinoline quinone, heme, or cofactor F420; and flavin adenine dinucleotide [12]. AdhD falls into the first category, but is a unique alcohol dehydrogenase because it is monomeric, with a molecular weight of around 32 kDa, and does not require a metal ion for catalysis [11].

AdhD is an ideal catalyst because of its extreme thermostability which allows it to withstand detrimental effects upon protein engineering approaches. Studies have shown that mutations can

destabilize enzymes, meaning the more stable the initial scaffold, the more changes it can accept. Also, thermostable enzymes are more resistant to denaturation, they can work at higher temperatures which makes their purification easier and their chance of getting contaminated lower, increases their reaction rates, and decreases the diffusional and mass transfer constraints. Thermophilic enzymes (compared to mesophilic enzymes) can also work well in various organic solvents, have higher substrate solubilities, and overall, can be used for longer periods of time in various operations [11].

AdhD follows an ordered bi-bi mechanism with the cofactor binding first, followed by the binding of the substrate, this is proceeded by the release of the substrate followed by the cofactor. The cofactor binds in a cleft at the C-terminal region of the protein. The binding of the cofactor results in the structural rearrangement of the active site allowing for catalysis [14]. The amino acids that interact with the cofactor and make up the cofactor binding pocket include Tyr205, Lys249, and His255 (**Figure 1.1**). The four amino acids, catalytic tetrad, that aid in catalysis by transferring hydride ions between the cofactor and substrate include Asp59, Tyr64, Lys90, and His122 (**Figure 1.1**) [12]. Lys90 makes a charged hydrogen bond with the hydroxyl group of Tyr64, which makes a salt bridge with Asp59. When a hydrogen bond is formed between Lys90 and Tyr64, the lone pair of electrons on the oxygen in the hydroxyl group of Tyr64 is delocalized which allows for the lowering of its pKa. This results in a pKa similar to that of the carbonyl group on the substrate, which starts catalysis. His122 is responsible for the binding and orientation of the substrate which gives the enzyme its substrate specificity and stereochemical selectivity [15]. Many members of the AKR superfamily are thought be active because of a “push-pull” mechanism [16]. His122 wants the reaction to proceed towards reduction by facilitating proton donation of Tyr64 while Lys90 wants the reaction to proceed towards oxidation by Tyr64 acting as a base and

accepting electrons from the substrate. However, in some members of the AKR family, the tyrosine and histidine are too far apart for this “push-pull” mechanism to occur. Therefore, although AdhD has the catalytic tetrad, it is unclear if it follows this push-pull mechanism.

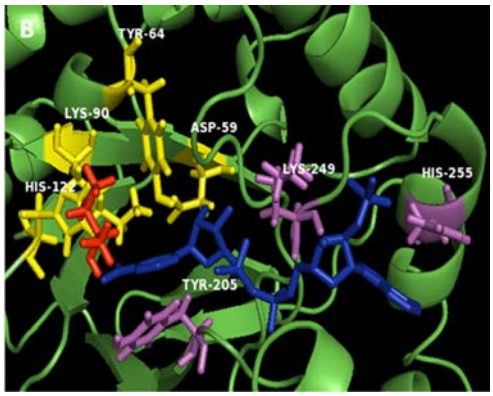

Figure 1.1 Homology model of AdhD. Catalytic tetrad in yellow, residues comprising the cofactor binding pocket in purple, 2,3-butanediol in red, and $NADP^+$ in blue [11].

AdhD works well with medium carbon chain lengths and prefers secondary alcohols over primary with its preferred substrate being 2,3-butanediol (acetoin in the reductive direction). Its preferred cofactor is NAD(H) and its optimum pH is 8.8 for alcohol oxidation and 6.1 for aldehyde/ketone reduction [12]. The Banta Lab has worked extensively with this enzyme to alter its cofactor specificity [17], introduce additional functionality [18], control cofactor and substrate selectivity [19], and to develop biofuel cells [20].

Here, extensive work has been done to develop tools and approaches to engineer AdhD to develop biomimetic multi-step cascades. Work involving AdhD will be addressed in chapters 2-5.

1.3 Methods to Control Cofactor Selectivity

Two predominant redox cofactors found in many biological systems include the nicotinamide nucleotides, nicotinamide adenine dinucleotide (NAD^+) and nicotinamide adenine dinucleotide

phosphate ($NADP^+$), as well as their reduced forms NADH and NADPH. The structural difference between NAD^+ and $NADP^+$ is the phosphate group attached to the adenosine ribose moiety in $NADP^+$. In terms of function, both NAD^+ and $NADP^+$ have similar redox potentials but play different roles in the cell. NAD(H) is involved in catabolic reactions, while NADP(H) is involved in anabolic reactions [21]. Additionally, the oxidation of NADH results in ATP in aerobic organisms, while NADPH is used in reductive biosynthesis [22].

AdhD uses both NAD(H) and NADP(H), with a preference for NAD(H). When these cofactors bind AdhD, the nicotinamide and adenosine ring bind in an anti-conformation compared to the pyrophosphate. The adenosine sticks outside of the barrel between β-strands 7 and 8 and α-helices 7 and 8. The nicotinamide sits in a cavity leading towards the center of the barrel with the pyrophosphate group in a tunnel between the nicotinamide and the adenosine. For hydride transfer to occur, the nicotinamide needs to be orientated with its 4-pro-hydrogen facing upwards and directed to the open side of the active site allowing the cofactor to be closer to the substrate. In terms of interactions with surrounding residues, Tyr205 is close to the nicotinamide ring allowing for a stacking interaction with its benzene ring. In terms of interactions with the pyrophosphate, some AKR'S undergo these interactions through the "seatbelt" mechanism where the pyrophosphate group is held down through a salt bridge between a lysine and aspartate on one side and a lysine on the other [11, 23]. AdhD does not have many positively charged residues in that position so the salt bridge is unlikely [11, 19]. However, there may be a cationic-pi interaction between tryptophan 27 and lysine 210 that covers the pyrophosphate, which can also function as a seat belt [11, 24].

Extensive work has been in done in the Banta lab to regulate the cofactor specificity of AdhD, which is important as NAD^+ is more stable and cheaper than $NADP^+$. Additionally, being able to

selectivity regulate activity can prove useful in multi-step cascades. One of the first engineering efforts to control cofactor specificity was done by Scrutton et al. in the 1990's where work was done with glutathione reductase to convert its specificity from $NADP^+$ to NAD^+ [22]. Previous work in the Banta Lab has altered cofactor specificity by point mutations and grafting substrate loops from another member of the AKR superfamily onto AdhD [17, 19]. The results indicated that making changes in the cofactor binding pocket or substrate binding loops can affect cofactor specificity.

In this work, two ways to regulate cofactor specificity have been achieved. One way involved the insertion of single amino acids or single point mutations distal to the phosphate group of $NADP^+$ to broaden/reverse cofactor specificity (chapter 2) [25]. However, this approach did not allow for dynamic control.

A second approach is through domain insertion, which allowed for external dynamic regulation of cofactor specificity (chapter 3) [26]. Dynamic regulation is commonly found in nature where feedback loops are used to respond to environmental changes without having to wait for a change in gene expression [1]. Many engineering approaches have focused on developing protein switches which respond to external stimuli allowing for regulation and cellular control. This specific thesis work involves allosteric regulation, where the conformational change in one protein can affect the other, and can cause a change in the local environment [1].

Both methods will be described in-depth in chapters 2 and 3.

1.4 Expanding the Genetic Code - Unnatural Amino Acid Incorporation

One way to expand the capabilities of an enzyme is to introduce novel functional groups that were previously not present. This can be achieved through unnatural amino acid incorporation. There is a myriad of unnatural amino acids with different capabilities that can be used to increase

the potential applications of enzymes. Commonly used unnatural amino acids contain functional groups such as azides and alkynes, which allows for a selective method of conjugating enzymes.

There are two ways to incorporate unnatural amino acids: global/residue-specific incorporation and site-specific incorporation. Residue-specific incorporation involves the use of cells that are auxotroph's for one canonical amino acid [27]. Supplementing the cells with the unnatural amino acid (UAA) analog results in the replacement of the canonical amino acid. In this approach, all sites in the protein containing the canonical amino acid are replaced with the UAA. If only specific sites are desired, then the remaining positions containing the canonical amino acid need to be mutated to an alternate amino acid. The second approach is site-specific incorporation, which involves the introduction of an amber stop codon (TAG) at the desired position of unnatural amino acid incorporation [27]. This approach limits the incorporation to one single site. There are three stop or nonsense codons: UAG (amber), UGA (opal), and UAA (ochre), with the rarest being the amber stop codon leading to its use in incorporation [28].

When performing site-specific unnatural amino acid incorporation, the cells are provided with the unnatural amino acid, which is used to replace the amber stop codon in the gene of interest. The orthogonal aminoacyl-tRNA synthetase, an enzyme responsible for attaching an amino acid onto its tRNA and is unique to each tRNA, attaches the unnatural amino acid to the orthogonal amber suppressor tRNA [29]. This is referred to as nonsense codon suppression and results in orthogonal tRNA with the unnatural amino acid [29]. tRNA's generally do not recognize the amber stop codon, therefore an engineered tRNA is used in this process. The ribosome decodes this tRNA-unnatural amino acid complex when it recognizes the amber stop codon (UAG) in the gene, resulting in the protein being synthesized with the unnatural amino acid [29].

The incorporation of unnatural amino acids into proteins requires the use of two plasmids. The first plasmid contains the gene of the target protein with the amber stop codon. The second is the helper plasmid containing the tRNA synthetase and amber suppressing tRNA. In this work, two aminoacyl-tRNA synthetase/tRNA pairs are used: pDule2 pCNF and pULTRA pCNF, which has greater suppression [30, 31]. They both come from archaea *Methanocaldococcus jannaschii* [32]. This system is orthogonal only in bacteria not in eukaryotic cells [29]. Additionally, these plasmids can work with azide and alkyne containing unnatural amino acids, such as para-azidophenylalanine and o-propargyl-tyrosine (**Figure 1.2**). These are the two unnatural amino acids used in this thesis work.

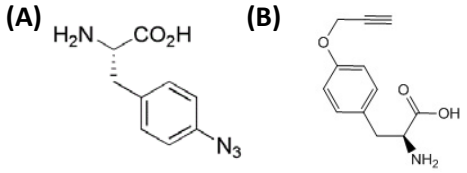

Figure 1.2 Structures of unnatural amino acids. (A) para-azidophenylalanine (from Chem-Impex) (B) o-propargyl-tyrosine (from Psyclo Peptide)

There has been advancement in numerous areas through the use of unnatural amino acids. The Dougherty Lab replaced key residues with unnatural amino acids to study magnesium binding in mammalian central nervous systems [33]. The Lewis Lab used it to merge metal and biological catalysts by clicking a functional group on the metal to an incorporated functional group on the enzyme [34]. This gave the metal selectivity that was previously not present. Unnatural amino acids were also used as an NMR probe to study structure and activity [35]. These are just a few of many examples of unnatural amino acid applications. In this work, unnatural amino acids were

used to merge organic catalysts and enzymes to enable selective alcohol oxidation and to impart enzymatic selectivity onto organic catalysts. Essentially, the unnatural amino acids were used as a conjugation tool and as a way to expand protein functionality.

Unnatural amino acid incorporation will be addressed in chapters 4 and 6.

1.5 Hydrogels for Dual Functionality

The ability to add extra functions to enzymes was also addressed through the use of hydrogels. Hydrogels are polymeric networks that can absorb water, are flexible, and biocompatible [36]. The hydrogels used here are made from HSH, a triblock forming polypeptide which is composed of two alpha helical leucine zipper domains (H) separated by a random domain (S) [37, 38]. Hydrogels form when the leucine zipper domains cross-link through protein-protein interactions resulting in a supramolecular hydrogel [37, 39]. The cross-linking is based on various interactions and is reversible based on pH making these hydrogels physical gels [36, 40]. It was observed that as the pH increases, the leucine zippers lose their alpha helical structure [40].

The leucine zippers found in HSH are formed through the helical wheel (**Figure 1.3**) [41]. The hydrophobic plane along the helix (residues *a* and *d*) is composed of leucine, isoleucine, or valine with leucine being predominant (hence the name). Due to the hydrophobic effect, *a* and *d* are buried in the core during the formation of the coiled coil. The remainder of the residues are charged (*e* and *g*) or neutral (*b, c,* and *f*). The backbone is made of alpha helices with *a* & *g* and *d* & *e* making the rungs [41]. The porosity can be controlled by varying the length and position of the S domain and there must be at least two H domains per monomer to cross-link [18, 39].

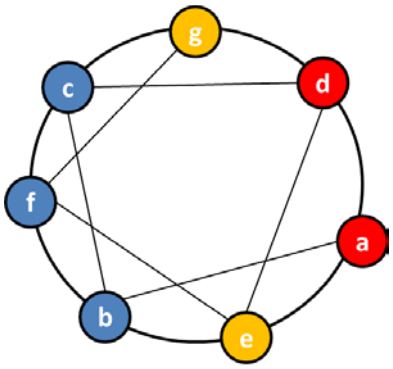

Figure 1.3 Alpha helical leucine heptad. Hydrophobic resides in red, charged residues in yellow, and neutral residues in blue.

Previous work in the Banta Lab focused on developing chimeric enzymes with hydrogels [18]. AdhD in particular was fused to a hydrogel, resulting in HS-AdhD-H, an enzyme that had the ability to oxidize alcohols while forming hydrogels [18]. In this work, HSH, HS-AdhD-H, and HSH with an unnatural amino acid were combined to form hydrogels. The hydrogel containing unnatural amino acid has the ability to be clicked to an alkyne-containing organic catalyst (TEMPO) to introduce selectivity of alcohol oxidation (with AdhD and TEMPO) along with hydrogel formation.

Hydrogels as a network are important as they are biocompatible and can be used in the development of numerous products. They are found in contact lenses, dressings for wounds, drug delivery, and much more [36].

Hydrogels will be discussed in chapter 4.

1.6 TEMPO

TEMPO, (2,2,6,6-tetramethylpiperidin-1-yl)oxyl, is an organic catalyst that has the ability to oxidize oxygen, nitrogen, and sulfur-containing functional groups [7]. Although its broad

reactivity can be seen as an advantage, TEMPO is known to work in basic pH's and cannot break carbon-carbon bonds. However, one of the advantages of TEMPO is its ability to be modified. Previous work has shown that 4-amino-TEMPO (TEMPO-NH_2) can oxidize alcohols and aldehydes and can work in acidic pH's [7]. Advancements have also been made to oxidize alcohols using TEMPO in the presence of copper at room temperature with air as the oxidant [42]. This set-up was selective toward primary alcohols and worked with allylic, benzylic, and aliphatic forms. This advancement removed the need for pure oxygen and removed the need for protecting groups to oxidize primary alcohols over secondary [42]. Additionally, as TEMPO has a high turnover rate with various alcohols, it has been used for electro-organic synthesis and for energy conversion processes [43]. For example, TEMPO has been used on electrodes to oxidize alcohols to carbonyl compounds for industrial applications [44].

Technically, TEMPO by itself is not a catalyst as it needs to be oxidized for activity, making its active form the oxoammonium ion [45, 46]. It has the ability to oxidize primary alcohols and in turn it is reduced. Laccase can be used to revert the reduced form back to TEMPO and to convert TEMPO to the active form, the oxoammonium ion [46]. TEMPO can also be regenerated to its active form with an electrode [45].

Since TEMPO can oxidize primary alcohols and AdhD can oxidize secondary alcohols, a hybrid of these two catalysts opens up the possibility of selectively oxidizing alcohols. TEMPO must be regenerated to maintain activity and AdhD cannot proceed without a cofactor. Therefore, the direction the reaction proceeds can also be controlled. To develop these hybrids and to do so in a site-selective manner, functional groups are needed. AdhD was incorporated with an azide-containing unnatural amino acid using the site-specific method previously described and TEMPO

was synthesized with an alkyne group. The chemistry required to conjugate the two will be described in the next section.

Although previous work has shown the ability to develop AdhD-TEMPO hybrids, the methods used do not allow TEMPO to attach in a site-specific manner [45]. The site-specific hybrids in solution and hydrogels developed in this thesis work will be discussed in chapter 4.

1.7 Conjugation Methods - Click Chemistry, SpyTag/SpyCatcher, SnoopTag/SnoopCatcher

The incorporation of unnatural amino acids containing an azide or alkyne functional group adds an extra method for conjugating two entities. Reactions between azides and alkynes were studied in the 1800's by Huisgen, who showed that 1,3-dipolar cycloaddition reactions resulting in triazoles were possible [47]. The drawbacks of this reaction involved excessive temperature and pressure, which are not feasible in many systems. As a result, advances have been made resulting in two main types of "click reactions": copper-catalyzed and strain-promoted.

The bioconjugation of azides and terminal alkynes can be completed in the presence of copper (I). The copper ligand reacts with the alkyne to form a copper acetylide [48]. The azide and acetylide then react forming a 5-triazolyl copper intermediate. The carbon-nitrogen bond occurs between the nucleophilic carbon of the acetylide and the electrophilic nitrogen of the azide [49]. The addition of copper increases the rate of reaction by seven orders of magnitude compared to the Huisgen technique [47]. Additionally, copper allows for the regioselectivity of the reaction with only the 1,4-disubstituted 1,2,3-triazole forming [49]. This reaction is referred to as copper-catalyzed azide-alkyne cycloaddition (CuAAC).

The problem with the use of copper is that it can be toxic to living cells. One way to circumvent this is to use water soluble ligands. They increase the rate of reaction and are sacrificial reductants, protecting the cells and biomolecules from copper [50]. This has been successfully performed with sodium ascorbate and tris(3-hydroxypropyltriazoyl-methyl)amine (THPTA) [51]. The click reaction requires copper in the +1-oxidation state, but a common way to introduce copper as a catalyst for click reactions is through copper sulfate. Sodium ascorbate is a reducing agent that has been effective in reducing copper to the cuprous (+1) state. A copper-binding ligand that works well with sodium ascorbate is THPTA, which acts as a "sacrificial reductant" to prevent the oxidation of the biomolecules. It has been shown that reactive oxygen species can result from the reaction and can oxidize amino acids such as histidine, which is why THPTA is needed [51].

A second approach to circumvent the effects of copper is a second type of click reaction, strain-promoted cycloaddition, which proceeds in the absence of copper. The reaction occurs between a cyclooctyne and an azide and proceeds because it releases ring strain [52]. Different variations of the cyclooctyne (various functional groups) have all been used successfully, especially those with electron withdrawing groups, which increases reaction rates [47]. The various groups on the cyclooctyne have been observed to decrease the activation energy for the transition states [52]. However, it should be noted that the fastest reaction between a cyclooctyne and an azide is around ten times slower than a reaction between a terminal alkyne and an azide [50]. Additionally, the products include the 1,4-disubstitued triazole and its regioisomer [47]. Both copper-catalyzed and strain-promoted cycloaddition will be described in chapter 4.

Another tool to combine two enzymes is through a covalent attachment between SpyTag peptide and SpyCatcher protein. These peptide tags originate from the fibronectin binding protein found in the gram positive bacteria *Streptococcus pyogenes*, specifically in its adhesion domain

(CnaB2), which has an isopeptide bond between Lys31 and Asp117 [53, 54]. When this bond is broken with lysine in the N-terminus fragment and aspartic acid in the C-terminus, the fragments combine spontaneously to reform that bond [53]. The two halves of this domain were modified and renamed SpyTag and SpyCatcher [53]. The formation of the bond can occur in as little as minutes and works in various conditions (temperature, pH, buffers) and results in a bond that can resist boiling [54]. This reaction will be discussed in chapters 5 and 6.

A second method of covalent attachment through tags is SnoopTag and SnoopCatcher. These are from the RrgA adhesion from the gram-positive bacterium *Streptococcus pneumoniae*, responsible for septicemia, pneumonia, and meningitis [55]. It has been shown that if the D4 Ig-like domain is split, it can spontaneously re-form a peptide bond between Lys742 and Asn854. This domain was split and re-named SnoopTag, which is composed of residues 734-745, and SnoopCatcher, which is composed of residues 749-860 [55]. This system is orthogonal to the SpyTag/SpyCatcher system and will be discussed in chapter 6.

1.8 Engineering Protein Microenvironments with sfGFP Scaffolds

The final goal of this thesis was to alter enzyme kinetics through microenvironment engineering. Supercharged superfolder green fluorescent protein (sfGFP) was used as a scaffold to alter the microenvironment of AdhD and as a platform for electrostatic guidance.

The scaffold used here is a modified version of green fluorescent protein (GFP). The source is GFP from jellyfish *Aequorea Victoria* made of 11 β-strands wrapped around a central helix (PDB 1EMA) [56]. Folding reporter GFP, which contains the cycle 3 mutations F99S, M153T, and V163A, allowed GFP to be grown recombinantly in *E. coli* at 37 °C and allowed it to fold properly thereby resulting in fluorescence [57]. The chromophore consists of Ser65-Tyr66-Gly67

[58]. An absorbance scan of cycle 3 GFP shows the presence of a major peak at 397 nm and a minor peak at 475 nm, which are the excitation wavelengths [59]. The major peak corresponds to the GFP population with a neutral or protonated chromophore. The minor peak corresponds to the GFP population that has an anionic or deprotonated chromophore.

The enhanced GFP mutations, F64L and S65T, increased the fluorescence of GFP. A superfolder GFP (sfGFP) variant was made that combined these previous mutations with six new ones (PDB 2B3P) [60]. This resulted in a more stable GFP that can be fused to various polypeptides while retaining the ability to properly fold and fluoresce through the maturation of its chromophore, T65-Y66-G67 [58, 60]. Additionally it was able to allow for circular permutation and chemical denaturants making it an ideal starting scaffold [60].

As this sfGFP is more stable than its predecessors, the Liu Lab was able to create supercharged versions of this variant while increasing its stability [61]. sfGFP has a net charge of -7 so mutations within the amino sequence along the surface of the protein were made to develop variants with very positive or negative charges. Residues that contributed to more positively charged variants included arginine and lysine, while aspartic acid and glutamic acid contributed to the negative charge. This resulted in the development of many sfGFP variants, which were done by mutating the solvent exposed residues to charged residues [61]. An advantage of charging proteins is less protein aggregation. There has been research indicating that there is a relationship between solubility and net charge - as proteins develop a net charge, their percent aggregation decreases. Protein aggregation is a problem in human disease and is one of the reasons why proteins are not commonly used as therapeutic or diagnostic agents [61].

A spectral scan of sfGFP shows a major peak at 490 nm, corresponding to the anionic chromophore, and a minor peak at 390 nm, corresponding to the neutral or protonated

chromophore [62]. As the pH decreases, the hydrogen ions in solution allow sfGFP to become protonated, increasing the peak at 390 nm and decreasing the peak at 490 nm. This protonation quenches the fluorescence because it inhibits proton transfer [62]. The fluorescent properties of these supercharged variants were similar to sfGFP. However, when a charged variant and sfGFP were boiled and then cooled, sfGFP precipitated out indicating the loss of its fluorescence is irreversible, while the charged variants were able to retain some of their fluorescence [61]. These charged variants were also able to demonstrate a reversible affinity and subsequent complex with molecules of the opposite charge [61].

In this work, sfGFP was used to alter the microenvironment of AdhD. There has been extensive work done on altering proteins on the nanoscale level to alter their kinetics. More recently, the idea of controlling the local chemical and physical environment of proteins has been focused on, allowing proteins to retain their structure while enhancing their catalysis [1]. These efforts include changing the pH profile, engineering specificity, external regulation, and more, which can result in substrate channeling.

In the first part of this engineering approach, sfGFP was used to alter the local environment of AdhD by introducing supercharged sfGFP proteins, while allowing AdhD to retain its structure. This technique allows for *in vivo* and *in vitro* applications and provides a way to enhance the catalytic efficiency of AdhD. This project will be discussed in chapter 5.

In the final section of this work, previous tools and approaches were used to develop a multi-step catalytic cascade through substrate channeling with enzymes other than AdhD. Substrate channeling allows chemical reaction intermediates to go from one enzyme to another without being released into the bulk solution [63]. The problem with channeling arises from the fact that the diffusion of the intermediate is usually faster than the catalytic rates of the enzymes [63]. If this

issue can be circumvented, substrate channeling can be achieved, which increases both yields and efficiencies. Therefore, another definition of channeling involves the ability to increase the kinetics of the system [64]. However, it should be noted that the rate of the cascade is limited by the rate-limiting enzyme [63, 65]. In nature, many enzymes that participate in these channeling reactions have active sites positioned so that the mass transport of the reactants is controlled. These intermediates are usually sequestered next to the active site, which decreases their exposure to side reactions and can protect the cells from intermediates that may be unstable or toxic [63]. If these metabolites are sequestered at a high enough concentration, they can also overcome thermodynamic limitations in the bulk environment. In nature, channeling occurs via: intramolecular tunnels, electrostatic guidance, covalent swing arms, and spatial organization [63]. In nature, these "intracellular multienzyme structures" are referred to as metabolons.

Intramolecular tunnels refer to a hydrophobic tunnel that connects two active sites such as those found in tryptophan synthase and bifunctional aldolase-dehydrogenase, among others. In tryptophan synthase the two active sites are connected by a 2.5 nm tunnel that essentially results in a bifunctional enzyme that can catalyze a two-step reaction [63]. The intermediate rapidly diffuses along the tunnel and the protein undergoes a conformational change at the active site. Electrostatic guidance refers to the ability of ionic strength to move intermediates along a surface of the opposite charge [63]. This results in bounded diffusion allowing the movement of an intermediate between two active sites. An example of this includes enzymes involved in the tricarboxylic acid (TCA) cycle, malate dehydrogenase and citrate synthase [63]. This mechanism of channeling with these enzymes was thoroughly studied in the Banta Lab. It was determined that a mutation in the highly conserved positive patch connecting these two enzymes results in a loss of substrate channeling [64]. The third method involves the intermediates binding to a swing arm

transferring it from one enzyme to another. An example of this includes the multienzyme pyruvate dehydrogenase complex, which participates in glycolysis and leads into the TCA cycle. The key concept in all methods includes the spatial organization of the enzymes to allow the active sites to be oriented appropriately [63]. The challenges that arise when developing these systems biomimetically stems from the fact that diffusion is usually faster than the catalytic rate so orientating two active sites close to one another is usually not strong enough to result in channeling.

There are many ways to measure substrate channeling. One way is to measure the transient time (Ƭ), which is the time it takes the intermediate to reach steady state [63]. This value is a function of the maximum velocity and Michaelis constant of the second enzyme and the reaction velocity of the first enzyme in a two-step process [63]. Ideally, the transient time will approach zero in a perfect system. The reason for this is that if an intermediate is diffusing from one site to the next without any assembly between the two sites, it will require more time to reach its destination [64]. This can also be measured by plotting the product concentration as a function of time. Once the system reaches steady state, a linear fit can be determined and the point at which the concentration equals zero is the transient time [66]. A second method is the isotope dilution and enrichment method [63]. Here, if we monitor the reaction of A to B by enzyme 1 (E1) and B to C by enzyme 2 (E2), we can measure channeling by adding isotopically labeled A* in the presence of B. If the two enzymes sequester the intermediate, then A* should be converted to B* by E1 and B* should be converted to C* by E2. However, if the intermediates are not sequestered, then B can also be used by E2 to make C. The ratio of the labeled to unlabeled product (C* versus C) can be used to determine the degree of substrate channeling. Another method is to add a competing enzyme to the cascade [63]. If the enzyme can utilize the intermediate, this suggests the intermediate is being released into the bulk, signifying leaky or no channeling depending on the

extent of the side reaction. A fourth method is to add an inhibitor to the bulk environment that inhibits the second enzyme from reacting [63]. Again, if a change in catalytic rate is observed, this signifies a decrease in substrate channeling.

Here, sfGFP with varying charge was used as a scaffold for substrate channeling between recombinant human hexokinase II (HK2) and human glucose-6-phosphate-dehydrogenase (G6PD) through electrostatic guidance.

Hexokinases are responsible for catalyzing sugar phosphorylation (first step of glycolysis) and sending signals of glucose levels to the nucleus in a variety of organisms ranging from bacteria to mammals [67]. Glycolysis occurs in the cytosol in eukaryotic cells, making this a cytosolic protein. Additionally, studies have shown that hexokinase found in the mitochondria is involved in controlling apoptosis in mammals. This is significant as glucose metabolism is one of the main pathways used by all organisms to make energy in the form of ATP. Hexokinases in humans can be divided into four different types based on their kinetics and where they are in tissues. Interestingly, the amino acid sequence within each type of hexokinase is very similar between different organisms [67]. The three types of isozymes are referred to as type I, II, III and IV, with IV commonly referred to as glucokinase. The first three are approximately 100 kDa. They all contain a similar amino acid distribution in their N and C terminal halves, which suggests a duplication and fusion of a 50 kDa protein, presumably hexokinase IV, which corresponds to the correct molecular weight. This work focuses on hexokinase type II from humans, which is approximately 100 kDa and contains both an N and C domain with catalytic activity [67].

Glucose-6-phosphate-dehydrogenase (G6PD) is an enzyme that participates in the first step of the pentose phosphate pathway, which aids in biosynthesis, prevents against oxidative stress, provides pentoses, and produces NADPH, which is the reducing power of the cell [68]. Here, work

is being done with human G6PD, which studies have shown has a catalytic and structural $NADP^+$ site [69]. The structural site is required for the stability and refolding of the enzyme [69]. One of the main goals of G6PD is the production of NADPH. G6PD takes D-glucose-6-phosphate along with magnesium chloride and $NADP^+$ to produce 6-phospho-D-gluconate and NADPH.

Here we are monitoring the conversion of ATP and glucose to glucose-6-phosphate and ADP by HK2, followed by the conversion of glucose-6-phosphate and $NADP^+$ by G6PD to 6-phospho-gluconolactone and NADPH [70]. The intermediate, glucose-6-phosphate is negatively charged and therefore, should be guided along a positive patch. Previous work has shown that connecting HK2 and G6PD with a cationic peptide bridge (lysine residues) helped facilitate substrate channeling through electrostatic guidance as the intermediate, glucose-6-phosphate, is negatively charged [70]. In this thesis work, channeling was tested by fusing HK2 and G6PD to -30, 0, and +36 sfGFP to determine the extent of substrate channeling. This work will be addressed in chapter 6.

The following are the specific aims of this thesis:

In chapter 2, we address the cofactor specificity of AdhD. We identified a position distal to the cofactor binding pocket of AdhD that alters cofactor specificity with a single point mutation or insertion. This demonstrates that amino acids involved in substrate interactions can also affect cofactor specificity. This approach should be applicable to other members of the AKR superfamily.

In chapter 3, we further examine the effect of insertions in AdhD and how this affects cofactor selectivity. This was done by domain insertion where an RTX domain from the adenylate cyclase of *Bordetella Pertussis* was inserted into substrate loop A of AdhD. Once again, we show

that cofactor specificity is affected. Additionally, the insertion allowed for dynamic regulation of cofactor specificity with calcium.

In chapter 4, we continue working with AdhD to expand its catalytic properties by introducing a functionalized unnatural amino acid for click chemistry. The reaction between azide-AdhD and alkyne-TEMPO results in an organic/enzyme catalytic hybrid. This hybrid allows for the selective oxidation of alcohols. This work was extended to hydrogels, by incorporating HSH, and to AdhD mutants with substrate loops from human aldose reductase to modify substrate and cofactor selectivity.

In chapter 5, we alter the microenvironment of AdhD by using sfGFP to enhance catalysis. Fusions of AdhD with supercharged sfGFP demonstrate the ability to alter the local environment of AdhD while allowing AdhD to retain its structure.

The tools and engineering approaches from chapters 2-5, which focused on AdhD, were used in chapter 6 to develop a multi-step cascade with sfGFP acting as the scaffold for electrostatic guidance between HK2 and G6PD.

CHAPTER 2

ENGINEERING THE COFACTOR SPECIFICITY OF AN ALCOHOL DEHYDROGENASE VIA SINGLE MUTATIONS OR INSERTIONS DISTAL TO THE 2'-PHOSPHATE GROUP OF NADP(H)

Project Collaborators: Walaa Abdallah, Kusum Solanki, and Scott Banta

A version of this chapter entitled "Engineering the cofactor specificity of an alcohol dehydrogenase via single mutations or insertions distal to the 2'-phosphate group of NADP(H)" was published in Protein Engineering, Design & Selection in 2017 in volume 30, issue 5, pages 373-380. WA was responsible for helping with protein characterization, including enzyme kinetics and circular dichroism studies.

2.1 Abstract

There have been many reports exploring the engineering of the cofactor specificity of aldo-keto reductases (AKRs), as this class of proteins is ubiquitous and exhibits many useful activities. A common approach is the mutagenesis of amino acids involved in interactions with the 2'-phosphate group of NADP(H) in the cofactor binding pocket. We recently performed a "loop-grafting" approach to engineer the substrate specificity of the thermostable alcohol dehydrogenase D (AdhD) from *Pyrococcus furiosus* and we found that a loop insertion after residue 211, which is on the back side of the cofactor binding pocket, could also alter cofactor specificity. Here we further explore this approach by introducing single point mutations and single amino acid insertions at the loop insertion site. Six different mutants of AdhD were created by either converting glycine 211 to cysteine or serine or by inserting alanine, serine, glycine or cysteine between the 211 and 212 residues. Several mutants gained activity with $NADP^+$ above the wild-type enzyme. And remarkably, it was found that all of the mutants investigated resulted in some degree of reversal of cofactor specificity in the oxidative direction. These changes were generally a result of changes in conformations of the ternary enzyme/cofactor/substrate complexes as opposed to changes in affinities or binding energies of the cofactors. This study highlights the role that amino acids which are distal to the cofactor binding pocket but are involved in substrate interactions can influence cofactor specificity in AdhD, and this strategy should translate to other AKR family members.

2.2 Introduction

The aldo-keto reductase (AKR) superfamily is comprised of over 100 oxidoreductases with importance in both health and industrial applications [23]. They are found in all organisms and play an important role in many physiological processes. All AKRs share a common $(\alpha/\beta)_8$-barrel

(also known as triphosphate isomerase motif (TIM barrel)) three-dimensional structural motif and they utilize NAD(P)(H) as a cofactor. The active sites of the AKRs bind the cofactor in an extended conformation within a cleft that runs through the carboxy-terminal face of barrel, which is unlike other nicotinamide-dependent dehydrogenases that contain the Rossman-fold motif.

The AKRs are generally categorized into three classes. Class I is the most studied and includes mammalian AKRs, which catalyze steroid and prostaglandin metabolism [71, 72]. Members belonging to this class have long substrate binding loops, which confer specific substrate specificity to AKRs. Class II comprises aldo reductases (ARs), which catalyze interconversion of glucose to sorbitol and have been studied as drug targets for the treatment of diabetes [73]. Class III AKRs are not yet assigned specific functions, but they have truncated substrate binding loops [74]. One of the enzymes belonging to Class III is the alcohol dehydrogenase D (AdhD) from the hyperthermophilic archaea *Pyrococcus furiosus* (**Figure 2.1**). This reversible enzyme has been well-characterized by our group and others [12] and we have been engineering various aspects of AdhD for several years [11].

Engineering of the cofactor specificity of dehydrogenases has been of interest not only to understand the properties of the cofactor binding site, but also to redesign enzymes for various applications. The only difference between NAD(H) and NADP(H) is the 2'-monophosphate group attached to the ribose ring of the adenine moiety. The cofactor specificity of an AKR is thought to be determined by the presence of favorable interactions between the 2'-monophosphate group of NADP(H) and amino acids in the cofactor binding pocket. Generally, alteration in cofactor specificity can be achieved by systematic site directed mutagenesis of the side chains interacting with the 2'-phosphate group of NADP(H) and investigating the effect of mutations on cofactor specificity [75-80]. For example, Banta *et al.* made site-directed mutations at every amino acid

that interacted with the 2'-phosphate group in the 2,5-diketo-D-gluconic acid reductase (2,5-DKGR) from *Corynebacterium*, and mutants were identified with cofactor specificity broadening such that mutants with NAD(H) were more active than wild-type with NADP(H) [76, 81]. Computational strategies for altering enzymes for cofactor preference have also been explored [82-84]. Xia *et al.* (2013) utilized a molecular simulations approach to construct a 3D-structure model of xylose reductase to obtain favorable binding modes for both cofactors NAD^+ and $NADP^+$ based on hydrophobic and hydrophilic interactions. Others have used *in silico* approaches to calculate cofactor binding energy approximations and strength of hydrogen bond interactions to predict the relative affinity of an enzyme for the cofactor [82, 84]. All these reports, whether computational or experimental, utilize direct interactions (i.e. electrostatic, hydrophilic, hydrophobic, hydrogen bonding or steric) to stabilize or destabilize the 2'-phosphate group of NADP(H) in the cofactor binding pocket. We have also used this approach to engineer the cofactor specificity of AdhD, which has a natural preference for NAD(H) especially in the reductive direction. Lys249 and His255, which bind to the 2'-phosphate of NADP(H), were mutated to Gly and Arg respectively leading to cofactor specificity broadening with increased activity with both cofactors in the reductive direction [17] (**Figure 2.1B**).

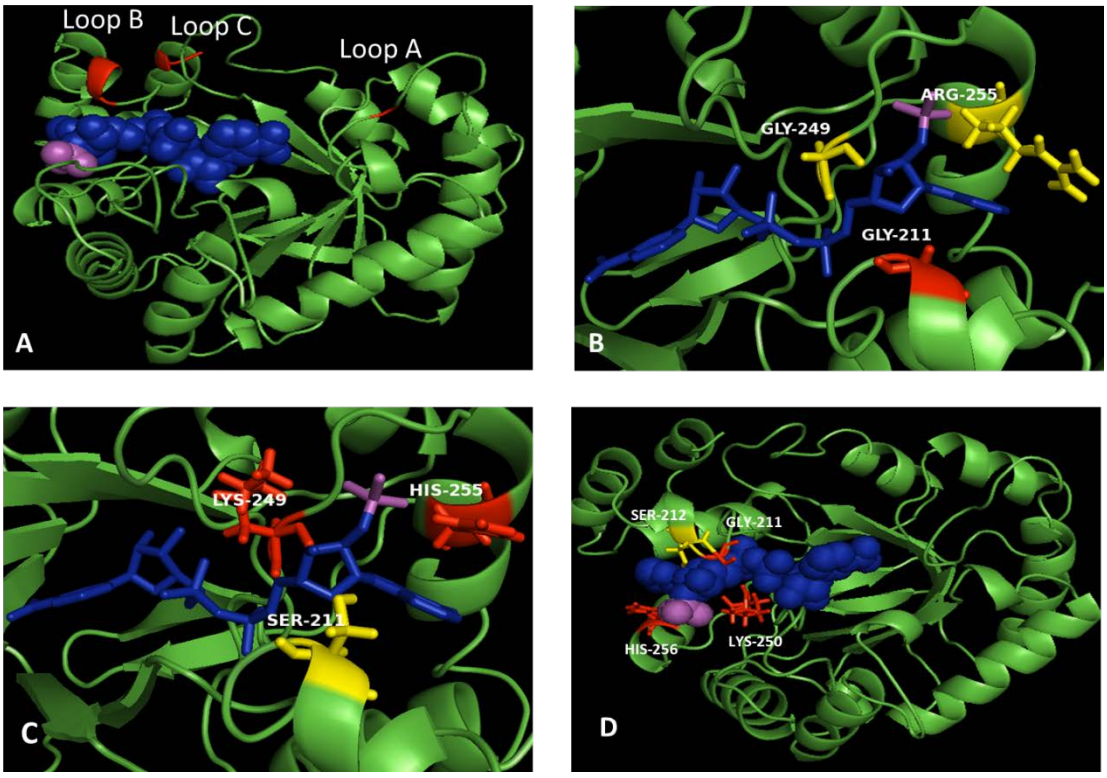

Figure 2.1 Homology model of AdhD. (A) Wild-type AdhD with loops A, B and C indicated. Homology models of cofactor binding pocket of (B) double mutant K249G/H255R (C) mutant G211S and (D) mutant G211InsS with bound $NADP^+$. The $NADP^+$ backbone is shown as blue sticks or spheres and the 2'monophosphate group is highlighted in magenta. Cofactor interacting residues, His 255 and Lys249, are shown as red sticks and labeled. Also, Glycine 211 is shown as red sticks and mutations are depicted in yellow.

There have also been a few reports of engineering cofactor specificity of various oxo-reductases by making mutations distal to the 2'-phosphate group of NADP(H) [85, 86]. Cahn et al. (2016) demonstrated that cofactor specificity of various NAD(P)H dependent enzymes can be altered by mutating amino acids distal to 2' position of ribose, located within 5 Å of the N6 atom of NAD(P)(H) adenine. They have shown that single mutations at distal positions were beneficial for changing cofactor specificity in several enzymes with Rossmann and DHQS folds, but this approach did not work with the TIM barrel fold found in the AKRs.

Substrate specificity in the AKRs is imparted by three mobile loops A, B and C located at the top of the $(\alpha/\beta)_8$-barrel structure. Sequence alignments between Class I mesophilic AKRs and Class III thermophilic AdhD indicated that they differ at the substrate loops A, B and C (**Figure 2.1A**). Loops A and B are significantly truncated in AdhD while loop C is absent. We recently reported the grafting of loops from mesophilic human aldose reductase (hAR, Class I) onto the AdhD core protein and this led to the grafting of hAR activity into the AdhD scaffold. And surprisingly, this loop-grafting approach led to a loss of NAD^+-dependent activity while retaining $NADP^+$-dependent activity in two mutants. Thus the grafted loops led to a significant change in cofactor specificity in the oxidative direction as compared to the wild-type enzyme [19]. The most active mutants were then combined with the previously identified K249G/H255R cofactor specificity mutations (which interact with the 2'-phosphate group of NADP(H)) and surprisingly the impacts were not additive as these combined mutations inactivated the enzyme (**Figure 2.1B**). This led to the conclusion that there were two orthogonal pathways to altering cofactor specificity in AdhD – alter interactions with the 2'-phosphate of NADP(H) or insert new amino acids in a loop on the substrate binding site distal to the cofactor binding pocket to reduce NAD^+-dependent activity [19].

Based on this prior work, here we have investigated the minimal mutations or insertions required for altering the cofactor specificity in the oxidative direction at the loop B insertion site. A homology model of AdhD (**Figure 2.1A**) shows the location of loop B on the distal side of the cofactor binding pocket from the 2'-phosphate group of NADP(H). We have investigated single point mutations by converting Gly211 to Ser or Cys and inserting single amino acids (Ala, Gly, Ser or Cys) between the 211 and 212 positions. The effect of these mutations on cofactor specificity were determined, and we found that all of the site-directed mutations (**Figure 2.1C**) or

single amino acid insertions (**Figure 2.1D**) at the 211-position resulted in reversal of cofactor specificity in the oxidative direction.

2.3 Materials and Methods

2.3.1 Materials

2,3-Butanediol, NAD^+, $NADP^+$, media, and buffer components were purchased from Sigma-Aldrich (St Louis, MO, USA). Oligonucleotides were from Integrated DNA Technologies (Coralville, IA, USA). Isopropyl-ß-D-1-thiogalactopyranoside (IPTG) and ampicillin were purchased from Promega (Madison, WI, USA). *Escherichia coli* BL21(DE3) competent cells and Phusion high-fidelity DNA polymerase were from New England Biolabs (Ipswich, MA, USA). Pierce Commassie (Bradford) protein assay kit was from Thermo Fisher Life Technologies (New York, NY, USA). Precast sodium dodecyl sulfate-polyacrylamide gels, NuPAGE MOPS running buffer, and Novex sharp pre-stained protein standard molecular weight marker were from Invitrogen (Carlsbad, CA, USA). Gel filtration column Superdex 16/200 was from GE Healthcare (Piscataway, NJ, USA). Of note, 30 KDa MWCO centrifugal filters were from EMD Millipore (Billerica, MA, USA).

2.3.2 Site-Directed Mutagenesis

Mutants G211S, G211C, and the insertion of Ala, Gly, Ser or Cys between 211 and 212 residues (termed G211InsA, G211InsG, G211InsS, and G211InsC, respectively) were created by site-directed mutagenesis of the wild-type AdhD gene in pET-20b vector [12] using the Phusion high-fidelity DNA polymerase. Sequences of the primers used are given in supporting information. All mutations and insertions were verified by DNA sequencing.

2.3.3 AdhD Expression and Purification

Expression and purification of AdhD and mutants were performed using a previously established protocol [17]. A single colony harboring the wild-type AdhD or mutant plasmid was expanded in 10 ml of Luria-Bertani (LB) media supplemented with 0.1 mg/ml of ampicillin and grown overnight at 37°C with shaking at 200 rpm. The overnight cultures were then transferred into 1 L of LB medium containing 0.1 mg/ml ampicillin and grown at 37°C with shaking at 200 rpm until the O.D. reached 0.6. Cultures were then induced with 0.5 mM of IPTG followed by overnight incubation at 25°C shaken at 200 rpm. Cells were harvested by centrifugation at 5000g for 20 min, resuspended in 30 ml of Tris-HCl (pH 7.5), and were lysed by incubating at 80 °C for 1 h. Endogenous proteins and cell debris were removed by centrifugation at 10,000g for 30 min. Supernatant was concentrated using a 30 KDa MWCO centrifugal filter before being loaded onto a gel filtration column with 20 mM Tris-HCl (pH 7.5) containing 100 mM NaCl as an equilibrating and eluting buffer at a flow rate of 1.5 ml/min. Fractions containing active enzyme solutions were pooled and concentrated to working concentration in 20 mM Tris-HCl buffer (pH 7.5) before use.

2.3.4 Protein Concentrations and Purity

The protein concentrations were determined using a Pierce Coomassie (Bradford) protein assay kit with bovine serum albumin as a standard protein. Homogeneity of purified AdhD and the mutants were determined by using NuPAGE 4-12 % Bis-Tris Gels with a Novex Mini-Cell system using novex sharp pre-stained protein standards for molecular weight estimation. Samples were prepared as described previously [12].

2.3.5 Protein Denaturation Studies

Thermal denaturation of wild-type AdhD and mutants was studied by measuring circular dichroic absorbance at 222 nm between 25°C and 90 °C with rate of 1 °C/min. Of note, 1 ml of 5 µM protein samples were made in 10 mM phosphate buffer, pH 8.0 and spectra were recorded using JascoJ-815 spectrometer.

2.3.6 Homology Modeling

A homology model of AdhD and its mutants were generated using SWISS MODEL [87] using Prostaglandin F synthase from *Trypanosoma brucei* (1VBJ, 40.26 % identities). The homology models were aligned with the structure of 2,5-DKGR from *Cornybacterium* (1A80 with bound NADPH, 1M9H with bound NADH) [81] and the interactions of cofactor with mutants were explored using PYMOL. **Figure 2.1** was generated using PYMOL.

2.3.7 Kinetic Parameter Estimation

The full kinetic parameters of AdhD and the mutants were determined for the oxidation reaction with both NAD^+ and $NADP^+$ by using previously described methodology [17]. Briefly, initial rates at 45°C were measured using a SpectraMax M2 plate reader by following the production of NAD(P)H at 340 nm (ε = 6.22 per mM/cm). Initially, kinetics of all the mutants were studied by using reaction mixtures containing 1-100 mM 2,3 butanediol and an appropriate amount of enzyme in 50 mM Glycine-NaOH buffer (pH 8.8). Mixtures were incubated in a 96-well plate at 45 °C and the reactions were initiated by addition of 1-1,000 µM NAD(P)H. For some mutants (G211S, G211C, G211InsA, and G211InsS), with NAD^+ as a cofactor, the K_A or K_B values were observed to be higher than the maximum concentration of substrate or cofactor utilized. So, for mutants G211S, G211C, G211InsA and G211InsS, kinetic data were also measured using assay reaction

mixtures containing 1-450 mM 2,3 butanediol and 1-5500 μM NAD^+. Control reactions in the absence of enzyme confirmed that cofactor degradation was insignificant at 45°C over the timescale used. Data was collected in at least triplicate and was fit to the ordered bi-bi rate equation (Equation 2.1) [18, 88] using nonlinear least-squares regression (Igor Pro, Wavemetrics, Inc., Portland, OR, USA). Errors are reported as standard errors.

$$v = \frac{E_t k_{cat} AB}{K_D K_B + K_A B + K_B A + AB} \tag{2.1}$$

2.3.8 Fluorescence Titrations

Dissociations constants for cofactor binding were determined using fluorescence titrations [17, 89]. Briefly, 1 ml of 3 μM enzyme (in 50 mM glycine-NaOH buffer, pH 8.8) was stirred in a 1 cm quartz cuvette at 45 °C in a J-815 Spectrometer (Jasco, Inc., Easton, MD, USA) equipped with a Peltier junction temperature control and titrated with $NAD(P)^+$ in solution. Samples were excited at 280 nm and fluorescence changes were monitored at 330 nm. Concentrations of cofactor were chosen so that total volume of cofactor added was <2 % (v/v) of the total reaction volume. Experiments were performed in triplicate and data were fit to a saturation adsorption isotherm (Equation 2.2) using Igor Pro.

$$\phi = \frac{[NAD(P)]}{K_D + [NAD(P)]} \tag{2.2}$$

2.3.9 Cofactor Binding Energies

Changes in the cofactor binding energies in the ground-state ($\Delta\Delta G_b$) and transition-state ($\Delta\Delta G_b^{\neq}$) were calculated from equations 2.3 and 2.4 [90] utilizing cofactor dissociation constants and steady-state kinetic parameters. R is the gas constant (1.9872041 cal/mol/K) and T is temperature (318 K).

$$\Delta\Delta G_b = -RT \ln[(K_d)_{wt}/(K_d)_{mut}] \tag{2.3}$$

$$\Delta\Delta G_b^{\neq} = RT \ln\left[\left(\frac{k_{cat}}{K_A}\right)_{wt} \Big/ \left(\frac{k_{cat}}{K_A}\right)_{mut}\right] \tag{2.4}$$

2.4 Results

2.4.1 Expression, Purification, and Thermostability of AdhD and Mutants

Six different mutants were created by single amino acid mutations or insertions in the AdhD gene. The mutations were G211C and G211S (**Figure 2.1C**). The insertion mutants were G211InsA, G211InsG, G211InsC, and G211InsS (**Figure 2.1D**). After expression in E. coli, proteins were first purified by incubation at high temperature in order to exploit the thermostability of the AdhD structure. Following gel filtration chromatography, the proteins were purified to greater than 98% as observed on SDS-PAGE (**Figure 2.3**). The effect of the mutations on the thermostability of AdhD were studied by monitoring far UV circular dichroic spectra at 25°C and 80°C (**Figure 2.4**). Just as is observed with the wild-type, no apparent structural unfolding was observed for any of the mutants at 80°C.

2.4.2 Homology Modeling

Homology models of AdhD and the mutants were generated and interactions with the cofactors were analyzed by aligning homology models with the crystal structure of a similar AKR (2,5-DKGR) containing bound NADP(H) using PYMOL. Lys249 and His255 of AdhD are known to have favorable interactions with 2'phosphate group of NADP(H) [17]. Analysis of the homology models of all mutants suggested that interactions with these amino acids are not affected by the mutations or insertions at loop B (**Figure 2.1B-D**).

2.4.3 Fluorescence Titrations

Fluorescence titration measurements were performed at 45 °C to determine cofactor dissociation constants ($K_{D's}$) for the oxidized cofactors by the AdhD mutants. Fluorescence quenching of tryptophan located at the 92nd position in AdhD following cofactor binding was monitored. Titration curves for AdhD and the mutants with NAD^+ and $NADP^+$ are shown in **Figure 2.5** and **Figure 2.6**. Dissociation constants were calculated using equation 2.2 and are shown in **Table 2.1** and **Table 2.2** for NAD^+ and $NADP^+$. Only minor differences in $K_{D's}$ for both NAD^+ and $NADP^+$ were observed between wild-type AdhD and the mutants (**Table 2.1** and **Table 2.2**). The K_D values of wild-type AdhD and mutants varied between 8.6 - 37 μM and 56 - 78 μM, for NAD^+ and $NADP^+$ respectively, indicating that the mutations led to only marginal changes in affinity for the cofactor molecules. This is in contrast to results obtained with the K249G/H255R mutant where the K_D for NAD^+ increased to 45 μM while the K_D for $NADP^+$ decreased to 0.66 μM [17].

Table 2.1 Steady-state kinetic parameters for wild-type AdhD and mutants with NAD^+. Full parameters with NAD^+ as a cofactor for oxidation reactions.

Enzyme	K_D (μM)	k_{cat} (s^{-1})	K_A (μM)	K_B (mM)
Wild-type	11 ± 1	2.6 ± 0.4	230 ± 50	12 ± 6
G211S	19 ± 1	4.0 ± 0.6	100 ± 40	100 ± 20
G211C	37 ± 4	1.1 ± 0.1	480 ± 70	240 ± 40
G211InsG	23 ± 3	6.5 ± 0.5	290 ± 50	110 ± 10
G211InsC	33 ± 6	0.43 ± 0.02	97 ± 13	76 ± 6
G211InsA	31 ± 5	1.7 ± 0.3	120 ± 10	260 ± 110
G211InsS	8.6 ± 1.0	6.7 ± 2.3	1600 ± 600	1100 ± 500
K249G/H255R[a]	45 ± 2	15 ± 2	460 ± 60	690 ± 80

Enzyme	k_1^{ss} ($\mu M^{-1} s^{-1}$)	k_2^{ss} (s^{-1})	k_3^{ss} ($\mu M^{-1} s^{-1}$) x10^{-3}	$(k_1 k_3/k_2)^{ss}$ ($\mu M^{-2} s^{-1}$) x10^{-6}
Wild-type	0.011 ± 0.003	0.12 ± 0.04	0.21 ± 0.11	20 ± 11
G211S	0.040 ± 0.017	0.76 ± 0.32	0.040 ± 0.010	2.1 ± 0.5
G211C	0.0023 ± 0.0004	0.087 ± 0.017	0.0046 ± 0.0009	0.12 ± 0.02
G211InsG	0.022 ± 0.004	0.51 ± 0.15	0.059 ± 0.007	2.6 ± 0.5
G211InsC	0.0044 ± 0.0006	0.15 ± 0.03	0.0057 ± 0.0005	0.17 ± 0.04
G211InsA	0.014 ± 0.003	0.44 ± 0.11	0.0065 ± 0.0030	0.21 ± 0.10
G211InsS	0.0042 ± 0.0022	0.036 ± 0.019	0.0061 ± 0.0035	0.71 ± 0.41
K249G/H255[a]	0.033 ± 0.006	1.5 ± 0.3	0.022 ± 0.004	0.48 ± 0.09

Oxidation reactions were performed at 45°C in 50 mM glycine-NaOH buffer (pH 8.8) with 2,3-butanediol as a substrate. K_D is the cofactor dissociation constant as determined by fluorescence titrations, K_A and K_B are Michaelis constants for cofactor and substrate, respectively. For mutants G211S, G211C, G211InsA and G211InsS, kinetics data were measured using higher substrate and cofactor concentrations as described in the 'Materials and Methods' section. Reactions were performed in at least triplicate, and errors shown are standard errors of at least three independent measurements.

Rate constants calculated from relationships: $k_1^{SS} = k_{cat}/K_A$, $k_2^{ss} = k_{cat}/K_D$, $k_3^{ss} = k_{cat}/K_B$

[a]The K249G/H255R mutant data were determined by *Campbell et.al* (2010) under identical conditions.

Table 2.2 Steady-state kinetic parameters for wild-type AdhD and mutants with $NADP^+$. Full parameters with $NADP^+$ as a cofactor for oxidation reactions.

Enzyme	K_D (μM)	k_{cat} (s^{-1})	K_A (μM)	K_B (mM)
Wild-type	64 ± 2	0.073 ± 0.002	7.4 ± 0.9	0.44 ± 0.10
G211S	67 ± 4	0.29 ± 0.01	15 ± 2	0.91 ± 0.16
G211C	65 ± 3	0.92 ± 0.07	25 ± 9	9.6 ± 2.5
G211InsG	75 ± 5	0.52 ± 0.10	33 ± 29	1.5 ± 0.5
G211InsC	78 ± 6	0.86 ± 0.09	120 ± 40	5.5 ± 1.2
G211InsA	56 ± 4	2.1 ± 0.2	360 ± 90	90 ± 4
G211InsS	59 ± 5	2.1 ± 0.1	66 ± 24	17 ± 2
K249G/H255R[a]	0.66 ± 0.10	4.7 ± 0.2	78 ± 5	200 ± 10

Enzyme	k_1^{ss}($\mu M^{-1}s^{-1}$)	k_2^{ss} (s^{-1})	k_3^{ss}($\mu M^{-1}s^{-1}$) x10^{-3}	$(k_1k_3/k_2)^{ss}$ ($\mu M^{-2}s^{-1}$) x10^{-6}
Wild-type	0.0098 ± 0.0012	0.63 ± 0.08	0.16 ± 0.04	2.6 ± 0.6
G211S	0.019 ± 0.02	1.3 ± 0.2	0.31 ± 0.06	4.7 ± 0.9
G211C	0.037 ± 0.013	2.4 ± 0.9	0.096 ± 0.026	1.5 ± 0.4
G211InsG	0.016 ± 0.014	1.2 ± 1.0	0.34 ± 0.12	4.5 ± 1.8
G211InsC	0.0074 ± 0.0025	0.58 ± 0.20	0.16 ± 0.04	2.0 ± 0.5
G211InsA	0.0057 ± 0.0015	0.32 ± 0.09	0.023 ± 0.002	0.41 ± 0.05
G211InsS	0.032 ± 0.012	1.9 ± 0.70	0.12 ± 0.02	2.1 ± 0.3
K249G/H255R[a]	0.060 ± 0.005	0.040 ± 0.007	0.024 ± 0.002	36 ± 6

Oxidation reactions were performed at 45°C in 50 mM glycine-NaOH buffer (pH 8.8) with 2,3-butanediol as a substrate. K_D is the cofactor dissociation constant as determined by fluorescence titrations, K_A and K_B are Michaelis constants for cofactor and substrate, respectively. Reactions were performed in at least triplicate, and errors shown are standard deviations.

Rate constants calculated from relationships: $k_1^{ss}=k_{cat}/K_A$, $k_2^{ss}=k_{cat}K_D/K_A$, $k_3^{ss}=k_{cat}/K_B$

[a]The K249G/H255R mutant data was determined by Campbell *et al* (2010) under identical conditions.

2.4.4 Steady State Kinetic Analyses

Steady state kinetic experiments were carried out in the oxidative direction for all the mutants and wild-type AdhD using either NAD^+ or $NADP^+$ as a cofactor (**Table 2.1** and **Table 2.2**). With NAD^+, three mutants G211S, G211InsG, and G211InsS exhibited improvement in k_{cat} over the wild-type enzyme. G211InsG and G211InsS mutant exhibited 2.5-fold enhancement in the k_{cat} value and mutant G211S showed 1.5-fold enhancement over wild-type. The mutant with Cys insertion, G211InsC, exhibited the lowest k_{cat} value with a 6-fold decrease as compared to the wild-type AdhD. The impact on the activity with $NADP^+$ was even greater, as all the mutants exhibited improvement over wild-type. Mutants with Ala and Ser insertion showed a 29-fold increase in k_{cat}, respectively (**Table 2.2**). An order of magnitude improvement was observed for other mutants as well. The K_A varied from 97 to 1600 μM for NAD^+ and from 7.4 to 360 μM for $NADP^+$ in the wild-type and mutants. Similarly, variations observed for K_B ranged from 12 to 1100 mM for NAD^+ and 0.44 to 90 mM for $NADP^+$ in the wild-type and mutants. This is also in contrast to results obtained with the K249G/H255R mutant where the K_B for $NADP^+$ exhibited the largest increase observed, 200 mM [17].

In order to simplify the comparison of the impacts of the mutations on the steady-state kinetics, the individual microscopic rate constants for the reaction mechanism were calculated according to Equation 2.5 (**Table 2.1** and **Table 2.2**). In the case of NAD^+, the on-rate of cofactor (k_1^{ss}) was found to decrease in all of the mutants except for the G211S and insertion of Gly (G211InsG), which was measured to be 0.04 and 0.022 $\mu M^{-1}s^{-1}$, respectively, as compared to 0.011 $\mu M^{-1}s^{-1}$ for wild-type AdhD. The mutant with the Ala insertion (G211InsA) showed a similar k_1^{ss} as that of wild-type. The off-rate (k_2^{ss}) increased for all the mutants except G211C and G211InsS. The off-rate value for the mutant with the Cys insertion (G211InsC) was measured to be similar

to that of the wild-type enzyme. An approximately 6-fold enhancement was observed for mutant G211S and 3 to 4-fold for the Ala (G211InsA) and Gly insertion (G211InsG) mutants. All of the mutants demonstrated decreases in the on-rate of the substrate (k_3^{ss}) after binding NAD^+ as a cofactor, with decreases between 32-fold and 46-fold for mutants, G211InsA, G211InsS, G211InsC, and G211C. The highest decrease of 46-fold was shown by G211C. The composite rate constant $(k_1k_3/k_2)^{ss}$ is a useful parameter that can be used to compare the catalytic performances of ordered bi-bi enzymes [76]. All of the mutants resulted in substantial decreases in catalytic performance with NAD^+ (**Table 2.1**). The catalytic performance decreased by two orders of magnitude for G211C and G211InsC. Mutants, G211InS and G211InsA exhibited 28-fold and 100-fold decreases, respectively. The G211InsG exhibited the highest catalytic performance among mutants, but the value was still only 13% of the wild-type value.

With $NADP^+$ as a cofactor, all of the mutants produced an increase in both the on-rate (k_1^{ss}) and the off-rate constants (k_2^{ss}) for the cofactor, except mutant G211InsC and G211InsA, which showed a decrease in values compared to the wild-type (**Table 2.2**). Mutants G211S, G211C, G211InsS, and G211InsG exhibited between 2-fold to 4-fold enhancement for both k_1^{ss} and k_2^{ss} (**Table 2.2**). The net on-rate of the substrate following $NADP^+$-binding (k_3^{ss}) increased by approximately 2-fold for mutants G211S and G211InsG and decreased by 7-fold for G211InsA. The G211InsC and G211InsS mutants showed similar net on-rates as that of wild-type, whereas G211C showed a 40% decrease. The mutants that showed an increase in the net on-rate of substrate with $NADP^+$ were G211S and G211InsG, both with 0.31×10^{-3} $\mu M^{-1}s^{-1}$ compared to 0.16×10^{-3} $\mu M^{-1}s^{-1}$ for the wild-type. G211S also exhibited a 2-fold improvement in overall catalytic performance $(k_1k_3/k_2)^{ss}$. In terms of catalytic performance with $NADP^+$, the least active mutant

was G211InsA, which decreased 6-fold compared to wild-type AdhD. The catalytic performances of G211InsC and G211InsS were similar to that of wild-type.

$$E + A \underset{k_2^{ss}}{\overset{k_1^{ss}}{\rightleftarrows}} EA \qquad\qquad EA + B \xrightarrow{k_3^{ss}} EAB \tag{2.5}$$

Wild-type AdhD is able to use both cofactors in both directions, but it exhibits a strong preference for NADH over NADPH in the reductive direction [17] and a slight preference for NAD^+ over $NADP^+$ in the oxidative direction. The ratio of $k_{cat}(NADP^+)/k_{cat}(NAD^+)$ for wild-type AdhD was 0.028 (**Table 2.3**). All of the mutants showed higher $k_{cat}(NADP^+)/k_{cat}(NAD^+)$ ratios compared to wild-type AdhD. Mutants G211S and G211InsG showed an enhancement of approximately 3-fold and mutants G211InsS, G211C, and G211InsA, the enhancement observed was 11-, 30-, and 43-fold,respectively. The G211InsC mutant possessed the highest $k_{cat}(NADP^+)/k_{cat}(NAD^+)$ ratio of 2.0, which is 71 times higher than the wild-type enzyme and more than 6-fold higher than the K249G/H255R mutant (**Table 2.3**). In contrast to the large changes seen in the k_{cat} values, all of the $K_d(NADP^+)/K_d(NAD^+)$ ratios were of the same order of magnitude as the wild-type enzyme. The Michaelis constants for the enzymes were more affected by the mutations. G211C and G211InsS had $K_A(NADP^+)/K_A(NAD^+)$ values similar to the wild-type with a ratio of 0.032 for wild-type AdhD. G211InsC and G211InsA had 38-fold and 94-fold increases in the $K_A(NADP^+)/K_A(NAD^+)$ ratio, respectively. The wild-type enzyme had a $K_B(NADP^+)/K_B(NAD^+)$ ratio of 0.037, which was similar to the G211C mutant value of 0.040. The values for G211InsG and G211InsS were approximately 40% of the wild-type value while the values for G211InsC and G211InsA were 2- and 9-fold higher than the wild-type.

Table 2.3 Ratio of steady-state parameters and composite microscopic rates for Wt AdhD and mutants. Studies with NAD^+ versus $NADP^+$ as cofactors for oxidation reactions.

Enzyme	$K_D(NADP^+)/K_D(NAD^+)$	$k_{cat}(NADP^+)/k_{cat}(NAD^+)$	$K_A(NADP^+)/K_A(NAD^+)$	$K_B(NADP^+)/K_B(NAD^+)$
Wild-type	5.8 ± 0.7	0.028 ± 0.004	0.032 ± 0.080	0.037 ± 0.020
G211S	3.5 ± 0.3	0.072 ± 0.011	0.15 ± 0.06	0.0091 ± 0.0024
G211C	1.7 ± 0.2	0.83 ± 0.09	0.052 ± 0.020	0.040 ± 0.012
G211InsG	3.3 ± 0.5	0.081 ± 0.017	0.12 ± 0.10	0.014 ± 0.005
G211InsC	2.4 ± 0.5	2.0 ± 0.2	1.2 ± 0.4	0.072 ± 0.017
G211InsA	1.8 ± 0.3	1.2 ± 0.2	3.0 ± 0.8	0.35 ± 0.15
G211InsS	6.9 ± 1.0	0.31 ± 0.11	0.041 ± 0.022	0.016 ± 0.007
K249G/H255R[a]	0.015 ± 0.002	0.31 ± 0.04	0.17 ± 0.02	0.29 ± 0.04

Enzyme	$(k_1k_3/k_2)^{ss}$ $(NADP^+)/(k_1k_3/k_2)^{ss}$ (NAD^+)
Wild-type	0.13 ± 0.08
G211S	2.2 ± 0.7
G211C	12 ±4
G211InsG	1.7 ± 0.7
G211InsC	12 ± 4
G211InsA	2.0 ± 1.0
G211InsS	2.9 ± 1.8
K249G/H255R[a]	74 ±18

[a]The K249G/H255R mutant data was determined by Campbell *et al* (2010) under identical conditions.

The $(k_1k_3/k_2)^{ss}(NADP^+)/(k_1k_3/k_2)^{ss}(NAD^+)$ provides a clear comparison of the catalytic efficiencies of ordered bi-bi enzymes with the different cofactors. Cofactor specificity reversal was observed with every mutant explored (**Table 2.3**). The value for the wild-type is 0.13 and this increased for every mutant explored with the biggest changes seen with the G211C and G211InsC mutants exhibiting a two order of magnitude increase with a value of 12 for each (**Table 2.3** and **Figure 2.2**)

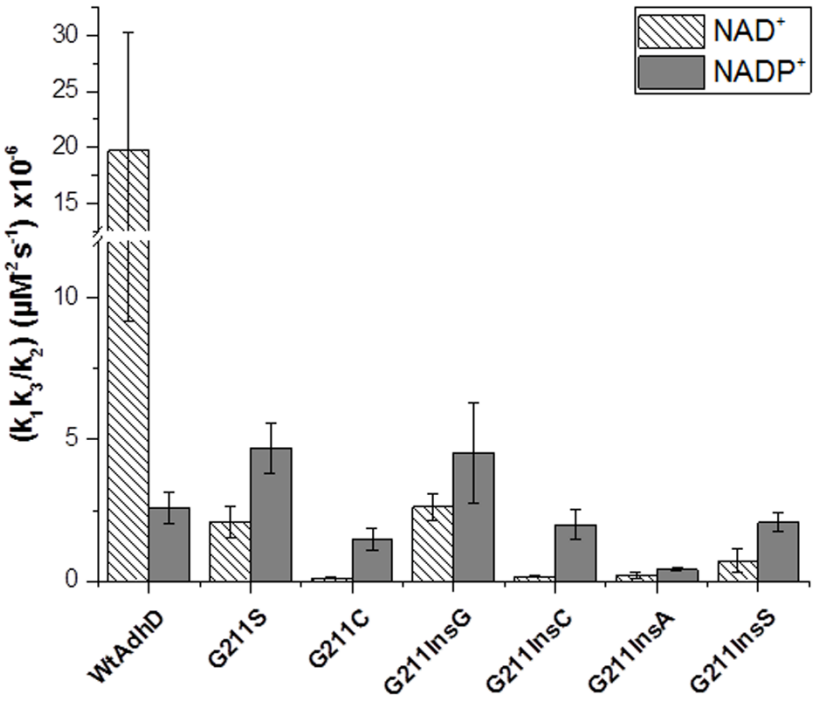

Figure 2.2 Catalytic performance of wild-type AdhD and mutants. Comparison of catalytic performance $(k_1k_3/k_2)^{ss}$ of wild-type AdhD and mutants with NAD^+ and $NADP^+$ in the oxidation reaction. Error bars shown are standard errors of at least three independent measurements.

2.4.5 Cofactor Binding Energies

Changes in the ground-state and transition-state binding energies of the cofactors and the mutants compared to the wild-type enzyme were calculated from cofactor dissociation constants

and kinetic data using equations 2.3 and 2.4, respectively (**Table 2.4** and **Table 2.5**). With NAD^+ as a cofactor, all of the mutants lost ground-state binding energy ranging from 0.35 to 0.76 kcal/mol except for G211InsS, which gained 0.15 kcal/mol. The transition-state binding energies with NAD^+ were more variable, with G211S, G211InsG, and G211InsA gaining energies and G211C, G211InsC, and G211InsS losing binding energies with the biggest changes in ground-state and transition-state binding energies observed for G211C (0.76 and 1.0 kcal/mol, respectively). Similar results were seen with the previously described K249G/H255R mutant [19], which lost 0.88 kcal/mol of ground-state binding energy, but gained 0.67 kcal/mol transition-state binding energy (**Table 2.4**).

Table 2.4 Change in the ground- and transition-state binding energies with NAD^+ as a cofactor

Enzyme	$\Delta\Delta G_b$ (kcal/mol)	$\Delta\Delta G_b^{\neq}$(kcal/mol)
G211S	0.35	-0.79
G211C	0.76	1.0
G211InsG	0.46	-0.43
G211InsC	0.69	0.59
G211InsA	0.65	-0.14
G211InsS	-0.15	0.62
K249G/H255R[a]	0.88	-0.67

[a]The K249G/H255R mutant data was determined by Campbell *et al* (2010) under identical conditions

With $NADP^+$, the G211InsC mutant showed the maximum change of 0.12 kcal/mol in the ground-state binding energy. With $NADP^+$ as a cofactor, the changes in ground-state binding energy were smaller, with G211InsG and G211InsC exhibiting the largest losses of 0.10 and 0.12 kcal/mol. The transition-state binding energy changes were larger, with G211C and G211InsS

showing the highest gains of 0.84 and 0.74 kcal/mol, respectively (**Table 2.5**). These results are much different from what was observed with the K249G/H255R mutant [19], which gained 2.9 kcal/mol of ground-state binding energy and gained 1.1 kcal/mol transition-state binding energy (**Table 2.5**).

Table 2.5 Change in the ground- and transition-state binding energies with $NADP^+$ as a cofactor

Enzyme	$\Delta\Delta G_b$ (kcal/mol)	$\Delta\Delta G_b^{\neq}$ (kcal/mol)
G211S	0.029	-0.45
G211C	0.0098	-0.84
G211InsG	0.10	-0.29
G211InsC	0.12	0.20
G211InsA	-0.084	0.33
G211InsS	-0.051	-0.74
K249G/H255R[a]	-2.9	-1.1

[a]The K249G/H255R mutant data was determined by Campbell *et al* (2010) under identical conditions

2.5 Discussion

Enzymes of the AKR superfamily generally exhibit cofactor specificities and there have been a number of reports aiming to explore the basis of this molecular recognition [75-77, 80, 91]. The general approach in all of these reports has been to apply site-directed mutagenesis to the

amino acids interacting with the cofactor, especially those that interact with the 2'-phosphate group of $NADP^+$.

While studying the structural differences between a mesophilic AKR (human aldose reductase) and the thermophilic AdhD, our group found that there is a truncation of loops A and B and an absence of loop C in AdhD [19] and that the insertion of these loops in AdhD altered the substrate specificity along with a concomitant alteration in cofactor specificity in the oxidative direction. This motivated further investigation into the minimum insertion length required to alter the cofactor specificity of AdhD in the loop regions as opposed to the amino acids directly interacting with the 2'-phosphate group of NADP(H). Loop B is located at the back side of the adenine binding site of cofactor binding pocket and has no apparent interaction with the 2'-phosphate group of NADP(H) (**Figure 2.1A**). Thus, we decided to study the effect of mutations and single amino acid insertions at the loop B position. Homology models of AdhD and the mutants with $NADP^+$ suggest that the distance between loop B of AdhD and the 2'-phosphate group of $NADP^+$ is greater than 10 Å (**Figure 2.1B-D**). Yet surprisingly, these conservative changes led to increased activity in some and alteration of cofactor preference in all of the mutants evaluated.

Similar effects have been reported upon mutation of side chains away from the 2'-phosphate group of NADP(H) in other nicotinamide cofactor-dependent dehydrogenase enzymes [86]. Cahn *et al.* explored engineering cofactor-specificity in NAD(P)(H)-dependent enzymes with different folds and identified a position on a helix (within 5 Å of the N6 atom of the NAD(P)H adenine moiety) that runs parallel to the cofactor adenine moiety. Mutations at this position led to changes in catalytic activity and cofactor specificity. However, this approach was ineffective for an enzyme with a TIM-barrel fold, as is found in the AKRs.

Based on previous mutagenesis work from our group in AKR enzymes, we made single mutations at loop B, which begins at 211th amino acid of AdhD. A homology model of AdhD shows that the distance between from N6 atom of the adenine moiety and amino acid 211 is 7-8 Å and the distance to amino acid 212 is 5-6 Å. The largest impacts on cofactor specificity were observed when G211 was mutated to cysteine (G211C) and when cysteine was inserted between the 211 and 212 amino acids (G211InsC) of AdhD.

When mutations are made in the cofactor binding pocket at amino acid side chains interacting with the 2'-phosphate group of NADP(H), changes in the dissociation constant (K_D, **Table 2.3**) and the ground- and transition-state binding energies can be observed as can be seen in the K249G/H255R mutant [19] (**Table 2.5**). The mutants created in this work also resulted in a substantial change in cofactor specificity in the oxidative direction (**Figure 2.2**); however, these changes are not due to large changes in the dissociation constants for the cofactors (K_D, **Table 2.3**) or in the ground- or transition-state binding energies of either cofactor (**Table 2.4** and **Table 2.5**).

These results indicate that the mutations are instead affecting the interactions of the ternary enzyme/cofactor/substrate transition state. This is evidenced by the full steady-state kinetic behavior of all the mutants in the forward direction in the absence of products for the oxidation reaction using NAD^+ or $NADP^+$ as cofactors (**Table 2.1**, **Table 2.2**, and **Table 2.3**). The mutations led to many changes in the kinetic parameters, but there was a striking increase (6-fold up to 90-fold) in every Michaelis constant for substrate (K_B), when NAD^+ was used as a cofactor. The results were more mixed when $NADP^+$ was used, where the K_B values also increased for very mutant, but some of the mutants exhibited only 2- to 4-fold differences. And, there was a consistent increase in the k_{cat} value for every mutant with $NADP^+$, which was not observed when NAD^+ was used as a cofactor.

There are several ways to compare the catalytic performance of mutant enzymes. For the ordered bi-bi enzymes, there are two Michaelis constant (K_m) values, thus complicating the comparison of the traditional k_{cat}/K_m. An alternative choice is to use the steady-state kinetic parameters to calculate on- and off-rates of the individual reaction steps and compare a ratio such as k_1k_3/k_2. All of the mutants created exhibited a decrease in overall catalytic performance $(k_1k_3/k_2)^{ss}$ with NAD^+ as compared to wild-type (**Table 2.1**). With $NADP^+$, several mutants exhibited similar or decreased performance, while mutants, G211S and G211InsG, had a 1.8- and 1.7-fold increase in this parameter, respectively. By comparing the ratio of this parameter between $NADP^+$ and NAD^+ as a cofactor, every mutant investigated resulted in a reversal of cofactor specificity. Two of the mutants (G211S and G211InsG) demonstrated activity with $NADP^+$ that exceeds that of the wild-type, and two of the mutants (G211C and G211InsC) exhibit almost complete reversals in cofactor specificity (**Table 2.3**, **Figure 2.2**).

The fact that single amino acid mutations or insertions at a site away from the 2'-phosphate group of NADP(H) affect cofactor specificity as dramatically as mutations within the cofactor binding pocket is useful. There are many reports of cofactor specificity engineering in the AKR family, but there are only few reports where reversal of cofactor specificity is achieved with retention or enhanced catalytic efficiency as compared to the wild-type. Furthermore, in all these reports at least triple or quadruple mutations of amino acids involved in the binding of the 2'-phosphate group were required for switch in cofactor specificity [92-94]. There have been reports on effects of distal single mutation on various NAD(P)H-dependent enzymes with different folds; however, they could not find beneficial mutation for enzymes with TIM barrel fold. Here, we have discovered a position in AdhD, an enzyme with TIM barrel fold, distal to the 2'phosphate group, which can create mutants with activities with the non-preferred cofactor that exceeds the parental

activity and can lead to mutants with reversal of the cofactor specificity. This represents an extended approach for cofactor engineering in the AKR enzyme family with the TIM barrel fold.

2.6 Conclusion

There are well-established locations for mutagenesis to alter cofactor specificity in the aldo-keto reductases. We identified a position on the other side of the cofactor binding pocket where point mutations or single amino acid insertions produced increased activities and every mutant exhibited altered cofactor specificity. This mutation site may be useful in related enzymes.

2.7 Supporting Information

AdhD amino acid sequence:

```
MGDYKDDDDK AKRVNAFNDL KRIGDDKVTA IGMGTWGIGG RETPDYSRDK ESIEAIRYGL        60
ELGMNLIDTA EFYGAGHAEE IVGEAIKEFE REDIFIVSKV WPTHFGYEEA KKAARASAKR       120
LGTYIDLYLL HWPVDDFKKI EETLHALEDL VDEGVIRYIG VSNFNLELLQ RSQEVMRKYE       180
IVANQVKYSV KDRWPETTGL LDYMKREGIA LMAYTPLEKG TLARNECLAK IGEKYGKTAA       240
QVALNYLIWE ENVVAIPKAS NKEHLKENFG AMGWRLSEED REMARRCVED PNSSSVD          297
```

Oligonucleotides used for site-directed mutagenesis (mutation in italics)

G211S:

Forward primer: ACGCCTCTAGAAAAA*TCC*ACCCTGGCGCGTAAC - 3'

Reverse primer: GTTACGCGCCAGGGT*GGA*TTTTTCTAGAGGCGT - 3'

G211C:

Forward primer: ACGCCTCTAGAAAAA*TGC*ACCCTGGCGCGTAAC - 3'

Reverse primer: GTTACGCGCCAGGGT*GCA*TTTTTCTAGAGGCGT - 3'

Glycine inserted between 211 & 212:

Forward primer: CCTCTAGAAAAAGGT*GGC*ACCCTGGCG - 3'

Reverse primer: CGCCAGGGT*GCC*ACCTTTTTCTAGAGG - 3'

Alanine inserted between 211 & 212:

Forward primer: GAAAAAGGT*GCC*ACCCTGGCG - 3'

Reverse primer: CGCCAGGGT*GGC*ACCTTTTTC - 3'

Serine inserted between 211 & 212:

Forward primer: GAAAAAGGT*TCC*ACCCTGGCG - 3'

Reverse primer: CGCCAGGGT*GGA*ACCTTTTTC - 3'

Cysteine inserted between 211 & 212:

Forward primer: CTAGAAAAAGGT*TGC*ACCCTGGCG - 3'

Reverse primer: CGCCAGGGT*GCA*ACCTTTTTCTAG - 3'

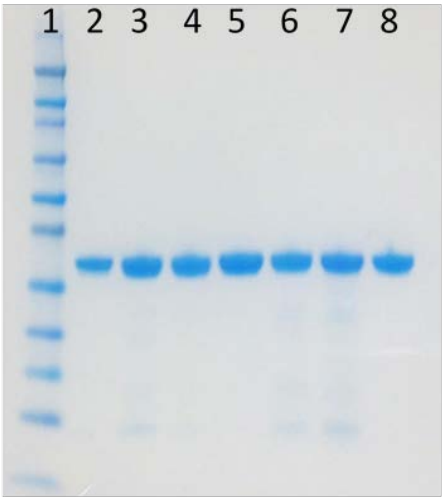

Figure 2.3 SDS-PAGE of wild-type AdhD and mutants. SDS-PAGE of wild-type AdhD and mutants after purification using gel filtration column (for details see materials and methods). Lane 1: molecular weight ladder, lane 2: wild-type AdhD, lane 3: G211S, lane 4: G211C, lane 5: G211InsA, lane 6: G211InsG, lane 7: G211InsC, and lane 8: G211InsS. A single band is observed at ~34 KDa, consistent with the calculated molecular mass of AdhD.

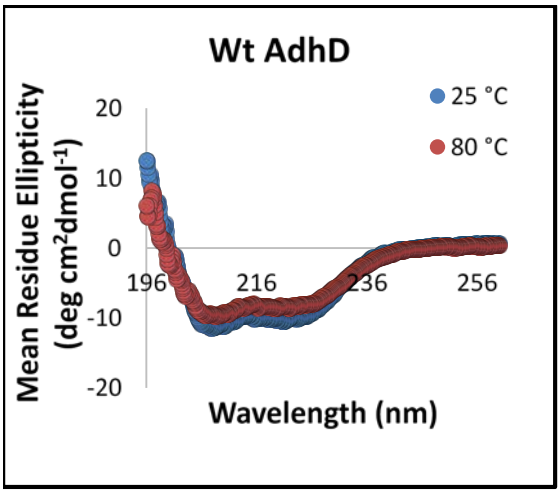
Wt AdhD
Mean Residue Ellipticity (deg cm²dmol⁻¹)
Wavelength (nm)
25 °C
80 °C
20
10
0
-10
-20
196
216
236
256

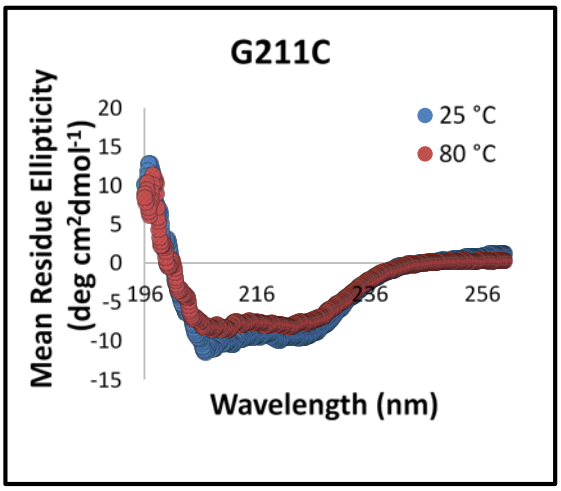
G211C
Mean Residue Ellipticity (deg cm²dmol⁻¹)
Wavelength (nm)
25 °C
80 °C
20
15
10
5
0
-5
-10
-15
196
216
236
256

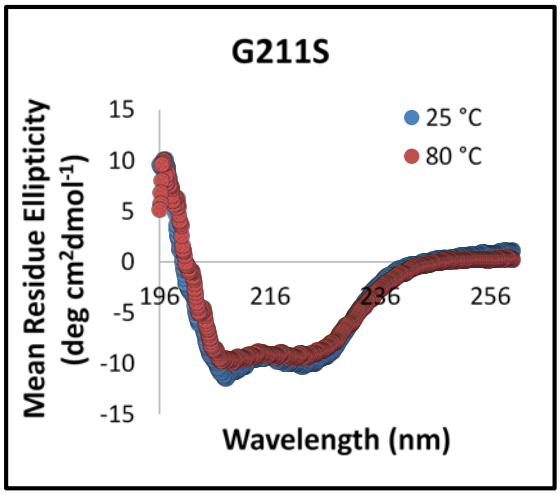
G211S
Mean Residue Ellipticity (deg cm²dmol⁻¹)
Wavelength (nm)
25 °C
80 °C
15
10
5
0
-5
-10
-15
196
216
236
256

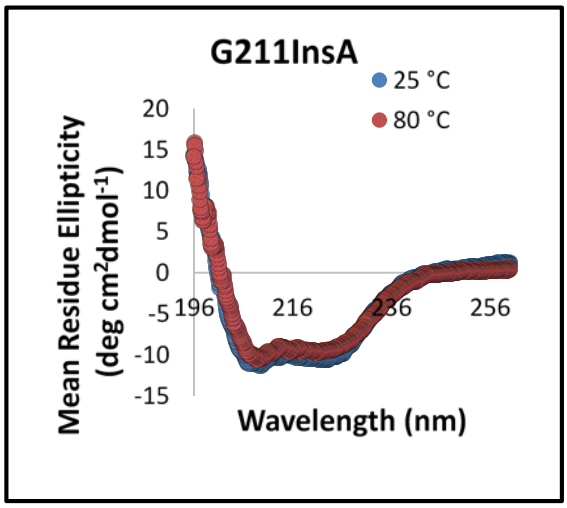
G211InsA
Mean Residue Ellipticity (deg cm²dmol⁻¹)
Wavelength (nm)
25 °C
80 °C
20
15
10
5
0
-5
-10
-15
196
216
236
256

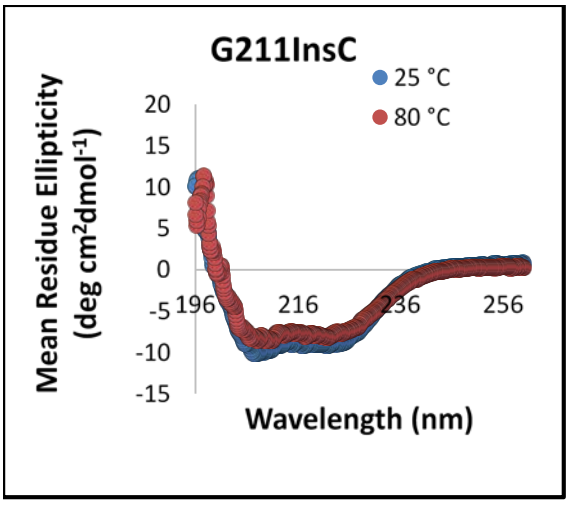
G211InsC
Mean Residue Ellipticity (deg cm²dmol⁻¹)
Wavelength (nm)
25 °C
80 °C
20
15
10
5
0
-5
-10
-15
196
216
236
256

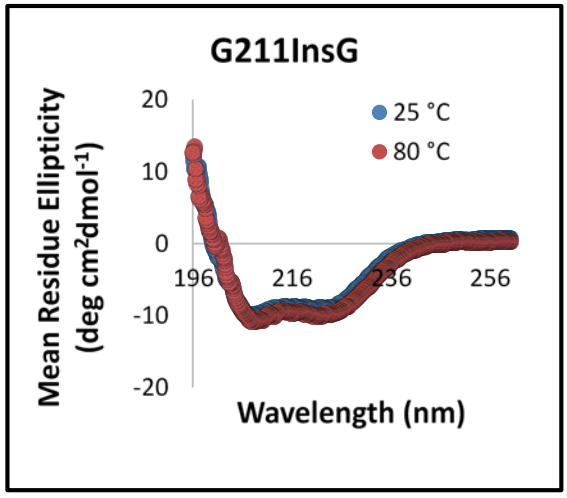
G211InsG
Mean Residue Ellipticity (deg cm²dmol⁻¹)
Wavelength (nm)
25 °C
80 °C
20
10
0
-10
-20
196
216
236
256

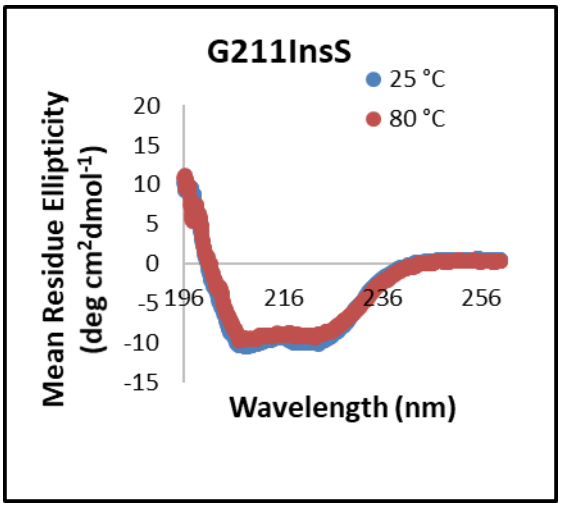

Figure 2.4 Circular dichroic absorbance spectra of wild-type AdhD and mutants. Far UV CD spectra of wild-type AdhD and mutants in 10 mM sodium phosphate buffer (pH 8.0) by measuring mean residue ellipticity between 195 to 260 nm at 25 and 80 °C in a J-815 spectrometer.

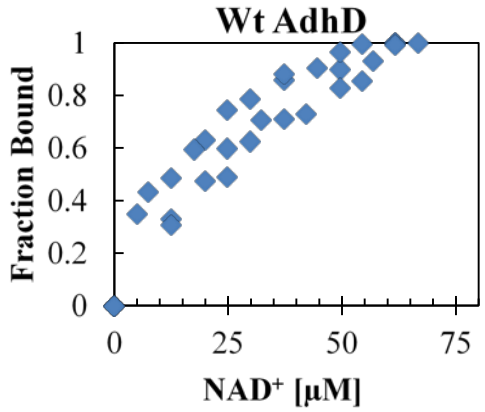
Wt AdhD
Fraction Bound
1
0.8
0.6
0.4
0.2
0
0
25
50
75
NAD+ [µM]

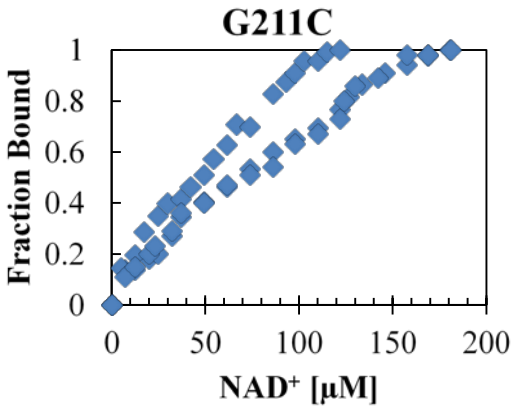
G211C
Fraction Bound
1
0.8
0.6
0.4
0.2
0
0
50
100
150
200
NAD+ [µM]

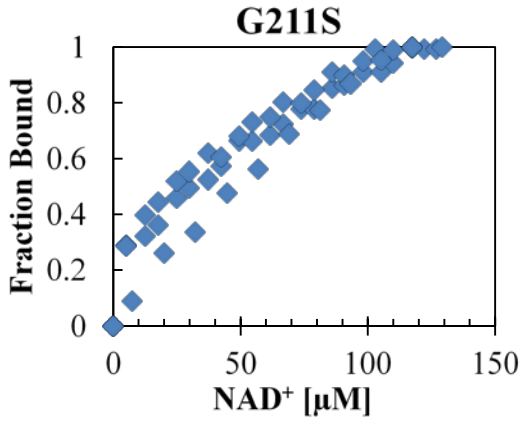
G211S
Fraction Bound
1
0.8
0.6
0.4
0.2
0
0
50
100
150
NAD+ [µM]

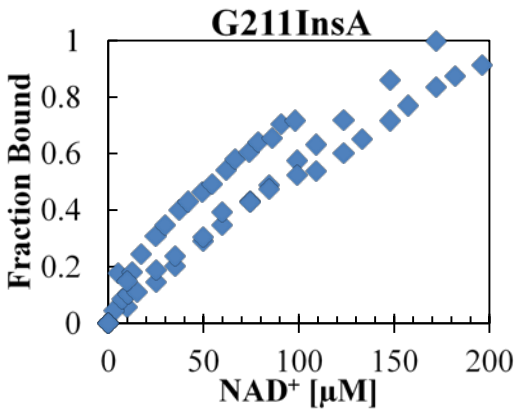
G211InsA
Fraction Bound
1
0.8
0.6
0.4
0.2
0
0
50
100
150
200
NAD+ [µM]

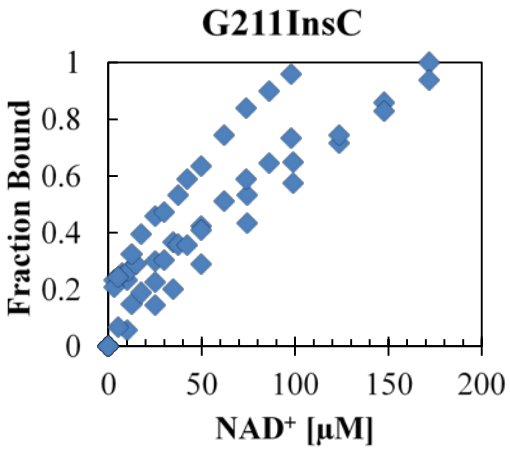
G211InsC
Fraction Bound
1
0.8
0.6
0.4
0.2
0
0
50
100
150
200
NAD+ [µM]

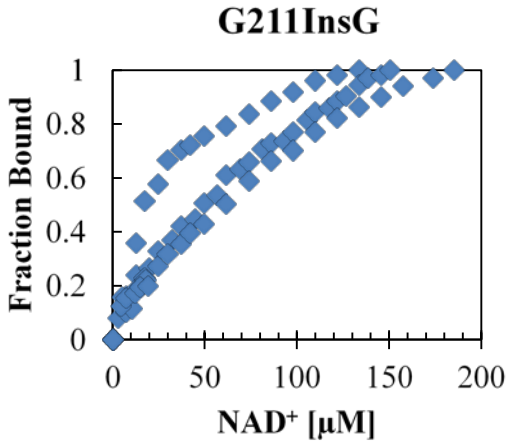
G211InsG
Fraction Bound
1
0.8
0.6
0.4
0.2
0
0
50
100
150
200
NAD+ [µM]

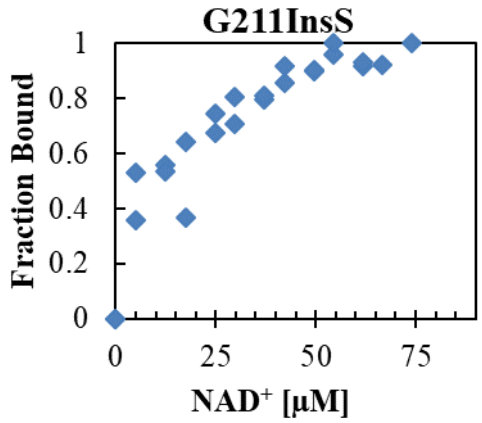

Figure 2.5 Fluorescence titrations of wild-type AdhD and mutants with NAD^+. These were used for K_D determination. 3 µM of enzyme was titrated with NAD^+ at 45 °C in a J-815 spectrometer equipped with a Peltier junction temperature control. Samples were excited at 280 nm and fluorescence change at 330 nm was monitored.

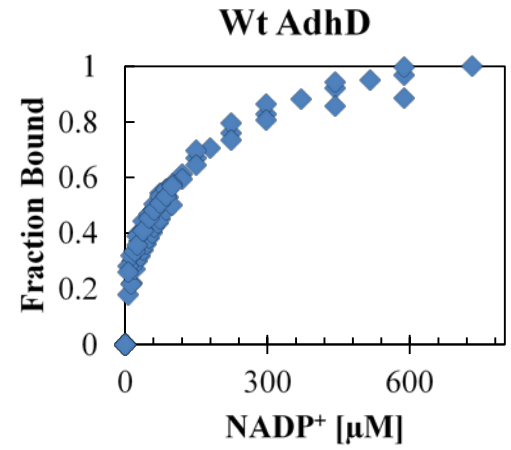
Wt AdhD
Fraction Bound
0
0.2
0.4
0.6
0.8
1
0
300
600
NADP+ [µM]

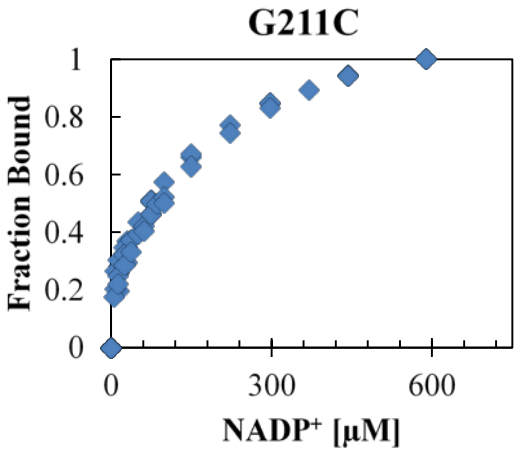
G211C
Fraction Bound
0
0.2
0.4
0.6
0.8
1
0
300
600
NADP+ [µM]

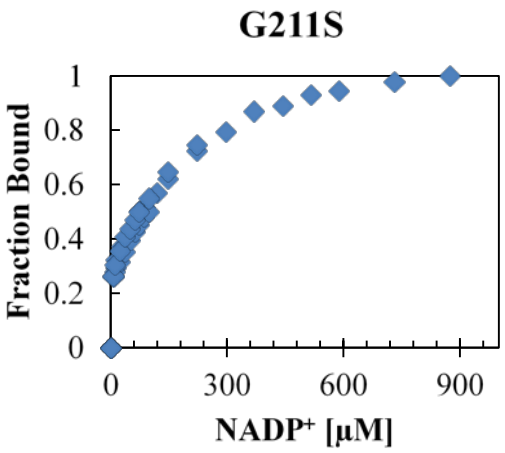
G211S
Fraction Bound
0
0.2
0.4
0.6
0.8
1
0
300
600
900
NADP+ [µM]

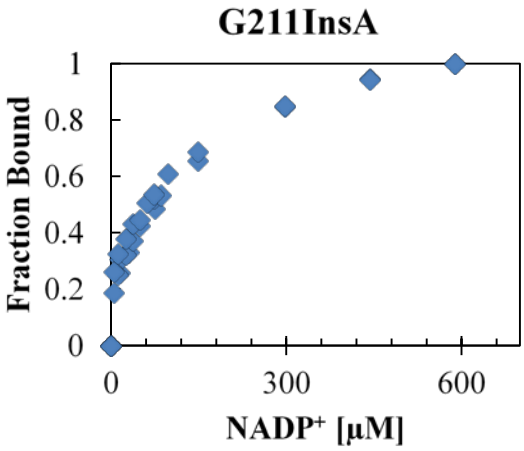
G211InsA
Fraction Bound
0
0.2
0.4
0.6
0.8
1
0
300
600
NADP+ [µM]

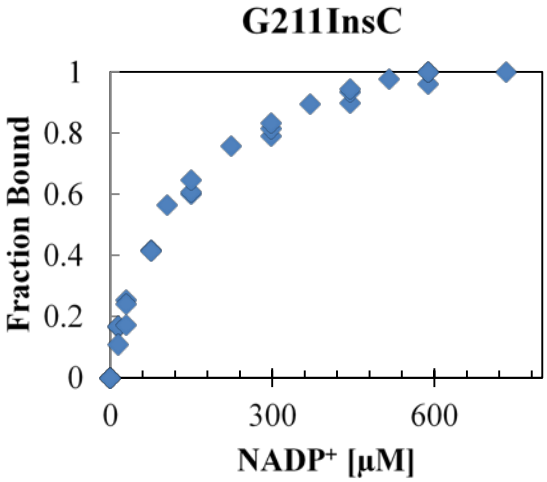
G211InsC
Fraction Bound
0
0.2
0.4
0.6
0.8
1
0
300
600
NADP+ [µM]

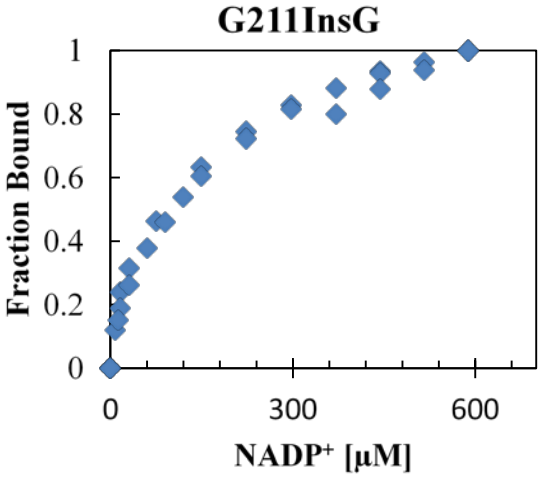
G211InsG
Fraction Bound
0
0.2
0.4
0.6
0.8
1
0
300
600
NADP+ [µM]

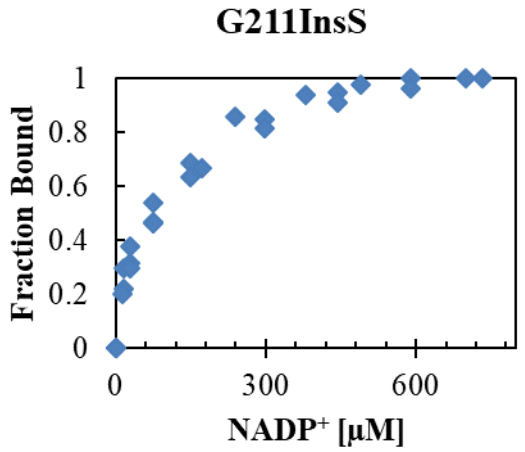

Figure 2.6 Fluorescence titrations of wild-type AdhD and mutants with $NADP^+$. These were used for K_D determination. 3 µM of enzyme was titrated with $NADP^+$ at 45 °C in a J-815 spectrometer equipped with a Peltier junction temperature control. Samples were excited at 280 nm and fluorescence change at 330 nm was monitored.

CHAPTER 3

INSERTION OF A CALCIUM-RESPONSIVE BETA ROLL DOMAIN INTO A THERMOSTABLE ALCOHOL DEHYDROGENASE ENABLES TUNABLE CONTROL OVER COFACTOR SELECTIVITY

Project Collaborators: Walaa Abdallah, Kusum Solanki, and Scott Banta

A version of this chapter entitled "Insertion of a calcium-responsive β-roll domain into a thermostable alcohol dehydrogenase enables tunable control over cofactor selectivity" was published in ACS Catalysis in 2018 in volume 8, pages 1602-1613. WA was responsible for molecular cloning and protein expression and characterization, including terbium studies, enzyme kinetics (with KS), circular dichroism studies (with KS), and kinetic model derivations.

3.1 Abstract

The RTX domains found in some secreted proteins fold into the β-roll secondary structure motif upon calcium binding, which enables folding to be localized extracellularly. We inserted an RTX domain from the adenylate cyclase of *Bordetella pertussis* into a loop near the catalytic active site of the thermostable alcohol dehydrogenase D (AdhD) from *Pyrococcus furiosus*. The resultant chimera, β-AdhD, gained the calcium-binding ability of the β-roll, retained the thermostable activity of AdhD, and exhibited reduced overall alcohol dehydrogenase activity. However, the addition of calcium to β-AdhD preferentially inhibited NAD^+-dependent activity in comparison to $NADP^+$-dependent activity. Calcium was found to be a competitive inhibitor of AdhD and the addition of the RTX domain introduced calcium-dependent non-competitive inhibition to β-AdhD affecting NAD^+-dependent activity. Thus, the insertion of an intrinsically disordered calcium-binding domain into a key loop in a cofactor-dependent enzyme results in an enzyme with tunable cofactor selectivity, reminiscent of a calcium-controlled cofactor selectivity rheostat switch.

3.2 Introduction

Nicotinamide cofactors are critical electron donors and acceptors necessary for the biocatalysis of a wide range of redox reactions essential for life. The ubiquitous NAD(H) and NADP(H) cofactors have similar redox potentials and only differ by a 2'-phosphate group on the adenosine ribose of the molecule. This difference is exploited so that NAD(H) is often involved in catabolic reactions, while NADP(H) is used in anabolic reactions. Most enzymes have evolved a selectivity for only one cofactor, allowing oxidation and reduction reactions to take place simultaneously in the same compartment without cross-reaction.

There has been almost three decades of research in protein engineering aimed at altering or reversing the cofactor selectivity of nicotinamide-dependent enzymes. Early pioneering work

by Scrutton *et al.* [22] demonstrated how amino acids in the "Rossman fold" could be mutated to reverse cofactor selectivity in glutathione reductase. Often the engineering of cofactor specificity in an enzyme is driven by the desire to enable the enzyme to use NAD(H) as opposed to NADP(H) since NAD(H) is more abundant, more stable, and less expensive [95]. In the aldo-keto reductases (AKRs), mutations have been identified in the 2,5-diketo-D-gluconic acid reductase (2,5-DKGR) to broaden cofactor specificity to use NAD(H) for the production of vitamin C [76, 96]. Ketol-acid reductoisomerases involved in the biosynthesis of branched amino acids have been engineered for increased NAD(H)-dependent activity [79]. Formate dehydrogenases are useful for the regeneration of cofactors driven by formate oxidation. Mutations were identified in the cofactor binding pocket to engineer the enzyme to use NADP(H) [97]. More recently, there have been efforts to use computational approaches to predict mutations needed to alter cofactor specificity in dehydrogenases and reductases [82, 98].

A central goal of biochemical engineering is the development of new biocatalysts that can be used to create novel biological processes. There has been a great deal of research aimed at designing and characterizing genetic circuit elements for dynamic and programmable control over protein expression [99]. In addition, there has been decades of research aimed at the development of inhibitors and other molecules that can be used for tunable control over enzymatic activity. We hypothesize that dynamic control over the cofactor selectivity of an enzyme could produce new biocatalytic capabilities. For *in vivo* applications, this could facilitate balancing of redox requirements under different growth conditions or it can enable dynamic control over the metabolic fluxes. Similarly, in *in vitro* systems, dynamic control over cofactor selectivity would enable control over pathway fluxes, energy utilization, and redox potential.

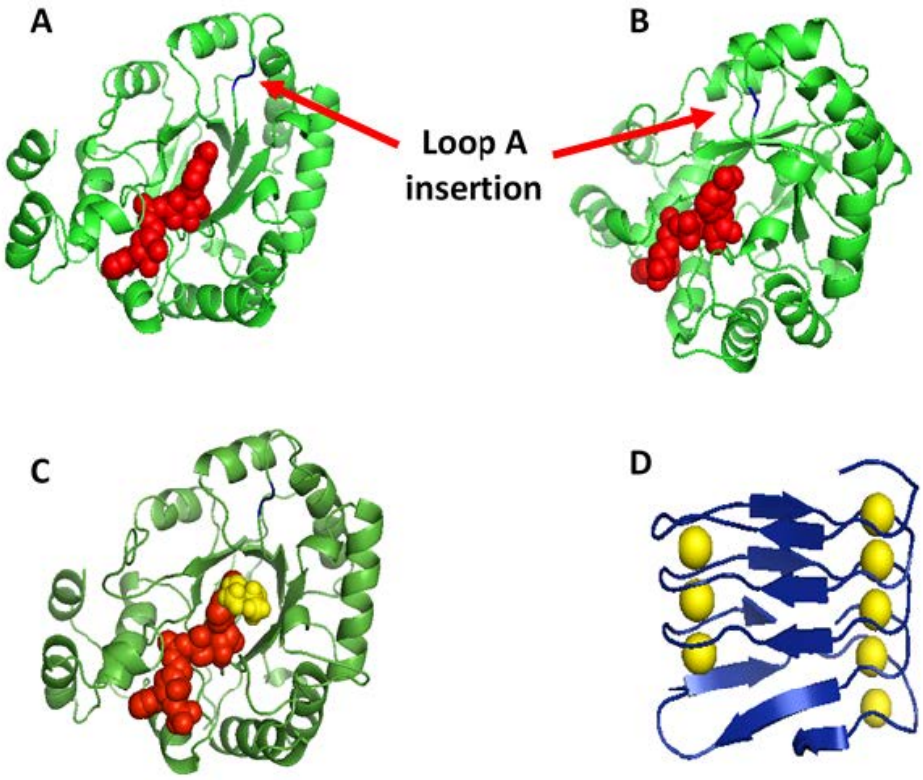

Figure 3.1 Structures of AdhD and the β-roll domain. Homology model of AdhD with bound cofactor highlighted in red and insertion sites in blue (A) looking down the α/β barrel and (B) rotated 90° with insertion sites in loop A indicated. (C) Homology model of ternary complex of AdhD with cofactor in red, 2,3-butanediol in yellow, and insertion site in blue. (D) Crystal structure of the fifth block β-roll domain from the adenylate cyclase protein with calcium ions in yellow (PDB ID 5CVW, Bumba et al., 2016).

We have a long-standing interest in engineering the activity of the alcohol dehydrogenase D (AdhD) isolated from *Pyrococcus furiosus* (**Figure 3.1**) [11, 17, 19, 20, 25]. This enzyme is a monomeric member of the AKRs, has a preference for NAD(H) in the reductive direction, and follows an ordered bi-bi rate mechanism where the cofactor binds first followed by the binding of the substrate [18]. It has activity with many substrates and is most active with 2,3-butanediol [12]. Mobile loops on the top of the barrel (loops A, B and C) are thought to be responsible substrate

specificity [14]. We have engineered just about every aspect of this enzyme including the use of two site-directed mutations in the cofactor binding pocket in AdhD to broaden cofactor selectivity and enhance catalysis [17]. Substrate specificity was engineered by swapping the three mobile loops in the substrate binding pocket with loops from human aldose reductase (hAR). Interestingly, this loop-switching approach also resulted in a reversal of cofactor selectivity from NAD(H) to NADP(H) [19]. More recently, mutations and insertions in one of the mobile loop positions, loop B on the back side of the cofactor binding pocket, resulted in an enzyme with broadened or reversed cofactor selectivity [25]. Therefore, we have created versions of this enzyme with varying cofactor selectivities. However, as with all other protein engineering approaches to altering cofactor utilization, these selectivities are not dynamically controllable.

It is becoming increasingly clear that nature uses conformationally dynamic peptides to regulate biomolecular functions [100]. Intrinsically disordered proteins (IDPs) can toggle between ordered and disordered structures, sometimes serving as regulatory elements. IDPs can be classified in two categories: systems that exploit entropic disorder (such as elastin-like peptides), and those which are involved in conditional molecular recognition (such as the N-terminal domain of the p53 transcription factor) [101]. Binding events by IDPs can be transient or irreversible, where transient binding allows IDPs to function as chaperones and permanent binding allows for modifications such as inhibition and activation [101]. We have been characterizing and exploring various applications using the β-roll secondary structure motif, which also seems to function physiologically as an IDP [102-108]. Specifically, we have been exploring the fifth block of the repeats-in-toxin (RTX) domain from the adenylate cyclase toxin of *Bordetella pertussis*, which is disordered in the absence of calcium and folds into the β-roll domain upon calcium binding [103]. The β-roll secondary structure domain is a flattened spiral shape with two parallel facing β-sheet

faces with turn regions in between that bind calcium via canonical aspartic acid side chains (**Figure 3.1D**) [102, 104]. β-roll domains fold through a polarized mechanism that begins on the C-terminal side of the peptide. The C-terminal capping group stabilizes the initial calcium-dependent folding of β-roll domain via an entropic stabilization. It is thought that the β-roll domain serves as a natural switching mechanism so that pathogenic proteins with the RTX domain are inactive inside of cells, and β-roll domains fold outside of the cell where calcium is more abundant [109]. Thus, the RTX/β-roll transition serves as a dynamic protein switch to localize activity to extracellular, calcium rich environments.

We hypothesized that the disordered to ordered transition of the RTX domain could be exploited for tunable, calcium-dependent modulation of enzymatic activity if it were inserted in the appropriate location of an enzyme. In this work, the RTX domain DNA sequence was cloned into a substrate binding loop (Loop A) of the AdhD sequence (**Figure 3.1**), resulting in the chimeric fusion protein β-AdhD. The Loop A site in AdhD was chosen as the insertion site because it is near the cofactor binding pocket and yet it can be substantially mutated without ablating enzymatic activity [19]. We explored the impact of calcium on the activity of the new β-AdhD fusion protein and found that calcium inhibited NAD^+-dependent activity while far less of an impact was observed for $NADP^+$-dependent activity. Thus, the introduction of the RTX domain into AdhD enables calcium addition to be used to regulate the cofactor selectivity of the new β-AdhD enzyme.

3.3 Materials and Methods

3.3.1 Materials

Oligonucleotides were purchased from Integrated DNA technologies (Coralville, IA). Phusion high fidelity DNA polymerase and *E. coli* BL21(DE3) expression cells were from New England Biolabs (Ipswich, MA). Isopropyl β-D-1-thiogalactopyranoside and ampicillin were from Promega (Madison, WI). NuPAGE SDS-PAGE gels, MOPS running buffer, and NOVEX Sharp pre-stained proteins standards were from Invitrogen (Carlsbad. CA). The gel filtration column, Superdex 16/200, was purchased from GE Healthcare (Piscataway, NJ). Molecular weight centrifugal filters were from EMD Millipore (Billerica, MA). All other chemicals were from Sigma Aldrich (St. Louis, MO).

3.3.2 Cloning, Expression, and Purification

The DNA sequence of the RTX domain from the fifth block of the RTX motifs in the CyaA toxin of *Bordetella pertussis* was cloned into the *adhD* gene from *Pyrococcus furiosus* in the pET-20b(+) vector, plasmid pWUR85 [12]. The plasmid was restriction digested with *Sal*I, so that the valine at the 125th position of AdhD was replaced with glycine followed by the DNA sequence of the fifth block of RTX and this was followed by phenylalanine, resulting in the final construct pWUR85-β-roll (complete sequences can be found in the Supporting Information). Final sequences were verified by DNA sequencing.

The pWUR85 and pWUR85-β-roll plasmids were transformed into *E. coli* BL21(DE3) expression cells and plated onto Luria Broth (LB) plates supplemented with 0.1 mg/ml ampicillin. Single colonies were inoculated overnight in LB supplemented with 0.1 mg/ml ampicillin. Expression was performed at 37 °C in 1 L flasks containing the same medium. Induction was

performed with 0.5 mM final concentration Isopropyl β-D-1-thiogalactopyranoside (IPTG) at OD 0.6 and cultures were kept shaking at 200 rpm overnight.

The cells were harvested, re-suspended in 20 mM Tris-HCl buffer (pH 7.8, with 100 mM NaCl), and lysed at 80 °C for one hour to denature all proteins except for thermophilic AdhD. Cell debris was removed by centrifugation for 30 minutes at 9560 rpm and was concentrated using centrifugal filters (30 kDa MWCO) and purified using gel filtration chromatography (Superdex 16/200, GE Healthcare, Piscataway, NJ) using the lysis buffer of 20 mM Tris-HCl, 100 mM NaCl, pH 7.8. Samples were collected and pooled, and purity was ensured by electrophoresis on NuPAGE 4-12 % Bis-tris gels in MES running buffer (Invitrogen). Samples used were greater than 95% pure and were concentrated in 30 kDa MWCO centrifugal filters before use. The β-AdhD protein was purified by the same method, but a final buffer exchange was performed into 50 mM tris (pH 7.5) by centrifugation at 5560 rpm for 10 minutes three times. This was done to decrease the effect of ionic strength on the conformational change in the β-roll [104]. Protein concentrations were determined by measuring absorbances at 280 nm on a SpectraMax M2 plate reader and using the extinction coefficients of 53,985 and 58,455 M^{-1} cm^{-1} for AdhD and β-AdhD, respectively [110].

3.3.3 Circular Dichroic Absorbance

Circular dichroic absorbance measurements were performed to determine the thermal denaturation curves for AdhD and β-AdhD by monitoring the absorbance at 222 nm while heating from 45 to 90 °C in a Jasco J-815 spectrometer at a rate of 1 ºC/min. Protein samples were dialyzed into water with and without 2.5 mM $CaCl_2$ and a final concentration of 2 ml of 1.25 µM protein was used. Data were converted to mean residue ellipticities (Equation 3.1) and scans were performed in at least duplicate.

$$\theta\ (deg\ cm^2\ dmol^{-1}) = \frac{ellipticiy(mdeg)\ \times 10^6}{pathlength(mm)\ \times\ [protein](\mu M)\ \times\ n} \qquad (3.1)$$

Full length protein scans of AdhD and β-AdhD were also performed at 45 °C from 195 to 260 nm. Data were converted to mean residue ellipticities (Equation 3.1) and experiments were performed in at least triplicate.

3.3.4 Terbium Förster Resonance Energy Transfer

Terbium binding assays were conducted to probe for the presence of calcium-binding sites as terbium is a fluorescent calcium analog with a similar ionic radius. 5 µM protein was incubated at 25 °C for 30 minutes in 20 mM PIPES (pH 6.8) supplemented with 120 mM NaCl and 10 mM KCl and varying terbium chloride hexahydrate concentrations in the same buffer. The samples were excited at 282 nm and emission at 545 nm was measured using a Spectramax M2 Plate Reader. Data were fit to a saturation adsorption isotherm (Equation 3.3).

3.3.5 Intrinsic Tryptophan Fluorescence Experiments

Cofactor dissociation constants (K_d or K_{ia} values) were determined by fluorescence titrations in a J-815 Spectrometer (Jasco, Inc., Easton, MD). Fluorescence titrations were performed by incubating 2 mL of a 3 µM enzyme solution in glycine-NaOH buffer (pH 9.3) in one-centimeter path-length cuvettes at 45 °C. Samples were excited at 280 nm and emission was recorded at 330 nm to detect $NAD(P)^+$ cofactor binding. Cofactors were titrated in and the total volume of the cofactor added was less than two percent of the total volume to avoid dilution effects. Data were fit to the saturation adsorption isotherm (Equation 3.2) and performed in at least triplicate.

$$\phi = \frac{K_d^{-1}[NAD(H)]}{1 + K_d^{-1}[NAD(H)]} \quad (3.2)$$

Dissociation constants were determined with varying calcium concentrations from 0 to 200 mM final concentrations (in 50 mM increments and at 25 mM).

3.3.6 Kinetic Activity Assays

Initial rate date for oxidation reactions in the forward direction were determined by conducting activity assays at 45 °C in 96-welled plates where substrate (2,3-butanediol), enzyme, and glycine buffer (pH 9.3) were initially incubated for 20 minutes. Cofactor (NAD^+ or $NADP^+$) was added and absorbance at 340 nm was measured continuously for 20 minutes. The initial alcohol concentrations ranged from 2 mM to 100 mM and the initial cofactor concentrations ranged from 1 µM to 1000 µM. Studies were performed with calcium (or other salt) concentrations ranging from 0 and 200 mM. The final reaction volumes were 250 µL. To ensure initial rates were collected, data was only used within the first 10% of the conversion of the added cofactor. The absorbance values were converted to cofactor concentrations, and linear regression was used to calculate initial rates. These rates were divided by the enzyme concentration to obtain initial specific rates (**Table 3.7** - **Table 3.16**). All measurements were made in at least triplicate.

3.3.7 Kinetic Rate Data Fitting

To determine parameters for various kinetic rate equations, nonlinear regression was performed using fits to the entire data sets using least squares curve fitting in MATLAB. Measured dissociation constants were used for the K_{ia} values in the equations. Parameters were estimated and 95% confidence intervals were reported. For the fit of the full β-AdhD data set to the derived

equation with competitive and non-competitive inhibition (Equation 3.10) several of the parameters were not well fit leading to error bars at least 3 orders of magnitude larger than values and thus these parameters were reported without error bars (**Table 3.5**).

3.3.8 Statistical Analysis

One-way and two-way analysis of variance (ANOVA) as well as Student's t-test were completed using Microsoft Excel. At least three data sets were used per study. Statistical significance was indicated by $p<0.05$.

3.4 Results and Discussion

3.4.1 Expression and Purification of AdhD and β-AdhD

The DNA sequence corresponding to the RTX peptide in the fifth block of the RTX motif in the CyaA toxin of *Bordetella pertussis* was cloned into plasmid pWUR85, which contains the AdhD gene from thermostable *Pyrococcus furiosus*. The 84-amino acid insertion began with an added glycine, ended with a phenylalanine, and replaced a valine at position 125 in the AdhD gene, resulting in the construct, pWUR85-β-roll. This site in AdhD (Loop A) was chosen for insertion as it has previously been shown that this loop region could be swapped with a loop from a related enzyme (hAR) without eliminating AdhD activity [19]. The pWUR85 and pWUR85-β-roll plasmids were transformed into BL21(DE3) cells and both proteins were expressed. Cloning of the RTX domain into Loop A of AdhD resulted in the formation of a new 42 kDa fusion protein, β-AdhD, with the parent enzyme, AdhD, having a molecular weight of around 34 kDa. The full amino acid and DNA sequences of AdhD and β-AdhD can be found in the Supporting Information.

The resulting proteins, AdhD and β-AdhD, were routinely produced at 50-100 mg of protein per liter of *E. coli* culture. After induction, the pelleted cells were re-suspended and heat-

treated for cell lysis and to denature endogenous mesostable *E. coli* proteins. The whole cell lysates were centrifuged and both proteins were found in the soluble fractions. This suggests the insertion of the RTX domain did not drastically affect the intrinsic thermostability of AdhD. The soluble fractions were concentrated, and the proteins were further purified using size exclusion chromatography and yielded the expected molecular masses to greater than 95% purity as seen on SDS-PAGE (**Figure 3.9**).

3.4.2 Effect of RTX Domain on Protein Thermal Stability

To further characterize the thermal stability of β-AdhD, denaturation studies were conducted where unfolding was monitored by measuring the circular dichroic absorbance at 222 nm, where a prominent negative signal for alpha helices is observed. The absorbance signals for AdhD and β-AdhD with and without 2.5 mM calcium chloride in water were found to be relatively constant up to 90°C, confirming that the insertion did not dramatically perturb native AdhD thermostability (**Figure 3.10**).

3.4.3 Terbium Förster Resonance Energy Transfer (FRET) Studies to Probe the Presence of Calcium-Binding Sites in β-AdhD

The ability of the β-roll to bind calcium after its insertion into the AdhD protein was assessed using FRET upon Tb^{3+} binding (**Figure 3.2**). Terbium was used to probe for the presence of calcium-binding sites in the RTX domain as it has a similar ionic radius to calcium and can be observed via fluorescence. When the RTX domain folds into the β-roll structure, tyrosine residues are localized close to the calcium-binding sites, allowing energy transfer between tyrosine and terbium. FRET data at different Tb^{3+} concentrations were fit to Equation (3.3).

$$\phi = \frac{K_d^{-1}[Tb^{3+}]}{1 + K_d^{-1}[Tb^{3+}]} \tag{3.3}$$

For additions up to 100 μM Tb^{3+}, the change in fluorescence was similar for AdhD and β-AdhD. At concentrations above 100 μM, the fluorescence signal continued to increase for β-AdhD but stayed relatively constant for AdhD. This suggests the β-roll domain in AdhD binds Tb^{3+} beyond what is bound by AdhD alone, indicating the presence of new Tb^{3+} binding sites. By two-way ANOVA, the changes in fluorescence as a function of Tb^{3+} concentration and the interaction parameter were statistically significant for AdhD and β-AdhD, indicating the enzymes interact differently with Tb^{3+}. These results are similar to what has previously been reported for Tb^{3+} binding by RTX peptide fusions to maltose binding protein [103].

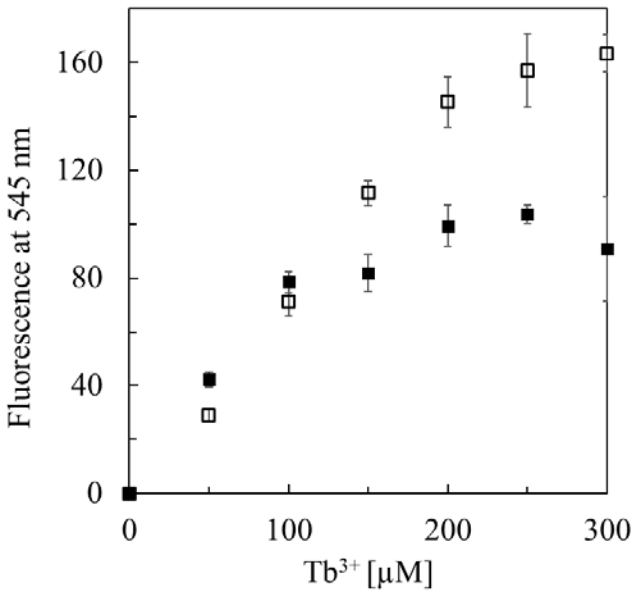

Figure 3.2 Fluorescence emission measurements at 545 nm as a function of terbium concentrations for the RTX domain inserted into AdhD (β-AdhD). The signal for β-AdhD (□) continues to increase at higher terbium concentrations as compared to AdhD alone (■), indicating calcium binding by the RTX domain beyond the calcium interactions with the AdhD protein alone.

Although the terbium binding data of the fusion protein, β-AdhD, is consistent with the folding of the RTX domain into the β-roll structure upon cation binding, 3-D structure determination will be required to definitively determine whether the β-roll structure is the same as observed when the same sequence is expressed recombinantly without insertion into another protein.

3.4.4 Impact of Calcium on Cofactor Binding Affinities

Dissociation constants (K_d values) for AdhD and β-AdhD binding cofactors were measured by fluorescence titration where the intrinsic fluorescence of the tryptophan in the 92nd position, in the cofactor binding pocket, was quenched by the addition of cofactor (NAD^+ or $NADP^+$) in the absence and presence of 50 mM Ca^{2+} (**Table 3.1** and **Figure 3.13**). This calcium concentration was chosen as this is well above the calcium concentration needed for the isolated RTX domain to fold into the β-roll structure.

Table 3.1 Dissociation constants (K_d values, μM) for AdhD and β-AdhD. Data collected with NAD^+ and $NADP^+$ in the presence and absence of 50 mM calcium[a].

	K_d with 0 mM Ca^{2+}	K_d with 50 mM Ca^{2+}
AdhD, $\mathbf{NAD^+}$	12 ± 2	18 ± 3
AdhD, $\mathbf{NADP^+}$	67 ± 6*,†	44 ± 1†
β-AdhD, $\mathbf{NAD^+}$	12 ± 3 ⁑	19 ± 2 ⁑
β-AdhD, $\mathbf{NADP^+}$	38 ± 3*	48 ± 4

[a]All data were collected in at least triplicate. Error bars represent standard deviations. Statistically significant differences by one-way ANOVA are denoted with *, †, and ⁑ ($p<0.05$)

The K_d values in the absence of calcium show that the insertion of the RTX domain improved the binding of $NADP^+$, but changes in the binding of NAD^+ were not statistically significant. Upon the addition of calcium, the K_d values increased for AdhD and β-AdhD with

NAD^+. The K_d of AdhD for NAD^+ increased by 50%, while that of β-AdhD increased by 58%, but only the change for β-AdhD reached statistical significance. Two-way ANOVA with both proteins at 0 and 50 mM calcium revealed that the calcium concentration influenced the dissociation constants, whereas the effect of RTX domain insertion was not significant.

With $NADP^+$ as a cofactor, the K_d values increased for both AdhD and β-AdhD compared to NAD^+, but the trend for cofactor affinities upon calcium addition were different between the enzymes. The K_d values for AdhD decreased by 34% in the presence of calcium but increased by 26% for β-AdhD. Only the change for AdhD reached statistical significance. Two-way ANOVA revealed that the effect of the calcium concentration was insignificant, but the effects of the RTX domain insertion and the interaction parameter were significant.

A significant change was observed when comparing enzyme binding affinities to NAD^+ and $NADP^+$ in the presence and absence of calcium. Two-way ANOVA comparing the K_d values for AdhD with NAD^+ and $NADP^+$ demonstrate that the type cofactor, as well as the interaction parameter, are significantly different, whereas the effect of the calcium concentration was not. The same was done for β-AdhD and it was determined that the effects of the cofactor type and the calcium concentrations are significant, but the interaction parameter was not.

Overall these results indicate that the insertion of the RTX domain into AdhD and the addition of 50 mM calcium resulted in some significant impacts on the binding of the cofactors, but these changes were modest (not reaching an order of magnitude) indicating relatively minor impacts on the functions of the cofactor binding pockets.

3.4.5 Effect of the RTX Domain on Enzyme Activity in the Absence of Calcium

AdhD follows the ordered bi-bi kinetic mechanism, where cofactor binding necessarily occurs before substrate (2,3-butanediol) to form a ternary enzyme/cofactor/substrate complex. Initial rate data were collected at varying cofactor (A, 1 - 1000 µM) and 2,3-butanediol substrate (B, 2 - 100 mM) concentrations. There are four parameters in the ordered bi-bi rate Equation (3.4). The dissociation constants (K_d or K_{ia} values) were measured independently using fluorescence titration (as previously described, **Table 3.1**), so three parameters were used to fit the data (**Table 3.7**, **Table 3.9**, **Table 3.11**, and **Table 3.13**). Experiments were performed with either NAD^+ and $NADP^+$ in the absence of calcium and the data were used to estimate the kinetic parameters (**Table 3.2**) using non-linear least squares regression.

$$v = \frac{E_t k_{cat} AB}{K_{ia}K_B + K_A B + K_B A + AB} \tag{3.4}$$

The insertion of the RTX domain into AdhD in the absence of calcium resulted in a substantial overall reduction in AdhD activity. The rate data also indicated that substrate saturation was not reached for β-AdhD, which prevented the data from being accurately fitted by the ordered bi-bi rate equation (**Figure 3.16** and **Figure 3.17**). Therefore, only AdhD kinetic parameters were determined at 0 mM calcium with NAD^+ and $NADP^+$ (**Table 3.2**, **Table 3.7**, and **Table 3.11**). The parameters are consistent with previously published results [17].

Table 3.2 Ordered bi-bi kinetic parameters for AdhD (Equation 3.4). Data collected in the oxidation reaction with 2,3–butanediol and $NAD(P)^+$ in the presence and absence of 50 mM calcium[a].

	Cofactor	K_{ia} (μM)	k_{cat} (s^{-1})	K_A (μM)	K_B (mM)
AdhD	NAD^+	12 ± 2	1.5 ± 0.2	44 ± 56	5.8 ± 4.0
AdhD w/50 mM Ca^{2+}	NAD^+	18 ± 3	2.0 ± 0.8	140 ± 140	71 ± 47
AdhD	$NADP^+$	67 ± 6*	0.039 ± 0.003†	31 ± 35	1.1 ± 0.5 ‡
AdhD w/50 mM Ca^{2+}	$NADP^+$	44 ± 1*	0.24 ± 0.01†	23 ± 12	5.1 ± 0.6 ‡

[a] K_{ia} values were obtained from fluorescence titrations (**Table 3.1**). All data were collected in at least triplicate. Error bars represent 95% confidence intervals. Statistically significant differences by t-test of calcium addition are denoted with *, †, and ‡ ($p<0.05$).

3.4.6 Effect of Calcium on Steady-State Kinetic Parameters of AdhD with NAD^+ and $NADP^+$ as Cofactors

Steady state kinetic data were measured for AdhD and β-AdhD in the presence of 50 mM calcium, as this should be a sufficient calcium concentration to transition the RTX domain into the β-roll fold [103]. β-AdhD activity was affected by calcium addition. However, as was seen in the absence of calcium, the data with either cofactor could not be accurately fit to Equation 3.4 as substrate saturation was not reached (**Figure 3.16** and **Figure 3.17**).

The dissociation constants (K_d or K_{ia} values) from **Table 3.1** were used, and the remaining kinetic parameters for AdhD with NAD^+ as a cofactor were fit and found to change slightly in the presence of calcium (**Table 3.2**). The K_A and K_B increased by an order of magnitude, but none of the changes reached statistical significance. The same studies were also conducted with $NADP^+$ (**Table 3.2**, **Table 3.8**, and **Table 3.12**). Unlike with NAD^+, the K_A and K_B values for AdhD with $NADP^+$ were the same order of magnitude, while the k_{cat} increased by an order of magnitude in

the presence of 50 mM calcium. In the presence of calcium, the k_{cat} value increased by around 500%, the K_A decreased by almost 30% and the K_B value increased by almost 400%, but only the change in k_{cat} and K_B reached statistical significance. Therefore, the maximum turnover rate of the wild type enzyme increased in the presence of 50 mM calcium when $NADP^+$ was used as a cofactor. These results suggest that the addition of calcium increases the turnover rate of the enzyme/$NADP^+$/substrate complex into products. The reason for this calcium-induced enhancement of $NADP^+$-dependent activity are not clear.

To shed some light on the structural impact of the calcium addition, circular dichroic absorbance studies were performed in the presence and absence of 10 μM $NAD(P)^+$ with and without 2.5 mM calcium at 45 °C, the temperature at which the kinetic assays were performed. Those concentrations were the highest that could be used, as the spectra became noisy at higher concentrations. The addition of cofactor with and without calcium had no effect on the secondary structure of AdhD (**Figure 3.3A**). Similarly, the addition of NAD^+ had no effect on the β-AdhD secondary structure. However, the addition of $NADP^+$, calcium, or both resulted in significant upward shifts in the spectra (**Figure 3.3B**). Further 3-D structural studies of the enzymes in the presence of calcium and cofactors would need to be performed to understand how calcium affects the formation of the enzyme/cofactor complexes.

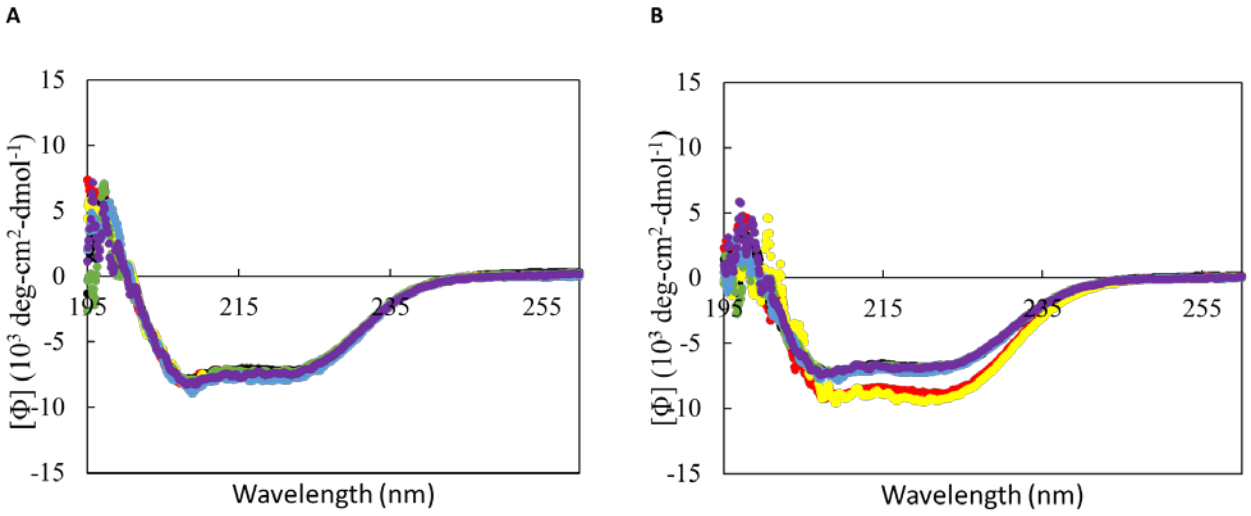

Figure 3.3 Circular dichroic absorbance at 45 °C for (A) AdhD and (B) β-AdhD. Spectra were measured in the absence of calcium and cofactor (red), and in the presence of 2.5 mM Ca^{2+} (black), 10 µM NAD^+ (yellow), 10 µM NAD^+ with 2.5 mM Ca^{2+} (green), 10 µM $NADP^+$ (blue), and 10 µM $NADP^+$ with 2.5 mM Ca^{2+} (purple). All measurements were made in triplicate and average values are shown.

3.4.7 Effect of Calcium on Steady-State Kinetic Parameters Using a Simplified Rate Equation for β-AdhD with NAD^+ and $NADP^+$ as Cofactors

To obtain a meaningful analysis of the kinetic data for the β-AdhD, the ordered bi-bi rate equation (Equation 3.4) was simplified to Equation 3.5 by dividing by the K_B term and assuming that the substrate values (B) were small as compared to the K_B value. Thus, the equation captures activity where the reaction is first order with respect to substrate (B) and the data could be more readily fit using this equation. This approach has previously been used for exploring mutations in a similar AKR enzyme (2,5-DKGR) [96] and is appropriate for exploring kinetic behavior of an enzyme operating below the saturation conditions of the substrate ($B<<K_B$).

$$v = \frac{E_t \left({k_{cat}}/{K_B} \right) AB}{K_{ia} + A} \tag{3.5}$$

The fitted apparent K_{ia} value for β-AdhD was an order of magnitude lower than the measured K_d value and the fitted value for β-AdhD with 50 mM calcium was an order of magnitude higher than the measured K_d value (**Table 3.1**). As can be seen (**Table 3.3**), the lumped kinetic parameters indicate the overall activity of AdhD decreased by an order of magnitude with calcium addition, while β-AdhD decreased by three orders of magnitude in the presence of 50 mM calcium with NAD^+. By Student's t-test, the changes in these parameters for AdhD were insignificant, while changes in β-AdhD reached statistical significance. Thus, the addition of 50 mM calcium significantly reduced activity with NAD^+ as a cofactor in the β-AdhD enzyme.

Table 3.3 Kinetic parameters fit to simplified rate equation (Equation 3.5) for AdhD and β-AdhD with NAD^+. Data collected in the oxidation reaction with 2,3–butanediol and NAD^+ in the presence and absence of calcium.

	k_{cat}/K_B ($\mu M^{-1}s^{-1}$)	K_{ia} (μM)	$(k_{cat}/K_B)/K_{ia}$ ($\mu M^{-2}s^{-1}$)
[a]AdhD	$(2.6 \pm 1.8) \times 10^{-4}$	12 ± 2	$(2.2 \pm 1.6) \times 10^{-5}$
[a]AdhD w/50 mM Ca^{2+}	$(2.8 \pm 2.2) \times 10^{-5}$	18 ± 3	$(1.6 \pm 1.2) \times 10^{-6}$
β-AdhD	$(2.0 \pm 0.1) \times 10^{-7}$*	0.63 ± 1.10†	$(3.2 \pm 5.6) \times 10^{-7}$
β-AdhD w/50 mM Ca^{2+}	$(1.3 \pm 0.2) \times 10^{-7}$*	630 ± 190†	$(2.1 \pm 0.7) \times 10^{-10}$

[a]K_{ia} values were obtained from fluorescence titrations (**Table 3.1**) and k_{cat}/K_B data were obtained from **Table 3.2**. All data were collected in at least triplicate. Error bars represent 95% confidence intervals. Statistically significant differences by t-test of calcium addition are denoted with * and † ($p<0.05$).

The $NADP^+$ data were also fit to the modified rate Equation 3.5. The fitted apparent K_{ia} value for β-AdhD was an order of magnitude higher than the measured K_d value and the fitted value for β-AdhD with 50 mM calcium was similar to the measured K_d value (**Table 3.1**). With $NADP^+$ as a cofactor, the addition of calcium increased the catalytic efficiency of AdhD by an order of magnitude, while the catalytic efficiency of β-AdhD doubled. However, these changes did not reach statistical significance (**Table 3.4**). Overall the addition of 50 mM calcium increased the activity with $NADP^+$ as a cofactor.

Table 3.4 Kinetic parameters fit to simplified rate equation (Equation 3.5) for AdhD and β-AdhD with $NADP^+$. Data collected in the oxidation reaction with 2,3–butanediol and $NADP^+$ in the presence and absence of calcium.

	k_{cat}/K_B ($\mu M^{-1}s^{-1}$)	K_{ia} (μM)	$(k_{cat}/K_B)/K_{ia}$ ($\mu M^{-2}s^{-1}$)
[a]AdhD	$(3.6 \pm 1.5) \times 10^{-5}$	67 ± 6*	$(5.3 \pm 2.3) \times 10^{-7}$
[a]AdhD w/50 mM Ca^{2+}	$(4.7 \pm 0.6) \times 10^{-5}$	44 ± 1*	$(1.1 \pm 0.1) \times 10^{-6}$
β-AdhD	$(5.1 \pm 0.8) \times 10^{-7}$	160 ± 100	$(3.3 \pm 2.1) \times 10^{-9}$
β-AdhD w/50 mM Ca^{2+}	$(4.7 \pm 0.2) \times 10^{-7}$	70 ± 20	$(6.7 \pm 1.9) \times 10^{-9}$

[a] K_{ia} values were obtained from fluorescence titrations (**Table 3.1**) and k_{cat}/K_B data were obtained from **Table 3.2**. All data were collected in at least triplicate. Error bars represent 95% confidence intervals. Statistically significant differences by t-test of calcium addition are denoted with * ($p<0.05$).

Taken together, these results indicate that calcium addition (50 mM) has much different effects on AdhD versus β-AdhD activity. For AdhD, calcium increases activity with $NADP^+$. When the β-roll domain is inserted into AdhD, calcium was also found to increase $NADP^+$-dependent activity. However, the more dramatic observation is the significant reduction in NAD^+-dependent activity that was seen for β-AdhD and not AdhD alone. Therefore, the calcium-induced folding of the RTX domain selectively perturbs the formation of the enzyme/NAD^+/substrate complex.

Studies were performed with different salts to confirm the selectivity of this system with calcium (**Figure 3.18**). Magnesium, which has the same cationic charge as calcium, was even more inhibitory to AdhD activity with NAD^+ than was observed for calcium, and thus magnesium was not used as a control for the β-AdhD. Sodium chloride, like calcium, has no significant effects on AdhD activity at 50 mM or less with NAD^+. With AdhD and $NADP^+$, calcium and sodium chloride have a similar effect on AdhD, making it an appropriate control. Although calcium and sodium chloride have a similar effect on β-AdhD in the presence of NAD^+ and $NADP^+$, the calcium-induced inhibition of β-AdhD with NAD^+ was greater than what was observed sodium chloride, which is consistent with the calcium selectivity of the RTX- β-roll transition.

3.4.8 Effect of Calcium Titration on Cofactor Specificity of β-AdhD

In order to further explore the impact of calcium on β-AdhD activity, additional kinetic rate experiments were performed with varying cofactor and a wider range of calcium concentrations (10 - 200 mM), but with constant substrate concentrations (100 mM 2,3–butanediol) (**Figure 3.4**). At lower concentrations of calcium, the rates were generally found to increase, and then as the calcium concentration was increased further (especially above the 50 mM concentration used before), the rates for β-AdhD further decreased in the presence of NAD^+ (**Figure 3.4A**). A pseudo-exponential decay as a function of calcium concentration was observed, which resulted in the rate decreasing by an order of magnitude at high calcium concentrations. The same study was conducted with $NADP^+$; as the calcium concentration increased the rates either increased or stayed the same, except for 200 μM $NADP^+$, where a slight decrease in activity was observed at around 100 mM calcium or higher (**Figure 3.4B**). However, unlike NAD^+, none of these effects altered the rate by an order of magnitude. This is consistent with the observation that

calcium has a much larger effect on NAD^+-dependent activity in β-AdhD, whereas calcium has a mixed effect on $NADP^+$-dependent activity (which is mostly beneficial).

The insertion of the RTX domain led to a decrease in the affinity of the enzyme/cofactor complex for substrate, as evidenced by the fact that the kinetic data collected before were below the saturation levels for the enzyme with the substrate, 2,3-butanediol. Therefore, data from **Figure 3.4** were fit to the ordered bi-bi rate equation (Equation 3.4) where the concentration of substrate (B) is held constant (but not saturating), which produces an apparent Michaelis Menton type equation (Equation 3.6).

$$v = \frac{E_t\left(\frac{k_{cat}B}{K_B + B}\right)A}{\left(\frac{K_{ia}K_B + K_AB}{K_B + B}\right) + A} = \frac{E_t k_{cat,app} A}{K_{A,app} + A} \tag{3.6}$$

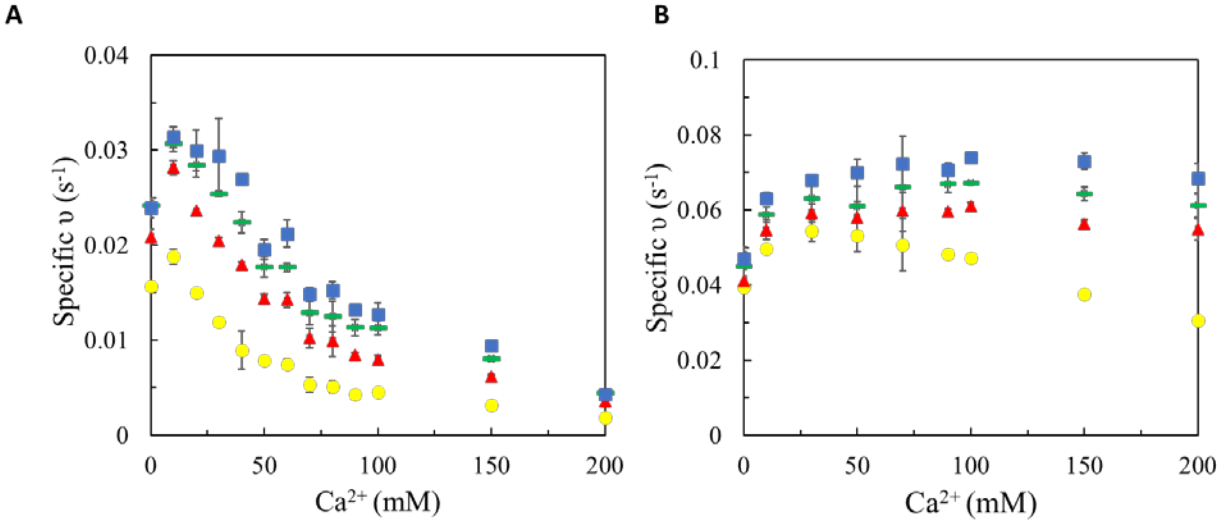

Figure 3.4 Specific rates as a function of calcium concentration for β-AdhD with varying $NAD(P)^+$. 200 (•), 500 (▲), 750 (-), and 1000 (■) μM cofactor were used all at 100 mM 2,3–butanediol. (A) Specific rates decrease with NAD^+ as a cofactor as calcium concentration increases. (B) Specific rates generally are affected differently with $NADP^+$ as a cofactor as calcium concentration increases. All measurements were made in triplicate and error bars represent 95% confidence intervals.

These apparent catalytic efficiencies ($k_{cat,app}/K_{A,app)}$ for AdhD and β-AdhD (at 100 mM 2,3–butanediol and varying cofactor) were determined as a function of varying calcium concentrations (**Figure 3.5A**, **Figure 3.5B**, and **Figure 3.11**). Changes in the apparent catalytic efficiencies of AdhD with NAD^+ were insignificant at calcium concentrations below 100 mM calcium, and a significant decrease in activity was only seen at 200 mM calcium. For β-AdhD, decreases in the apparent catalytic efficiencies with NAD^+ were significant for all calcium concentrations except for 10 mM calcium. Upon the addition of 20 mM calcium, the apparent catalytic efficiency decreased by 43% and decreased continuously so that the efficiency decreased by 93% with 200 mM calcium. These results extend the striking trend that was observed before, where the addition of calcium dramatically inhibits NAD^+-dependent activity in β-AdhD, but not AdhD.

The same study was conducted with $NADP^+$ for both AdhD and β-AdhD (**Figure 3.5A, Figure 3.5B**, and **Figure 3.12**). Here, calcium addition had much less of an impact. All changes in apparent catalytic efficiency for AdhD were insignificant. The same was true for β-AdhD, with the exception of 200 mM calcium, where a significant decrease was observed.

Thus, **Figure 3.5A** shows that the addition of calcium does not have a large impact on the apparent catalytic efficiency of either NAD^+ or $NADP^+$ for AdhD, but **Figure 3.5B** shows there is large effect on the catalytic efficiency of β-AdhD for NAD^+, which is not seen for $NADP^+$. The addition of calcium had a small, but significant effect on the binding of NAD^+ by β-AdhD (**Table 3.1**), but this data suggests the dominant effect of calcium addition on β-AdhD is the perturbation of the ternary complex formed between enzyme/NAD^+/substrate.

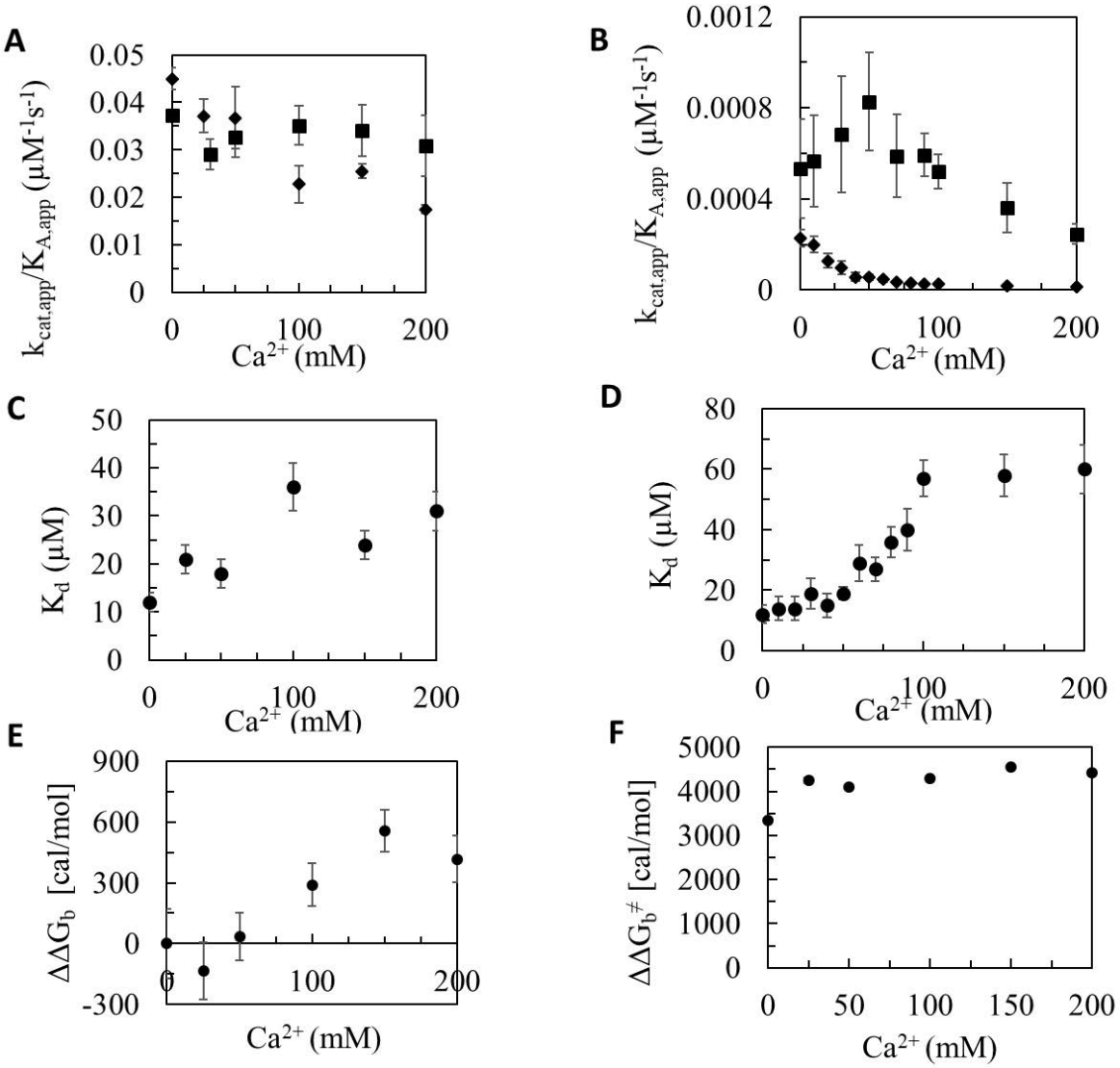

Figure 3.5 Apparent catalytic efficiencies, cofactor dissociation constants, and binding energies for AdhD and β-AdhD. Apparent catalytic efficiencies ($k_{cat,app}/K_{A,app}$) for AdhD (A) and β-AdhD (B) with NAD^+ (♦) and $NADP^+$ (■) as a function of calcium concentrations with 100 mM 2,3 – butanediol as the substrate. Insignificant changes were observed for AdhD with NAD^+ at calcium concentrations lower than 100 mM, while insignificant changes observed with $NADP^+$ at all calcium concentrations. A significant decrease in catalytic efficiencies is observed with β-AdhD with NAD^+, but not $NADP^+$, as a function of increasing calcium concentration. Error bars represent 95% confidence intervals. Cofactor dissociation constants for NAD^+ as a function of calcium concentration for AdhD (C) and β-AdhD (D). Data were fit to the saturation adsorption isotherm and calculated by equation 10. Error bars represent standard deviations. Changes in ground-state and transition state binding energies between AdhD and β- AdhD as a function of calcium concentrations. The differences in the ground state binding energy increase as a function of calcium concentration (E), while changes in transition-state binding energy as a function of calcium concentration (F) plateau after an increase upon calcium addition. The changes in

ground state and transition state binding energies were calculated by equations 3.7 and 3.8. Error bars represent standard deviations.

3.4.9 Effect of Calcium on Changes in Ground State and Transition State Binding Energies Between AdhD and β-AdhD

Steady state kinetic experiments with AdhD and β-AdhD revealed that the addition of the RTX domain significantly reduced the activity under all conditions. The apparent kinetic parameters obtained from the modified ordered bi-bi rate equation when the substrate is held constant (Equation 3.6) can be used to calculate the effect of the mutations and calcium on the thermodynamic binding energies of the enzyme/cofactor binary complex (ground state) and the enzyme/cofactor/substrate ternary complex (transition state) [90].

Since the activity of the β-AdhD enzyme was most affected with NAD^+ as a cofactor, the majority of the analysis was focused on these reactions. Additional dissociation constants for NAD^+ were determined at varying calcium concentrations (**Table 3.6** and **Figure 3.13**) for AdhD and β-AdhD. A sigmoidal relationship between calcium concentration and dissociation constants was observed for β-AdhD, but not AdhD (**Figure 3.5C** and **Figure 3.5D**). Fitting the NAD^+ dissociation constant data for β-AdhD as a function of calcium suggests a dissociation constant for calcium of 63±1 mM (**Figure 3.19**). This is larger than the K_d values for calcium that we have previously reported using circular dichroism [108], FRET using fluorescent proteins appended to the ends of the RTX domain [104], and by following the RTX folding using a quartz crystal microbalance (QCM) [105]. However, we have observed K_d values for calcium of this magnitude and even higher when the RTX domain repeats were rearranged into non-native orderings, likely leading to perturbations in the polarized folding mechanism of the β-roll domain [102]. Since AdhD is a very stable scaffold, perhaps the insertion of the domain into

Loop A of AdhD also adds steric hindrance to the folding of the RTX domain, resulting in an increase in the calcium needed to enable folding into the β-Roll structure.

These dissociation constants (as a function of calcium) were used to calculate changes in the ground-state binding energies between the proteins and cofactors at different calcium concentrations (Equation 3.7) [90].

$$\Delta\Delta G_b = -RT \ln[(K_d)_{wt}/(K_d)_{mut}] \tag{3.7}$$

The insertion of the RTX domain into AdhD resulted in almost no change in the ground state binding energy of NAD^+ and this continued up to 50 mM calcium. However, as more calcium was added to the system, surpassing the apparent K_d for calcium, the β-AdhD binary complex lost ground state binding energy as compared to the wild type protein (**Figure 3.5E**). This suggests a modulation of the cofactor binding pocket leading to the observed calcium-dependent loss of activity with NAD^+. Two-way ANOVA revealed the impact of the calcium concentration on the ground state binding energies was significant between the two proteins.

Using the apparent catalytic efficiencies ($k_{cat,app}/K_{A,app}$) for NAD^+ at varying calcium concentrations (**Figure 3.5A** and **Figure 3.5B**), the changes in the transition-state binding energies between the protein/cofactor/substrate complexes were determined using equation (3.8) [90].

$$\Delta\Delta G_b^{\neq} = RT \ln\left[\left(\frac{k_{cat}}{K_A}\right)_{wt} \Big/ \left(\frac{k_{cat}}{K_A}\right)_{mut}\right] \tag{3.8}$$

The addition of the RTX domain significantly reduced the transition state binding energy of the β-AdhD/NAD^+/2,3-butanediol ternary complex as compared to the wild type suggesting the addition

perturbs the ability of the enzyme to create this complex. However, this was not further affected by the addition of calcium (**Figure 3.5F**). Two-way ANOVA analysis determined that the effect of the mutation is significant, whereas the effect of the calcium concentration is insignificant.

These data suggest that the addition of the RTX sequence into AdhD perturbs the transition state with NAD^+ as a cofactor under all calcium conditions. As calcium is added above the K_d of the RTX domain for calcium, the binding of the calcium also impacts the ground state binding of the NAD^+ cofactor as well. The reason why this effect occurs with NAD^+ as a cofactor while far less of an impact with $NADP^+$ is observed is not clear. Crystal studies of the apo- and holo- forms of other members of the AKR superfamily suggest a rearrangement of these enzymes upon cofactor binding [14]. The catalytic tetrad residues are highly conserved in the AKR superfamily, including 2,5-DKGR [23]. In particular, regions of 2,5-DKGR near the catalytic tetrad lack electron density suggesting a poorly defined structure, which becomes well-defined upon the binding of cofactor. This suggests the binding of cofactor facilitates the organization of the active site [14]. On the other hand, the residues that comprise the cofactor-binding pocket undergo minimal changes upon cofactor binding, suggesting the enzyme is always ready to interact with the cofactor. This implies that the cofactor does not only undergo hydride ion transfer with the substrate, but is also responsible for the orientation of the residues in the catalytic tetrad and substrate-binding pocket [14]. Therefore, we can speculate that when $NADP^+$ is used as a cofactor, the active site organization is less affected by calcium as compared to when NAD^+ is used. This is consistent with the circular dichroism data where $NADP^+$ and calcium affected the β-AdhD secondary structure differently than NAD^+ alone (**Figure 3.3**), but structural studies of β-AdhD with cofactors and calcium would shed more light on these interactions.

Another interesting feature of AKR enzymes is the fact that many are NADP(H)-dependent and it has been shown that a canonical arginine residue (R276 in rat 3α- hydroxysteroid dehydrogenase) makes an ionic interaction with the phosphate group of NADP(H). This coincides with a conformational change where a salt bridge is able to form over the bound NADP(H) molecule, which is thought to enhance the kinetic mechanism [23]. We have previously studied these features in AdhD, which has a histidine (H255) at the position corresponding to R276 and the putative salt bridge is missing [17]. Despite these differences, pre-steady state kinetics showed a range of conformational dynamics in the wild type and an H255R mutant with both NAD(H) and NADP(H). Most interestingly, we observed a difference in the conformational dynamics between the cofactors, and this could also explain the asymmetry of the effect of calcium addition to the β-AdhD enzyme [17]. The two different cofactors require different protein conformational changes during cofactor binding, and the insertion and calcium-dependent folding of the β-roll may affect these dynamics differently.

3.4.10 Inhibition Analyses Suggest Calcium Acts as a Competitive Inhibitor in AdhD and a Mixed Inhibitor in β-AdhD

We combined all the steady state kinetic data collected to attempt to complete the full forward kinetic analysis of the impacts of calcium on AdhD and β-AdhD activity. Therefore, Lineweaver-Burk plots were used to qualitatively evaluate the calcium inhibition mechanisms using the data collected over the wide range of calcium concentrations. The inverse of specific activity as a function of inverse cofactor concentration depicts similar y-intercepts for AdhD at varying calcium concentrations with an increase in slope, suggesting calcium acts as a competitive inhibitor of AdhD (**Figure 3.6A**). To quantify the inhibition constant, the data were fit to the ordered bi-bi rate equation with competitive inhibition of cofactor (Equation 3.9) [111].

$$v = \frac{k_{cat}AB}{K_{ia}K_B + K_BA + AB + K_AB(1 + \frac{I}{K_I})} \quad (3.9)$$

Data with zero calcium (no inhibition) and varying cofactor and substrate were combined with data obtained with varying calcium and cofactor and 100 mM 2,3-butanediol and all of the data collected (254 reaction rates over a range of cofactor, substrate, and calcium concentrations, **Table 3.15**) were fit by Equation 7 using least square regression to determine the kinetic constants (**Table 3.5, Figure 3.6B**). The measured values of the dissociation constants at each calcium concentration were input as constants. The calcium inhibition constant, K_I, was found to be 7.6 ± 7.4 mM (**Table 3.5, Figure 3.6B**). The remainder of the parameters provided a good fit to the data, and the k_{cat}, K_A, and K_B values from the global fit (**Table 3.5**) were not statistically significantly different from the same values obtained with zero calcium (**Table 3.2**). However, it was clear by observing the fits of the data at different calcium and substrate conditions that this equation did not fully capture all the features in the data (**Figure 3.6C**). This suggests that the interactions of AdhD with calcium may be more complex than just competitive inhibition in the active site. This is not surprising given the fact that calcium seemed to accelerate AdhD activity with $NADP^+$ as a cofactor and thus, it is unlikely that calcium just acts as a classic competitive inhibitor. Lineweaver-Burk plots were created for $NADP^+$, but no obvious qualitative trend was observed (**Figure 3.14**).

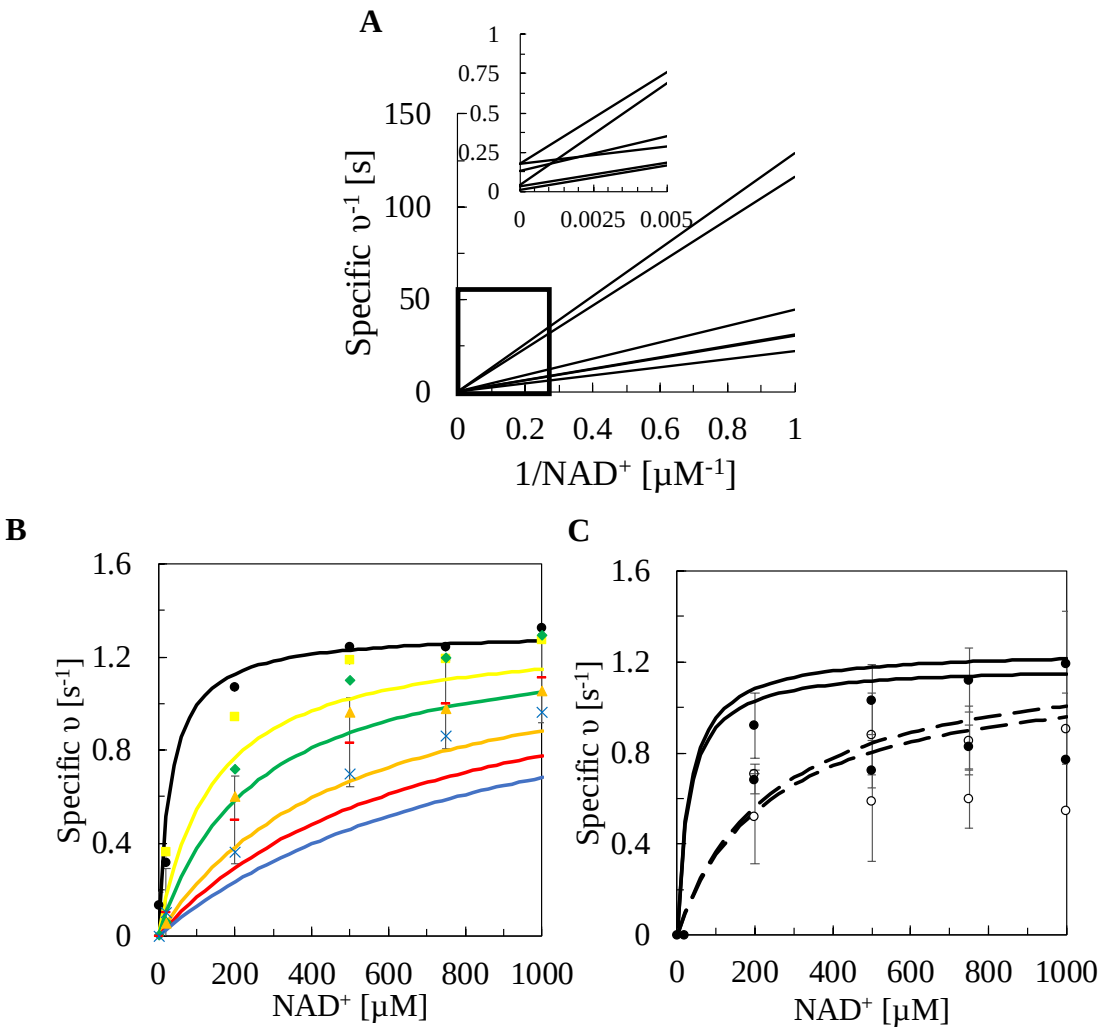

Figure 3.6 AdhD calcium inhibition study. (A) Double reciprocal plot showing inverse AdhD specific activity vs inverse NAD^+ with 100 mM 2,3-butanediol with increasing calcium concentrations as slope increases with inset of higher NAD^+ concentrations depicted on top-left. This shows qualitatively that calcium acts as a competitive inhibitor with AdhD. (B) The same experimental rate data from panel (A) for AdhD with constant 100 mM 2,3-butanediol and varying NAD^+ with 0 (•), 25 (■), 50 (♦), 100 (▲), 150 (—), and 200 (x) mM calcium depicted as data points. The least squares fitted rate equation at these concentrations using equation 3.9 and the parameters from **Table 3.5** are depicted as solid lines. (C) AdhD with 40 and 60 mM 2,3-butanediol and varying NAD^+ with 0 (•) and 50 (°) mM calcium. The least squares fitted rate equation at these concentrations using equation 3.9 and the parameters from **Table 3.5** are depicted as solid lines for 0 mM calcium and dashed lines for 50 mM calcium.

We assumed that the addition of the RTX domain into AdhD would add an orthogonal inhibition site, and since this was located away from the cofactor binding pocket, this could introduce a different inhibition mechanism. The Lineweaver-Burk plot for β-AdhD over a range of calcium concentrations shows an increasing slope at increasing calcium concentrations qualitatively suggesting competitive inhibition. However, a large change in the y-intercept is also observed suggesting non-competitive inhibition (**Figure 3.7A**). Calcium binding to the active site of AdhD is most likely contributing to competitive inhibition, while calcium binding to the β-roll and decreasing the affinity of the substrate to β-AdhD leads to an orthogonal non-competitive inhibition effect. Calcium inhibition of β-AdhD in the presence of $NADP^+$ was also explored using Lineweaver Burke plots, but like AdhD, no clear qualitative trend was observed (**Figure 3.15**).

A mixed inhibition equation was derived (Supporting Information) for the ordered bi-bi mechanism (Equation 3.10). Although only one inhibitor is present (calcium), it acts in two different locations in the protein and thus, the rate equation was derived to accommodate competitive inhibition by calcium (I) in the active site of β-AdhD and non-competitive inhibition in the RTX site by calcium (J), so that two different inhibition constants could be determined.

$$v = \frac{E_t\begin{pmatrix} k_{cat}K_{iaJ}K_{BJ}K_I K_J K_{JI}[A][B] + k_{cat}K_{AJ}K_I K_J K_{JI}[A][B]^2 + \\ k_{catJ}K_{ia}K_B K_I K_{JI}[A][B][J] + k_{catJ}K_A K_I K_{JI}[A][B]^2[J] \end{pmatrix}}{\left[\begin{array}{c} K_{ia}K_{iaJ}K_B K_{BJ}K_J K_I K_{JI} + K_{iaJ}K_B K_{BJ}K_J K_I K_{JI}[A] + \\ (K_{ia}K_{AJ}K_B + K_{iaJ}K_A K_{BJ})K_J K_I K_{JI}[B] + K_A K_{AJ}K_I K_J K_{JI}[B]^2 + \\ K_J K_I K_{JI}(K_B K_{AJ} + K_{iaJ}K_{BJ})[A][B] + (K_{AJ}K_J K_I K_{JI})[A][B]^2 + \\ K_{ia}K_B K_{BJ}K_I K_{JI}[A][J] + (K_{ia}K_{AJ}K_B + K_{iaJ}K_A K_{BJ})K_I K_{JI}[B][J] + \\ (K_{ia}K_{AJ}K_B + K_{iaJ}K_A K_{BJ})K_J K_{JI}[B][I] + \\ (K_{ia}K_{AJ}K_B K_I + K_{iaJ}K_A K_{BJ}K_I)[B][I][J] + (K_A K_{AJ}K_J K_{JI})[B]^2[I] + \\ K_A K_{AJ}K_I K_{JI}[B]^2[J] + K_I K_A K_{AJ}[B]^2[I][J] + K_I K_{JI}K_A K_{BJ}[A][B][J] + \\ K_I K_{JI}K_{ia}K_B[A][B][J] + K_I K_{JI}K_A[A][B]^2[J] + \\ K_{ia}K_{iaJ}K_B K_{BJ}K_J K_{JI}[I] + K_{ia}K_{iaJ}K_B K_{BJ}K_I K_{JI}[J] + K_{ia}K_{iaJ}K_B K_{BJ}K_I[I][J] \end{array}\right]} \tag{3.10}$$

Using a global least squares fit, all kinetic parameters were determined, with the exception of K_{ia}, which was set to the K_d values from fluorescence titrations (**Figure 3.13**). Despite fitting 331 reaction rates (**Table 3.16**) at varying cofactor, substrate, and calcium concentrations, the error bars for several of the parameters were orders of magnitude larger than the values. This suggests that despite the large data set used, additional data would be necessary to fully determine the remaining kinetic parameters. Pre-steady state or other methods may be necessary to determine these parameters with acceptable precision. In addition, it is also likely that calcium has other effects or interactions with the enzyme that may not be captured by just competitive and non-competitive inhibition. However, the values provide a reasonable fit to the experimental data (**Figure 3.7B**).

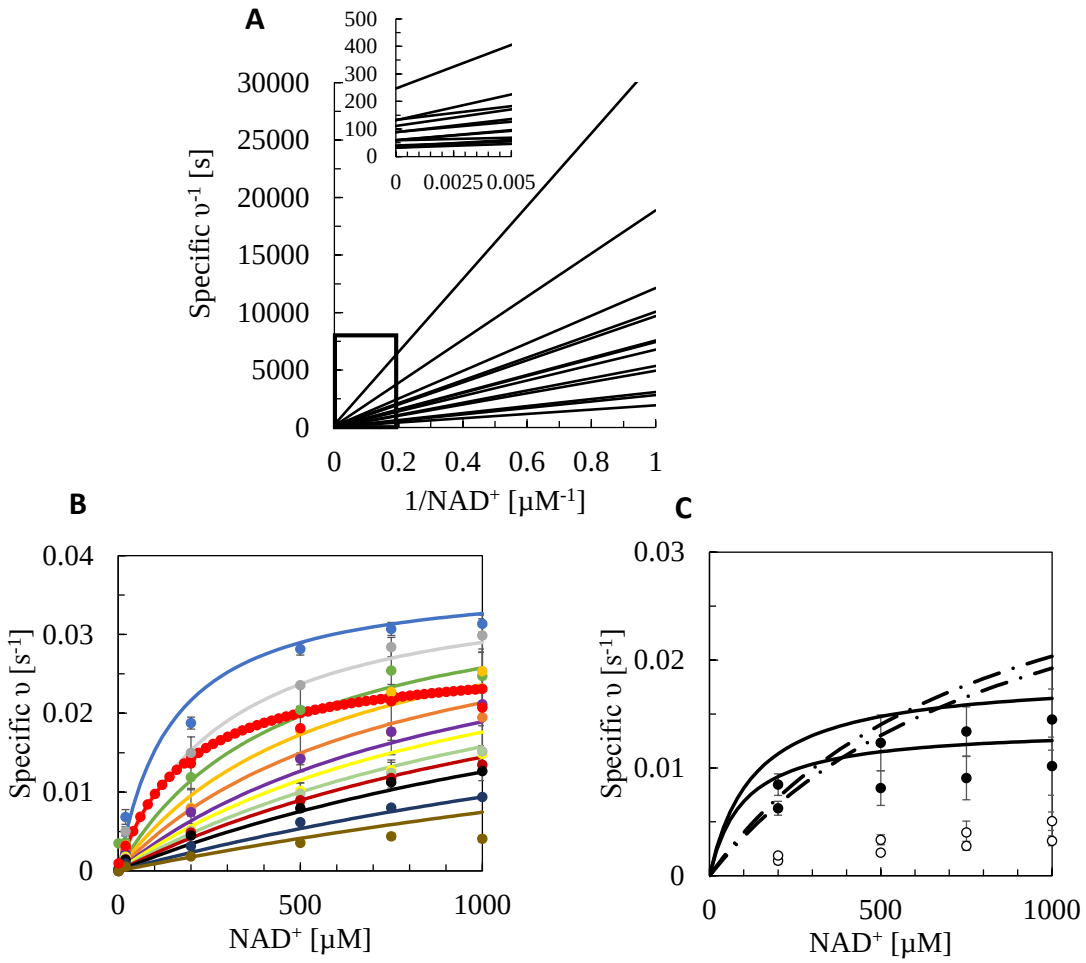

Figure 3.7 β-AdhD calcium inhibition study. (A) Double reciprocal plot showing inverse β-AdhD specific activity vs inverse NAD^+ with 100 mM 2,3-butanediol with increasing calcium concentrations as slope increases with inset of higher NAD^+ concentrations depicted on top-left. This shows qualitatively that calcium acts as a mixed inhibitor with β-AdhD. (B) The same experimental rate data from panel (A) for β-AdhD with constant 100 mM 2,3-butanediol and varying NAD^+ with experimental rates depicted as data points. The least squares fitted rate equation at these concentrations using equation 3.10 and the parameters from **Table 3.5** are depicted as solid lines. (C) β-AdhD with 40 and 60 mM 2,3-butanediol and varying NAD^+ with 0 (•) and 50 (°) mM calcium. The least squares fitted rate equation at these concentrations using equation 3.10 and the parameters from **Table 3.5** are depicted as solid lines for 0 mM calcium and dashed lines for 50 mM calcium.

The k_{cat}/K_B value from the global fit (**Table 3.5**) was found to be similar to the same parameters from the modified rate equation fit to the data in the absence of calcium (**Table 3.3**). And a comparison of the fitted parameters (**Table 3.5**) suggests the concentration of calcium required to

inhibit the system non-competitively is much less than the calcium required to inhibit AdhD competitively.

Table 3.5 Calcium inhibition constants for AdhD and β-AdhD. Competitive inhibition constants (Equation 3.9) for AdhD and mixed inhibition constants (Equation 3.10) for β-AdhD with 100 mM 2,3–butanediol, 1 to 1000 μM NAD^+ and 0 to 200 mM calcium[a].

	k_{cat} (s^{-1})	K_A (μM)	K_B (mM)	K_I (mM)
AdhD	1.4 ± 0.2	34 ± 34	7.7 ± 4.7	7.6 ± 7.4
β-AdhD	0.18 ± 0.21	1100 ± 1500	610 ± 830	0.38[b]

	k_{catJ} (s^{-1})	K_{AJ} (μM)	K_{BJ} (mM)	K_J (μM)	K_{JI} (μM)
AdhD	N/A	N/A	N/A	N/A	N/A
β-AdhD	0.038[b]	1.1[b]	1.1[b]	85[b]	86[b]

[a]All data was collected in at least triplicate. Error bars represent 95% confidence intervals.

[b]Confidence intervals are at least 3 orders of magnitude larger than values and thus are omitted for clarity.

There are several figures of merit that could be used to compare the different enzymes at different calcium concentrations. The modified rate equation where the substrate concentration is low (Equation 3.5) provides a good fit to the data at 0 and 50 mM calcium, and this equation can be used to calculate an apparent k_{cat}/K_M for the two enzymes (**Figure 3.8**). The wild type protein is affected by calcium such that its activity with NAD^+ is reduced but its activity with $NADP^+$ is increased. The cofactor selectivity is broadened, but the preference for NAD^+ remains. The addition of the RTX domain to create β-AdhD results in much different behavior. In the absence

of calcium, the β-AdhD enzyme has a strong preference for NAD^+ over $NADP^+$. However, as calcium is increased, the $NADP^+$-dependent activity is enhanced, while the NAD^+-dependent activity is dramatically inhibited. Thus, the addition of the RTX domain introduces calcium-dependent control over the cofactor selectivity of AdhD.

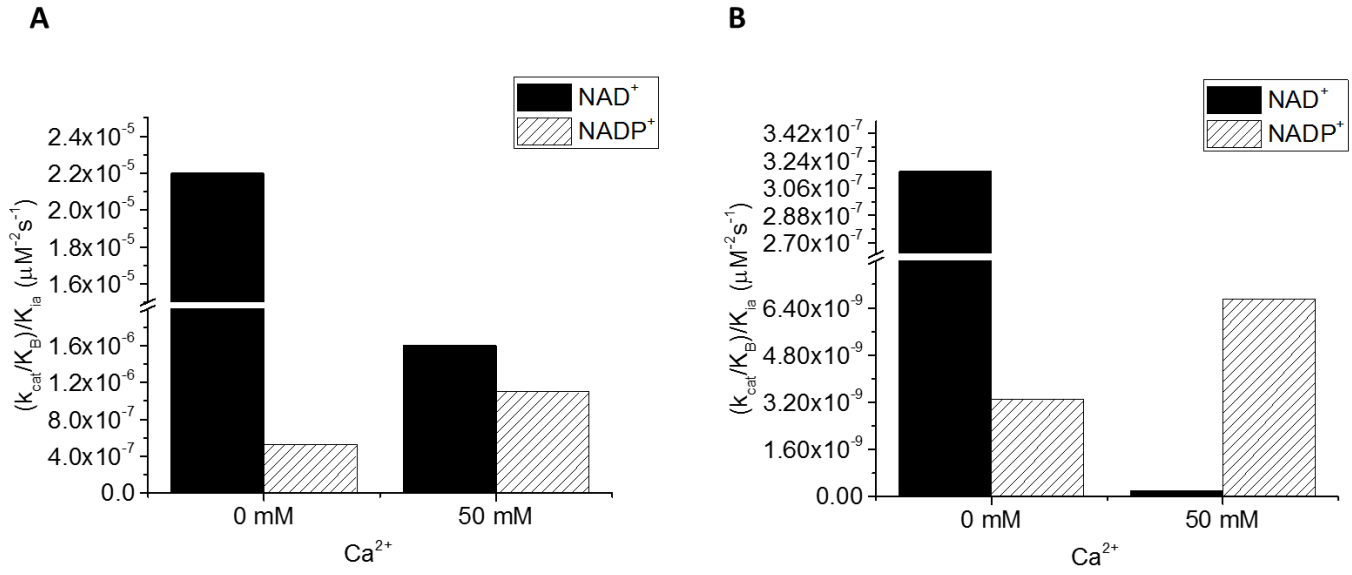

Figure 3.8 Apparent catalytic efficiency of (A) AdhD and (B) β-AdhD with NAD^+ and $NADP^+$ at 0 and 50 mM calcium. Cofactor specificity of β-AdhD reverses upon the addition of calcium. The catalytic efficiency of β-AdhD in the absence of calcium is greater with NAD^+, while in the presence of 50 mM Ca^{2+}, activity is greater with $NADP^+$.

This new IDP/enzyme chimera, whose activity and relative cofactor selectivity can be controlled externally through the addition or removal of calcium, is reminiscent of a protein switch. In these systems, protein structures change in response to input signals (ligands, pH, etc.) leading to outputs such as altered ligand affinities or enzymatic activities [112-114]. Examples of protein switches include a barnase/ubiquitin system and a maltose binding protein/beta-lactamase system where catalytic activity is modulated by maltose [113, 115-119]. These switches can be used in applications including biosensors, therapeutic agents, and smart biomaterials.

3.5 Conclusion

In conclusion, the insertion of a conformationally dynamic IDP domain into a loop near the active site of an enzyme, β-AdhD, resulted in a novel thermostable chimera. The RTX domain introduces a new non-competitive calcium-binding inhibition site that preferentially impacts NAD^+-dependent activity. Thus, in the new protein, calcium functions as a novel "rheostat"-like switching mechanism, where cofactor selectivity can be tuned with calcium. This approach should be modular and could be used to introduce calcium-dependent modulation of activity in any other member of the AKR superfamily, which are ubiquitous and are known to participate in many physiological roles [120]. The use of IDP domains to dynamically modify enzymatic activity, especially cofactor selectivity, is an important new approach in biocatalyst development.

3.6 Supporting Information

AdhD and β-AdhD amino acid sequences

AdhD

```
MGDYKDDDDK AKRVNAFNDL KRIGDDKVTA IGMGTWGIGG RETPDYSRDK ESIEAIRYGL        60
ELGMNLIDTA EFYGAGHAEE IVGEAIKEFE REDIFIVSKV WPTHFGYEEA KKAARASAKR       120
LGTYIDLYLL HWPVDDFKKI EETLHALEDL VDEGVIRYIG VSNFNLELLQ RSQEVMRKYE       180
IVANQVKYSV KDRWPETTGL LDYMKREGIA LMAYTPLEKG TLARNECLAK IGEKYGKTAA       240
QVALNYLIWE ENVVAIPKAS NKEHLKENFG AMGWRLSEED REMARRCVED PNSSSVD          297
```

β-AdhD

```
MGDYKDDDDK AKRVNAFNDL KRIGDDKVTA IGMGTWGIGG RETPDYSRDK ESIEAIRYGL        60
ELGMNLIDTA EFYGAGHAEE IVGEAIKEFE REDIFIVSKV WPTHFGYEEA KKAARASAKR       120
LGTYIDLYLL HWPGGSARDD VLIGDAGANV LNGLAGNDVL SGGAGDDVLL GDEGSDLLSG       180
DAGNDDLFGG QGDDTYLFGV GYGHDTIYES GGGHDTIRFD DFKKIEETLH ALEDLVDEGV       240
IRYIGVSNFN LELLQRSQEV MRKYEIVANQ VKYSVKDRWP ETTGLLDYMK REGIALMAYT       300
PLEKGTLARN ECLAKIGEKY GKTAAQVALN YLIWEENVVA IPKASNKEHL KENFGAMGWR       360
LSEEDREMAR RCVEDPNSSS VD                                                382
```

AdhD and β-AdhD DNA sequences

AdhD

```
ATGGGGGACT ACAAAGACGA TGACGACAAG GCAAAACGCG TGAATGCATT TAACGACCTG        60
AAACGTATTG GTGATGACAA AGTAACCGCT ATCGGCATGG GTACTTGGGG CATCGGTGGT       120
CGTGAAACCC CGGATTACAG CCGCGACAAA GAGTCCATCG AGGCGATCCG TTATGGCCTG       180
GAGCTGGGTA TGAACCTGAT TGACACGGCG GAGTTTTATG GTGCCGGCCA CGCTGAAGAG       240
ATTGTCGGTG AAGCCATCAA AGAGTTCGAA CGCGAGGACA TCTTCATTGT TTCGAAGGTC       300
TGGCCGACCC ACTTTGGTTA TGAAGAGGCG AAGAAAGCTG CACGCGCCAG CGCGAAGCGT       360
CTGGGCACCT ACATTGATCT GTACCTGTTG CATTGGCCGG TCGACGACTT TAAAAAGATT       420
GAAGAAACCC TGCACGCACT CGAGGATTTG GTGGATGAGG GTGTCATTCG CTACATCGGC       480
GTTTCCAATT TCAATCTGGA GTTGCTGCAA CGTAGCCAGG AAGTGATGCG TAAGTACGAG       540
ATCGTGGCGA ACCAGGTCAA ATACAGCGTG AAGGACCGTT GGCCAGAAAC GACCGGCCTG       600
CTGGACTATA TGAAACGTGA GGGTATCGCG CTGATGGCCT ATACGCCTCT AGAAAAAGGT       660
ACCCTGGCGC GTAACGAGTG CCTGGCAAAG ATCGGTGAGA AGTACGGTAA GACGGCGGCA       720
CAAGTTGCCC TGAATTACCT GATTTGGGAA GAGAATGTTG TGGCGATTCC GAAGGCGAGC       780
AACAAAGAGC ATCTGAAAGA GAACTTCGGC GCGATGGGCT GGCGCCTGAG CGAAGAAGAT       840
CGTGAGATGG CGCGCCGGTG TGTTGAGGAT CCGAATTCGA GCTCCGTGGA C                 891
```

β-AdhD

```
ATGGGGGACT ACAAAGACGA TGACGACAAG GCAAAACGCG TGAATGCATT TAACGACCTG        60
AAACGTATTG GTGATGACAA AGTAACCGCT ATCGGCATGG GTACTTGGGG CATCGGTGGT       120
CGTGAAACCC CGGATTACAG CCGCGACAAA GAGTCCATCG AGGCGATCCG TTATGGCCTG       180
GAGCTGGGTA TGAACCTGAT TGACACGGCG GAGTTTTATG GTGCCGGCCA CGCTGAAGAG       240
ATTGTCGGTG AAGCCATCAA AGAGTTCGAA CGCGAGGACA TCTTCATTGT TTCGAAGGTC       300
TGGCCGACCC ACTTTGGTTA TGAAGAGGCG AAGAAAGCTG CACGCGCCAG CGCGAAGCGT       360
CTGGGCACCT ACATTGATCT GTACCTGTTG CATTGGCCGG GGGGCAGCGC GCGTGATGAC       420
GTGCTGATCG GCGACGCAGG CGCCAACGTC CTCAATGGCC TGGCGGGCAA CGACGTGCTG       480
TCCGGCGGCG CTGGCGACGA TGTGCTGCTG GGCGACGAGG GCTCGGACCT GCTCAGCGGC       540
```

```
GATGCGGGCA ACGACGATCT GTTCGGCGGG CAGGGCGATG ATACTTATCT GTTCGGGGTC       600
GGGTACGGGC ACGACACGAT CTACGAATCG GGCGGCGGCC ATGACACCAT CCGCTTCGAC       660
GACTTTAAAA AGATTGAAGA AACCCTGCAC GCACTCGAGG ATTTGGTGGA TGAGGGTGTC       720
ATTCGCTACA TCGGCGTTTC CAATTTCAAT CTGGAGTTGC TGCAACGTAG CCAGGAAGTG       780
ATGCGTAAGT ACGAGATCGT GGCGAACCAG GTCAAATACA GCGTGAAGGA CCGTTGGCCA       840
GAAACGACCG GCCTGCTGGA CTATATGAAA CGTGAGGGTA TCGCGCTGAT GGCCTATACG       900
CCTCTAGAAA AAGGTACCCT GGCGCGTAAC GAGTGCCTGG CAAAGATCGG TGAGAAGTAC       960
GGTAAGACGG CGGCACAAGT TGCCCTGAAT TACCTGATTT GGGAAGAGAA TGTTGTGGCG      1020
ATTCCGAAGG CGAGCAACAA AGAGCATCTG AAAGAGAACT TCGGCGCGAT GGGCTGGCGC      1080
CTGAGCGAAG AAGATCGTGA GATGGCGCGC CGGTGTGTTG AGGATCCGAA TTCGAGCTCC      1140
GTGGAC                                                                 1146
```

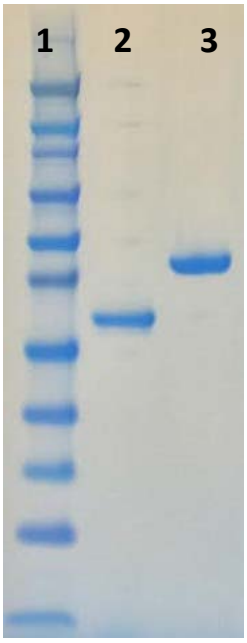

Figure 3.9 SDS-PAGE of AdhD and β-AdhD after gel filtration. Lane 1: molecular weight marker, lane 2: AdhD, lane 3: β-AdhD. Samples were lysed by heating for 1 h at 80°C prior to purification. A distinct band at approximately 34 kDa for AdhD and 42 kDa for β-AdhD is observed, consistent with the theoretical molecular masses.

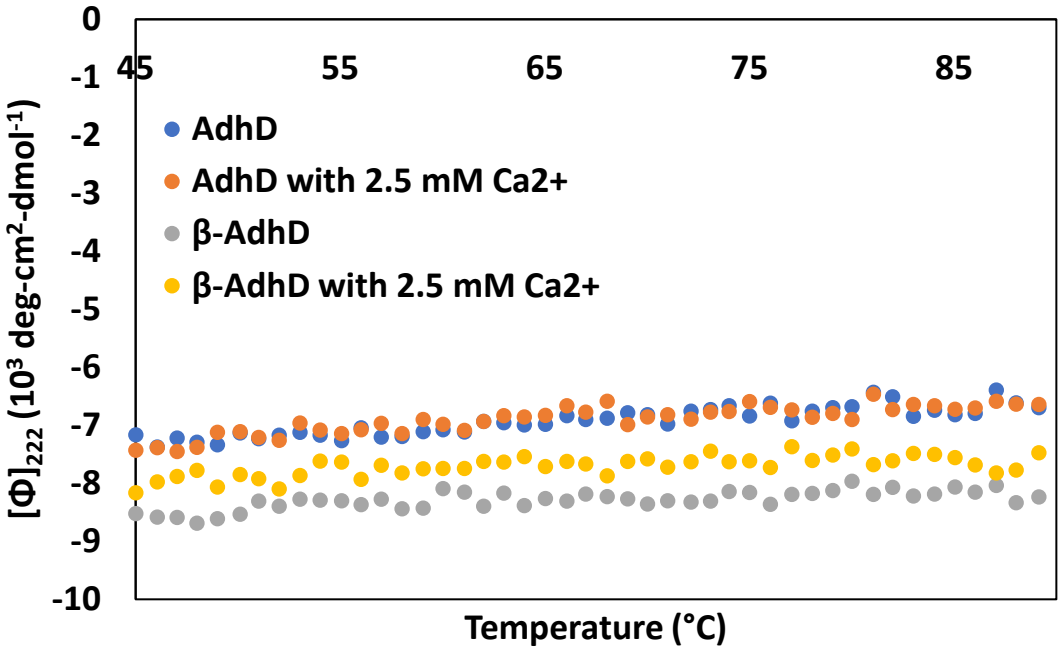

Figure 3.10 Thermal denaturation curves for AdhD and β-AdhD. Studies were done in the absence and presence of calcium as measured by the circular dichroic absorbance at 222 nm as temperature was varied from 25 to 90 °C. 1.25 µM samples were prepared in water and runs were performed in at least duplicate.

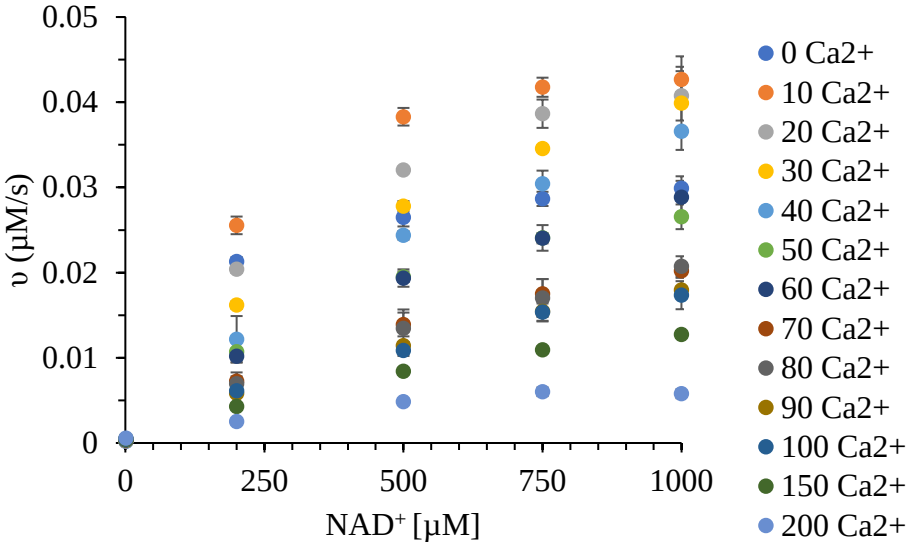

Figure 3.11 Rate versus NAD^+ at varying calcium concentrations for β-AdhD. Data were collected in at least triplicate.

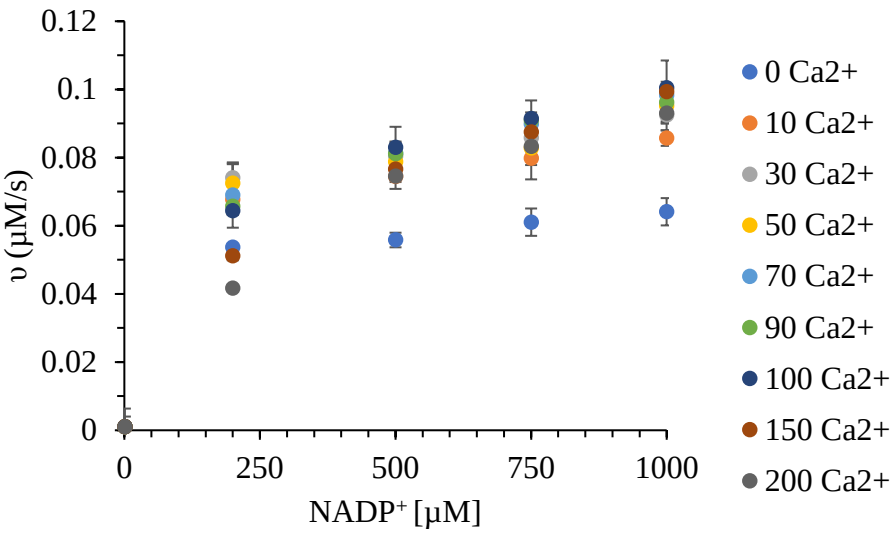

Figure 3.12 Rate versus $NADP^+$ at varying calcium concentrations for β-AdhD. Data were collected in at least triplicate.

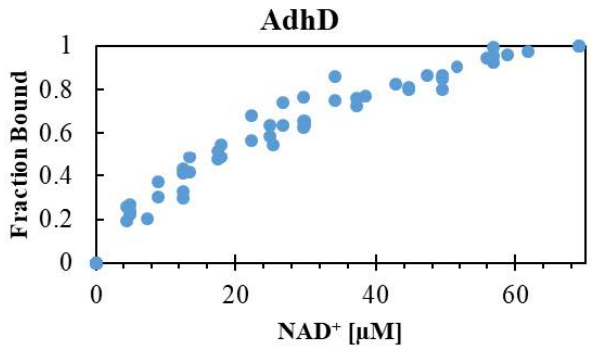
AdhD
Fraction Bound
NAD+ [µM]

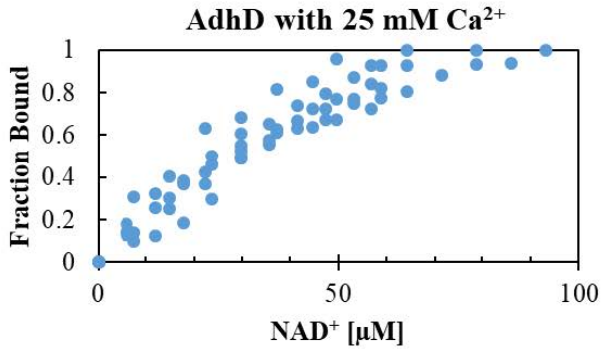
AdhD with 25 mM Ca2+
Fraction Bound
NAD+ [µM]

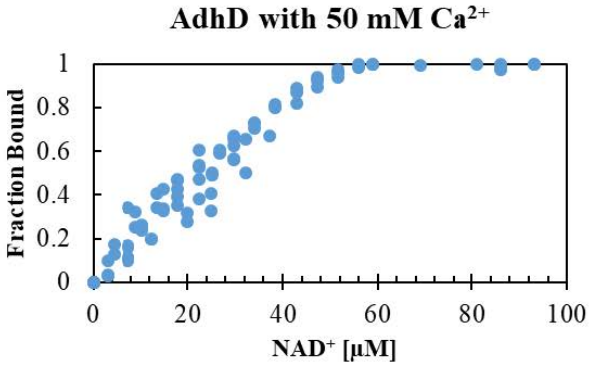
AdhD with 50 mM Ca2+
Fraction Bound
NAD+ [µM]

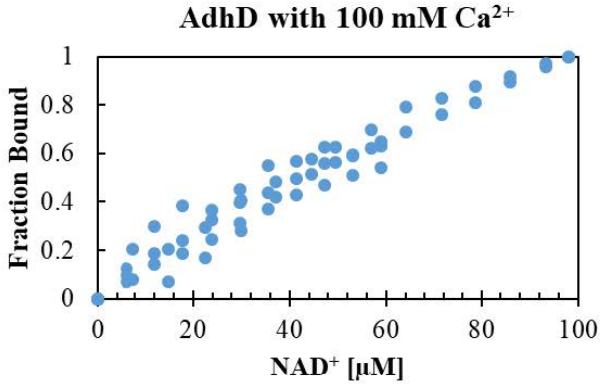
AdhD with 100 mM Ca2+
Fraction Bound
NAD+ [µM]

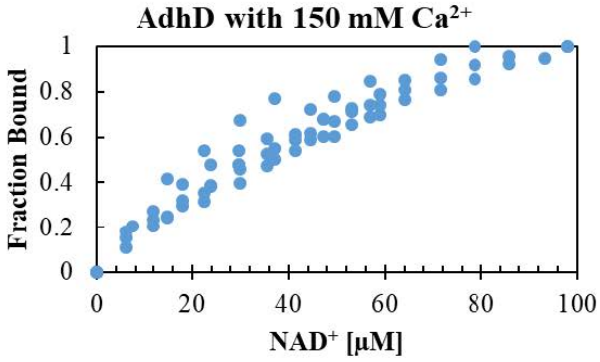
AdhD with 150 mM Ca2+
Fraction Bound
NAD+ [µM]

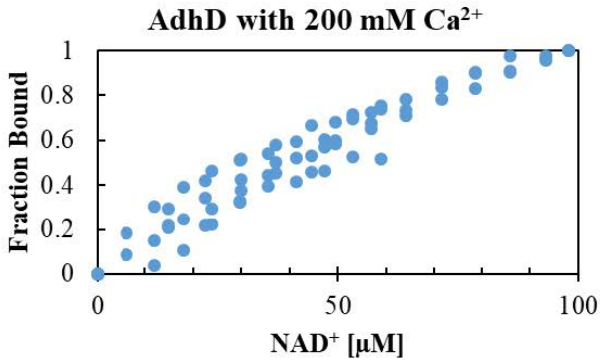
AdhD with 200 mM Ca2+
Fraction Bound
NAD+ [µM]

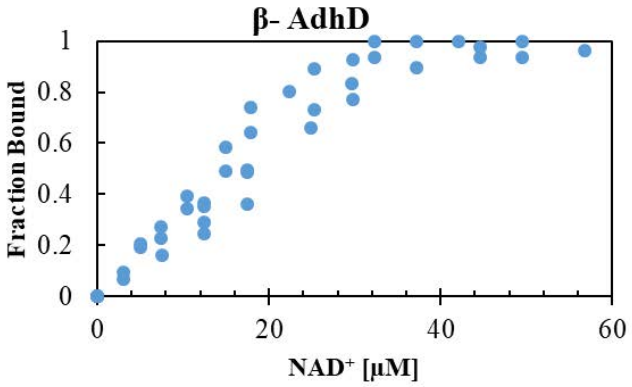
β- AdhD
Fraction Bound
NAD+ [µM]

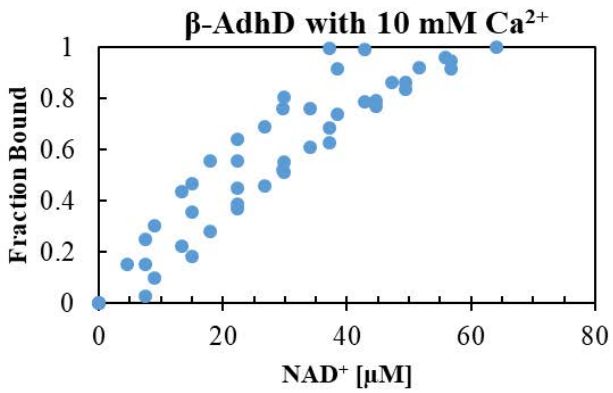
β-AdhD with 10 mM Ca2+
Fraction Bound
NAD+ [µM]

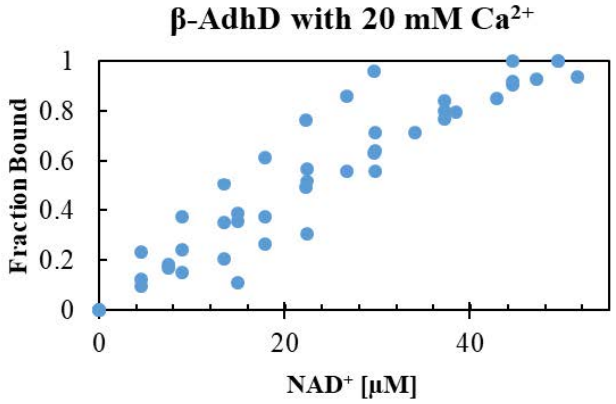
β-AdhD with 20 mM Ca2+
Fraction Bound
NAD+ [µM]

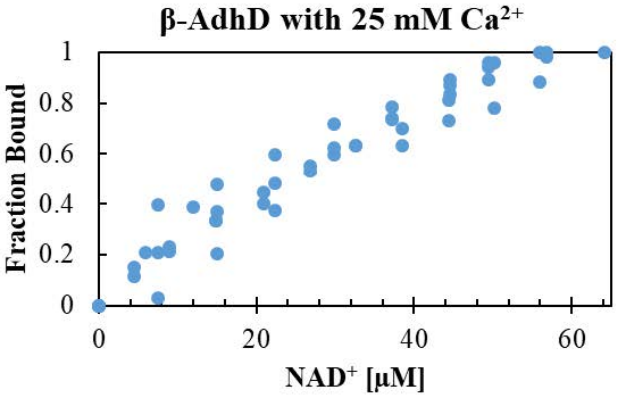
β-AdhD with 25 mM Ca2+
Fraction Bound
NAD+ [µM]

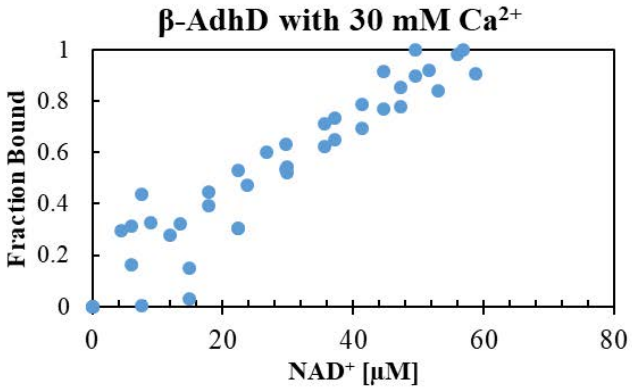
β-AdhD with 30 mM Ca2+
Fraction Bound
NAD+ [µM]

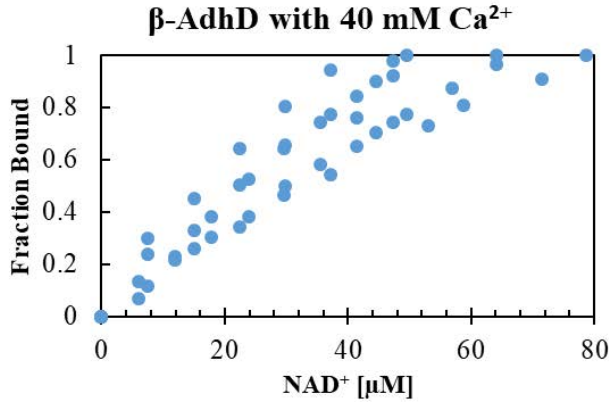
β-AdhD with 40 mM Ca2+
Fraction Bound
NAD+ [µM]

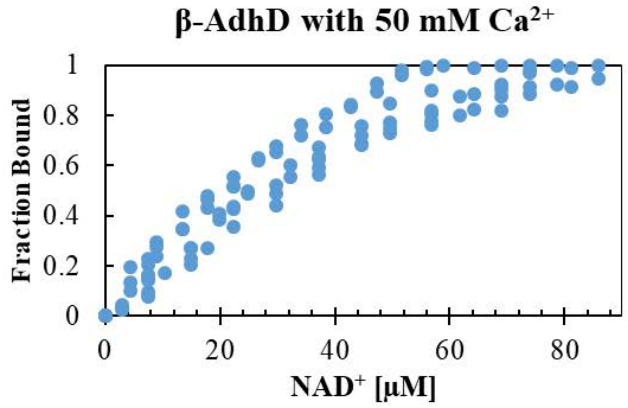
β-AdhD with 50 mM Ca2+
Fraction Bound
NAD+ [µM]
0
0.2
0.4
0.6
0.8
1
0
20
40
60
80

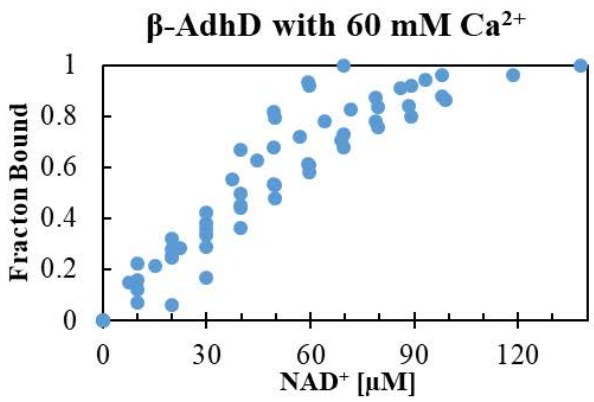
β-AdhD with 60 mM Ca2+
Fracton Bound
NAD+ [µM]
0
0.2
0.4
0.6
0.8
1
0
30
60
90
120

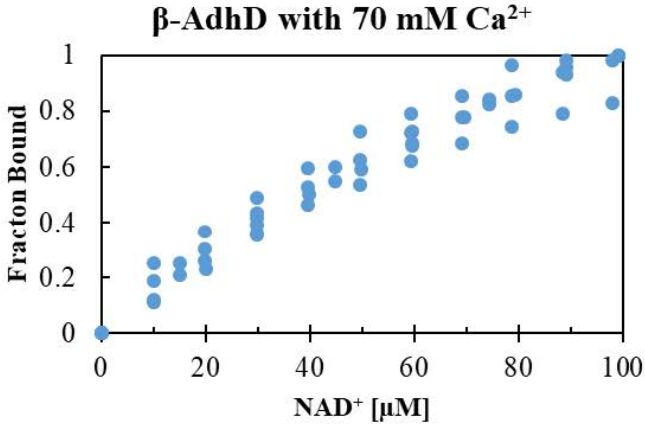
β-AdhD with 70 mM Ca2+
Fracton Bound
NAD+ [µM]
0
0.2
0.4
0.6
0.8
1
0
20
40
60
80
100

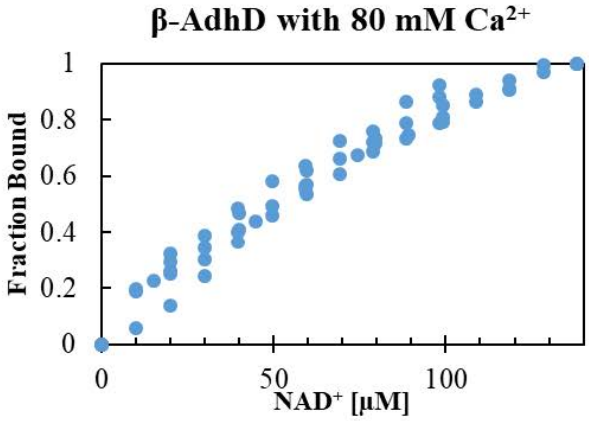
β-AdhD with 80 mM Ca2+
Fraction Bound
NAD+ [µM]
0
0.2
0.4
0.6
0.8
1
0
50
100

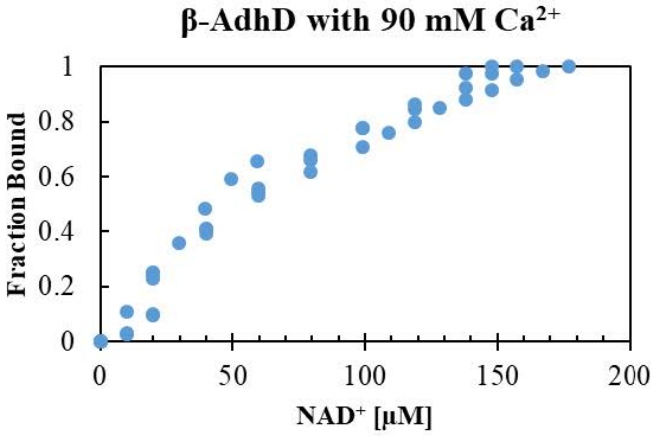
β-AdhD with 90 mM Ca2+
Fraction Bound
NAD+ [µM]
0
0.2
0.4
0.6
0.8
1
0
50
100
150
200

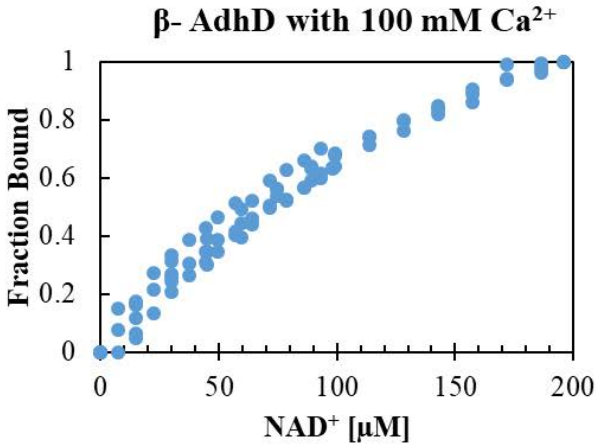
β- AdhD with 100 mM Ca2+
Fraction Bound
NAD+ [µM]
0
0.2
0.4
0.6
0.8
1
0
50
100
150
200

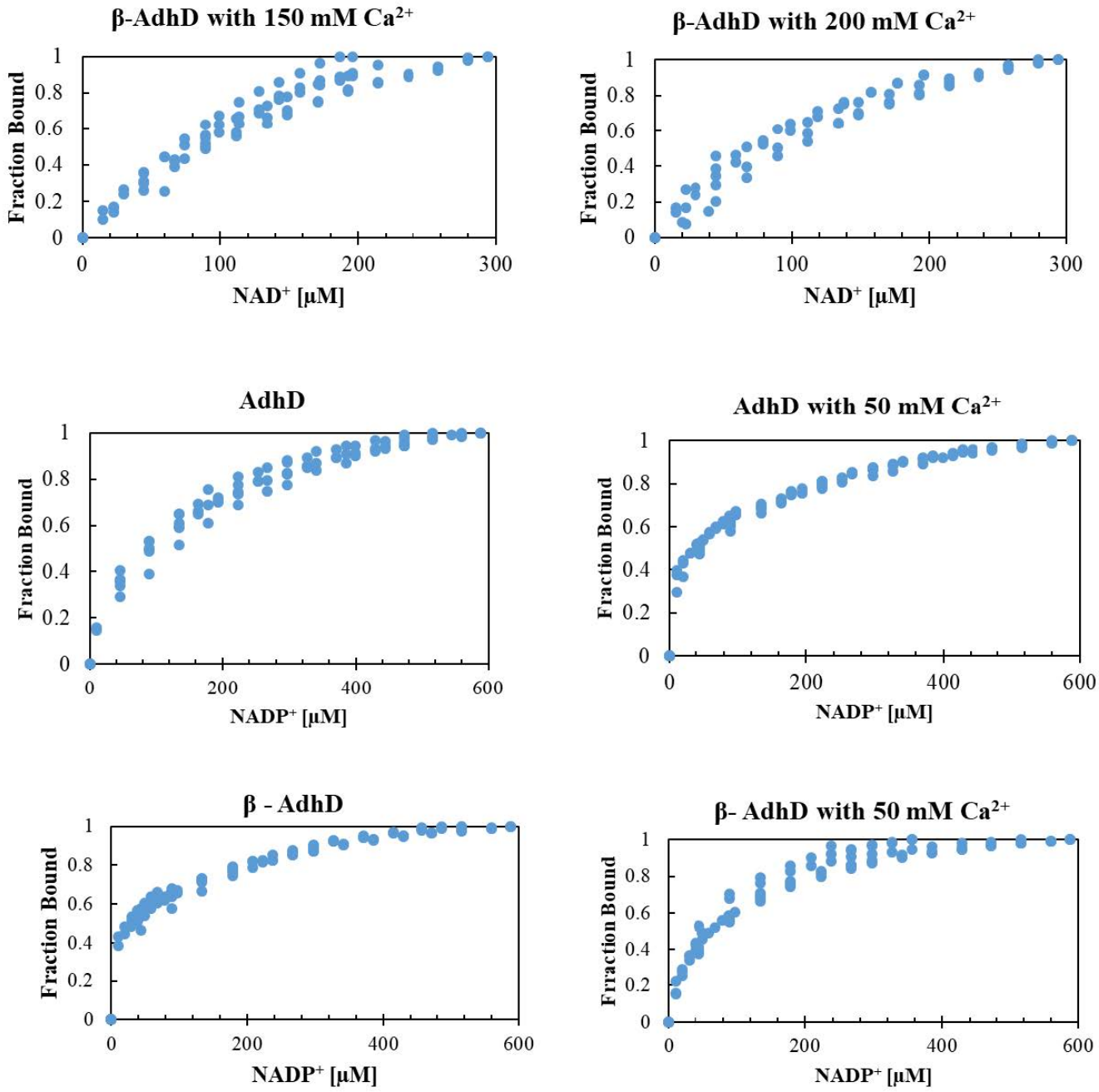

Figure 3.13 Fluorescence titrations for AdhD and β-AdhD. From 0 to 200 mM calcium with NAD^+ and at zero and 50 mM calcium with $NADP^+$. Data were collected in at least triplicate.

Table 3.6 Dissociation constants for cofactor (NAD^+) for AdhD and β-AdhD at various calcium concentrations.

Ca^{2+} (mM)	AdhD K_d, NAD^+ (μM)	β-AdhD K_d, NAD^+ (μM)
0	12 ± 2	12 ± 3
10		14 ± 4
20		14 ± 4
25	21 ± 3	17 ± 3
30		19 ± 5
40		15 ± 4
50	18 ± 3	19 ± 2
60		29 ± 6
70		27 ± 4
80		36 ± 5
90		40 ± 7
100	36 ± 5	57 ± 6
150	24 ± 3	58 ± 7
200	31 ± 4	60 ± 8

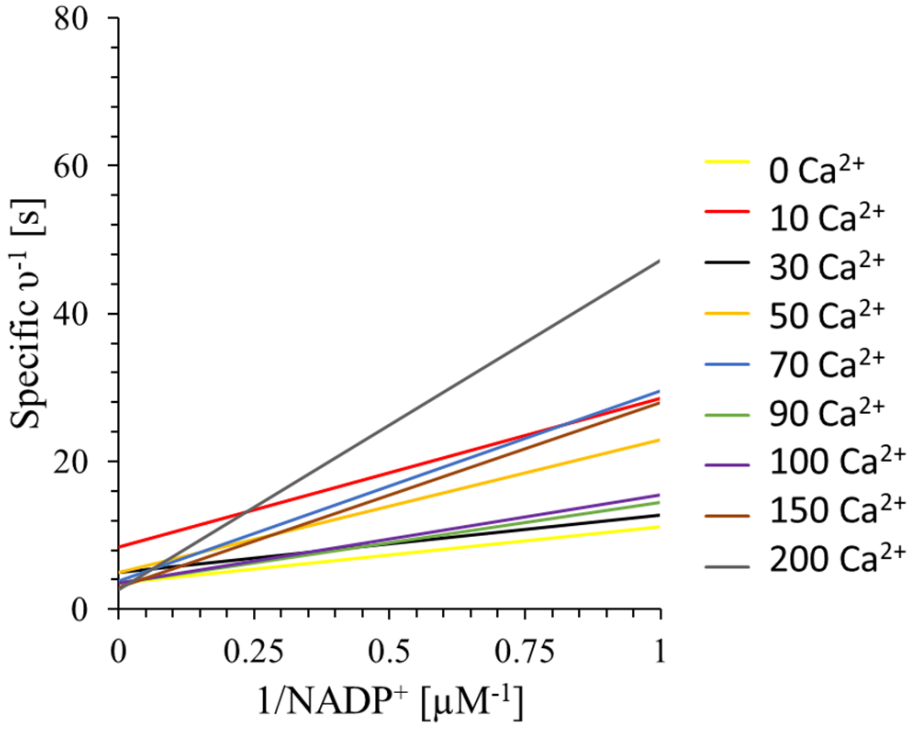

Figure 3.14 Double reciprocal plot of inverse specific activity for AdhD vs inverse $NADP^+$. Reactions run with 100 mM 2,3-butanediol with increasing calcium concentrations. There is no clear tend as a function of increasing calcium concentration, indicating a mixed inhibition.

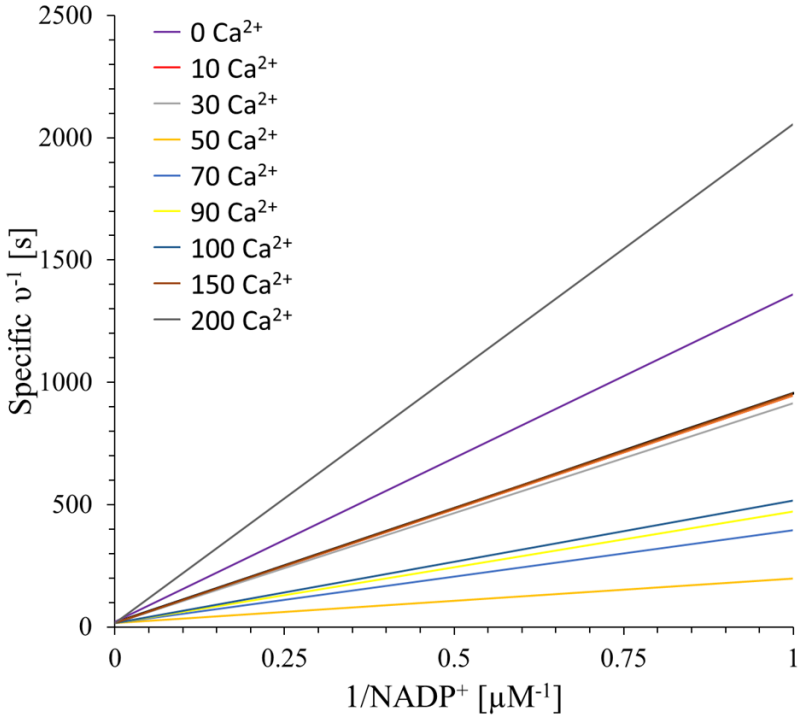

Figure 3.15 Double reciprocal plot of inverse specific activity for β-AdhD vs $NADP^+$. Reactions run with 100 mM 2,3-butanediol with increasing calcium concentrations. There is no clear trend as a function of increasing calcium concentration, indicating a mixed inhibition.

β-AdhD, 0 Ca^{2+}, NAD^{+}

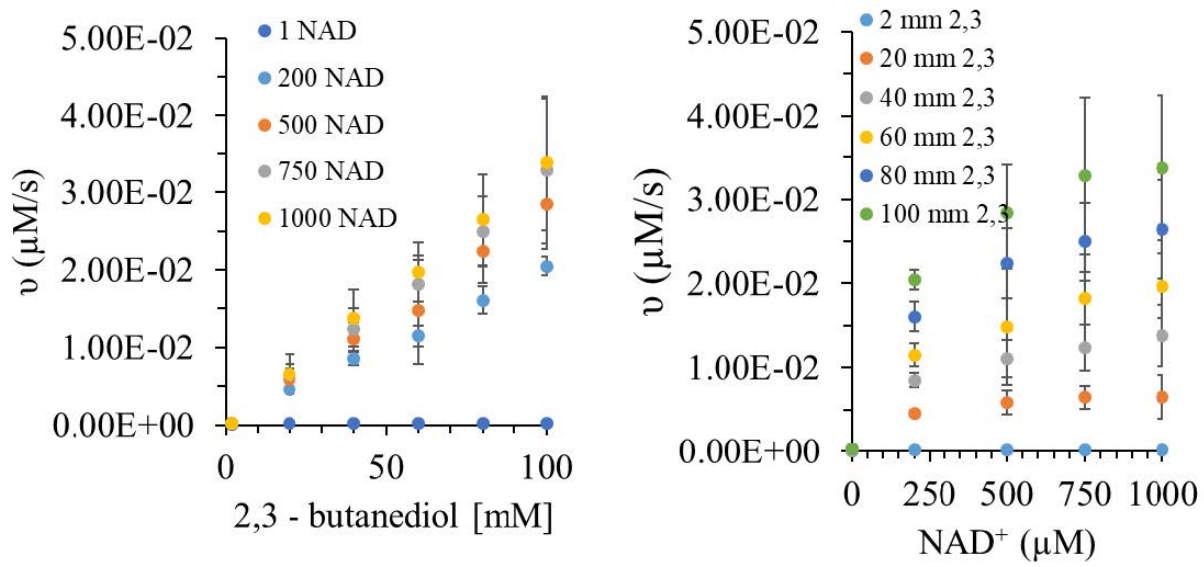

β-AdhD, 50 Ca^{2+}, NAD^{+}

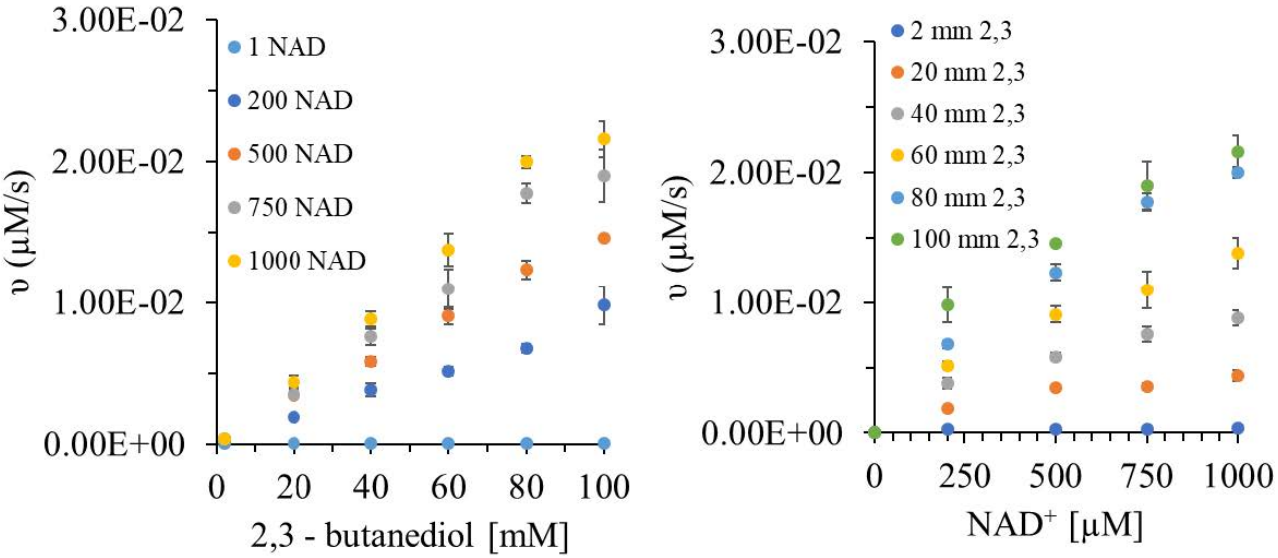

Figure 3.16 Steady state kinetic rate data for β-AdhD at 0 and 50 mM calcium with NAD^{+}. Data were collected in at least triplicate.

β-AdhD, 0 Ca^{2+}, $NADP^{+}$

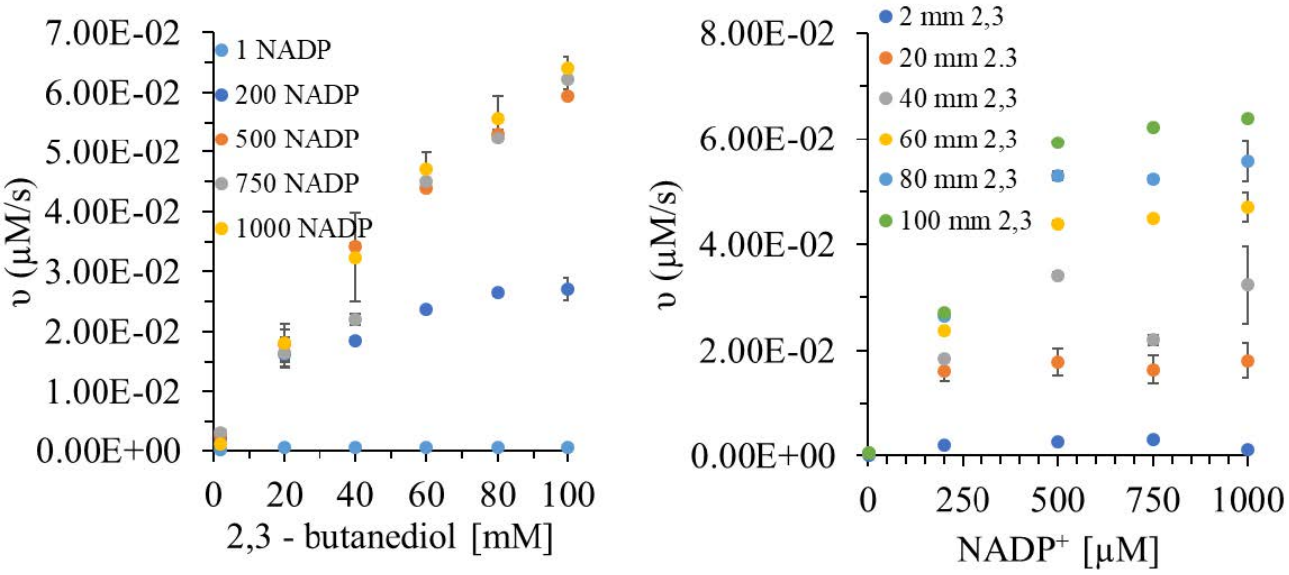

β-AdhD, 50 Ca^{2+}, $NADP^{+}$

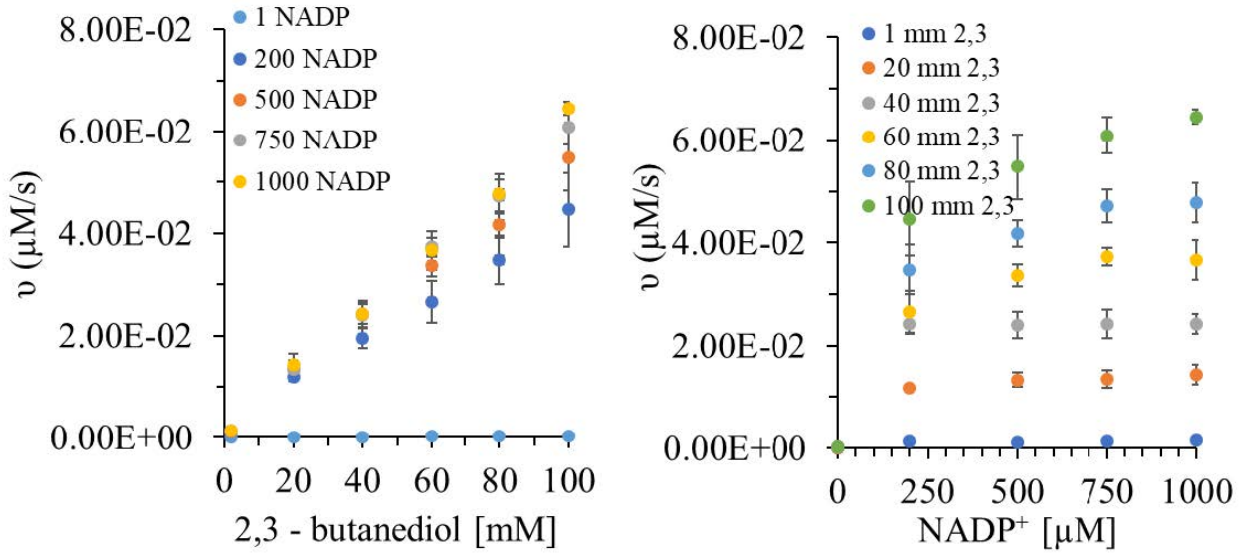

Figure 3.17 Steady state kinetic rate data for β-AdhD at 0 and 50 mM calcium with $NADP^{+}$. Data were collected in at least triplicate.

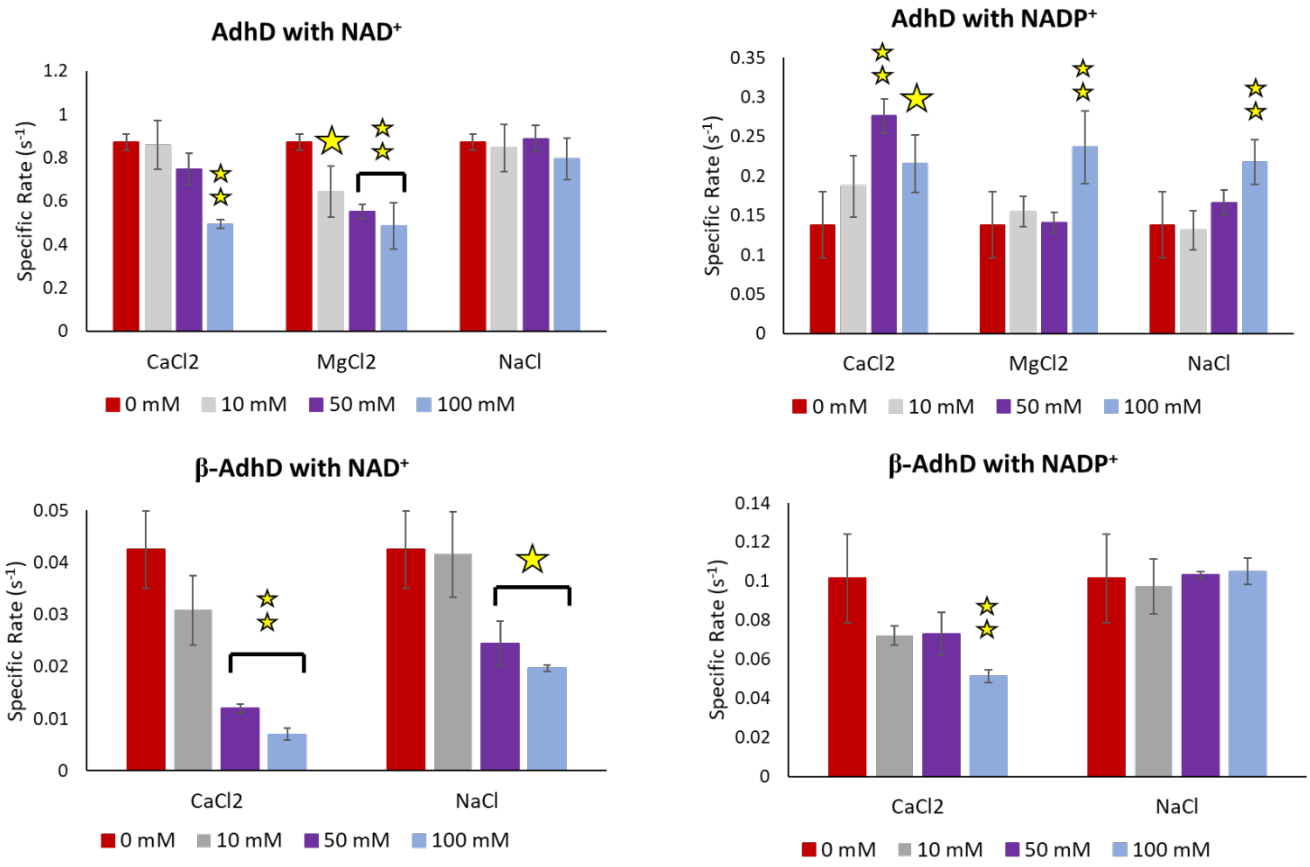

Figure 3.18 Specific rates for AdhD and β-AdhD with 0, 10, 50, and 100 mM salts with NAD^+ and $NADP^+$ as cofactors. Magnesium has a strong inhibitor effect on the activity of AdhD with NAD^+, and therefore was not an appropriate control. NaCl was used as a control to compare with $CaCl_2$ with β-AdhD. Stars indicate statistically significant rates (*$p<0.05$, **$p<0.005$) compared to the protein in the absence of the salt (red bars). Data were collected in at least triplicate.

Ordered Bi Bi Derivations

Case 1: varying [B]

V = Et * kcat * A * B / (Kia*Kb + Ka*B + A*Kb + AB)

Case 2: Constant [B]

- Ordered bi-bi rate equation

V = Et * kcat * A * B / (Kia*Kb + Ka*B + A*Kb + AB)

- Constant B so can divide by B and Kb (both constants)

V = [(Et * kcat * A * B)/(Kb*B)] / (Kia*Kb/(Kb*B) + Ka*B/(B*Kb) + A*Kb/(B*Kb) + AB/(Kb*B)

V = (Et * (kcat *B/Kb + B) * A) / ((KiaKb + KaB)/(Kb + B) + A)

V = Et * kcat,app * A / (Ka,app + A)

** Same form as Michaelis-Menton Equation; used to determine apparent parameters

Case 3: Kb >> B

V = Et * kcat * A * B / (Kia*Kb + Ka*B + A*Kb + AB)

- Divide by Kb (Kb values exceed B)

V = (Et * kcat * A * B / Kb) / (Kia*Kb/Kb + Ka*B/Kb + A* Kb/Kb + AB/Kb)

V = (Et * kcat * A * B / Kb) / (Kia + 0 [kb >> B] + A + 0 [kb >> B])

V = (Et*kcat*A*B /kb) / (Kia + A)

Mixed competitive and non-competitive inhibition derivation for β-AdhD

- **The following script was entered into DynaFit**

```
reaction A + B  ---> P + Q
modifiers I, J

E + A  <==> EA      :    k1  k-1
EA + B <=> EAB      :    k2  k-2
EAB   <=> EPQ       :    kp  k-p
EPQ  <=> EQ + P     :    k3  k-3
```

EQ <=> E + Q : k4 k-4

E + I <=> EI : k5 k-5

E + J <=> EJ : k6 k-6

EJ + I <=> EJI : k7 k-7

EJ + A <=> EJA : k8 k-8

EJA + B <=> EJAB : k9 k-9

EJAB <=> EJPQ : k10 k-10

EJPQ <=> EJQ + P : k11 k-11

EJQ <=> EJ + Q : k12 k-12

Notes:

- Competitive inhibition, where calcium competes with the substrate, was previously shown to be true for AdhD
- Non-competitive inhibition, where calcium binds at a site other than the active site and decreases the affinity of the enzyme for the substrate, is assumed to represent the β-roll binding sites
- "I" represents calcium binding to AdhD
- "J" represents calcium binding to the β-roll
- There are no steps following the EJI complex because it is a dead end complex with calcium binding to the β-roll and the active site of AdhD. "I" is competing with cofactor so the calcium attachment is reversible. When calcium binds the β-roll it is not reversible. Therefore, EJI is used as opposed to EIJ.
- The following model output was obtained (based on the King-Altman method):

Rate Equation

V = [E]0 N/D = d[P]/dt = + k3 [EPQ] - k-3 [EQ] [P] + k11 [EJPQ] - k-11 [P] [EJQ]

N = n1 [P][Q] + n2 [A][B] + n3 [P][Q][J] - n4 [P]2[Q] - n5 [B][P][Q] + n6 [A][B][J] + n7 [A][B][P] + n8 [A][B]2 - n9 [P]2[Q][J] - n10 [B][P][Q][J] + n11 [A][B][P][J] + n12 [A][B]2[J]

D = d1 + d2 [J] + d3 [I] + d4 [Q] + d5 [P] + d6 [B] + d7 [A] + d8 [I][J] + d9 [Q][J] + d10 [P][J] + d11 [P][I] + d12 [P][Q] + d13 [P]2 + d14 [B][J] + d15 [B][I] + d16 [B][Q] + d17 [B][P] + d18 [B]2 + d19 [A][J] + d20 [A][P] + d21 [A][B] + d22 [P][I][J] + d23 [P][Q][J] + d24 [P]2[J] + d25 [P]2[I] + d26 [P]2[Q] + d27 [B][I][J] + d28 [B][Q][J] + d29 [B][P][J] + d30 [B][P][I] + d31 [B][P][Q] + d32 [B]2[J] + d33 [B]2[I] + d34 [B]2[Q] + d35 [A][P][J] + d36 [A][P]2 + d37 [A][B][J] + d38 [A][B][P] + d39 [A][B]2 + d40 [P]2[I][J] + d41 [P]2[Q][J] + d42 [B][P][I][J] + d43 [B][P][Q][J] + d44 [B][P]2[Q] + d45 [B]2[I][J] + d46 [B]2[Q][J] + d47 [B]2[P][Q] + d48

[A][P]2[J] + d49 [A][B][P][J] + d50 [A][B][P]2 + d51 [A][B]2[J] + d52 [A][B]2[P] + d53 [B][P]2[Q][J] + d54 [B]2[P][Q][J] + d55 [A][B][P]2[J] + d56 [A][B]2[P][J]

Terms:

n1 = k-1 k-2 k-p k-3 k-4 k-5 k-6 k-7 k-8 k12 (- k-9 k-10 - k-9 k11 - k10 k11)

n2 = k1 k2 kp k3 k4 k-5 k-6 k-7 k-8 k12 (+ k-9 k-10 + k-9 k11 + k10 k11)

n3 = k-1 k4 k-5 k6 k-7 k-8 k-9 k-10 k-11 k-12 (- k-2 k-p - k-2 k3 - kp k3)

n4 = - k-1 k-2 k-p k-3 k-4 k-5 k-6 k-7 k-8 k-9 k-10 k-11

n5 = - k-1 k-2 k-p k-3 k-4 k-5 k-6 k-7 k9 k10 k11 k12

n6 = k-1 k4 k-5 k6 k-7 k8 k9 k10 k11 k12 (+ k-p k-2 + kp k3)

n7 = + k1 k2 kp k3 k4 k-5 k-6 k-7 k-8 k-9 k-10 k-11

n8 = + k1 k2 kp k3 k4 k-5 k-6 k-7 k9 k10 k11 k12

n9 = - k-1 k-2 k-p k-3 k-5 k6 k-7 k-8 k-9 k-10 k-11 k-12

n10 = - k2 kp k3 k4 k-5 k6 k-7 k-8 k-9 k-10 k-11 k-12

n11 = + k-1 k-2 k-p k-3 k-5 k6 k-7 k8 k9 k10 k11 k12

n12 = + k2 kp k3 k4 k-5 k6 k-7 k8 k9 k10 k11 k12

d1 = k-1 k4 k-5 k-6 k-7 k-8 k12 (k-2 k-p k-9 k-10 + k-2 k-p k-9 k11 + k-2 k-p k10 k11 + k-2 k3 k-9 k-10 + k-2 k3 k-9 k11 + k-2 k3 k10 k11 + kp k3 k-9 k-10 + kp k3 k-9 k11 + kp k3 k10 k11)

d2 = k-1 k4 k-5 k6 k-7 k-8 k12 (k-2 k-p k-9 k-10 + k-2 k-p k-9 k11 + k-2 k-p k10 k11 + k-2 k3 k-9 k-10 + k-2 k3 k-9 k11 + k-2 k3 k10 k11 + kp k3 k-9 k-10 + kp k3 k-9 k11 + kp k3 k10 k11)

d3 = k-1 k4 k5 k-6 k-7 k-8 k12 (k-2 k-p k-9 k-10 + k-2 k-p k-9 k11 + k-2 k-p k10 k11 + k-2 k3 k-9 k-10 + k-2 k3 k-9 k11 + k-2 k3 k10 k11 + kp k3 k-9 k-10 + kp k3 k-9 k11 + kp k3 k10 k11)

d4 = k-1 k-4 k-5 k-6 k-7 k-8 k12 (k-2 k-p k-9 k-10 + k-2 k-p k-9 k11 + k-2 k-p k10 k11 + k-2 k3 k-9 k-10 + k-2 k3 k-9 k11 + k-2 k3 k10 k11 + kp k3 k-9 k-10 + kp k3 k-9 k11 + kp k3 k10 k11)

d5 = k-1 k-5 k-6 k-7 k-8 (k-2 k-p k4 k-9 k-10 k-11 + k-2 k-p k-3 k-9 k-10 k12 + k-2 k-p k-3 k-9 k11 k12 + k-2 k-p k-3 k10 k11 k12 + k-2 k3 k4 k-9 k-10 k-11 + kp k3 k4 k-9 k-10 k-11)

d6 = k4 k-5 k-6 k-7 k12 (k-1 k-2 k-p k9 k10 k11 + k-1 k-2 k3 k9 k10 k11 + k-1 kp k3 k9 k10 k11 + k2 kp k3 k-8 k-9 k-10 + k2 kp k3 k-8 k-9 k11 + k2 kp k3 k-8 k10 k11)

d7 = k1 k4 k-5 k-6 k-7 k-8 k12 (k-2 k-p k-9 k-10 + k-2 k-p k-9 k11 + k-2 k-p k10 k11 + k-2 k3 k-9 k-10 + k-2 k3 k-9 k11 + k-2 k3 k10 k11 + kp k3 k-9 k-10 + kp k3 k-9 k11 + kp k3 k10 k11)

d8 = k-1 k4 k-5 k6 k7 k-8 k12 (k-2 k-p k-9 k-10 + k-2 k-p k-9 k11 + k-2 k-p k10 k11 + k-2 k3 k-9 k-10 + k-2 k3 k-9 k11 + k-2 k3 k10 k11 + kp k3 k-9 k-10 + kp k3 k-9 k11 + kp k3 k10 k11)

d9 = k-1 k4 k-5 k6 k-7 k-8 k-12 (k-2 k-p k-9 k-10 + k-2 k-p k-9 k11 + k-2 k-p k10 k11 + k-2 k3 k-9 k-10 + k-2 k3 k-9 k11 + k-2 k3 k10 k11 + kp k3 k-9 k-10 + kp k3 k-9 k11 + kp k3 k10 k11)

d10 = k-1 k-5 k6 k-7 k-8 (k-2 k-p k4 k-9 k-10 k-11 + k-2 k-p k-3 k-9 k-10 k12 + k-2 k-p k-3 k-9 k11 k12 + k-2 k-p k-3 k10 k11 k12 + k-2 k3 k4 k-9 k-10 k-11 + kp k3 k4 k-9 k-10 k-11)

d11 = k-1 k5 k-6 k-7 k-8 (k-2 k-p k4 k-9 k-10 k-11 + k-2 k-p k-3 k-9 k-10 k12 + k-2 k-p k-3 k-9 k11 k12 + k-2 k-p k-3 k10 k11 k12 + k-2 k3 k4 k-9 k-10 k-11 + kp k3 k4 k-9 k-10 k-11)

d12 = k-4 k-5 k-6 k-7 k-8 (k-2 k-p k-3 k-9 k-10 k12 + k-2 k-p k-3 k-9 k11 k12 + k-2 k-p k-3 k10 k11 k12 + k-1 k-p k-3 k-9 k-10 k12 + k-1 k-p k-3 k-9 k11 k12 + k-1 k-p k-3 k10 k11 k12 + k-1 k-2 k-3 k-9 k-10 k12 + k-1 k-2 k-3 k-9 k11 k12 + k-1 k-2 k-3 k10 k11 k12 + k-1 kp k-3 k-9 k-10 k12 + k-1 kp k-3 k-9 k11 k12 + k-1 kp k-3 k10 k11 k12 + k-1 k-2 k-p k-9 k-10 k-11 + k-1 k-2 k3 k-9 k-10 k-11 + k-1 kp k3 k-9 k-10 k-11)

d13 = k-1 k-2 k-p k-3 k-5 k-6 k-7 k-8 k-9 k-10 k-11

d14 = k4 k-5 k6 k-7 k12 (k-1 k-2 k-p k9 k10 k11 + k-1 k-2 k3 k9 k10 k11 + k-1 kp k3 k9 k10 k11 + k2 kp k3 k-8 k-9 k-10 + k2 kp k3 k-8 k-9 k11 + k2 kp k3 k-8 k10 k11)

d15 = k4 k5 k-6 k-7 k12 (k-1 k-2 k-p k9 k10 k11 + k-1 k-2 k3 k9 k10 k11 + k-1 kp k3 k9 k10 k11 + k2 kp k3 k-8 k-9 k-10 + k2 kp k3 k-8 k-9 k11 + k2 kp k3 k-8 k10 k11)

d16 = k-4 k-5 k-6 k-7 k12 (k-1 k-2 k-p k9 k10 k11 + k-1 k-2 k3 k9 k10 k11 + k-1 kp k3 k9 k10 k11 + k2 kp k3 k-8 k-9 k-10 + k2 kp k3 k-8 k-9 k11 + k2 kp k3 k-8 k10 k11)

d17 = k-5 k-6 k-7 (k-1 k-2 k-p k-3 k9 k10 k11 k12 + k2 kp k3 k4 k-8 k-9 k-10 k-11)

d18 = k2 kp k3 k4 k-5 k-6 k-7 k9 k10 k11 k12

d19 = k-1 k4 k-5 k6 k-7 k8 k12 (k-2 k-p k-9 k-10 + k-2 k-p k-9 k11 + k-2 k-p k10 k11 + k-2 k3 k-9 k-10 + k-2 k3 k-9 k11 + k-2 k3 k10 k11 + kp k3 k-9 k-10 + kp k3 k-9 k11 + kp k3 k10 k11)

d20 = k1 k-5 k-6 k-7 k-8 (k-2 k-p k4 k-9 k-10 k-11 + k-2 k-p k-3 k-9 k-10 k12 + k-2 k-p k-3 k-9 k11 k12 + k-2 k-p k-3 k10 k11 k12 + k-2 k3 k4 k-9 k-10 k-11 + kp k3 k4 k-9 k-10 k-11)

d21 = k1 k-5 k-6 k-7 k12 (k-2 k-p k4 k9 k10 k11 + k-2 k3 k4 k9 k10 k11 + kp k3 k4 k9 k10 k11 + k2 k-p k4 k-8 k-9 k-10 + k2 k-p k4 k-8 k-9 k11 + k2 k-p k4 k-8 k10 k11 + k2 k3 k4 k-8 k-9 k-10 + k2 k3 k4 k-8 k-9 k11 + k2 k3 k4 k-8 k10 k11 + k2 kp k4 k-8 k-9 k-10 + k2 kp k4 k-8 k-9 k11 + k2 kp k4 k-8 k10 k11 + k2 kp k3 k-8 k-9 k-10 + k2 kp k3 k-8 k-9 k11 + k2 kp k3 k-8 k10 k11)

d22 = k-1 k-5 k6 k7 k-8 (k-2 k-p k4 k-9 k-10 k-11 + k-2 k-p k-3 k-9 k-10 k12 + k-2 k-p k-3 k-9 k11 k12 + k-2 k-p k-3 k10 k11 k12 + k-2 k3 k4 k-9 k-10 k-11 + kp k3 k4 k-9 k-10 k-11)

d23 = k-1 k-5 k6 k-7 k-12 (k-2 k-p k4 k-9 k-10 k-11 + k-2 k3 k4 k-9 k-10 k-11 + kp k3 k4 k-9 k-10 k-11 + k-2 k-p k4 k-8 k-10 k-11 + k-2 k3 k4 k-8 k-10 k-11 + kp k3 k4 k-8 k-10 k-11 + k-2 k-p k4 k-8 k-9 k-11 + k-2 k-p k4 k-8 k10 k-11 + k-2 k3 k4 k-8 k-9 k-11 + k-2 k3 k4 k-8 k10 k-11 + kp k3 k4 k-8 k-9 k-11 + kp k3 k4 k-8 k10 k-11 + k-2 k-p k-3 k-8 k-9 k-10 + k-2 k-p k-3 k-8 k-9 k11 + k-2 k-p k-3 k-8 k10 k11)

d24 = k-1 k-2 k-p k-3 k-5 k6 k-7 k-8 k-9 k-10 k-11

d25 = k-1 k-2 k-p k-3 k5 k-6 k-7 k-8 k-9 k-10 k-11

d26 = k-3 k-4 k-5 k-6 k-7 k-8 k-9 k-10 k-11 (k-2 k-p + k-1 k-p + k-1 k-2 + k-1 kp)

d27 = k4 k-5 k6 k7 k12 (k-1 k-2 k-p k9 k10 k11 + k-1 k-2 k3 k9 k10 k11 + k-1 kp k3 k9 k10 k11 + k2 kp k3 k-8 k-9 k-10 + k2 kp k3 k-8 k-9 k11 + k2 kp k3 k-8 k10 k11)

d28 = k4 k-5 k6 k-7 k-12 (k-1 k-2 k-p k9 k10 k11 + k-1 k-2 k3 k9 k10 k11 + k-1 kp k3 k9 k10 k11 + k2 kp k3 k-8 k-9 k-10 + k2 kp k3 k-8 k-9 k11 + k2 kp k3 k-8 k10 k11)

d29 = k-5 k6 k-7 (k-1 k-2 k-p k-3 k9 k10 k11 k12 + k2 kp k3 k4 k-8 k-9 k-10 k-11)

d30 = k5 k-6 k-7 (k-1 k-2 k-p k-3 k9 k10 k11 k12 + k2 kp k3 k4 k-8 k-9 k-10 k-11)

d31 = k-4 k-5 k-6 k-7 (k-2 k-p k-3 k9 k10 k11 k12 + k-1 k-p k-3 k9 k10 k11 k12 + k2 k-p k-3 k-8 k-9 k-10 k12 + k2 k-p k-3 k-8 k-9 k11 k12 + k2 k-p k-3 k-8 k10 k11 k12 + k-1 k-2 k-3 k9 k10 k11 k12 + k-1 kp k-3 k9 k10 k11 k12 + k2 kp k-3 k-8 k-9 k-10 k12 + k2 kp k-3 k-8 k-9 k11 k12 + k2 kp k-3 k-8 k10 k11 k12 + k2 kp k3 k-8 k-9 k-10 k-11)

d32 = k2 kp k3 k4 k-5 k6 k-7 k9 k10 k11 k12

d33 = k2 kp k3 k4 k5 k-6 k-7 k9 k10 k11 k12

d34 = k2 kp k3 k-4 k-5 k-6 k-7 k9 k10 k11 k12

d35 = k-1 k-5 k6 k-7 k8 (k-2 k-p k4 k-9 k-10 k-11 + k-2 k-p k-3 k-9 k-10 k12 + k-2 k-p k-3 k-9 k11 k12 + k-2 k-p k-3 k10 k11 k12 + k-2 k3 k4 k-9 k-10 k-11 + kp k3 k4 k-9 k-10 k-11)

d36 = k1 k-2 k-p k-3 k-5 k-6 k-7 k-8 k-9 k-10 k-11

d37 = k4 k-5 k6 k-7 k8 (k2 kp k3 k-9 k-10 k12 + k2 kp k3 k-9 k11 k12 + k2 kp k3 k10 k11 k12 + k-1 k-2 k-p k9 k-10 k12 + k-1 k-2 k-p k9 k11 k12 + k-1 k-2 k3 k9 k-10 k12 + k-1 k-2 k3 k9 k11 k12 + k-1 kp k3 k9 k-10 k12 + k-1 kp k3 k9 k11 k12 + k-1 k-2 k-p k9 k10 k12 + k-1 k-2 k3 k9 k10 k12 + k-1 kp k3 k9 k10 k12 + k-1 k-2 k-p k9 k10 k11 + k-1 k-2 k3 k9 k10 k11 + k-1 kp k3 k9 k10 k11)

d38 = k1 k-5 k-6 k-7 (k-2 k-p k-3 k9 k10 k11 k12 + k2 k-p k4 k-8 k-9 k-10 k-11 + k2 k-p k-3 k-8 k-9 k-10 k12 + k2 k-p k-3 k-8 k-9 k11 k12 + k2 k-p k-3 k-8 k10 k11 k12 + k2 k3 k4 k-8 k-9 k-10 k-11 + k2 kp k4 k-8 k-9 k-10 k-11 + k2 kp k-3 k-8 k-9 k-10 k12 + k2 kp k-3 k-8 k-9 k11 k12 + k2 kp k-3 k-8 k10 k11 k12 + k2 kp k3 k-8 k-9 k-10 k-11)

d39 = k1 k2 k-5 k-6 k-7 k9 k10 k11 k12 (k-p k4 + k3 k4 + kp k4 + kp k3)

d40 = k-1 k-2 k-p k-3 k-5 k6 k7 k-8 k-9 k-10 k-11

d41 = k-1 k-2 k-p k-3 k-5 k6 k-7 k-11 k-12 (k-9 k-10 + k-8 k-10 + k-8 k-9 + k-8 k10)

d42 = k-5 k6 k7 (k-1 k-2 k-p k-3 k9 k10 k11 k12 + k2 kp k3 k4 k-8 k-9 k-10 k-11)

d43 = k-5 k6 k-7 k-12 (k2 kp k3 k4 k-9 k-10 k-11 + k-1 k-2 k-p k4 k9 k-10 k-11 + k-1 k-2 k3 k4 k9 k-10 k-11 + k-1 kp k3 k4 k9 k-10 k-11 + k2 kp k3 k4 k-8 k-10 k-11 + k-1 k-2 k-p k4 k9 k10 k-11 + k-1 k-2 k3 k4 k9 k10 k-11 + k-1 kp k3 k4 k9 k10 k-11 + k2 kp k3 k4 k-8 k-9 k-11 + k2 kp k3 k4 k-8 k10 k-11 + k-1 k-2 k-p k-3 k9 k10 k11)

d44 = k2 k-3 k-4 k-5 k-6 k-7 k-8 k-9 k-10 k-11 (k-p + kp)

d45 = k2 kp k3 k4 k-5 k6 k7 k9 k10 k11 k12

d46 = k2 kp k3 k4 k-5 k6 k-7 k9 k10 k11 k-12

d47 = k2 k-3 k-4 k-5 k-6 k-7 k9 k10 k11 k12 (k-p + kp)

d48 = k-1 k-2 k-p k-3 k-5 k6 k-7 k8 k-9 k-10 k-11

d49 = k-5 k6 k-7 k8 (k2 kp k3 k4 k-9 k-10 k-11 + k-1 k-2 k-p k4 k9 k-10 k-11 + k-1 k-2 k-p k-3 k9 k-10 k12 + k-1 k-2 k-p k-3 k9 k11 k12 + k-1 k-2 k3 k4 k9 k-10 k-11 + k-1 kp k3 k4 k9 k-10 k-11 + k-1 k-2 k-p k4 k9 k10 k-11 + k-1 k-2 k-p k-3 k9 k10 k12 + k-1 k-2 k3 k4 k9 k10 k-11 + k-1 kp k3 k4 k9 k10 k-11 + k-1 k-2 k-p k-3 k9 k10 k11)

d50 = k1 k2 k-3 k-5 k-6 k-7 k-8 k-9 k-10 k-11 (k-p + kp)

d51 = k2 kp k3 k4 k-5 k6 k-7 k8 k9 (k-10 k12 + k11 k12 + k10 k12 + k10 k11)

d52 = k1 k2 k-3 k-5 k-6 k-7 k9 k10 k11 k12 (k-p + kp)

d53 = k-1 k-2 k-p k-3 k-5 k6 k-7 k9 k-11 k-12 (k-10 + k10)

d54 = k2 kp k3 k4 k-5 k6 k-7 k9 k-11 k-12 (k-10 + k10)

d55 = k-1 k-2 k-p k-3 k-5 k6 k-7 k8 k9 k-11 (k-10 + k10)

d56 = k2 kp k3 k4 k-5 k6 k-7 k8 k9 k-11 (k-10 + k10)

Simplification #1:

- All terms with P and Q are cancelled as reactions were performed in the absence of products

N = n2 [A][B] + n6 [A][B][J] + n8 [A][B] + n12 [A][B]2[J]

D = d1 + d2 [J] + d3 [I] + d6 [B] + d7 [A] + d8 [I][J] + d14 [B][J] + d15 [B][I] + d18 [B]2 + d19 [A][J] + d21 [A][B] + d27 [B][I][J] + d32 [B]2[J] + d33 [B]2[I] + d37 [A][B][J] + d39 [A][B]2 + d45 [B]2[I][J] + d51 [A][B]2[J]

Simplification #2:

- All terms were simplified by canceling terms that contained k-2, k-p, k-9, and k-10 as we assume enzyme is irreversible

Simplification #3:

- Define dissociation constants and inhibition constants and simplify

  k-1/k1 = Kia
  k-5/k5 = KI
  k-6/k6 = KJ
  k-7/k7 = KJI
  k-8/k8 = Kiaj

Simplification #4:

- Kpk3k4 are part of kcat term in ordered bi bi derivation, analogously, k10k11k12 are part of kcatj. Divide all terms by kpk3k4k10k11k12
  k1 = kcat/Ka
  k2 = kcat/Kb
  k8 = kcat/Kaj
  k9 = kcat/Kbj

Simplification #5:

- Re-write all terms into kinetic parameters (Equation 3.10)

$$v = \frac{E_t\begin{pmatrix} k_{cat}K_{iaJ}K_{BJ}K_IK_JK_{JI}[A][B] + k_{cat}K_{AJ}K_IK_JK_{JI}[A][B]^2 + \\ k_{catJ}K_{ia}K_BK_IK_{JI}[A][B][J] + k_{catJ}K_AK_IK_{JI}[A][B]^2[J] \end{pmatrix}}{\begin{bmatrix} K_{ia}K_{iaJ}K_BK_{BJ}K_JK_IK_{JI} + K_{iaJ}K_BK_{BJ}K_JK_IK_{JI}[A] \\ +(K_{ia}K_{AJ}K_B + K_{iaJ}K_AK_{BJ})K_JK_IK_{JI}[B] + K_AK_{AJ}K_IK_JK_{JI}[B]^2 \\ + K_JK_IK_{JI}(K_BK_{AJ} + K_{iaJ}K_{BJ})[A][B] + (K_{AJ}K_JK_IK_{JI})[A][B]^2 \\ + K_{ia}K_BK_{BJ}K_IK_{JI}[A][J] + (K_{ia}K_{AJ}K_B + K_{iaJ}K_AK_{BJ})K_IK_{JI}[B][J] \\ +(K_{ia}K_{AJ}K_B + K_{iaJ}K_AK_{BJ})K_JK_{JI}[B][I] + \\ (K_{ia}K_{AJ}K_BK_I + K_{iaJ}K_AK_{BJ}K_I)[B][I][J] + (K_AK_{AJ}K_JK_{JI})[B]^2[I] + \\ K_AK_{AJ}K_IK_{JI}[B]^2[J] + K_IK_AK_{AJ}[B]^2[I][J] + K_IK_{JI}K_AK_{BJ}[A][B][J] + \\ K_IK_{JI}K_{ia}K_B[A][B][J] + K_IK_{JI}K_A[A][B]^2[J] + \\ K_{ia}K_{iaJ}K_BK_{BJ}K_JK_{JI}[I] + K_{ia}K_{iaJ}K_BK_{BJ}K_IK_{JI}[J] + K_{ia}K_{iaJ}K_BK_{BJ}K_I[I][J] \end{bmatrix}}$$

- **Note:** Setting I and J equal to zero and re-arranging the equation results in the ordered bi-bi rate equation

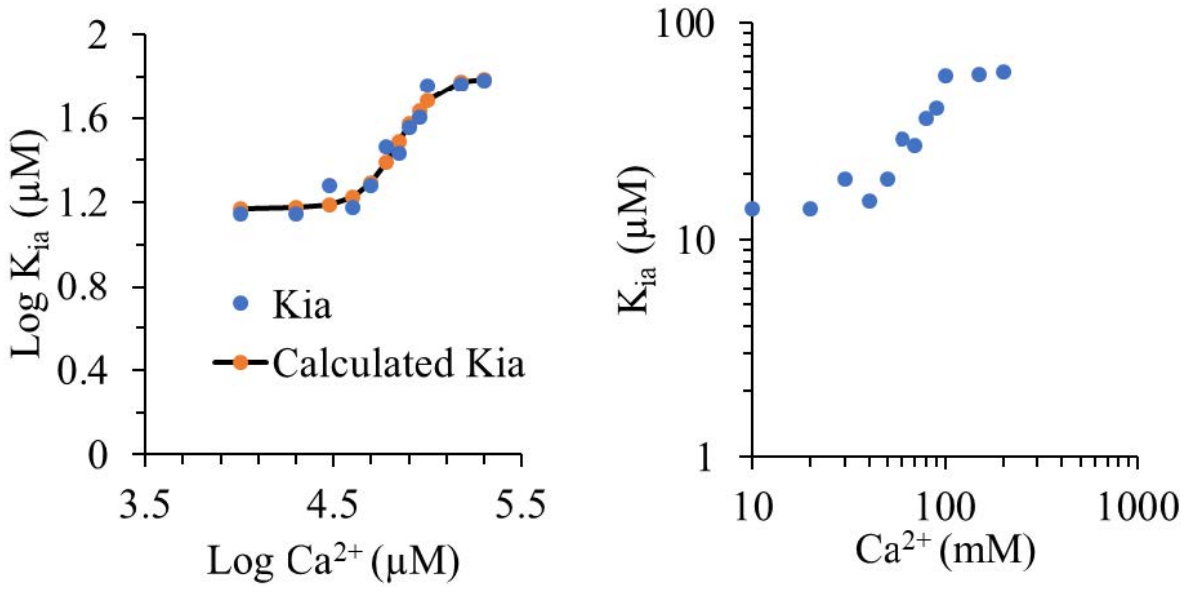

Figure 3.19 Sigmoidal relationship between calcium concentration and K_{ia} values for β-AdhD. The following values were obtained for the sigmoidal fit to the Log data:

$$y = base + \frac{max}{1 + \exp((x_{half} - x)/rate))} \tag{3.11}$$

base = 1.2 ± 0.085
max = 0.63 ± 0.16
x_{half} = 4.8 ± 0.072
rate = 0.10 ± 0.067

The concentration at the inflection point is 63±1 mM calcium.

Specific Initial Rate Kinetic Data

Table 3.7 Specific rate data for AdhD at varying NAD^+ and 2,3-butanediol concentration with zero calcium

AdhD, NAD, No Ca^{2+}

Rate (1/s)	NAD^+ (µM)	2,3-butanediol (µM)
0.228	200	2000
0.292	500	2000
0.496	750	2000
0.474	500	4000
0.488	750	4000
0.524001	1000	4000
1.223938	200	20000
1.676643	500	20000
1.946813	750	20000
1.23562	500	60000
1.310444	750	60000
1.456876	1000	60000
1.448604	750	80000
1.636246	1000	80000
1.713312	200	100000
1.727727	500	100000
1.818645	750	100000
1.849095	1000	100000
0.302	500	2000
0.592	750	2000
0.698	1000	2000
0.496	500	4000
0.508	750	4000
0.617999	1000	4000
1.766582	200	20000
1.830731	500	20000
2.071161	750	20000
1.683814	750	100000
1.917748	1000	100000
0.592759	200	20000
0.636689	500	20000
0.803461	500	40000
0.935139	750	40000
1.020002	200	60000
1.110001	500	60000
1.142002	750	60000
1.224537	200	80000
1.273342	500	80000

1.373617	750	80000
1.362036	200	100000
1.47894	500	100000
1.588096	750	100000
0.64492	500	40000
0.756061	750	40000
0.773461	1000	40000
0.99004	500	60000
1.00014	750	60000
1.033138	1000	60000
1.082943	500	80000
1.170837	750	80000
1.230739	1000	80000
1.419003	750	100000
1.43736	1000	100000
0.442706	750	20000
0.443198	1000	20000
0.729999	200	40000
0.776181	500	40000
0.788581	750	40000
1.008822	500	60000
1.028658	750	60000
1.086478	1000	60000
0.881679	200	80000
1.216183	500	80000
1.249922	750	80000
1.308541	1000	80000
1.413497	500	100000
1.474165	750	100000
1.531077	1000	100000
0.640921	200	40000
0.667481	500	40000
0.820001	200	60000
0.822	500	60000
0.998582	200	80000
1.013223	500	80000
0.13214	1	100000
0.87	20	100000
1.426005	200	100000
1.560002	500	100000
1.419003	750	100000
1.437205	1000	100000
0.195601	20	100000
1.465996	200	100000
1.413398	500	100000

1.474002	750	100000
1.529999	1000	100000
0.037948	20	100000
1.178002	200	100000
1.242321	500	100000
1.179997	750	100000
1.102317	1000	100000
0.652554	200	100000
0.860045	500	100000
0.925549	750	100000
0.953284	1000	100000
0.650656	200	100000
0.856788	500	100000
1.193766	750	100000
0.927007	1000	100000

Table 3.8 Specific rate data for AdhD at varying NAD^+ and 2,3-butanediol concentration with 50 mM calcium

AdhD, NAD, 50 mM Ca^{2+}

Rate (1/s)	NAD^+ (µM)	2,3-butanediol (µM)
0.50854	200	40000
0.5253	750	40000
0.76278	750	60000
0.84206	1000	60000
0.89546	200	100000
1.12294	1000	100000
0.36778	200	20000
0.420476	500	20000
0.55962	750	40000
0.70824	200	60000
0.7542	500	60000
0.77412	750	60000
0.79434	1000	60000
0.78166	200	80000
0.92974	500	80000
0.95674	1000	80000
0.82382	200	100000
0.986	750	100000
0.60926	500	20000
0.31936	200	40000
0.40178	500	40000
0.52294	750	40000

0.54642	1000	40000
0.5941	200	80000
0.92448	500	80000
0.97788	1000	80000
0.86766	500	100000
1.04338	750	100000
0.4427	750	20000
0.44352	1000	20000
0.73	200	40000
0.77618	500	40000
0.78858	750	40000
1.00882	500	60000
1.02866	750	60000
1.08648	1000	60000

Table 3.9 Specific rate data for β-AdhD at varying NAD^+ and 2,3-butanediol concentration with zero calcium

β-AdhD, NAD^+, No Ca^{2+}

Rate (1/s)	NAD^+ (μM)	2,3-butanediol (μM)
0.003551	200	20000
0.005748	500	20000
0.005706	750	20000
0.007289	200	40000
0.009838	500	40000
0.011242	750	40000
0.013043	1000	40000
0.016202	500	60000
0.016557	750	60000
0.018727	1000	60000
0.013388	200	80000
0.020021	500	80000
0.022265	750	80000
0.024566	1000	80000
0.016243	200	100000
0.028195	500	100000
0.036482	750	100000
0.017567	1000	100000
0.001316	1000	4000
0.003814	200	20000
0.005521	500	20000
0.00628	750	20000

0.006711	1000	20000
0.006007	200	40000
0.010515	500	40000
0.011997	750	40000
0.013062	1000	40000
0.016818	750	60000
0.016002	1000	60000
0.012743	200	80000
0.020559	500	80000
0.023007	750	80000
0.025038	1000	80000
0.036113	1000	100000
0.000926	750	4000
0.000787	1000	4000
0.003197	200	20000
0.003906	500	20000
0.004166	750	20000
0.002904	1000	20000
0.005436	200	40000
0.0067	500	40000
0.007611	750	40000
0.008042	1000	40000
0.007304	200	60000
0.01196	750	60000
0.012279	750	60000
0.009195	200	80000
0.013052	500	80000
0.015533	750	80000
0.015404	1000	80000
0.011577	200	80000
0.017643	500	100000
0.020965	750	100000
0.022091	1000	100000
0.003064	200	20000
0.003718	500	20000
0.004141	750	20000
0.006109	200	40000
0.007321	500	40000
0.008048	750	40000
0.010879	500	60000
0.011969	750	60000
0.012213	1000	60000
0.012069	200	80000
0.015293	500	80000
0.016579	750	80000

0.017172	1000	80000
0.014175	200	100000
0.020174	500	100000
0.021676	750	100000
0.022	1000	100000
0.003283	200	20000
0.003777	500	20000
0.004508	750	20000
0.004846	1000	20000
0.006692	200	40000
0.007362	500	40000
0.008042	750	40000
0.009131	1000	40000
0.009007	200	60000
0.011069	500	60000
0.012638	750	60000
0.013356	1000	60000
0.011827	200	80000
0.015403	500	80000
0.016776	750	80000
0.018456	1000	80000
0.014671	200	100000
0.019759	500	100000
0.021211	750	100000
0.023069	1000	100000
0.003195	200	20000
0.003231	500	20000
0.003687	750	20000
0.006048	200	40000
0.007091	500	40000
0.007404	750	40000
0.007546	1000	40000
0.009051	200	60000
0.011157	500	60000
0.011447	750	60000
0.012146	1000	60000
0.011857	200	80000
0.014639	500	80000
0.015882	750	80000
0.015938	1000	80000
0.01504	200	100000
0.018651	500	100000
0.020409	750	100000
0.020926	1000	100000
0.000971	1	100000

0.000971	1	100000
0.004243	20	100000
0.015191	200	100000
0.020147	500	100000
0.021618	750	100000
0.021985	1000	100000
0.00475	20	100000
0.015882	200	100000
0.019706	500	100000
0.021176	750	100000
0.023015	1000	100000
0.003235	20	100000
0.015882	200	100000
0.018603	500	100000
0.020409	750	100000
0.020926	1000	100000
0.002029	20	100000
0.007941	200	100000
0.009191	500	100000
0.009679	750	100000
0.010382	1000	100000
0.001809	20	100000
0.007721	200	100000
0.009117	500	100000
0.009835	1000	100000

Table 3.10 Specific rate data for β-AdhD at varying NAD^+ and 2,3-butanediol concentration with 50 mM calcium

β-AdhD, NAD^+, 50 mM Ca^{2+}

Rate (1/s)	NAD^+ (µM)	2,3-butanediol (µM)
0.001063	750	20000
0.00136	1000	20000
0.001959	200	40000
0.002225	500	40000
0.002742	750	40000
0.003213	1000	40000
0.003252	500	60000
0.004366	750	60000
0.004574	1000	60000
0.002464	200	80000
0.004871	500	80000
0.006048	750	80000
0.00714	1000	80000

0.003432	200	100000
0.005335	500	100000
0.006971	750	100000
0.00841	1000	100000
0.001121	750	20000
0.001317	1000	20000
0.001219	200	40000
0.002135	500	40000
0.002831	750	40000
0.003345	1000	40000
0.00202	200	60000
0.003429	500	60000
0.002273	750	60000
0.005646	1000	60000
0.002724	200	80000
0.004474	500	80000
0.006119	750	80000
0.006916	1000	80000
0.004925	200	100000
0.005505	500	100000
0.007375	750	100000
0.008517	1000	100000
0.001849	500	40000
0.00204	750	40000
0.002447	1000	40000
0.001563	200	60000
0.002577	500	60000
0.003232	750	60000
0.003635	1000	60000
0.002078	200	80000
0.003971	500	80000
0.0074	750	80000
0.002566	200	100000
0.005324	500	100000
0.005176	750	100000
0.006866	1000	100000
0.001367	750	20000
0.001571	1000	20000
0.001375	200	40000
0.001935	500	40000
0.003136	750	40000
0.003417	1000	40000
0.003175	500	60000
0.004657	750	60000
0.005201	1000	60000

0.002721	200	80000
0.004078	500	80000
0.006307	750	80000
0.007479	1000	80000
0.003461	200	100000
0.005269	500	100000
0.008423	750	100000
0.001263	500	20000
0.001554	750	20000
0.001684	1000	20000
0.001284	200	40000
0.002489	500	40000
0.003196	750	40000
0.003605	1000	40000
0.002034	200	60000
0.003946	500	60000
0.004785	750	60000
0.005288	1000	60000
0.002422	200	80000
0.005231	500	80000
0.006566	750	80000
0.007457	1000	80000
0.000682	200	20000
0.00126	500	20000
0.001408	750	20000
0.002095	1000	20000
0.001168	200	40000
0.002236	500	40000
0.002719	750	40000
0.0034	1000	40000
0.00195	200	60000
0.003624	500	60000
0.004809	750	60000
0.006033	1000	60000
0.002493	200	80000
0.004568	500	80000
0.006704	750	80000
0.007706	1000	80000

Table 3.11 Specific rate data for AdhD at varying $NADP^+$ and 2,3-butanediol concentration with zero calcium

AdhD, NADP, No Ca^{2+}

Rate (1/s)	NAD^+ (µM)	2,3-butanediol (µM)
0.020594	500	2000
0.024027	750	2000
0.022797	200	4000
0.026127	500	4000
0.030825	500	40000
0.034249	750	40000
0.033239	500	80000
0.034313	750	80000
0.038253	500	100000
0.036685	750	100000
0.0271	200	2000
0.027408	500	2000
0.028176	500	4000
0.029764	750	4000
0.033008	200	40000
0.034649	500	40000
0.030174	200	60000
0.033049	500	60000
0.034174	200	80000
0.034626	500	80000
0.034137	750	100000
0.038213	1000	100000
0.033043	500	20000
0.030072	750	20000
0.032028	750	40000
0.046321	1000	40000
0.039991	500	100000
0.042613	750	100000
0.042589	200	40000
0.039216	500	40000
0.038748	750	40000
0.032766	1000	40000
0.022442	200	60000
0.039449	500	60000
0.038206	750	60000
0.034613	500	80000
0.037133	750	80000
0.036543	500	100000
0.040179	750	100000

0.038322	200	20000
0.042783	500	20000
0.03626	750	40000
0.038465	1000	40000
0.037345	750	60000
0.039647	1000	60000
0.037691	750	100000
0.038607	1000	100000
0.033998	1000	40000
0.040369	500	60000

Table 3.12 Specific rate data for AdhD at varying $NADP^+$ and 2,3-butanediol concentration with 50 mM calcium

AdhD, $NADP^+$, 50 mM Ca^{2+}

Rate (1/s)	NAD^+ (µM)	2,3-butanediol (µM)
0.007223	200	2000
0.094775	500	2000
0.093238	750	2000
0.103996	1000	2000
0.030576	200	60000
0.236363	500	60000
0.224841	750	60000
0.21481	1000	60000
0.213012	200	80000
0.249488	500	80000
0.246737	750	80000
0.230379	1000	80000
0.023924	200	100000
0.258811	500	100000
0.265215	750	100000
0.24166	1000	100000
0.081967	200	2000
0.09375	500	2000
0.098873	750	2000
0.121414	200	4000
0.139344	500	4000
0.154713	750	4000
0.181865	200	20000
0.199621	500	20000
0.196834	750	20000
0.202049	1000	20000
0.244826	200	40000
0.236901	500	40000

0.226947	750	40000
0.232418	1000	40000
0.224027	200	60000
0.239933	500	60000
0.232121	750	60000
0.24772	1000	60000
0.237613	200	80000
0.250415	500	80000
0.247111	750	80000
0.256522	1000	80000
0.228586	200	100000
0.260963	500	100000
0.267587	750	100000
0.253519	1000	100000
0.049488	200	2000
0.078381	500	2000
0.095287	750	2000
0.13627	200	20000
0.018955	500	20000
0.019416	750	20000
0.194672	200	40000
0.214139	500	40000
0.145492	200	60000
0.222848	500	60000
0.230533	750	60000
0.194672	200	80000
0.215164	500	80000
0.220287	750	80000
0.189549	200	100000
0.240779	500	100000
0.306352	750	100000
0.056352	200	4000
0.079918	750	4000
0.060451	1000	4000
0.167008	200	20000
0.169057	500	20000
0.172643	750	20000
0.185963	500	40000
0.193135	750	40000
0.024744	200	60000
0.196209	500	60000
0.196721	750	60000
0.204918	500	80000
0.204918	750	80000
0.209529	200	100000

0.209529	500	100000
0.210041	750	100000
0.090164	200	4000
0.098361	500	4000
0.177254	200	20000
0.177766	500	20000
0.190574	750	40000
0.197234	1000	40000
0.197746	750	60000
0.207403	1000	60000
0.206455	200	100000
0.211066	750	100000
0.218238	1000	100000
0.082992	500	4000
0.085041	750	4000
0.162398	500	20000
0.165471	750	20000
0.179303	500	40000
0.189549	750	40000
0.186988	500	60000
0.196209	750	60000
0.204406	1000	60000
0.199795	500	80000
0.194672	750	80000
0.194672	200	100000
0.199795	500	100000
0.199795	750	100000

Table 3.13 Specific rate data for β-AdhD at varying $NADP^+$ and 2,3-butanediol concentration with zero calcium

β-AdhD, $NADP^+$, No Ca^{2+}

Rate (1/s)	NAD^+ (µM)	2,3-butanediol (µM)
0.001176	200	2000
0.002	500	2000
0.002221	750	2000
0.003176	200	4000
0.003449	500	4000
0.004588	750	4000
0.010882	750	20000
0.010882	1000	20000
0.013971	200	40000

0.016176	500	40000
0.016176	750	40000
0.004559	200	60000
0.019485	500	60000
0.019191	200	80000
0.022206	500	80000
0.020588	200	100000
0.023529	500	100000
0.024191	750	100000
0.003397	200	4000
0.00375	500	4000
0.004338	750	4000
0.010662	200	20000
0.011176	500	20000
0.011176	750	20000
0.012059	1000	20000
0.013529	200	40000
0.016471	500	40000
0.017647	200	60000
0.019118	500	60000
0.019485	750	60000
0.019265	200	80000
0.021471	750	80000
0.021471	1000	80000
0.018382	200	100000
0.024265	500	100000
0.024265	750	100000
0.024265	1000	100000
0.001471	200	2000
0.002279	750	2000
0.000846	1000	2000
0.002868	500	4000
0.003456	750	4000
0.010956	200	20000
0.01125	500	20000
0.013309	200	40000
0.015588	500	40000
0.015735	1000	40000
0.017279	200	60000
0.018603	500	60000
0.019853	200	80000
0.020882	500	80000
0.020882	200	100000
0.022279	500	100000
0.001684	200	2000

0.001838	500	2000
0.003559	200	4000
0.003618	500	4000
0.01375	500	20000
0.014265	750	20000
0.022059	200	40000
0.024779	500	40000
0.025368	1000	40000
0.004412	200	60000
0.031838	500	60000
0.033015	750	60000
0.033088	1000	60000
0.039706	500	80000
0.038235	750	80000
0.039706	1000	80000
0.041618	200	100000
0.044118	500	100000
0.044853	750	100000
0.047059	1000	100000
0.003632	200	4000
0.003662	500	4000
0.012059	200	20000
0.014338	500	20000
0.014265	1000	20000
0.022279	200	40000
0.025221	500	40000
0.026471	1000	40000
0.032353	500	60000
0.033088	750	60000
0.036029	1000	60000
0.038603	500	80000
0.038971	750	80000
0.044118	1000	80000
0.043382	500	100000
0.047059	750	100000
0.048529	1000	100000
0.001618	200	2000
0.001838	500	2000
0.003699	500	4000
0.003743	750	4000
0.004779	1000	4000
0.013897	200	20000
0.015221	500	20000
0.016176	1000	20000
0.023897	200	40000

0.025441	500	40000
0.0275	1000	40000
0.031765	200	60000
0.032574	500	60000
0.033088	750	60000
0.038529	500	80000
0.038235	750	80000
0.038971	1000	80000
0.040441	200	100000
0.043382	500	100000
0.045221	750	100000
0.045588	1000	100000

Table 3.14 Specific rate data for β-AdhD at varying $NADP^+$ and 2,3-butanediol concentration with 50 mM calcium

β-AdhD, $NADP^+$, 50 mM Ca^{2+}

Rate (1/s)	NAD^+ (μM)	2,3-butanediol (μM)
0.000632	500	2000
0.000882	750	2000
0.000904	1000	2000
0.001412	200	4000
0.003074	500	4000
0.008824	200	20000
0.010588	750	20000
0.014412	200	40000
0.019118	500	40000
0.020221	750	40000
0.025	500	60000
0.028676	750	60000
0.028676	1000	60000
0.026691	200	80000
0.031618	500	80000
0.036691	750	80000
0.036765	1000	80000
0.040441	500	100000
0.045956	750	100000
0.001029	200	2000
0.001397	200	4000
0.002353	500	4000
0.008603	200	20000
0.010588	500	20000

0.010662	750	20000
0.013897	200	40000
0.020074	500	40000
0.017794	200	60000
0.025368	500	60000
0.02875	750	60000
0.024926	200	80000
0.032132	500	80000
0.036471	750	80000
0.038235	200	100000
0.045588	500	100000
0.046471	1000	100000
0.001669	750	4000
0.002397	1000	4000
0.011838	200	40000
0.014706	500	40000
0.015441	750	40000
0.016176	1000	40000
0.016544	200	60000
0.021912	500	60000
0.022279	1000	60000
0.019779	200	80000
0.027353	500	80000
0.030809	750	80000
0.030882	1000	80000
0.024559	200	100000
0.031765	500	100000
0.040368	750	100000
0.048456	1000	100000
0.000824	200	2000
0.000949	500	2000
0.001074	750	2000
0.001809	500	4000
0.001772	750	4000
0.002743	1000	4000
0.015074	200	40000
0.017794	500	40000
0.024559	500	60000
0.025809	750	60000
0.026397	1000	60000
0.028529	200	80000
0.03125	500	80000
0.035294	750	80000
0.035882	1000	80000
0.033382	200	100000

0.040368	500	100000
0.045294	750	100000
0.047353	1000	100000
0.000853	200	2000
0.001037	500	2000
0.001397	750	2000
0.001838	500	4000
0.002404	750	4000
0.004044	1000	4000
0.008456	750	20000
0.011618	1000	20000
0.015	200	40000
0.016985	500	40000
0.017059	750	40000
0.01875	1000	40000
0.020956	200	60000
0.025294	500	60000
0.026397	750	60000
0.028676	1000	60000
0.027868	200	80000
0.031176	500	80000
0.034191	750	80000
0.036985	1000	80000
0.031544	200	100000
0.040441	500	100000
0.045	750	100000
0.001265	1000	2000
0.001478	200	4000
0.001735	500	4000
0.001882	1000	4000
0.008676	200	20000
0.009118	500	20000
0.000956	1000	20000
0.015735	200	40000
0.017941	500	40000
0.017941	750	40000
0.018456	1000	40000
0.023088	200	60000
0.026471	500	60000
0.027426	750	60000
0.02875	1000	60000
0.036397	200	100000
0.043088	500	100000
0.047353	750	100000

Table 3.15 Complete specific rate data for AdhD at varying NAD^+ and 2,3-butanediol concentration with varying calcium

AdhD, varying calcium

Rate (1/s)	NAD^+ (µM)	2,3-Butandediol (µM)	Ca^{2+} (µM)
0.228	200	2000	0
0.292	500	2000	0
0.496	750	2000	0
0.474	500	4000	0
0.488	750	4000	0
0.524	1000	4000	0
1.224	200	20000	0
1.6766	500	20000	0
1.9468	750	20000	0
1.2356	500	60000	0
1.3104	750	60000	0
1.4568	1000	60000	0
1.4486	750	80000	0
1.6362	1000	80000	0
1.7134	200	100000	0
1.7278	500	100000	0
1.8186	750	100000	0
1.849	1000	100000	0
0.302	500	2000	0
0.592	750	2000	0
0.698	1000	2000	0
0.496	500	4000	0
0.508	750	4000	0
0.618	1000	4000	0
1.7666	200	20000	0
1.8308	500	20000	0
2.0712	750	20000	0
1.6838	750	100000	0
1.9178	1000	100000	0
0.5928	200	20000	0
0.6366	500	20000	0
0.8034	500	40000	0
0.9352	750	40000	0
1.02	200	60000	0
1.11	500	60000	0
1.142	750	60000	0
1.2246	200	80000	0
1.2734	500	80000	0

1.3736	750	80000	0
1.362	200	100000	0
1.479	500	100000	0
1.588	750	100000	0
0.645	500	40000	0
0.756	750	40000	0
0.7734	1000	40000	0
0.99	500	60000	0
1.0002	750	60000	0
1.0332	1000	60000	0
1.083	500	80000	0
1.1708	750	80000	0
1.2308	1000	80000	0
1.419	750	100000	0
1.4374	1000	100000	0
0.4428	750	20000	0
0.4432	1000	20000	0
0.73	200	40000	0
0.7762	500	40000	0
0.7886	750	40000	0
1.0088	500	60000	0
1.0286	750	60000	0
1.0864	1000	60000	0
0.8816	200	80000	0
1.2162	500	80000	0
1.25	750	80000	0
1.3086	1000	80000	0
1.4134	500	100000	0
1.4742	750	100000	0
1.531	1000	100000	0
0.641	200	40000	0
0.6674	500	40000	0
0.82	200	60000	0
0.822	500	60000	0
0.9986	200	80000	0
1.0132	500	80000	0
0.43	20	100000	25000
1.042	200	100000	25000
1.206	500	100000	25000
1.238	750	100000	25000
1.24	1000	100000	25000
0.36	20	100000	25000
0.944	200	100000	25000
1.102	750	100000	25000
1.192	1000	100000	25000

0.358	20	100000	25000
0.958	200	100000	25000
1.136	500	100000	25000
1.1822	750	100000	25000
0.9726	20	100000	25000
1.226	500	100000	25000
1.2056	750	100000	25000
1.384	1000	100000	25000
0.366	20	100000	25000
0.932	200	100000	25000
1.19	500	100000	25000
1.252	750	100000	25000
1.405	1000	100000	25000
0.39	200	100000	50000
0.47	750	100000	50000
0.494	1000	100000	50000
1.4134	500	100000	50000
1.474	750	100000	50000
1.531	1000	100000	50000
0.2152	200	100000	50000
0.238	750	100000	50000
0.2266	1000	100000	50000
0.7722	200	100000	50000
1.16	500	100000	50000
1.1938	750	100000	50000
1.2094	1000	100000	50000
0.7722	200	100000	50000
1.0992	500	100000	50000
1.1858	750	100000	50000
1.223	1000	100000	50000
0.386	200	100000	100000
0.618	500	100000	100000
0.6634	750	100000	100000
0.7706	1000	100000	100000
0.378	200	100000	100000
0.624	500	100000	100000
0.722	750	100000	100000
0.746	1000	100000	100000
0.428	200	100000	100000
0.622	500	100000	100000
0.758	750	100000	100000
0.8332	1000	100000	100000
0.5854	200	100000	100000
0.962	500	100000	100000
1.1314	750	100000	100000

1.2248	1000	100000	100000
0.6176	200	100000	100000
0.9664	500	100000	100000
1.1548	750	100000	100000
1.216	1000	100000	100000
0.1906	200	100000	150000
0.342	500	100000	150000
0.466	750	100000	150000
0.596	1000	100000	150000
0.1034	20	100000	150000
0.174	200	100000	150000
0.304	500	100000	150000
0.348	750	100000	150000
0.478	1000	100000	150000
0.181	200	100000	150000
0.306	500	100000	150000
0.42	750	100000	150000
0.476	1000	100000	150000
0.8306	500	100000	150000
0.997	750	100000	150000
1.0802	1000	100000	150000
0.5008	200	100000	150000
0.835	500	100000	150000
0.9986	750	100000	150000
1.1402	1000	100000	150000
0.386	200	100000	200000
0.46	500	100000	200000
0.834	750	100000	200000
1.022	1000	100000	200000
0.165	200	100000	200000
0.272	500	100000	200000
0.4	750	100000	200000
0.658	1000	100000	200000
0.128	200	100000	200000
0.2722	500	100000	200000
0.3758	750	100000	200000
0.467	1000	100000	200000
0.3824	200	100000	200000
0.6876	500	100000	200000
0.857	750	100000	200000
0.949	1000	100000	200000
0.3474	200	100000	200000
0.708	500	100000	200000
0.8672	750	100000	200000
0.9782	1000	100000	200000

0.296	1000	80000	50000
0.5086	200	40000	50000
0.5252	750	40000	50000
0.7628	750	60000	50000
0.842	1000	60000	50000
0.8954	200	100000	50000
1.123	1000	100000	50000
0.3678	200	20000	50000
0.4204	500	20000	50000
0.3944	200	40000	50000
0.5596	750	40000	50000
0.7082	200	60000	50000
0.7542	500	60000	50000
0.7742	750	60000	50000
0.7944	1000	60000	50000
0.7816	200	80000	50000
0.9298	500	80000	50000
0.9568	1000	80000	50000
0.8238	200	100000	50000
0.986	750	100000	50000
1.2636	1000	100000	50000
0.3582	200	20000	50000
0.6092	500	20000	50000
0.3194	200	40000	50000
0.4018	500	40000	50000
0.523	750	40000	50000
0.5464	1000	40000	50000
0.594	200	80000	50000
0.9244	500	80000	50000
0.9778	1000	80000	50000
0.8676	500	100000	50000
1.0434	750	100000	50000
0.292	500	40000	50000
0.3096	500	60000	50000
0.3246	750	60000	50000
0.3408	200	80000	50000
0.382	500	80000	50000
0.3848	750	80000	50000
0.387	1000	80000	50000
0.3902	200	100000	50000
0.4716	750	100000	50000
0.4956	1000	100000	50000
0.4428	750	20000	50000
0.4436	1000	20000	50000
0.73	200	40000	50000

0.7762	500	40000	50000
0.7886	750	40000	50000
1.0088	500	60000	50000
1.0286	750	60000	50000
1.0864	1000	60000	50000
1.2078	200	80000	50000
1.2162	500	80000	50000
1.25	750	80000	50000
1.3086	1000	80000	50000
1.4674	200	100000	50000
1.4742	750	100000	50000
1.531	1000	100000	50000
0.1322	1	100000	0
0.87	20	100000	0
1.426	200	100000	0
1.56	500	100000	0
1.419	750	100000	0
1.4372	1000	100000	0
0.1956	20	100000	0
1.466	200	100000	0
1.4134	500	100000	0
1.474	750	100000	0
1.53	1000	100000	0
0.038	20	100000	0
1.178	200	100000	0
1.2424	500	100000	0
1.18	750	100000	0
1.1024	1000	100000	0
0.6526	200	100000	0
0.86	500	100000	0
0.9256	750	100000	0
0.9532	1000	100000	0
0.6506	200	100000	0
0.8568	500	100000	0
1.1938	750	100000	0
0.927	1000	100000	0

Table 3.16 Complete specific rate data for β-AdhD at varying NAD^+ and 2,3-butanediol concentration with varying calcium

β-AdhD, varying calcium

Rate (1/s)	NAD^+ (μM)	2,3-butanediol (μM)	Ca^{2+} (μM)
0.000971	1	100000	0
0.004243	20	100000	0
0.015191	200	100000	0
0.020147	500	100000	0
0.021618	750	100000	0
0.021985	1000	100000	0
0.00475	20	100000	0
0.015882	200	100000	0
0.019706	500	100000	0
0.021176	750	100000	0
0.023015	1000	100000	0
0.003235	20	100000	0
0.015882	200	100000	0
0.018603	500	100000	0
0.020409	750	100000	0
0.020926	1000	100000	0
0.002029	20	100000	0
0.007941	200	100000	0
0.009191	500	100000	0
0.009679	750	100000	0
0.010382	1000	100000	0
0.001809	20	100000	0
0.007721	200	100000	0
0.009117	500	100000	0
0.009835	1000	100000	0
0.003551	200	20000	0
0.005748	500	20000	0
0.005706	750	20000	0
0.007289	200	40000	0
0.009838	500	40000	0
0.011242	750	40000	0
0.013043	1000	40000	0
0.016202	500	60000	0
0.016557	750	60000	0
0.018727	1000	60000	0
0.013388	200	80000	0
0.020021	500	80000	0

0.022265	750	80000	0
0.024566	1000	80000	0
0.016243	200	100000	0
0.028195	500	100000	0
0.036482	750	100000	0
0.001316	1000	4000	0
0.003814	200	20000	0
0.005521	500	20000	0
0.00628	750	20000	0
0.006711	1000	20000	0
0.006007	200	40000	0
0.010515	500	40000	0
0.011997	750	40000	0
0.013062	1000	40000	0
0.016818	750	60000	0
0.016002	1000	60000	0
0.012743	200	80000	0
0.020559	500	80000	0
0.023007	750	80000	0
0.025038	1000	80000	0
0.036113	1000	100000	0
0.000926	750	4000	0
0.000787	1000	4000	0
0.003197	200	20000	0
0.003906	500	20000	0
0.004166	750	20000	0
0.005436	200	40000	0
0.0067	500	40000	0
0.007611	750	40000	0
0.008042	1000	40000	0
0.007304	200	60000	0
0.01196	750	60000	0
0.012279	750	60000	0
0.009195	200	80000	0
0.013052	500	80000	0
0.015533	750	80000	0
0.015404	1000	80000	0
0.011577	200	80000	0
0.017643	500	100000	0
0.020965	750	100000	0
0.022091	1000	100000	0
0.003064	200	20000	0
0.003718	500	20000	0

0.004141	750	20000	0
0.006109	200	40000	0
0.007321	500	40000	0
0.008048	750	40000	0
0.010879	500	60000	0
0.011969	750	60000	0
0.012213	1000	60000	0
0.012069	200	80000	0
0.015293	500	80000	0
0.016579	750	80000	0
0.017172	1000	80000	0
0.014175	200	100000	0
0.020174	500	100000	0
0.021676	750	100000	0
0.022	1000	100000	0
0.003283	200	20000	0
0.003777	500	20000	0
0.004508	750	20000	0
0.004846	1000	20000	0
0.006692	200	40000	0
0.007362	500	40000	0
0.008042	750	40000	0
0.009131	1000	40000	0
0.009007	200	60000	0
0.011069	500	60000	0
0.012638	750	60000	0
0.013356	1000	60000	0
0.011827	200	80000	0
0.015403	500	80000	0
0.016776	750	80000	0
0.018456	1000	80000	0
0.014671	200	100000	0
0.019759	500	100000	0
0.021211	750	100000	0
0.023069	1000	100000	0
0.003195	200	20000	0
0.003231	500	20000	0
0.003687	750	20000	0
0.006048	200	40000	0
0.007091	500	40000	0
0.007404	750	40000	0
0.007546	1000	40000	0
0.009051	200	60000	0

0.011157	500	60000	0
0.011447	750	60000	0
0.012146	1000	60000	0
0.011857	200	80000	0
0.014639	500	80000	0
0.015882	750	80000	0
0.015938	1000	80000	0
0.01504	200	100000	0
0.018651	500	100000	0
0.020409	750	100000	0
0.020926	1000	100000	0
0.000324	1	100000	10000
0.007773	20	100000	10000
0.018483	200	100000	10000
0.029027	500	100000	10000
0.030228	750	100000	10000
0.030134	1000	100000	10000
0.007125	20	100000	10000
0.018218	200	100000	10000
0.02784	500	100000	10000
0.030228	750	100000	10000
0.031929	1000	100000	10000
0.005911	20	100000	10000
0.019648	200	100000	10000
0.02761	500	100000	10000
0.031659	750	100000	10000
0.032091	1000	100000	10000
0.005182	20	100000	20000
0.01483	200	100000	20000
0.023602	500	100000	20000
0.028407	750	100000	20000
0.030863	1000	100000	20000
0.005571	20	100000	20000
0.014813	200	100000	20000
0.023575	500	100000	20000
0.027206	750	100000	20000
0.031497	1000	100000	20000
0.000162	1	100000	20000
0.004426	20	100000	20000
0.015341	200	100000	20000
0.023548	500	100000	20000
0.029648	750	100000	20000
0.027529	1000	100000	20000

0.00384	20	100000	30000
0.012226	200	100000	30000
0.020944	500	100000	30000
0.025208	750	100000	30000
0.027448	1000	100000	30000
0.003644	20	100000	30000
0.011606	200	100000	30000
0.020094	500	100000	30000
0.025654	750	100000	30000
0.003401	20	100000	30000
0.011889	200	100000	30000
0.020256	500	100000	30000
0.02537	750	100000	30000
0.026585	1000	100000	30000
0.00332	20	100000	40000
0.017462	500	100000	40000
0.022725	750	100000	40000
0.022725	1000	100000	40000
0.003167	20	100000	40000
0.010108	200	100000	40000
0.017705	500	100000	40000
0.021727	750	100000	40000
0.026949	1000	100000	40000
0.003279	20	100000	40000
0.006626	200	100000	40000
0.018339	500	100000	40000
0.023683	750	100000	40000
0.026801	1000	100000	40000
7.2E-05	1	100000	50000
0.002785	20	100000	50000
0.008056	200	100000	50000
0.014682	500	100000	50000
0.018339	750	100000	50000
0.019932	1000	100000	50000
4.05E-05	1	100000	50000
0.002562	20	100000	50000
0.007935	200	100000	50000
0.014534	500	100000	50000
0.018339	750	100000	50000
0.020323	1000	100000	50000
4.22E-05	1	100000	50000
0.002321	20	100000	50000
0.007611	200	100000	50000

0.013832	500	100000	50000
0.016423	750	100000	50000
0.018312	1000	100000	50000
0.001965	20	100000	60000
0.006963	200	100000	60000
0.013427	500	100000	60000
0.017192	750	100000	60000
0.020013	1000	100000	60000
0.002321	20	100000	60000
0.007517	200	100000	60000
0.014372	500	100000	60000
0.017773	750	100000	60000
0.020823	1000	100000	60000
0.002402	20	100000	60000
0.007975	200	100000	60000
0.014912	500	100000	60000
0.01807	750	100000	60000
0.022779	1000	100000	60000
0.002143	20	100000	70000
0.006181	200	100000	70000
0.011228	500	100000	70000
0.014345	750	100000	70000
0.015357	1000	100000	70000
0.00471	200	100000	70000
0.009176	500	100000	70000
0.012051	750	100000	70000
0.014183	1000	100000	70000
0.001534	20	100000	70000
0.005101	200	100000	70000
0.010283	500	100000	70000
0.012213	750	100000	70000
0.015047	1000	100000	70000
0.001822	20	100000	80000
0.005762	200	100000	80000
0.011606	500	100000	80000
0.014331	750	100000	80000
0.016167	1000	100000	80000
0.001457	20	100000	80000
0.004494	200	100000	80000
0.008353	500	100000	80000
0.01116	750	100000	80000
0.015141	1000	100000	80000
0.001547	20	100000	80000

0.005115	200	100000	80000
0.009716	500	100000	80000
0.012037	750	100000	80000
0.014439	1000	100000	80000
0.001483	20	100000	80000
0.004966	200	100000	80000
0.010108	500	100000	80000
0.012577	750	100000	80000
0.015101	1000	100000	80000
0.001373	20	100000	90000
0.004129	200	100000	90000
0.008623	500	100000	90000
0.010364	750	100000	90000
0.01336	1000	100000	90000
0.001342	20	100000	90000
0.004318	200	100000	90000
0.008056	500	100000	90000
0.011754	750	100000	90000
0.012915	1000	100000	90000
0.00108	20	100000	90000
0.004386	200	100000	90000
0.008529	500	100000	90000
0.011916	750	100000	90000
0.013373	1000	100000	90000
0.001342	20	100000	90000
0.004683	200	100000	90000
0.009082	500	100000	90000
0.011525	750	100000	90000
0.013792	1000	100000	90000
0.001281	20	100000	90000
0.004642	200	100000	90000
0.008866	500	100000	90000
0.011619	750	100000	90000
0.014318	1000	100000	90000
0.001266	20	100000	100000
0.004278	200	100000	100000
0.007503	500	100000	100000
0.010634	750	100000	100000
0.011363	1000	100000	100000
0.0015	20	100000	100000
0.004615	200	100000	100000
0.008434	500	100000	100000
0.012105	750	100000	100000

0.013549	1000	100000	100000
0.000162	1	100000	100000
0.0015	20	100000	100000
0.004656	200	100000	100000
0.008002	500	100000	100000
0.011147	500	100000	100000
0.01336	1000	100000	100000
0.000864	20	100000	150000
0.003077	200	100000	150000
0.006167	500	100000	150000
0.008083	750	100000	150000
0.009406	1000	100000	150000
0.001012	20	100000	150000
0.003225	200	100000	150000
0.006086	500	100000	150000
0.008259	750	100000	150000
0.009109	1000	100000	150000
0.000958	20	100000	150000
0.003144	200	100000	150000
0.006302	500	100000	150000
0.007759	750	100000	150000
0.009622	1000	100000	150000
0.000621	20	100000	200000
0.001835	200	100000	200000
0.00332	500	100000	200000
0.004021	750	100000	200000
0.003981	1000	100000	200000
0.000526	20	100000	200000
0.001835	200	100000	200000
0.00363	500	100000	200000
0.00448	750	100000	200000
0.004534	1000	100000	200000
0.000513	20	100000	200000
0.001903	200	100000	200000
0.003738	500	100000	200000
0.004764	750	100000	200000

CHAPTER 4

SITE-SPECIFIC INCORPORATION OF THE TEMPO ORGANIC CATALYST INTO A THERMOSTABLE ALCOHOL DEHYDROGENASE PRODUCES A SELECTIVE BIO/ORGANO-HYBRID CATALYST

Project Collaborators: Walaa Abdallah, Louis Lancaster, David Hickey, Ian Wheeldon, Shelley Minteer, and Scott Banta

WA was responsible for molecular cloning work and all enzyme work, including protein expression, protein purification, unnatural amino acid incorporation, and enzyme kinetics.

4.1 Abstract

Amber stop codons were introduced at three different positions in the thermostable alcohol dehydrogenase D, AdhD, from *Pyrococcus furiosus*. This enabled the incorporation of the unnatural amino acid, para-azidophenylalanine, to replace the initiation methionine (M1TAG), the catalytic tyrosine 64 (Y64TAG), and tyrosine 205 near the cofactor binding pocket (Y205TAG). The addition of the unnatural amino acid rendered Y64TAG inactive as its hydroxyl group, which participates in catalysis, was replaced with an azide group. The remaining mutants, M1TAG and Y205TAG, retained AdhD activity with 2,3-butanediol, its preferred substrate, and cofactor, NAD^+. An amber stop codon was also introduced into a hydrogel containing AdhD, HS-AdhD-H, to allow for the incorporation of the para-azidophenylalanine. This mutant retained the activity of AdhD. The azide in AdhD and HS-AdhD-H allowed for the site-specific attachment of an alkyne modified TEMPO organic catalyst via click chemistry. This resulted in an AdhD/TEMPO hybrid. AdhD prefers the oxidation of secondary alcohols with a specificity for medium carbon chain lengths while TEMPO prefers to oxidize primary alcohols of varying chain length. The bio/organo-hybrid catalysts demonstrate that enzymatic selectivity can be transferred to an organic catalyst by this approach. And this specificity can be altered by standard protein engineering methods.

4.2 Introduction

Biological and organic catalysts are two different classes of catalysts with varying properties. Enzymes are known for their enantioselectivity, substrate specificity, no byproduct formation, and their ability to be mass produced recombinantly [8]. Additionally, their ability to be engineered to increase stability and broaden potential applications makes them a desirable platform. Organic catalysts can be used homogenously or heterogeneously, can be modified to work in extreme

conditions, and can be synthesized with various functional groups. However, they lack the selectivity found in enzymes [7].

Bio-organo catalytic hybrids combines the properties of both classes, which was studied here. The enzyme chosen was alcohol dehydrogenase D, AdhD, from archaea *Pyrococcus furiosus,* which we have worked with extensively in our group [11, 17-20, 25]. It displays extreme thermostability, can be easily engineered, and exhibits substrate selectivity. AdhD prefers secondary alcohols over primary and works well with those with a medium carbon chain length [12]. The organic catalyst, TEMPO (2,2,6,6-tetramethylpiperidine-1-oxyl), prefers primary alcohols over secondary and works well with any chain length [7].

To expand the potential applications of a bio-organo hybrid, work was also done with an AdhD chimera. Chimeric fusion proteins allow for the functionalities of various protein domains to be combined into one system. Examples of these systems include fusion proteins designed to develop switches, study human drug therapy, drug targeting, production of antibodies, and much more [117, 121-123]. Previously, the Banta Lab fused a structural domain, hydrogel HSH, and an active domain, AdhD, to develop a chimeric fusion protein, HS-AdhD-H. HSH is a hydrogel forming triblock polypeptide with two-alpha helical leucine zipper domains (H), which reversibly cross-link resulting in a supramolecular hydrogel and are separated by a randomly coiled domain (S) [18, 37-40, 124]. HS-AdhD-H is a "novel bioactive material" that allowed AdhD to retain its activity while gaining the ability to form hydrogels [18].

We hypothesized that merging AdhD or HS-AdhD-H and TEMPO will result in selective alcohol oxidation (**Figure 4.1**). It can also allow for the selectivity of enzymes to be imparted onto organic catalysts. In the AdhD/TEMPO pathway, the alcohol being oxidized depends on which

catalyst can proceed. AdhD requires a cofactor and TEMPO must be regenerated, as the oxoammonium ion is the reactive species [45].

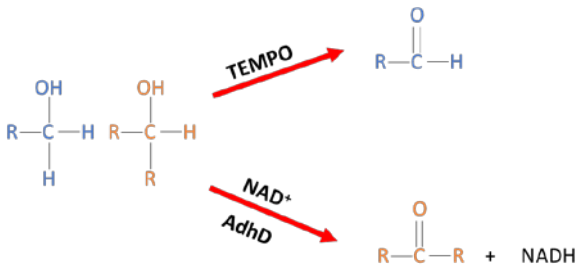

Figure 4.1 Alcohol oxidation reaction scheme with TEMPO and AdhD.

The AdhD-TEMPO and HS-AdhD-H/TEMPO hybrids were developed using azide-alkyne click chemistry. The reaction between azides and alkynes can be done in the presence or absence of copper. The use of copper requires a terminal alkyne, speeds up the reaction around seven orders of magnitude, and is selective [47]. However, the presence of copper can be toxic to some cells. The second pathway is referred to as strain-promoted cycloaddition, which occurs between a cyclooctyne and an azide. Since the reaction occurs through ring strain, this removes the need for toxic copper, however, two regioisomers result [47]. Both methods were studied.

To enable click chemistry, both AdhD and TEMPO required functional groups. Different versions of alkyne TEMPO (both terminal and internal) were synthesized by our collaborators. The azide group was incorporated into AdhD through site-specific unnatural amino acid incorporation, specifically through amber stop codon suppression. Unnatural amino acid incorporation has been utilized to study protein structure and activity, develop a responsive photo-switching mechanism, fuse the properties of metal catalysts and enzymes, and much more [34, 35,

125]. Here, we are using the azide functionality provided by the unnatural amino acid to develop site-selective hybrids. A TEMPO-AdhD hybrid has previously been made, but the sites of attachment were not selective [45].

In this work, three AdhD mutants were studied, each with a different location of the azide. The azide designates where TEMPO will attach. The following sites were mutated to an amber stop codon: initiation methionine (M1TAG), catalytic tyrosine (Y64TAG), and tyrosine near the cofactor binding pocket (Y205TAG) (**Figure 4.2**).

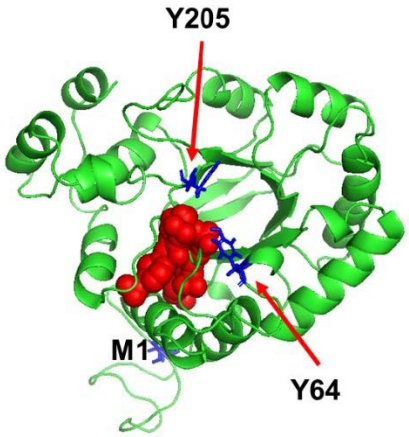

Figure 4.2 Homology model of AdhD with amber stop codon positions highlighted. Looking down the AdhD $(\alpha/\beta)_8$ barrel with mutations highlighted as blue sticks and cofactor, NAD^+, highlighted as red spheres. Figure generated using PYMOL.

M1TAG AdhD-TEMPO and Y205TAG AdhD-TEMPO may allow for the selective oxidation of primary and secondary alcohols, with Y205 providing steric hindrance. Y64TAG AdhD-TEMPO gained the substrate selectivity of AdhD suggesting enzymatic selectivity can be imparted onto organic catalysts.

The same techniques will be used to develop a three-component system containing TEMPO, HSH, and HS-AdhD-H to both selectively oxidize alcohols and form hydrogels.

4.3 Materials and Methods

4.3.1 Materials

Oligonucleotides were purchased from Integrated DNA Technologies (Coralville, IA). Phusion high fidelity DNA polymerase and *E. coli* BL21(DE3) and BL21-AI expression cells were from New England Biolabs (Ipswich, MA). NuPAGE SDS-PAGE gels, MOPS running buffer, and Novex sharp pre-stained protein standards were from Invitrogen (Carlsbad, CA). BugBuster protein extraction reagent was purchased from Millipore Sigma (Burlington, MA). Histidine purification Nickel-NTA resin and TAMRA was purchased from ThermoFisher Scientific (Waltham, MA). Chromatography columns were from Bio-Rad (Hercules, CA). Molecular weight centrifugal filters were from EMD Millipore (Billerica, MA). All other chemicals, including kanamycin and spectinomycin, were from Sigma Aldrich (St. Louis, MMO).

4.3.2 Cloning, Expression, and Purification of AdhD with Unnatural Amino Acids

The *adhD* gene from *Pyrococcus furiosus* in the pET-20b(+) vector, plasmid pWUR85, was re-cloned into the pET-28a(+) vector [12, 26]. The pET-28a(+) vector was restriction digested with *NdeI* such that the gene was preceded by the poly-histidine tag and the thrombin site. The resulting plasmid, AdhD-pet28a, was verified by DNA sequencing (complete sequence can be found in the Supporting Information). Site-directed mutagenesis was then used to introduce the amber stop codon (TAG) at the desired position for unnatural amino acid incorporation. Three different constructs were made: M1TAG (start methionine mutated to the amber stop codon), Y64TAG (catalytic tyrosine 64 mutated to the amber stop codon), and Y205TAG (tyrosine 205, which

participates in catalysis, mutated to the amber stop codon). Final sequences were verified by DNA sequencing (primers can be found in the Supporting Information).

The AdhD-pET-28a(+) plasmid, as well as the three different mutants (M1TAG, Y64TAG, Y205TAG), were co-transformed with aminoacyl-tRNA synthetase/tRNA pDule2 pCNF RS from *Methanocaldococcus jannaschii* into *E. coli* BL21-AI expression cells and plated onto Luria Broth (LB) plates supplemented with 0.1 mg/ml spectinomycin and 0.035 mg/ml kanamycin [126]. The pDule2 plasmid was a gift from Ryan Mehl. Prior to expression, media component stocks were prepared. 50x5052 solution was prepared by dissolving 125 g glycerol, 12.5 g glucose, and 50 g α-lactose in 365 mL water. 1 M MgSO4 was prepared by dissolving 60.18 g of $MgSO_4$ in 500 mL water. 40% glucose contained 20 g of D-(+)-glucose for every 30 mL of water. 20% arabinose was prepared by dissolving 2 g L-arabinose in 8 mL water and was sterile filtered and aliquoted into -20 °C. 25xM solution contained 44.36 g Na_2HPO_4, 42.55 g KH_2PO_4, 33.5 g NH_4Cl, and 8.9 g Na_2SO_4 in 500 mL water. ZY media contained 5 g N-Z amine AS (bovine casein enzymatic hydrolysate) and 2.5 g yeast extract in 500 mL water [126]. 200x trace metal solution contains the following in grams per liter: 0.5 EDTA, 3 $MgSO_4$-$7H_2O$, 0.5 $MnSO_4$-H_2O, 1 NaCl, 0.1 $FeSO_4$-$7H_2O$, 0.1 $Co(NO_3)_2$-$6H_2O$, 0.1 anhydrous $CaCl_2$, 0.1 $ZnSO_4$-$7H_2O$, anhydrous 0.01 $AlK(SO_4)_2$, 0.01 H_3BO_3, 0.01 Na_2MoO_4-$2H_2O$, 0.001 anhydrous Na_2SeO_3, 0.01 Na_2WO_4-2 H_2O, and 0.02 $NiCl_2$-$6H_2O$.

Single colonies were inoculated overnight in noninducing media, which contained the following for every 150 ml ZY media: 2 mM 1 M $MgSO_4$, 6 mL 25xM media, 750 µL of 200x trace metals, and 1.875 mL 40% glucose. Expression was performed the next day at 37 °C in 1L flasks containing 200 mL ZY media with 2 mL of the inoculated colonies. This media was then supplemented with autoinducing media containing the following for every 150 mL ZY media: 2

mM 1 M $MgSO_4$, 6 mL 25xM media, 750 µL of 200x trace metals, 3 mL 50x5052, and 375 uL 20% arabinose. The flasks were kept shaking at 200 rpm while the unnatural amino acid (UAA), para-azidophenylalanine, was prepared. 20 mg UAA per every 50 mL of media was added to each flask (M1TAG, Y64TAG, and Y205TAG positive controls) by pre-dissolving it in 0.5 M NaOH. Flasks containing the wild-type protein (AdhD-pET28a(+)) and negative controls (amber stop codon mutants) were not supplemented with the unnatural amino acid. The flasks were then returned to 37 °C and kept shaking overnight at 200 rpm.

The cells were harvested for purification with a portion resuspended in tris-buffer and lysed at 80 °C for 1 hour to denature all proteins except for thermophilic AdhD. This was done to confirm the presence of the protein, but was not used as a purification step as the unnatural amino acid is sensitive and although not studied at higher temperatures, it is known to photodegrade [127]. Therefore, the remainder of the cells were resuspended in 6 mL BugBuster protein extraction reagent and kept shaking at room temperature at 60 rpm for 20 minutes. The cells that were previously supplemented with para-azidophenylalanine were covered in foil to prevent azide degradation. Cell debris was removed by centrifugation for 30 minutes for the samples heated at 80 °C and for 1 hour at 7000xg for the samples treated with BugBuster. The clarified lysate from both the heated samples and the BugBuster samples were loaded onto NuPAGE 4-12% Bis-tris gels to confirm the expression of full-length protein in the wild-type and mutants supplemented with para-azidophenylalanine (**Figure 4.8**). The negative controls, mutants not supplemented with unnatural amino acid were also run on the gel to confirm the expression of the truncated protein. To confirm the expression of AdhD, the full-length protein for the wild-type and positive controls must have been present in the BugBuster samples (suggesting the incorporation of the UAA) and the supernatant of the 80 °C samples (suggesting the expression of AdhD as it is thermophilic).

Full-length proteins (wild-type and mutants with the UAA) that were lysed with BugBuster were loaded onto previously prepared chromatography columns containing 4 mL Ni-NTA resin. The resin was previously equilibrated with 20 mM sodium phosphate buffer with 500 mM NaCl, pH 7.4. The flow-through was collected and the column was washed with varying immidizole concentrations (75-500 mM immidizole) in 20 mM tris-HCl with 200 mM NaCl pH 7.4. Fractions were run on NuPAGE 4-12% Bis-tris gels in MES running buffer and those with 95% purity or more were pooled together and concentrated in 10 kDa MWCO centrifugal filters. The proteins were then buffer exchanged in 100 mM sodium phosphate buffer pH 7.4. Protein concentrations was measured by reading the absorbance at 280 nm on a SpectraMax M2 plate reader using an extinction coefficient of 52495 M^{-1} cm^{-1} for AdhD and M1TAG and 51005 M^{-1} cm^{-1} for Y64TAG and Y205TAG as the tyrosine is not present in the incorporated protein [110].

4.3.3 Cloning, Expression, and Purification of HSH, HS-AdhD-H, and HSH M1TAG

HSH and HS-AdhD-H (previously prepared in the Banta Lab) were cloned into pET28a(+) at *NdeI* (complete sequences can be found in supporting information) [18]. An amber stop codon was introduced at the initiation methionine of HSH, resulting in HSH M1TAG (primer can be found in supporting information). After verification of the sequences, constructs were co-transformed with the helper plasmid used for unnatural amino acid incorporation. The helper plasmid, pULTRA-CNF from *Methanocaldococcus jannaschii*, was prepared by the Schultz Lab and was ordered from Addgene (plasmid #48215). pULTRA was used instead of the previously used pDule2 because this helper plasmid has been shown to increase incorporation yields [30].

HSH, HSH M1TAG, and HS-AdhD-H were each co-transformed with pULTRA into *E. coli* BL21(DE3) cells onto Luria Broth (LB) plates supplemented with 0.035 mg/ml kanamycin and 0.1 mg/ml spectinomycin. Single colonies were inoculated at 37 ºC overnight in Terrific Broth (TB) supplemented with 0.035 mg/ml kanamycin and 0.1 mg/ml spectinomycin. Expression was performed the next day in the same media at 37 °C. When the cells reached on O.D. of approximately 1.0, induction was performed with 1 mM isopropyl β-D-1-thiogalactopyranoside (IPTG) and the cells were shaken at 200 rpm overnight at 27 °C. Cultures containing HSH M1TAG were supplemented with para-azidophenylalanine (20 mg of unnatural amino acid per 50 mL expression) during induction. A negative control was also done where HSH M1TAG was not supplemented with para-azidophenylalanine but was induced with IPTG.

The cells were harvested and resuspended in BugBuster and kept shaking at 60 rpm for 20 minutes. Those containing the unnatural amino acid were covered in foil. Cell debris was removed by centrifuging at 7000xg for 1 hour. The clarified lysate for the wild-type enzymes (HSH and HS-AdhD-H) and those containing the unnatural amino acid (HSH M1TAG with UAA) were loaded onto chromatography columns containing Ni-NTA resin previously equilibrated with 20 mM sodium phosphate buffer with 500 mM NaCl, pH 7.4. The clarified lysate of the negative control (HSH M1TAG without UAA) was run on SDS-PAGE to ensure no wild-type protein was expressed through read-through expression. Once this was confirmed, the columns incubated with clarified lysates were used to purify the proteins. The flow-through was collected and the column was washed with varying immidizole concentrations (75-500 mM immidizole) in 20 mM tris-HCl with 200 mM NaCl pH 7.4 (**Figure 4.11** and **Figure 4.12**). Fractions were run on NuPAGE 4-12% Bis-tris gels in MES running buffer and those containing protein greater than 95% pure were pooled together and concentrated in 20 kDa MWCO filters for HSH and 30 kDa MWCO filters

for HS-AdhD-H. It should be noted that the theoretical molecular weight of HSH is 24 kDa, but it runs at approximately 35 kDa, which matches previous work done in the Banta Lab [18]. The proteins were then buffer exchanged in 100 mM sodium phosphate buffer pH 7.4. A portion of HS-AdhD-H was buffer exchanged into 50 mM glycine (pH 9.3) for activity assays.

4.3.4 Kinetic Activity Assays

Kinetic assays were done with proteins that showed expression of the full-length protein and those containing the unnatural amino acid, para-azidophenylalanine. Specific activities for wild-type AdhD and its three mutants was determined by conducting assays at 45 °C in 96-well plates where enzyme, 100 mM substrate (2,3-butanediol), and 100 mM sodium phosphate buffer (pH 7.4) were incubated for 20 minutes. 100 µM cofactor (NAD^+) was then added and the absorbance at 340 nm was measured continuously for 20 minutes. Absorbance was converted to concentration using an extinction coefficient of 6.22 mM^{-1} cm^{-1}. The final reaction volume was 250 µL. To ensure initial rates, only data within the first 10% of the conversion of the added cofactor was used. Using enzyme concentration, rates were converted to initial specific rates. All measurements were made in at least triplicate.

The specific rate of wild-type AdhD with various alcohols, other than 2,3-butanediol, and sugars was measured at the exact same conditions.

Kinetic assays with HS-AdhD-H were performed to confirm the activity of AdhD in this chimeric fusion protein. Briefly, 100 mM 2,3-butanediol was incubated with enzyme and 50 mM glycine (pH 9.3) at 45 °C for approximately 20 minutes. 100 µM cofactor, NAD^+, was then added and the absorbance at 340 nm of NADH production was monitored. Specific rates were not determined as these were preliminary assays done only to ensure that HS-AdhD-H is active.

4.3.5 Click Chemistry with TAMRA

To further confirm the incorporation of the UAA (besides purification and activity assays), AdhD and the three mutants (M1TAG, Y64TAG, and Y205TAG) supplemented with para-azidophenylalanine were clicked to alkyne TAMRA. Steps 3.1 to 3.3 and 5.1 to 5.4 from protocol number MP33368 from ThermoFisher and steps 1.1 to 2.7 from protocol number MP33370 were followed. The samples were run on NuPAGE 4-12% Bis-tris gels in MES running buffer and prior to staining were observed under UV light.

HSH (as a control) and HSH M1TAG containing unnatural amino acid para-azidophenylalanine were also clicked to alkyne TAMRA to confirm incorporation and the ability to click onto HSH (same protocol as that used for AdhD). The samples were run on NuPAGE 4-12% Bis-tris gels in MES running buffer and prior to staining were observed under UV light (as the alkyne used for click chemistry is fluorescent). Once again, HSH should be observed at approximately 35 kDa, inconsistent with its theoretical molecular weight.

4.4 Results and Discussion

4.4.1 Expression and Purification of AdhD, M1TAG AdhD, Y64TAG AdhD, and Y205TAG AdhD and HSH, HSH TAG, and HS-AdhD-H

The DNA sequence corresponding to the AdhD gene from *Pyrococcus furiosus* was cloned into the pET28a(+) vector, resulting in the construct AdhD-pET28a(+). This same plasmid was used to introduce three unique amber stop codons in positions: methionine 1, tyrosine 64, and tyrosine 205. AdhD-pET28a(+) and the three mutants (M1TAG, Y64TAG, and Y205TAG) were co-transformed with pDule2 pCNF RS from *Methanocaldococcus jannaschii* into BL21-AI cells and all proteins were expressed. The wild-type enzyme and the three mutants had a molecular

weight of around 34 kDa consistent with its theoretical molecular weight. The full DNA and amino acid sequence of AdhD and the mutants can be found in the Supporting Information.

The resulting proteins, wild-type AdhD and the three mutants supplemented with para-azidophenylalanine, were routinely produced at 12 mg of protein per 200 mL *E. coli* culture. After expression and auto-induction, the pelleted cells were resuspended and extracted with BugBuster protein extraction reagent. The whole cell lysates were centrifuged, and the proteins were found in the soluble portion (**Figure 4.8**). The clarified lysate was purified using nickel-column chromatography and yielded the expected molecular masses with a purity of greater than 95% (**Figure 4.9** and **Figure 4.10**).

HSH and HS-AdhD-H (previously prepared in the Banta Lab) were cloned into pET28a(+), resulting in the plasmids HSH-pET28 and HS-AdhD-H pET28 (full DNA and amino acid sequences can be found in Supporting Information) [18]. The plasmids were co-transformed into *E. coli* BL21(DE3) cells with pULTRA-CNF. The proteins were purified on nickel resin to greater than 95% purity (**Figure 4.11** and **Figure 4.12**). The theoretical molecular weights are 24 kDa and 56 kDa for HSH and HS-AdhD-H, respectively, but HSH runs slightly higher at around 35 kDa, which was previously observed [18].

HSH and HS-AdhD-H were produced at around 10 to 15 mg of protein per liter of *E. coli* culture. HSH M1TAG with the unnatural amino acid had approximately half this yield.

4.4.2 Effect of the Unnatural Amino Acid, para-azidophenylalanine, on AdhD Specific Activity

The specific activity of AdhD and the three mutants, with para-azidophenylalanine replacing the amber stop codon, was determined with AdhD's preferred substrate, 2,3-butanediol (100 mM), and its cofactor NAD^+ (100 µM) (**Table 4.1**).

Table 4.1 Specific activity of AdhD and mutants (with para-azidophenylalanine) with 2,3-butanediol and NAD^+ Oxidation reaction with 100 mM 2,3 - butanediol and 100 µM NAD^+ in 100 mM sodium phosphate buffer pH 7.4. All data was collected in at least triplicate.

Mutant	Specific Activity (µmol min^{-1} mg^{-1})
AdhD	1.3 ± 0.05
M1TAG	1.0 ± 0.05
Y64TAG	Inactive
Y205TAG	0.62 ± 0.024

The activity of M1TAG AdhD was similar to that of AdhD, which was expected as the insertion was made at the N-terminus of the enzyme, away from the active site. The Y64TAG mutant was inactive. This was expected as the hydroxyl group of tyrosine 64, which participates in catalysis, was replaced with the functional azide group from para-azidophenylalanine [11]. The final mutant, Y205TAG was active, but less active than the wild-type enzyme. The benzene ring in Y205 is thought to participate in catalysis so the fact that the enzyme retained its activity is not unusual [11]. However, the decrease in activity could be due to insertion of a unique functional group previously not present.

4.4.3 Specific Activity of AdhD with Primary, Secondary, and Other Alcohols

AdhD prefers secondary alcohols over primary alcohols and works well with medium carbon chains. The preference of AdhD towards various alcohols, both with a varying number of hydroxyl groups and positions, and with varying carbon chain lengths was tested (**Figure 4.3**).

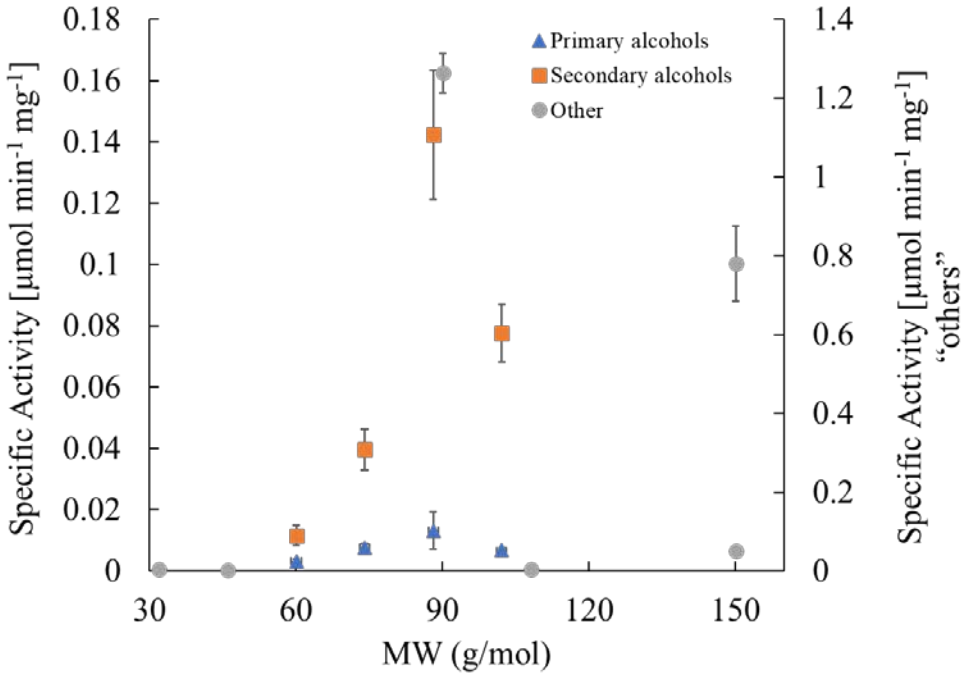

Figure 4.3 Specific activity of AdhD with various alcohols. Activity tested with 100 µM NAD^+ in 100 mM sodium phosphate buffer pH 7.4

Primary and secondary alcohols were varied from three to six carbon chains. AdhD consistently preferred the secondary alcohols over the primary regardless of chain length. Within the secondary alcohols, the maximum activity peaked at five carbon chains and then decreased, signifying AdhD's preference for secondary alcohols with medium chain length. The "other"

alcohols tested included methanol, ethanol, 2,3-butanediol, glucose, D-arabinose, and L-arabinose (list can be found in Supporting Information **Table 4.2**). AdhD showed minimal activity with most, except for arabinose and 2,3-butanediol. D-arabinose was more active than L-arabinose and the maximum activity was achieved with 2,3-butanediol, which is in accordance with previously published results [12].

4.4.4 HS-AdhD-H Activity Assay

One advantage of chimeric fusion proteins is their dual-functionality - HS-AdhD-H has the ability to form a hydrogel and retains the activity of AdhD [18]. To ensure HS-AdhD-H activity, assays with AdhD's preferred substrate 2,3-butanediol was done. Enzyme along with 100 mM substrate and 100 µM NAD^+ was incubated and monitored at 340 nm at 45 °C (**Figure 4.4**).

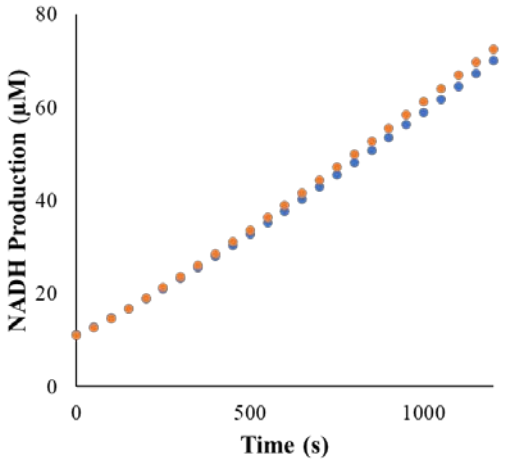

Figure 4.4 Rate of NADH production with HS-AdhD-H. HS-AdhD-H was incubated at 45 ºC with 2,3-butanediol and NAD^+ in 50 mM glycine (pH 9.3) and production of NADH at 340 nm was monitored. The slope increased suggesting HS-AdhD-H is active with these substrates at these conditions.

The enzymatic activity of HS-AdhD-H and its ability to form a hydrogel suggests a tri-functional system, that will have the ability to selectively oxidize secondary alcohols (AdhD) and primary alcohols (TEMPO), is possible.

4.4.5 Click Chemistry with TAMRA

AdhD and the three mutants, M1TAG, Y64TAG, and Y205TAG were clicked to alkyne-functionalized TAMRA to ensure the presence of para-azidophenylalanine and to test the accessibility of those sites for click chemistry. The use of copper ensures the formation of solely the 1,4-disubstituted 1,2,3-triazole [47]. After the reaction, the samples were run on SDS-PAGE and exposed to UV light (**Figure 4.5**). All three mutants labeled with para-azidophenylalanine were able to react with alkyne TAMRA and ran at the expected molecular weight of 34 kDa. AdhD alone was unable to form a bond with TAMRA as it does not contain the azide functional group required to react.

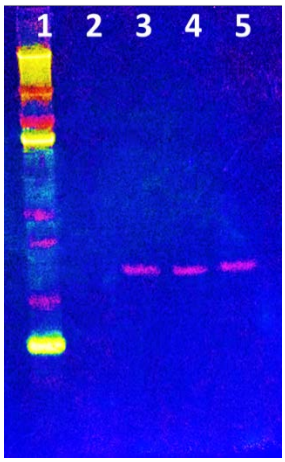

Figure 4.5 SDS-PAGE of azide-alkyne cycloaddition with AdhD. Protein gel exposed to UV light after copper-catalyzed azide-alkyne cycloaddition between para-azidophenylalanine labeled AdhD mutants M1TAG, Y64TAG, and Y205TAG and TAMRA (tetramethylrhodamine) fluorescent alkyne. Lane: (1) molecular weight ladder, (2) AdhD, (3) UAA labeled M1TAG, (4) UAA labeled Y64TAG, (5) UAA labeled Y205TAG. Expected bands observed at theoretical molecular weight, 34 kDa.

To ensure the incorporation of para-azidophenylalanine in HSH and to make sure the site is accessible for click chemistry, HSH para-azidophenylalanine was clicked to fluorescent-TAMRA (**Figure 4.6**). HSH without the unnatural amino acid was tested as a negative control.

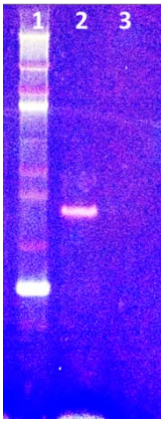

Figure 4.6 SDS-PAGE of HSH and HSH M1TAG with TAMRA. Protein gel exposed to UV light after click chemistry between HSH containing para-azidophenylalanine and alkyne TAMRA. Lane 1: molecular weight marker lane 2: HSH UAA, lane 3: HSH. An expected band at 35 kDa was observed for HSH with the unnatural amino acid.

HSH M1TAG (with the unnatural amino acid) lit up on SDS-PAGE under UV light. It ran at approximately the same size it normally runs on SDS-PAGE and a single band was fluorescent indicating HSH contains the unnatural amino acid and click chemistry was successful at this site. HSH alone does not have a band at the same molecular weight indicating the wild-type protein does not react with TAMRA alkyne.

4.4.6 Y64TAG AdhD-TEMPO Imparts AdhD Selectivity Onto TEMPO

Y64TAG AdhD was clicked to TEMPO via strain-promoted cycloaddition. Prior to the fusion, TEMPO preferred 1-propanol over 2,3-butanediol. After clicking TEMPO in the cofactor binding pocket of AdhD at Y64, the preference switched to 2,3-butanediol, a secondary alcohol (**Figure**

4.7). This suggests that selectivity can be imparted from one catalyst to another and that hybrids allowing for selective oxidation is possible.

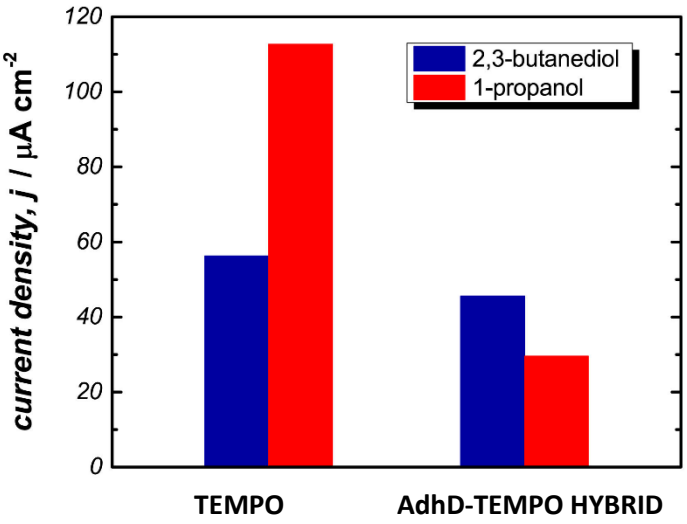

Figure 4.7 Activity of TEMPO before and after AdhD attachment at Y64. Collaborators performed electrochemical assay with TEMPO alone and AdhD-TEMPO after click chemistry at position Y64.

4.5 Conclusion

The ability to impart substrate selectivity onto an organic catalyst provides us with an extra tool we can use to develop multi-step cascades and merge different classes of catalysts. Here, we developed a technique that allows us to selectively oxidize a mixture of alcohols and in some cases, impart the selectivity of an enzyme, AdhD, onto an organic catalyst, TEMPO. The protein engineering methods used here can be readily applied to other systems. Work is still being completed on the other two mutants, M1TAG AdhD and Y205TAG AdhD. Additionally, work is being done with other organic catalysts besides TEMPO.

4.6 Future Work

Work with the three different mutants of AdhD and other alkyne modified moieties are currently being studied and tested by our collaborators.

Preliminary work has been done with new mutants of AdhD: hAR AdhD and hAR Y64TAG AdhD. Here, the AdhD gene containing human aldose reductase (hAR) loops A and B was synthesized, matching the protein sequence of a previous version of this fusion [19]. This construct was cloned into pET28a(+) using the same primers as those used when AdhD was cloned into this same vector. hAR is active with DL-glyceraldehyde and NADP(H), while AdhD is inactive with DL-glyceraldehyde. However, when hAR substrate loops A and B were grafted onto AdhD, hAR AdhD was found to be active with NADPH and DL-glyceraldehyde [19]. Its activity with 2,3-butanediol was still intact. However, hAR AdhD reversed cofactor specificity where now $NADP^+$ is preferred over NAD^+ [19].

Site-directed mutagenesis was performed on this new construct, hAR AdhD, to introduce an amber stop codon in the same position as tyrosine 64 in AdhD (sequence in Supporting Information).

Expression of hAR AdhD and incorporation of para-azidophenylalanine in Y64TAG hAR AdhD was achieved, as well as the ability to purify this protein on the nickel column (**Figure 4.13**). Preliminary TAMRA assays indicates the ability to click in the active site (**Figure 4.14**). Additionally, preliminary activity assays with hAR AdhD and Y64TAG hAR AdhD indicate the chimeric protein is active while the one lacking the hydroxyl group of tyrosine 64 is not (mutant with para-azidophenylalanine). Additionally, the enzyme is active with L-glyceraldehyde, but not D-glyceraldehyde. This chiral specificity gives us the ability to click TEMPO into the active site

of AdhD and impart not only its substrate selectivity, but its ability to distinguish between enantiomers as well.

4.7 Supporting Information

Primers to clone AdhD into pET28a(+) at *NdeI*

FWD: CCGCGCGGCAGCCATATGGCAAAAAGGGTAAATGCATTCAACGACCTTAAGCGTA

REV: AGTCATGCTAGCCATTCACACACACCTCCTTGCCATCTCTCTATCCTC

AdhD-pET28a(+) DNA sequence:

```
ATGGGCAGCA GCCATCATCA TCATCATCAC AGCAGCGGCC TGGTGCCGCG CGGCAGCCAT 60
ATGGCAAAAA GGGTAAATGC ATTCAACGAC CTTAAGCGTA TAGGAGATGA TAAGGTAACG 120
GCAATTGGAA TGGGAACATG GGGAATAGGA GGGAGAGAGA CCCCAGACTA TTCTAGGGAT 180
AAGGAAAGCA TAGAAGCAAT AAGATATGGA CTTGAATTAG GAATGAATTT AATCGACACA 240
GCGGAATTCT ATGGAGCTGG TCATGCTGAG GAAATAGTTG GAGAGGCCAT TAAAGAATTC 300
GAACGTGAGG ACATCTTCAT AGTGAGCAAG GTCTGGCCAA CTCACTTTGG GTATGAGGAA 360
GCAAAGAAGG CTGCTAGAGC AAGTGCTAAA AGGTTAGGAA CTTATATTGA CCTTTATTTG 420
TTGCACTGGC CCGTTGATGA CTTCAAGAAG ATAGAGGAGA CACTTCACGC TTTGGAAGAC 480
CTCGTAGATG AGGGAGTGAT AAGGTACATT GGAGTTAGCA ACTTCAATCT GGAACTTCTC 540
CAGCGCTCCC AGGAGGTCAT GAGGAAGTAT GAGATTGTAG CAAATCAAGT TAAATACTCA 600
GTGAAAGACC GCTGGCCCGA AACTACAGGA CTTCTCGACT ACATGAAGCG TGAAGGAATA 660
GCATTAATGG CGTACACACC TCTAGAAAAG GGAACTCTTG CAAGGAATGA ATGTCTAGCT 720
AAAATTGGAG AAAAATACGG AAAAACAGCT GCTCAAGTGG CTTTAAACTA CCTGATTTGG 780
GAGGAAAATG TTGTAGCAAT TCCAAAAGCA AGCAACAAGG AACACCTCAA AGAAAACTTT 840
GGAGCTATGG GATGGAGGCT TTCAGAGGAG GATAGAGAGA TGGCAAGGAG GTGTGTGTGA 900
```

AdhD Amino Acid Sequence

```
MGSSHHHHHH SSGLVPRGSH MAKRVNAFND LKRIGDDKVT AIGMGTWGIG GRETPDYSRD 60
KESIEAIRYG LELGMNLIDT AEFYGAGHAE EIVGEAIKEF EREDIFIVSK VWPTHFGYEE 120
AKKAARASAK RLGTYIDLYL LHWPVDDFKK IEETLHALED LVDEGVIRYI GVSNFNLELL 180
QRSQEVMRKY EIVANQVKYS VKDRWPETTG LLDYMKREGI ALMAYTPLEK GTLARNECLA 240
KIGEKYGKTA AQVALNYLIW EENVVAIPKA SNKEHLKENF GAMGWRLSEE DREMARRCV 299
```

AdhD Amino Acid Sequence with Mutations Highlighted in Red

```
MGSSHHHHHH SSGLVPRGSH MAKRVNAFND LKRIGDDKVT AIGMGTWGIG GRETPDYSRD 60
KESIEAIRYG LELGMNLIDT AEFYGAGHAE EIVGEAIKEF EREDIFIVSK VWPTHFGYEE 120
```

AKKAARASAK RLGTYIDLYL LHWPVDDFKK IEETLHALED LVDEGVIRYI GVSNFNLELL 180
QRSQEVMRKY EIVANQVKYS VKDRWPETTG LLDYMKREGI ALMAYTPLEK GTLARNECLA 240
KIGEKYGKTA AQVALNYLIW EENVVAIPKA SNKEHLKENF GAMGWRLSEE DREMARRCV 299

Amber stop codon primers:

M1TAG Primers:

FWD: GTGCCGCGCGGCAGCCATTAGGCAAAAAGGGTAAATGCATTCAACGACCTTAAGCGT

REV: ACGCTTAAGGTCGTTGAATGCATTTACCCTTTTTGCCTAATGGCTGCCGCGCGGCAC

Y64TAG Primers:

FWD: TAGGAATGAATTTAATCGACACAGCGGAATTCTAGGGAGCTGGTCATGCTGAGGAAATAG

REV: CTATTTCCTCAGCATGACCAGCTCCCTAGAATTCCGCTGTGTCGATTAAATTCATTCCTA

Y205TAG Primers:

FWD: GAAGCGTGAAGGAATAGCATTAATGGCGTAGACACCTCTAGAAAAGGGAACTCTTGCAAG

REV: CTTGCAAGAGTTCCCTTTTCTAGAGGTGTCTACGCCATTAATGCTATTCCTTCACGCTTC

** mutations highlighted in red in amino acid sequence

Primers for Hydrogels:

Primers to clone HSH and HS-AdhD-H into pET28a(+)

Forward: CCGCGCGGCAGCCATATGGGATCCGATGACGATGACAAATGGGCTAGCGGTGACCTGG

Reverse: AGTCATGCTAGCCATTTAGCAGCCACCCATACTAGTGTCTCGAGGCGCCACATGGTCA

Primers to clone HSH with M1TAG into pET28a(+)

Forward: CCGCGCGGCAGCCATTAGGGATCCGATGACGATGACAAATGGGCTAGCGGTGACCTGG

Reverse: CCAGGTCACCGCTAGCCCATTTGTCATCGTCATCGGATCCCTAATGGCTGCCGCGCGG

DNA Sequences:

HSH:

```
ATGGGCAGCA GCCATCATCA TCATCATCAC AGCAGCGGCC TGGTGCCGCG CGGCAGCCAT 60
ATGGGATCCG ATGACGATGA CAAATGGGCT AGCGGTGACC TGGAAAACGA AGTGGCCCAG 120
CTGGAAAGGG AAGTTAGATC TCTGGAAGAT GAAGCGGCTG AACTGGAACA AAAAGTCTCG 180
AGACTGAAAA ATGAAATCGA AGACCTGAAA GCCGAAATTG GTGACCATGT GGCGCCTCGA 240
GACACTAGCT ATCGCGATCC GATGGGTGCC GGCGCTGGTG CGGGCCCGGA AGGTGCAGGC 300
GCTGGTGCGG GCCCGGAAGG TGCCGGCGCT GGTGCGGGCC CGGAAGGTGC AGGCGCTGGT 360
GCGGGCCCGG AAGGTGCCGG CGCTGGTGCG GGCCCGGAAG GTGCAGGCGC TGGTGCGGGC 420
CCGGAAGGTG CCGGCGCTGG TGCGGGCCCG GAAGGTGCAG GCGCTGGTGC GGGCCCGGAA 480
GGTGCCGGCG CTGGTGCGGG CCCGGAAGGT GCAGGCGCTG GTGCGGGCCC GGAAGGTGCC 540
CGCATGCCGA CTAGCGGTGA CCTGGAAAAC GAAGTGGCCC AGCTGGAAAG GGAAGTTAGA 600
TCTCTGGAAG ATGAAGCGGC TGAACTGGAA CAAAAAGTCT CGAGACTGAA AAATGAAATC 660
GAAGACCTGA AAGCCGAAAT TGGTGACCAT GTGGCGCCTC GAGACACTAG TATGGGTGGC 720
TGCTAA 726
```

HS-AdhD-H:

```
ATGGGCAGCA GCCATCATCA TCATCATCAC AGCAGCGGCC TGGTGCCGCG CGGCAGCCAT 60
ATGGGATCCG ATGACGATGA CAAATGGGCT AGCGGTGACC TGGAAAACGA AGTGGCCCAG 120
CTGGAAAGGG AAGTTAGATC TCTGGAAGAT GAAGCGGCTG AACTGGAACA AAAAGTCTCG 180
AGACTGAAAA ATGAAATCGA AGACCTGAAA GCCGAAATTG GTGACCATGT GGCGCCTCGA 240
GACACTAGCT ATCGCGATCC GATGGGTGCC GGCGCTGGTG CGGGCCCGGA AGGTGCAGGC 300
GCTGGTGCGG GCCCGGAAGG TGCCGGCGCT GGTGCGGGCC CGGAAGGTGC AGGCGCTGGT 360
GCGGGCCCGG AAGGTGCCGG CGCTGGTGCG GGCCCGGAAG GTGCAGGCGC TGGTGCGGGC 420
CCGGAAGGTG CCGGCGCTGG TGCGGGCCCG GAAGGTGCAG GCGCTGGTGC GGGCCCGGAA 480
GGTGCCGGCG CTGGTGCGGG CCCGGAAGGT GCAGGCGCTG GTGCGGGCCC GGAAGGTGCC 540
CGCATGCCGC ATGGAATGGC AAAAAGGGTA AATGCATTCA ACGACCTTAA GCGTATAGGA 600
GATGATAAGG TAACGGCAAT TGGAATGGGA ACATGGGGAA TAGGAGGGAG AGAGACCCCA 660
GACTATTCTA GGGATAAGGA AAGCATAGAA GCAATAAGAT ATGGACTTGA ATTAGGAATG 720
AATTTAATCG ACACAGCGGA ATTCTATGGA GCTGGTCATG CTGAGGAAAT AGTTGGAGAG 780
GCCATTAAAG AATTCGAACG TGAGGACATC TTCATAGTGA GCAAGGTCTG GCCAACTCAC 840
TTTGGGTATG AGGAAGCAAA GAAGGCTGCT AGAGCAAGTG CTAAAAGGTT AGGAACTTAT 900
ATTGACCTTT ATTTGTTGCA CTGGCCCGTT GATGACTTCA AGAAGATAGA GGAGACACTT 960
CACGCTTTGG AAGACCTCGT AGATGAGGGA GTGATAAGGT ACATTGGAGT TAGCAACTTC 1020
AATCTGGAAC TTCTCCAGCG CTCCCAGGAG GTCATGAGGA AGTATGAGAT TGTAGCAAAT 1080
CAAGTTAAAT ACTCAGTGAA AGACCGCTGG CCCGAAACTA CAGGACTTCT CGACTACATG 1140
AAGCGTGAAG GAATAGCATT AATGGCGTAC ACACCTCTAG AAAAGGGAAC TCTTGCAAGG 1200
AATGAATGTC TAGCTAAAAT TGGAGAAAAA TACGGAAAAA CAGCTGCTCA AGTGGCTTTA 1260
AACTACCTGA TTTGGGAGGA AAATGTTGTA GCAATTCCAA AAGCAAGCAA CAAGGAACAC 1320
CTCAAAGAAA ACTTTGGAGC TATGGGATGG AGGCTTTCAG AGGAGGATAG AGAGATGGCA 1380
AGGAGGTGTG TGGGCATGCC GACTAGCGGT GACCTGGAAA ACGAAGTGGC CCAGCTGGAA 1440
AGGGAAGTTA GATCTCTGGA AGATGAAGCG GCTGAACTGG AACAAAAAGT CTCCAGACTG 1500
AAAAATGAAA TCGAAGACCT GAAAGCCGAA ATTGGTGACC ATGTGGCGCC TCGAGACACT 1560
AGTATGGGTG GCTGCTAG 1578
```

Protein Sequences

HSH:

```
MGSSHHHHHH SSGLVPRGSH MGSDDDDKWA SGDLENEVAQ LEREVRSLED EAAELEQKVS 60
RLKNEIEDLK AEIGDHVAPR DTSYRDPMGA GAGAGPEGAG AGAGPEGAGA GAGPEGAGAG 120
AGPEGAGAGA GPEGAGAGAG PEGAGAGAGP EGAGAGAGPE GAGAGAGPEG AGAGAGPEGA 180
RMPTSGDLEN EVAQLEREVR SLEDEAAELE QKVSRLKNEI EDLKAEIGDH VAPRDTSMGG 240
C 241
```

- Initiation methionine (in red) mutated to amber stop codon in M1TAG construct

HS-AdhD-H:

```
MGSSHHHHHH SSGLVPRGSH MGSDDDDKWA SGDLENEVAQ LEREVRSLED EAAELEQKVS 60
RLKNEIEDLK AEIGDHVAPR DTSYRDPMGA GAGAGPEGAG AGAGPEGAGA GAGPEGAGAG 120
AGPEGAGAGA GPEGAGAGAG PEGAGAGAGP EGAGAGAGPE GAGAGAGPEG AGAGAGPEGA 180
RMPHGMAKRV NAFNDLKRIG DDKVTAIGMG TWGIGGRETP DYSRDKESIE AIRYGLELGM 240
NLIDTAEFYG AGHAEEIVGE AIKEFEREDI FIVSKVWPTH FGYEEAKKAA RASAKRLGTY 300
IDLYLLHWPV DDFKKIEETL HALEDLVDEG VIRYIGVSNF NLELLQRSQE VMRKYEIVAN 360
QVKYSVKDRW PETTGLLDYM KREGIALMAY TPLEKGTLAR NECLAKIGEK YGKTAAQVAL 420
NYLIWEENVV AIPKASNKEH LKENFGAMGW RLSEEDREMA RRCVGMPTSG DLENEVAQLE 480
REVRSLEDEA AELEQKVSRL KNEIEDLKAE IGDHVAPRDT SMGGC 525
```

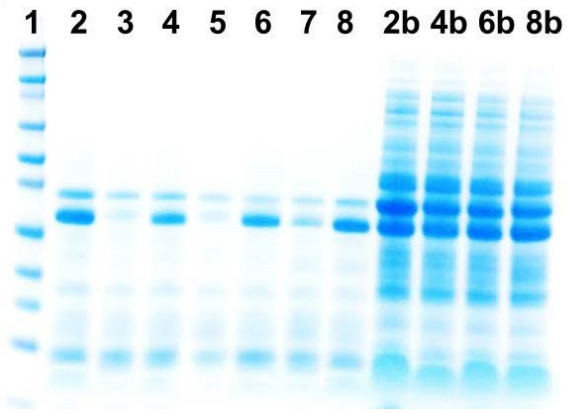

Figure 4.8 SDS-PAGE of AdhD and mutant cell lysates. Samples include M1TAG, Y64TAG, and Y205TAG with and without unnatural amino acid para-azidophenylalanine supplementation after heat treatment at 80 °C and after lysing with BugBuster detergent. 80 °C samples: (1) molecular weight marker, (2) AdhD, (3) M1TAG, (4) UAA labeled M1TAG, (5) Y64TAG, (6) UAA labeled Y64TAG, (7) Y205TAG, (8) UAA labeled Y205TAG. BugBuster samples: (2b) AdhD, (4b) UAA labeled M1TAG, (6b) UAA labeled Y64TAG, (8b) UAA labeled Y205TAG. A distinct band at approximately 34 kDa is observed for AdhD and mutants with UAA, consistent with calculated molecular weights.

Figure 4.9 SDS-PAGE after nickel column purification of AdhD and mutants. Mutants M1TAG, Y64TAG, and Y205TAG supplemented with unnatural amino acid para-azidophenylalanine. Lane 1: molecular weight marker, lane 2: flow-through, lane 3: 75 mM immidizole, lane 4: 100 mM immidizole, lane 5: 150 mM immidizole, lane 6: 300 mM immidizole, lane 7: 400 mM immidizole, lane 8: 500 mM immidizole. Samples were lysed using BugBuster detergent for 20 minutes at room temperature and purified by exploiting the poly-histidine tag at the N-terminus of the proteins. Proteins were eluted off the nickel column with increasing immidizole concentrations. Distinct bands at approximately 34 kDa are observed for AdhD and mutants with UAA, consistent with calculated molecular weights.

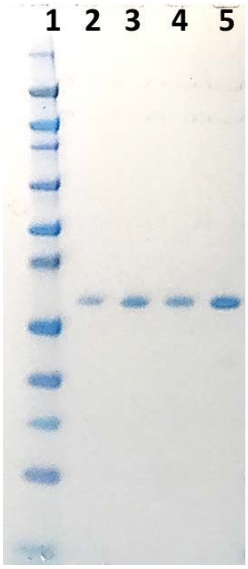

Figure 4.10 SDS-PAGE of AdhD and mutants. Lane 1: molecular weight marker, lane 2: AdhD, lane 3: M1TAG AdhD, lane 4: Y64TAG AdhD, and lane 5: Y205TAG AdhD. Bands are observed at the theoretical molecular weight, 34 kDa.

Figure 4.11 SDS-PAGE of HSH purification on nickel column. HSH and HSH M1TAG with para-azidophenylalanine. Protein was eluted off the column with increasing immidizole concentrations and purified protein boxed in red. Lane 1: molecular weight ladder, Lane 2-8: increasing immidizole concentrations. Protein runs at around 35 kDa, higher than the theoretical molecular weight of 24 kDa.

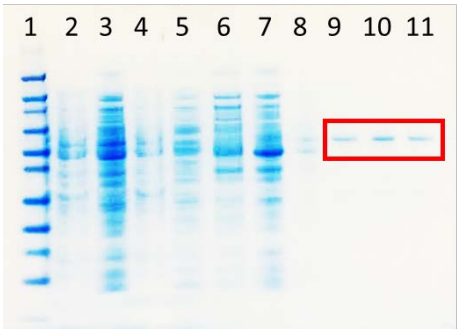

Figure 4.12 SDS-PAGE of HS-AdhD-H purification on nickel column. Protein was eluted off the column with increasing immidizole concentrations and purified protein boxed in red. Lane 1: molecular weight ladder, Lane 2-11: increasing immidizole concentrations. Band observed at 56 kDa, consistent with theoretical molecular weight.

Table 4.2 Specific activities of alcohols with AdhD

Alcohol	Specific Activity (μmol min^{-1} mg^{-1}) x 10^{-2}
1-propanol	0.32 ± 0.08
1-butanol	0.76 ± 0.14
1-pentanol	1.3 ± 0.6
1-hexanol	0.67 ± 0.09
2-propanol	1.2 ± 0.3
2-butanol	4.0 ± 0.7
2-pentanol	14 ± 2.0

2-hexanol	7.8 ± 0.9
2,3-butanediol	130 ± 4
L-arabinose	5 ± 0.2
D-arabinose	78 ± 10
D-Glucose	0.43 ± 0.04
Methanol	0.33 ± 0.02
Ethanol	0.19 ± 0.04

hAR AdhD DNA Sequence

```
ATGGGCAGCA GCCATCATCA TCATCATCAC AGCAGCGGCC TGGTGCCGCG CGGCAGCCAT 60
ATGGCAAAAA GGGTAAATGC ATTCAACGAC CTTAAGCGTA TAGGAGATGA TAAGGTAACG 120
GCAATTGGAA TGGGAACATG GGGAATAGGA GGGAGAGAGA CCCCAGACTA TTCTAGGGAT 180
AAGGAAAGCA TAGAAGCAAT AAGATATGGA CTTGAATTAG GAATGAATTT AATCGACACA 240
GCGGAATTCT ATGGAGCTGG TCATGCTGAG GAAATAGTTG GAGAGGCCAT TAAAGAATTC 300
GAACGTGAGG ACATCTTCAT AGTGAGCAAG GTCTGGCCAA CTCACTTTGG GTATGAGGAA 360
GCAAAGAAGG CTGCTAGAGC AAGTGCTAAA AGGTTAGGAA CTTATATTGA CCTTTATTTG 420
TTGCACTGGC CCACCGGCTT CAAACCAGGC AAAGAGTTCT TTCCGCTGGA TGAAAGCGGT 480
AACGTGCCGT CGGACAAGAA GATAGAGGAG ACACTTCACG CTTTGGAAGA CCTCGTAGAT 540
GAGGGAGTGA TAAGGTACAT TGGAGTTAGC AACTTCAATC TGGAACTTCT CCAGCGCTCC 600
CAGGAGGTCA TGAGGAAGTA TGAGATTGTA GCAAATCAAG TTAAATACTC AGTGAAAGAC 660
CGCTGGCCCG AAACTACAGG ACTTCTCGAC TACATGAAGC GTGAAGGAAT AGCATTAATG 720
GCGTACACAC CTCTAGAAAA GCCGGATCGC CCGTGGGCGA AACCGGAAGA CCCGTCTCTT 780
GCAAGGAATG AATGTCTAGC TAAAATTGGA GAAAAATACG GAAAAACAGC TGCTCAAGTG 840
GCTTTAAACT ACCTGATTTG GGAGGAAAAT GTTGTAGCAA TTCCAAAAGC AAGCAACAAG 900
GAACACCTCA AAGAAAACTT TGGAGCTATG GGATGGAGGC TTTCAGAGGA GGATAGAGAG 960
ATGGCAAGGA GGTGTGTGTG A 981
```

hAR AdhD Protein Sequence

```
MGSSHHHHHH SSGLVPRGSH MAKRVNAFND LKRIGDDKVT AIGMGTWGIG GRETPDYSRD 60
KESIEAIRYG LELGMNLIDT AEFYGAGHAE EIVGEAIKEF EREDIFIVSK VWPTHFGYEE 120
AKKAARASAK RLGTYIDLYL LHWPTGFKPG KEFFPLDESG NVPSDKKIEE TLHALEDLVD 180
EGVIRYIGVS NFNLELLQRS QEVMRKYEIV ANQVKYSVKD RWPETTGLLD YMKREGIALM 240
AYTPLEKPDR PWAKPEDPSL ARNECLAKIG EKYGKTAAQV ALNYLIWEEN VVAIPKASNK 300
EHLKENFGAM GWRLSEEDRE MARRCV 326
```

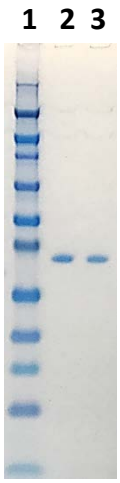

Figure 4.13 SDS-PAGE of hAR AdhD and Y64TAG hAR AdhD. (1) Molecular weight marker, (2) hAR AdhD, and (3) Y64TAG AdhD.

Figure 4.14 SDS PAGE of azide-alkyne cycloaddition with hAR AdhD. Protein gel exposed to UV light after copper-catalyzed azide-alkyne cycloaddition between hAR AdhD containing unnatural amino acid para-azidophenylalanine and fluorescent alkyne, tetramethylrhodamine (TAMRA). Lane: (1) molecular weight ladder, (2) hAR AdhD, and (3) UAA labeled Y64TAG.

CHAPTER 5

ENGINEERING THE MICROENVIRONMENT OF A THERMOSTABLE ALCOHOL DEHYDROGENASE VIA FUSION WITH SUPERCHARGED PROTEINS IMPROVES CATALYSIS

Project Collaborators: Walaa Abdallah, Vanessa Chirino, Ian Wheeldon, and Scott Banta

WA was responsible for molecular cloning and enzyme work, including protein expression, protein purification, unnatural amino acid incorporation, and enzyme kinetics with help from Vanessa.

5.1 Abstract

The chemical microenvironment near the active site of an enzyme can impact biocatalytic activity, however these effects can be difficult to investigate as mutations and fusions made near enzymatic active sites can introduce multiple variables and overlapping effects. Here we investigate the complexes made between the thermostable alcohol dehydrogenase D (AdhD) from *Pyrococcus furiosus* and superfolding green fluorescent protein (sfGFP) mutants that have extreme surface charges. Three charged sfGFP variants, -30, 0, and +36 were covalently attached to AdhD via the SpyCatcher/SpyTag system. Specific rates for the conversion of 2,3-butanediol and NAD^+ to acetoin and NADH were significantly increased in the -30 sfGFP complex, a mixed effect was seen for the 0 sfGFP complexes and the rates were unaffected by +36 sfGFP complexation. The effects of varying pH (7.8, 8.8 and 9.8) and salt (7.75 mM, 200 mM and 500mM) showed that there was a complex interplay between these effects which was consistent with fusion proteins affecting the local ionic strength near the AdhD active site as opposed to the local pH. A more complete steady state kinetic analysis was performed with of -30 and 0 AdhD-sfGFP complexes. The apparent k_{cat} and K_M parameters were affected by both salt and pH, but the overall catalytic efficiency was dependent on the charge of the fused sfGFP variant, and the -30 sfGFP fusions exhibited the largest beneficial effects at pH 8.8. The fusion of a supercharged protein is a facile means to alter the biocatalytic microenvironment of an enzyme and this approach could be used in *in vivo* catalytic cascades. The impact of the fusion protein on the apparent ionic strength of the active enzyme provides further insight into the potential effects charged patches observed on many metabolon forming complexes and has implications in our understanding of substrate channeling mechanisms.

5.2 Introduction

There have been decades of protein engineering research efforts aimed towards altering the active sites of enzymes to enhance catalytic performance [128-130]. Amino acid substitutions are frequently explored to alter the active site chemistry leading to changes in binding affinities, binding specificities, catalytic activities, and overall molecular stabilization. For example, site-directed mutations made in the cofactor binding pocket of the thermostable alcohol dehydrogenase D (AdhD) from *Pyrococcus furiosus* [11] were explored to broaden its cofactor specificity from NADH to enable activity with NADPH [17]. These mutations focused on interactions with the 2'-phosphate group of NADP(H). In a complimentary approach, amino acid mutations were made on the other side of the cofactor binding pocket, distal to the phosphate group in NADP(H), and this also resulted in broadened cofactor specificity [25]. These types of studies demonstrate the power of protein engineering, where mutations can be frequently found to create enzymes with improvements in reactant binding and/or transition state stabilization, leading to enhanced catalytic performance. However, a limitation of this approach is that it is time consuming and the engineering must generally be performed on a case by case basis for each new enzyme. Therefore, there is interest in developing strategies to potentially enhance enzyme performance characteristics without needing to perform a mutational analysis for every protein.

There has been recent interest in exploring the engineering of the enzyme microenvironments as a means to enhance catalytic activity. Protein immobilization efforts have demonstrated that the chemical environment of the supporting medium could influence biocatalytic activity [131-133]. Protein immobilization has been frequently investigated on charged resins to exploit electrostatic/ionic interaction with oppositely charged proteins [134]. For example, the immobilization of amyloglucosidase has been explored on cationic resins and when

amyloglucosidase conjugated to negative copolymers was immobilized, the enzyme was stabilized at higher temperatures, however the activity was found to decrease [135]. When invertase was immobilized on a DOWEX resin, the K_M of the enzyme was unaffected but an increase in the maximum velocity was reported [136]. The immobilization of enzymes on charged materials may result in the useful modulation of the local chemical microenvironment during *in vitro* biotransformations, however this approach will be limited for other applications including *in vivo* use.

Several molecular-scale approaches to modulating the microenvironment have also been reported which have led to desirable impacts on catalytic activity. The local pH of an active site is thought to be an important factor in the enzyme microenvironment as enzymatic activity is often pH-dependent. This effect has been used as an explanation for increased activity in the glucose oxidase (GOx)–horseradish peroxidase (HRP) cascade upon immobilized on a DNA scaffold [65]. The presence of the DNA reduces the local pH near the active sites, allowing the enzymes to operate closer to their optimal values. A similar effect was observed for a D-amino acid oxidase (DAAO) and Cytochrome C (Cyt c) cascade [137]. DAAO is active at alkaline pH values, while Cyt c is active at more acidic pH values. When a negative polyelectrolyte was fused to Cyt c, the local pH decreased which supported increased activity. Another means to modulate the catalytic microenvironment is through altering protein conformation. This was observed when a repeats-in-toxin (RTX) domain from the adenylate cyclase protein from *Bordetella pertussis* was inserted into a substrate binding look of AdhD [26]. The RTX domain is disordered in the absence of calcium and folds into the β-roll secondary structure upon calcium addition [138]. The fusion protein, β-AdhD, preferred $NADP^+$ in the presence of calcium and NAD^+ in the absence of calcium, which allows for tunable regulation of cofactor selectivity via addition of calcium as an

uncompetitive inhibitor. The microenvironment of an active site can also be modified to increase the local concentration of substrates. By concentrating reactants near the enzyme higher reaction rates can be achieved. This was observed with a modified version of AdhD that can accept nicotinamide mononucleotide NMN(H) as a cofactor [139]. dsDNA has a micromolar affinity for nicotinamide mono nucleotide (NMN(H)) so when dsDNA strands were conjugated to AdhD, the local concentration of NMN^+ was increased, enhancing the overall activity of the enzyme with this non-natural cofactor. A recently published review article discusses other approaches in engineering the microenvironment of enzymes [1].

In this report, we explore the fusion of supercharged proteins as a means to alter the microenvironment of an enzyme. We use the thermostable AdhD from *Pyrococcus furiosus* as a model enzyme (**Figure 5.1A**). AdhD is a monomeric member of the aldo-keto reductase superfamily and has the ability reversibly convert alcohols to aldehydes/ketones along with the concomitant reduction of $NAD(P)^+$ to NAD(P)H [11, 12]. It is enantioselective, highly thermostable, and has broad substrate specificity making it an interesting and useful potential industrial catalyst. The native enzyme has the highest activity with 2,3-butanediol which, in the presence of NAD^+, is converted to acetoin and NADH following an ordered bi-bi kinetic mechanism with the cofactor binding first [17, 18]. AdhD has been engineered to exhibit broadened cofactor specificity [17, 25], altered substrate specificity [19], activity with the non-natural cofactor NMN(H) [20], binding of a small molecule explosive molecule [140], and it has been engineered to form self-assembling catalytic hydrogels [18]. In order to rationally alter the microenvironment of AdhD without making site-directed mutations in the enzyme, we explored the fusion of the wild type enzyme to supercharged superfolder green fluorescent (sfGFP) proteins.

The supercharged sfGFP collection provides a set of well-characterized molecules that are structurally similar, yet have a wide range of calibrated surface charges (**Figure 5.1B**) [61]. The wild type GFP from *Aequorea victoria* consists of 11 β-strands wrapped around a central helix (PDB 1EMA) [56]. Several mutations have been made to enhance expression, folding and fluorescence [57]. The superfolder variant was used to create supercharged versions, where surface mutations were made, leading to remarkable increases in stability [61]. Here we explored a neutral GFP variant along with a mutant with 30 negative surface charges (-30) and a mutant with 36 positive charges (+36). The effective functional surface charge will depend on the solution pH.

We hypothesized that fusions of the supercharged sfGFP proteins to AdhD would lead to altered microenvironments, producing to altered kinetic activities. The nicotinamide cofactor NAD(H) is negatively charged and the AdhD enzyme has been reported to have an alkaline pH-optimum in the oxidative direction. Therefore, altering the charge near the active site should present an opportunity to enhance activity without making site directed mutations in the active site. To make the protein fusions, the SpyCatcher protein/SpyTag peptide system [141] (**Figure 5.1C**) was used to form a covalent bond between AdhD and sfGFP. This leads to the formation of tri-domain proteins where the sfGFP proteins and AdhD are fused by the SpyCatcher/SpyTag protein bridges (**Figure 5.1D**). The effects of different charges on the sfGFP on the kinetics of AdhD were explored and it was found that the addition of the negative charges leads to significant improvements in AdhD activity as compared to fusions made with the neutral and positively charged GFP and effects of salt and pH on this system was also explored.

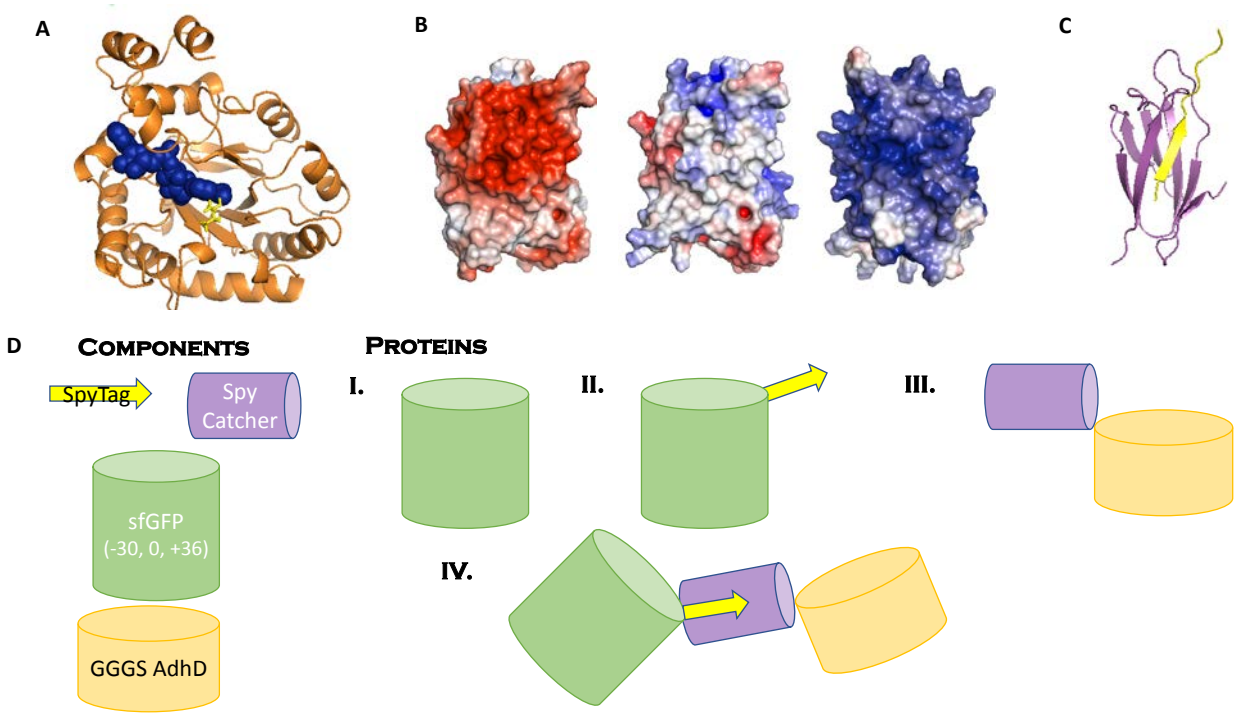

Figure 5.1 Structures of AdhD, sfGFP, and SpyTag/SpyCatcher. (A) Homology model of AdhD looking down the barrel with NAD^+ in blue and 2,3-butanediol in yellow. (B) Electrostatic surface potentials of -30, 0, and +36 sfGFP (PDB ID 2B3P). (C) SpyCatcher/SpyTag with catcher in purple and tag in yellow (PDB ID 4MLI). (D) Schematic of SpyCatcher-AdhD and SpyTag-sfGFP complexes.

5.3 Materials and Methods

5.3.1 Materials

DNA Oligonucleotides and ultramers were purchased from Integrated DNA Technologies (Coralville, IA). Phusion high fidelity DNA polymerase, Hi-Fi DNA assembly Master Mix, Q5 site-directed mutagenesis kit, and *E. coli* BL21(DE3) expression cells were from New England Biolabs (Ipswich, MA). In-Fusion cloning kit was from Takara Bio (Mountain View, CA). NuPAGE SDS-PAGE gels, MOPS running buffer, and Novex sharp pre-stained protein standards were from Invitrogen (Carlsbad, CA). Histidine purification Nickel-NTA resin was purchased from ThermoFisher Scientific (Waltham, MA). Chromatography columns were from Bio-Rad

(Hercules, CA). Molecular weight centrifugal filters were from EMD Millipore (Billerica, MA). All other chemicals, including kanamycin, were from Sigma Aldrich (St. Louis, MMO).

5.3.2 Cloning, Expression, Purification

Plasmids encoding for -30 and +36 sfGFP from jellyfish *Aequorea victoria* were a kind gift from the laboratory of David R. Liu [61] while the 0 sfGFP gene was a kind gift from the laboratory of Allie Obermeyer. A plasmid encoding the SpyCatcher gene was a kind gift from the laboratory of David Baker. The genes corresponding to sfGFPs flanked by SpyTag at their C-termini were produced by cloning into the *Hind III* linearized pET-28a(+) vector using ultramers containing the C-terminus sequence of sfGFP followed by the SpyTag sequence (see Supporting Information). This resulted in constructs -30 sfGFP SpyTag, 0 sfGFP SpyTag, and +36 sfGFP SpyTag. The genes were verified by DNA sequencing (complete sequences can be found in Supporting Information). The final charges on the sfGFP mutants were increased by 3 upon addition of the polyhistidine purification tag and thrombin site, artifacts of the cloning, and the SpyTag sequence.

Control sfGFP proteins lacking the C-terminal SpyTag, were prepared via site-directed mutagenesis by designing primers to insert a stop codon before the SpyTag (primers can be found in Supporting Information). This resulted in constructs -30, 0, and +36 sfGFP.

The sfGFP expression plasmids were transformed into *E. coli* BL21(DE3) cells and plated onto Luria Broth (LB) plates supplemented with 0.035 mg/ml kanamycin. Single colonies were inoculated overnight in LB media with 0.035 mg/ml kanamycin and kept shaking at 200 rpm at 37 °C. Expression was performed at 37 °C in the same media. Once the OD_{600} reached approximately 0.6, the cells were induced with 0.5 mM isopropyl β-D-1-thiogalactopyranside (IPTG) and kept shaking at 200 rpm at 25 °C overnight.

The cells were harvested and resuspended in 10 mM tris pH 7.5 with 1 M NaCl and sonicated. The crude lysate was then incubated at 70 °C for 10 minutes followed by centrifugation at 7000xg for 1 hour. The clarified lysate was loaded onto a pre-packed column containing nickel resin equilibrated with the resuspension buffer. The lysate with the resin was continuously rotated at 4 °C for 30 minutes. Following the collection of the flow-through, the column was washed with 10 column volumes of wash buffer (resuspension buffer with 20 mM immidizole, pH 7.5). The protein was eluted from the column with 500 mM immidizole.

Samples were loaded onto NuPAGE SDS-PAGE 4-12% Bis-tris gels in MES running buffer. Fractions containing protein greater than 95% pure were pooled together and briefly concentrated in 10 kDa MWCO filters. They were then dialyzed in 20 kDa MWCO cassettes in 50 mM glycine pH 8.8.

The *AdhD* gene from *Pyrococcus furiosus* in the pET-20b(+) vector, plasmid pWUR85, was cloned into the *NdeI*-digested pET-28a(+) vector (primers can be found in Supporting Information) [12]. The resulting plasmid (pET28a-AdhD), with a poly-histidine tag and the thrombin site, was verified by DNA sequencing (see Supporting Information).

To clone in SpyCatcher, the pET28a-AdhD plasmid was linearized via PCR prior to the initiation methionine of AdhD, between His20 and Met21 (primers can be found in Supporting Information). The SpyCatcher gene was amplified using PCR with another set of primers to clone it in at the N-terminus of AdhD (primers can be found in Supporting Information), resulting in pET28a-SpyCatcher-AdhD plasmid. A construct was also made with a short linker region (GGGS) inserted between the C-terminus of SpyCatcher (Ile136) and the N-terminus of AdhD (Met137) (primers can be found in Supporting Information), resulted in the pET28a-SpyCatcher-GGGS-AdhD plasmid (final sequences can be found in Supporting Information).

The pET28a-SpyCatcher-AdhD and pET28a-SpyCatcher-GGGS-AdhD plasmids were transformed into *E. coli* BL21(DE3) expression cells and plated onto Luria Broth (LB) plates supplemented with 0.035 mg/ml kanamycin. A single colony was inoculated overnight in LB supplemented with kanamycin. This was expressed at 37 ºC in a 1 L flask containing LB with 0.035 mg/ml kanamycin. When the cells reached an OD of approximately 0.6, they were induced with 0.5 mM IPTG and kept shaking at 37 ºC overnight.

Cells containing pET28a-SpyCatcher-AdhD were harvested in 20 mM tris-HCl (pH 7.8) buffer with 100 mM NaCl and lysed at 80 ºC for 1 hour to denature endogenous proteins. Crude lysate was spun down at 7000xg for 1 hour to remove cell debris. The clarified lysate was then concentrated in 30 kDa MWCO centrifugation filters. This was purified via gel filtration chromatography on a Superdex 16/200 (GE Healthcare, Piscataway, NJ) column using the lysis buffer. Samples were collected, and purity was ensured by running NuPAGE 4-12% Bis-tris gels in MES running buffer (Invitrogen). Samples containing protein greater than 95% pure was pooled together, concentrated in 30 kDa MWCO filters, and buffer exchanged into 50 mM glycine pH 8.8.

Cells containing pET28a-SpyCatcher-GGGS-AdhD were harvested and resuspended in 20 mM sodium phosphate buffer with 500 mM NaCl, pH 7.5. The cells were sonicated and centrifuged at 7000xg for 1 hour to remove cell debris. The clarified lysate was loaded onto a prepacked Ni column equilibrated with 20 mM Tris with 200 mM NaCl, pH 7.4. Following the collection of the flow-through, the column was washed with 4 column volumes of 20 mM sodium phosphate buffer with 500 mM NaCl, pH 7.5. The protein was then eluted off the column with steps of imidazole ranging from 50 to 500 mM imidazole, pH 7.5. Samples were loaded onto NuPAGE SDS-PAGE 4-12% Bis-tris gels in MES running buffer (Invitrogen). Fractions

containing protein with greater than 95% purity were pooled together and concentrated in 30 kDa MWCO filters and buffer exchanged into 50 mM glycine pH 8.8.

SpyCatcher-AdhD and SpyCatcher-GGGS-AdhD protein concentrations were determined by absorbance 280 nm on a SpectraMax M2 plate reader using an extinction coefficient of 63,955 M^{-1} cm^{-1} [142].

5.3.3 Determining sfGFP/ sfGFP SpyTag Concentrations

Spectral absorbance scans of different sfGFP proteins (in 50 mM glycine pH 8.8) were measured from 250 to 600 nm at 5 nm increments in triplicate and background was subtracted, revealing, an absorbance maximum of 485 nm, similar to what has been previously reported [61]. Beer's Law can be used to determine the protein concentration from the absorbance at 485 nm, however the extinction coefficient at 485 nm is needed. Using the ratio of the absorbance values at 485 nm and 280 nm, as well as the extinction coefficient at 280 nm (determined from ExPASy, 19,035 $M^{-1}cm^{-1}$ for sfGFP and 20,525 $M^{-1}cm^{-1}$ for sfGFP SpyTag) [142], the extinction coefficient at 485 nm can be calculated using equation 5.1 [143].

$$\varepsilon_{p,485\ nm} = \varepsilon_{p,280\ nm}\left(\frac{A_{p,485\ nm}}{A_{p,280\ nm}}\right) \tag{5.1}$$

To confirm the accuracy of the measurements, protein concentrations were normalized and the samples were scanned from 280 to 600 nm in triplicate. The absorbances at 485 nm were confirmed to be within 10% of each other (**Figure 5.6**). Equal concentrations of the sfGFP variants (-30, 0, and +36) were also run on NuPAGE 4-12% Bis-tris gels to ensure equal purity and concentration (**Figure 5.7**). The sfGFP-SpyTag proteins were treated similarly.

5.3.4 Complexation of sfGFP SpyTag and SpyCatcher-GGGS-AdhD

Equal concentrations of sfGFP or sfGFP-SpyTag and SpyCatcher-GGGS-AdhD were incubated together in the presence of 387.5 mM NaCl and 10 mM tris pH 7.5. Samples were vortexed and placed in a rotator at 4 °C overnight. Samples run on NuPAGE SDS-PAGE 4-12% Bis-tris gels in MES running buffer to follow the formation of a covalent bond between sfGFP-SpyTag and SpyCatcher-GGGS-AdhD and to ensure equal concentrations of the complexes were formed between the different charged sfGFP.

5.3.5 Kinetic Assays

Enzymes samples were taken directly from the complexation reaction for the kinetic assays to ensure equal concentration of SpyCatcher-GGGS-AdhD and each supercharged sfGFP. For specific rate data, equal concentrations from each reaction (between SpyCatcher-GGGS-AdhD and charged sfGFP tagged and untagged) was incubated with 50 mM glycine buffer and 100 mM substrate (2,3-butanediol) in 96-well plates at 45 °C for 15 minutes. Following incubation, 100 µM NAD^+ was added and absorbance at 340 nm was monitored. For pH studies, glycine buffers and 2,3-butanediol stocks were made at different pH values: 7.8, 8.8 or 9.8. For the salt studies, 1 M NaCl stocks were made in various 50 mM glycine buffers (pH 7.8, 8.8, and 9.8). The final reaction volume in the well was 250 µL. Initial rate data for the oxidation reaction was obtained by only using data within 10% of the conversion of NAD^+. Absorbance at 340 nm was converted to cofactor concentration ($\varepsilon = 6.22\ mM^{-1}\ cm^{-1}$) and the rates were divided by enzyme concentration to determine initial specific rates. All measurements were made in at least triplicate.

To determine the ordered bi-bi kinetic parameters of the different proteins, enzyme (SpyCatcher-GGGS-AdhD, -30 sfGFP-SpyTag + SpyCatcher-GGGS-AdhD, or 0 sfGFP-SpyTag + SpyCatcher-GGGS-AdhD) was incubated in 50 mM glycine buffer pH 7.8 or 8.8 with either

7.75 mM or 200 mM NaCl with substrate (2,3-butanediol) ranging from 2 to 30 mM. Following incubation, 1 to 200 µM NAD^+ was added bringing the final reaction volume to 250 µL. Initial rate data for the oxidation reaction was obtained by only using data within 10% of the conversion of NAD^+. Absorbance at 340 nm was converted to cofactor concentration and divided by enzyme concentration to determine initial specific rates. All measurements were made in at least triplicate.

5.3.6 Kinetic Rate Data Fitting

Kinetic parameters for simplified ordered bi-bi kinetic rate equation (5.3) were determined using nonlinear regression and least-squares in MATLAB. Parameters are reported with 95% confidence intervals.

5.3.7 Statistical Analysis

Three-way analysis of variance (ANOVA), two-factor interactions, and post-hoc analyses were done using MATLAB. To perform 3-way ANOVA with replicate for the simplified ordered bi-bi rate equation, individual data sets were used to determine three sets of parameters at one set of conditions (**Table 5.3**) and these values were used in the statistical analysis. Averages of the individual fits were confirmed to be similar to the global fit (**Table 5.4**). Student's t-test was completed using Microsoft Excel. Statistical significance was indicated by $p < 0.05$.

5.4 Results and Discussion

5.4.1 Expression and Purification of sfGFP, sfGFP SpyTag, and SpyCatcher-GGGS-AdhD

Supercharged sfGFP mutants (-30, 0 and +36) were expressed with and without an N-terminal SpyTag, resulting in 33 kDa proteins. The AdhD gene was expressed with an N-terminal

SpyCatcher domain, resulting in a 47 kDa protein. All of the proteins were expressed and purified to greater than 95% purity as seen on SDS-PAGE (**Figure 5.7**, **Figure 5.8**, and **Figure 5.9**).

5.4.2 Effect of SpyCatcher on AdhD Activity

To determine the effect of the SpyCatcher fusion on AdhD activity, kinetic assays with 100 mM 2,3-butanediol and 100 µM NAD^+ were conducted. Initial rate data was used to determine specific rates for the oxidation reaction (**Table 5.1**). The kinetic activity of the protein under these conditions with the SpyCatcher on the N-terminus was an order of magnitude lower than the wild type enzyme.

To obtain activity comparable to the wild type AdhD enzyme, a Gly-Gly-Gly-Ser (GGGS) linker was inserted between SpyCatcher and AdhD. The insertion of the linker reduced the fusion-induced inhibition, resulting in an order of magnitude increase in activity, making the difference in the specific rates between SpyCatcher-GGGS-AdhD and wild type AdhD insignificant by Student's t-test. Thus, the linker domain was included between SpyCatcher and AdhD in all subsequent experiments.

Table 5.1 Specific rate of AdhD and SpyCatcher-AdhD Variants. Rates collected from the oxidation reaction with 100 mM 2,3-butanediol and 100 µM NAD^+

Protein	Specific Rate (1/s)
AdhD	0.34 ± 0.01
SpyCatcher-AdhD	0.025 ± 0.002
SpyCatcher-GGGS-AdhD	0.39 ± 0.08

All data were collected in at least triplicate. Errors bars represent standard deviation.

5.4.3 Effect of Salt on sfGFP SpyTag and SpyCatcher-GGGS-AdhD Conjugation Reaction

Spectral scans of sfGFP proteins indicate a maximum absorbance at 485 nm (**Figure 5.6**), similar to previous reports [61]. Absorbance at 485 nm can be used as an indicator of the fluorescent protein concentration [144]. SDS-PAGE of normalized protein concentrations at 485 nm shows sfGFP variants with comparable concentrations (**Figure 5.7**). Normalizing proteins at this absorbance also showed similar absorbances at 280 nm, which is indicative of the total protein present, suggesting highly pure samples [144].

Mixing equimolar sfGFP-SpyTag proteins with SpyCatcher-GGGS-AdhD overnight at 4 ºC resulted in incomplete covalent bond formation (**Figure 5.8A**). The reaction with -30 sfGFP-SpyTag was unsuccessful, 0 sfGFP-SpyTag went to completion, and +36 sfGFP-SpyTag was partially reacted. The fact that the proteins with surface charge were less successful suggests a charge effect on the SpyTag/SpyCatcher reaction. To shield the charges, the reaction was repeated in the presence of approximately 400 mM NaCl. The reactions went to apparent completion in all three cases with SpyCatcher-GGGS-AdhD being fully consumed resulting in the formation of sfGFP-SpyTag/SpyCatcher-GGGS-AdhD and excess sfGFP-SpyTag (**Figure 5.8B**). SDS-PAGE analysis of the proteins suggested a similar concentration of SpyTag-SpyCatcher in all three cases. The same reactions were repeated with sfGFP without the SpyTag and no apparent complexes were formed, as expected (**Figure 5.9**).

5.4.4 Effect of Salt and pH on SpyCatcher-GGGS-AdhD Activity and Effect of pH on Net Charge of SpyCatcher-GGGS-AdhD and sfGFP-SpyTag

Previous work with AdhD has shown that the optimal pH for the oxidation of alcohols is pH 8.8 [12]. SpyCatcher-GGGS-AdhD activity was evaluated with 100 mM 2,3-butanediol and 100 µM NAD^+ with 0 – 500 mM NaCl at the reported optimal pH (**Figure 5.2A**). The addition of salt increased the specific rates until a maximum value was obtained at 125 mM NaCl. At higher salt concentrations the rates were found to plateau followed by a downward trend at the highest salt concentration of 0.5 M.

To test the effect of pH on SpyCatcher-GGGS-AdhD, additional assays were performed at one unit above and one unit below the optimal of 8.8 (**Figure 5.2B**). The specific activity with 7.75 mM NaCl was found to increase as the pH increased. Therefore, the observed optimal pH at low salt is pH 9.8 or higher. The same assay was repeated with 200 mM NaCl. Here, the rates at pH 7.8 and 8.8 were increased while at pH 9.8 a decrease was observed. The specific rates at each pH were significantly different from one another, with pH 8.8 being the optimal, as previously reported. Assays were performed at 500 mM NaCl, and the rate at pH 9.8 was again decreased compared to the lower salt concentrations, resulting in pH 8.8 being the optimal pH. The rates at the different pH values at the same salt concentration were significantly different by Student t-test. These results demonstrate a previously unreported interplay between salt and pH where an increase in ionic strength leads to a reduction in the pH-optima of the enzymatic activity (**Figure 5.2C**). Or conversely, the effect of salt on the activity at a given pH transitions from enhancing at low pH to inhibitory at high pH (**Figure 5.2B**).

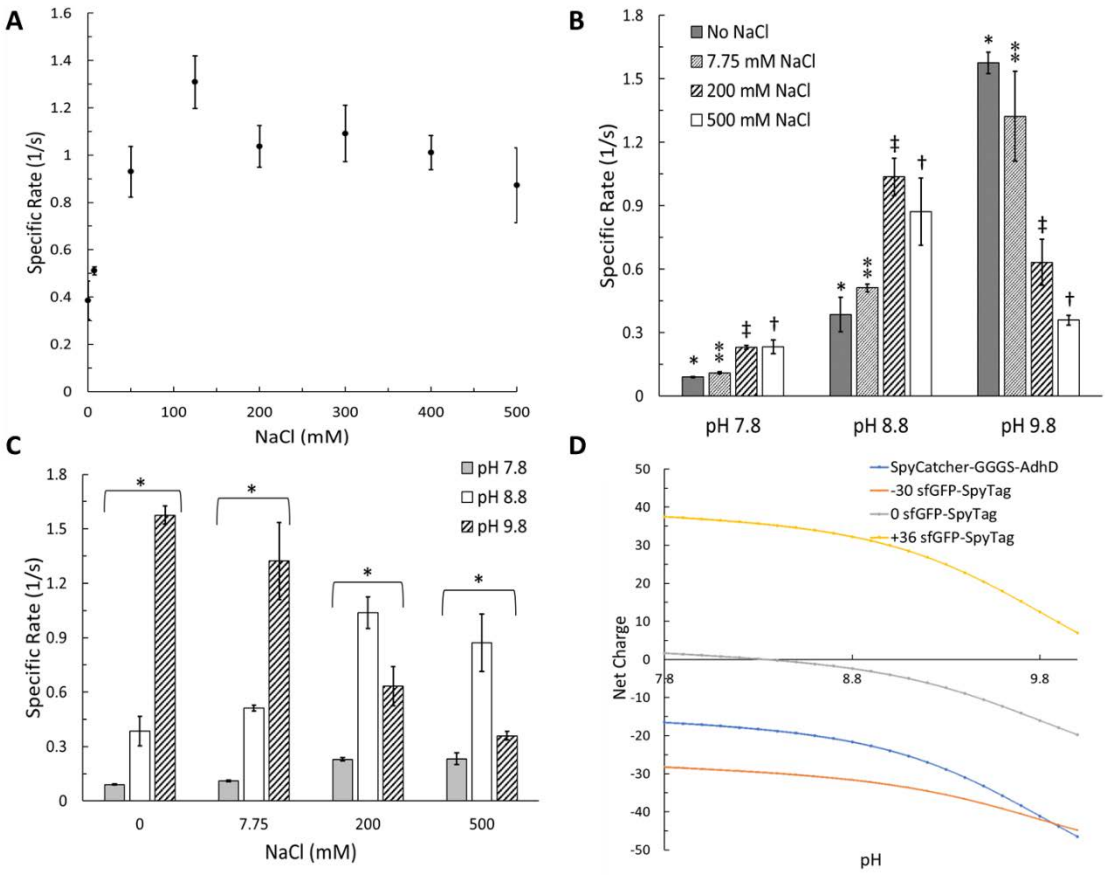

Figure 5.2 Specific rates for SpyCatcher-GGGS-AdhD with 100 mM 2,3-butanediol and 100 µM NAD^+. Assay performed at: (a) pH 8.8 as a function of varying salt concentrations, (b) varying salt as a function of pH and (c) varying pH as a function of salt. Statistically significant differences by Student's t-test denoted with * , ‡, and † ($p < 0.05$). (d) Net charge of SpyCatcher-GGGS-AdhD and sfGFP-SpyTag as a function of pH.

Along with changes in activity, pH also affects the net charge of SpyCatcher-GGGS-AdhD and sfGFP-SpyTag (**Figure 5.2D**). At pH 7.8, close to physiological pH, SpyCatcher-GGGS-AdhD has a net charge of approximately -17, while the sfGFP variants have a net charge approximately equivalent to the net charge calculated from the positive and negative residues. As the pH increases to 8.8, each protein is slightly more negative. This results in sfGFP-SpyTag variants with charges of -32, -2, and +32 and SpyCatcher-GGGS-AdhD with a net charge of -22.

As the pH increases to 9.8, the trend of becoming more negative continues, but the change is more drastic. SpyCatcher-GGGS-AdhD and -30 sfGFP have a net charge of approximately -41 while 0 sfGFP is now -16 and +36 sfGFP is 13. Therefore, as the pH increases, side chains are deprotonated resulting in a more negative net charge. From pH 7.8 to 9.8, 0 sfGFP attains a negative net charge, SpyCatcher-GGGS-AdhD and -30 stay negative while +36 remains positively charged.

5.4.5 Effect of sfGFP Complexation on AdhD Specific Activity

Kinetic rate experiments were performed in the presence of 100 mM 2,3-butanediol (substrate) and 100 µM NAD^+ (cofactor) and initial rates were collected to determine the effect of the charged sfGFP complexation on AdhD activity. The enzyme samples were added directly from the complexation reaction mixtures without further purification to ensure equal concentrations of active enzyme, SpyCatcher-GGGS-AdhD. Studies were performed with tagged and untagged sfGFP to determine the effect of the covalent bond formation on the catalytic efficiency.

Assays were first performed at pH 8.8, the reported optimal pH for the oxidation reaction [12] in the presence of 200 mM NaCl (**Figure 5.3D-F**). The conjugation of -30 sfGFP to the AdhD enzyme led to a significant increase in activity at 7.75 mM NaCl as compared to the untagged and mixed sfGFP control (**Figure 5.3D**). At higher NaCl concentrations, the rates for both the conjugated complexes and unconjugated mixtures significantly increased compared to 7.75 mM NaCl, but their differences between the conjugated and unconjugated proteins were statistically insignificant by a paired t-test. This increase in activity upon the addition of salt is similar to SpyCatcher-GGGS-AdhD at the same conditions **(Figure 5.2B**). The 0 sfGFP complex samples at pH 8.8 follow the same trend as both -30 sfGFP complexes and SpyCatcher-GGGS-AdhD, with an increase in rate upon salt addition followed by a slight decrease at the higher salt concentration

(**Figure 5.3E**). Like -30 sfGFP, AdhD conjugated with 0 sfGFP is significantly more active than the mixed proteins at 7.75 mM NaCl. However, the mixed versions are significantly more active than the conjugates at 200 and 500 mM NaCl. The +36 sfGFP samples followed a similar trend, however, none of the activities between the conjugated and mixed control versions reached statistical significance by a paired t-test (**Figure 5.3F**).

At pH 8.8, the complexation of -30 GFP and 0 GFP to AdhD appears to be similar to the addition of salt to unconjugated AdhD. At pH 8.8, both -30 and 0 sfGFP have a negative net charge, while +36 has a positive net charge. It is possible that the localization of negative charge near the enzyme introduces an increase in the apparent ionic strength, which increases the activity of SpyCatcher-GGGS-AdhD and then further salt addition leads to decreased activity at pH 8.8. With -30 sfGFP, the complexation at low salt increases the activity by 65 percent, and there was no effect of complexation at higher salt concentrations. With 0 sfGFP, a mixed effect was observed where at low salt the complexation with 0 sfGFP increased the activity by ~25 percent. Furthermore, although an increase in activity at higher salt is observed, the complexation of 0 sfGFP at 200 and 500 mM NaCl inhibited activity by ~30 percent compared to the untagged sfGFP. This inhibition is similar to what was observed with SpyCatcher-GGGS-AdhD where above 125 mM NaCl, inhibition was observed (**Figure 5.2A**). The effect is only observed for the addition of negative charges, as complexation of the +36 sfGFP protein have no effect on activity.

The effect of ionic strength on the activity of the uncomplexed AdhD was pH-dependent and thus the results were repeated at higher and lower pH values. At the lower pH 7.8, the addition of salt to AdhD led to increased activity, and inhibition at high salt was not observed (**Figure 5.2B**). When -30 sfGFP was conjugated to AdhD, no effect was seen at low salt, but at the higher salt concentrations the conjugation of sfGFP led to significant increases in the activity as compared

to the unconjugated mixed protein controls (**Figure 5.3A**). With 0 sfGFP, a similar trend was observed where, as the salt concentration increased, the activity increased and then plateaued. However, at 7.75 mM NaCl, the conjugated proteins were less active than the mixed proteins controls. A decrease was also seen at higher salt concentrations, but the effect of the complexation was statistically significant. The +36 sfGFP followed the same trend where the addition of salt increased activity, however, none of the differences between the conjugated and mixes protein controls were statistically significant by Student's t-test.

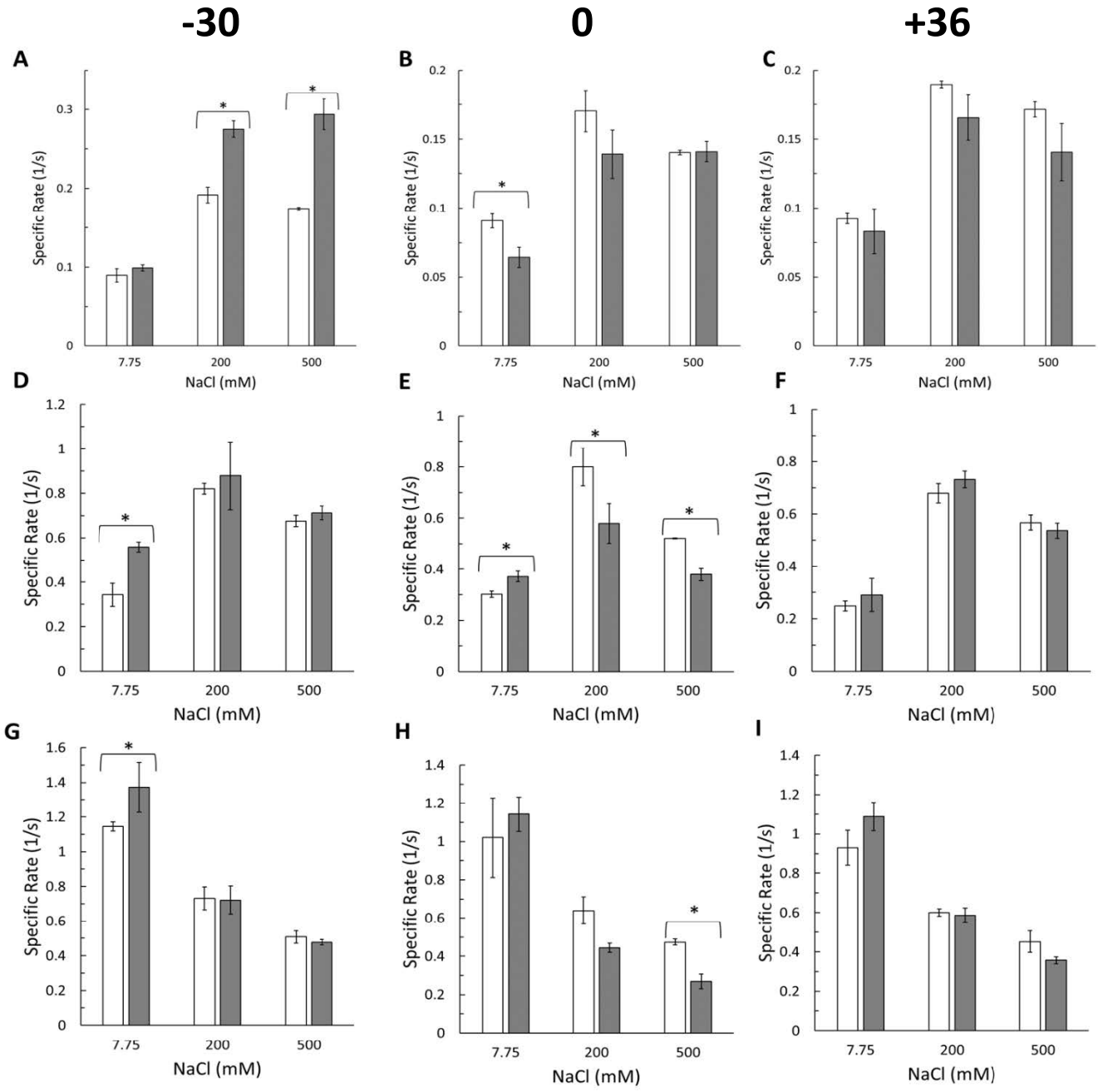

Figure 5.3 Specific rates of AdhD-sfGFP conjugates at varying pH as a function of NaCl. Rates collected at pH 7.8 (A-C), 8.8 (D-F), and 9.8 (G-I) as a function of NaCl. Conjugated proteins are shown with grey bars and controls consisting of unconjugated and mixed SpyCatcher-GGGS-AdhD and sfGFP are shown as white bars. All reactions were performed in triplicate with 100 mM 2,3-butanediol and 100 µM NAD^+. Statistically significant differences by Student's t-test of mixed sfGFP to conjugated sfGFP denoted with *($p < 0.05$).

At a pH of 7.8, the results for the complexation of the -30 sfGFP were qualitatively similar to what was observed pH 8.8 where the addition of the negative charges were consistent with an increase in the local ionic strength. However, the 0 sfGFP results were markedly different as the complexation of 0 sfGFP led to either an inhibition at low salt and no effect at higher salt. This is likely due to the fact that at pH 7.8 the net charge of 0 sfGFP transitions to an apparent positive charge (**Figure 5.2D**). When -30 sfGFP was conjugated to AdhD, the largest impacts were seen where at 200 and 500 mM NaCl, the conjugation of the -30 sfGFP led an increase in activity of 50 and 70 percent, respectively.

Kinetic assays were then performed at pH 9.8. At this pH, increasing salt had a consistently inhibitory effect on SpyCatcher-GGGS-AdhD (**Figure 5.2B**). However, this is a more optimal pH for activity in lows salt (7.75 mM NaCl or lower) (**Figure 5.2C**). A similar salt trend was observed with all three sfGFPs. Tethering the sfGFPs at 7.75 mM NaCl led to increased activity for all 3 sfGFP proteins but statistical significance was only reacted for -30 sfGFP as compared to the mixed protein controls. At higher salt, the tethering of the charged protein had no effect or was inhibitory, and this inhibition reached statistical significance for 0 sfGFP at 500 mM NaCl. As before, the tethering of +36 sfGFP had no effect on AdhD activity.

At pH 9.8, the 0 sfGFP protein has a net negative charge. At higher salt concentrations, the complexation of the charged proteins is consistent with an increase in ionic strength, and at this pH that effect is inhibitor. However, this effect only reached statistical significance for the 0 sfGFP at 500 mM salt, where a 45% reduction in activity was observed. The observation of increased activity upon complexation of all of the sfGFP proteins at low salt is not consistent with the ionic strength model.

Overall, these assays suggest that pH, salt, and the net charge of complexed sfGFP can all affect kinetic activity. However, these factors are not independent of each other and there is a complex the interplay between these effects. Previous work has shown that appending polymers with substantial negative or positive charges to enzymes can change the local pH, which can affect activity [133, 145]. Under this hypothesis, the complexation of -30 sfGFP should attract H^+ ions decreasing the local pH whereas complexation of +36 sfGFP should attract -OH ions increasing the local pH. If this were the case, the -30 sfGFP complexes would be most active at pH 9.8, as this would decrease the local pH and approach the optimum pH of 8.8 at higher salt concentrations. Similarly, the +36 sfGFP complexes would be most active at pH 7.8 as this would increase the local pH and approach the optimum pH of 8.8 at higher salt concentrations. However, no significant changes were observed upon tethering +36 sfGFP to SpyCatcher-GGGS-AdhD, suggesting the modulation of the local pH may not be occurring in this system. Instead, the results above are more consistent with the hypothesis that the appending of the negatively charged sfGFP proteins leads to local changes in ionic strength which can increase or decrease activity depending on the pH.

5.4.6 Effect of sfGFP-SpyTag on SpyCatcher-GGGS-AdhD Kinetics

In addition to affecting the apparent ionic strength, the appending of charged domains near enzyme active sites may also lead to changes in the local chemical environment that may impact different steps in the catalytic mechanism, such as the binding kinetics of the charged cofactor, NAD(H). To explore this, further kinetic assays were performed with 2,3-butanediol ranging from 2 to 30 mM and NAD^+ ranging from 1 to 200 µM NAD^+. Initial rates were measured at pH 7.8 and 8.8 with 7.75 and 200 mM NaCl. These pH values were chosen as pH 8.8 is the optimal pH for AdhD at the intermediate salt concentration, and experiments at pH 7.8 exhibited the greatest

differences between the uncharged 0 sfGFP and -30 sfGFP. The studies were completed with -30 sfGFP and 0 sfGFP complexes as the appending of -30 sfGFP significantly increased the activity at pH 7.8 and 8.8 while no significant effect was observed upon complexation with +36 sfGFP.

The AdhD enzyme follows an ordered bi-bi mechanism where cofactor (NAD^+) binds before substrate (2,3-butanediol) followed by the release of the product preceding that of the reduced cofactor (NADH). The ordered bi-bi rate law (Equation 5.2) has four parameters: k_{cat}, K_A, K_B, and K_{ia}, where K_A and K_B are Michaelis constants for cofactor and substrate, respectively, and K_{ia} is the dissociation constant for the cofactor.

$$v = \frac{E_t k_{cat} AB}{K_{ia}K_B + K_A B + K_B A + AB} \tag{5.2}$$

Initial rates were collected with varying NAD^+ (A) and 2,3-butanediol (B) concentrations to determine the kinetic parameters. The range of substrate used were near or below the previously published K_B value of the wild type enzyme (29 mM) [17]. Under these conditions the 2,3-butanediol concentrations did not reach saturation (**Figure 5.10** and **Table 5.5**). Therefore, as published previously [17, 25, 26, 76] we assume the rates will first order with respect to the substrate concentration (B) which leads to a simplified form of the ordered bi-bi rate equation, Equation 5.3. This equation retains saturating behavior with respect to the cofactor (A).

$$v = \frac{E_t \left({k_{cat}}/{K_B} \right) AB}{K_{ia} + A} \tag{5.3}$$

The fitting of data to this equation results in the determination of an apparent k_{cat} term (k_{cat}/K_B), and an apparent K_M term (K_{ia}). An apparent catalytic efficiency term can also be calculated ($(k_{cat}/K_B)/K_{ia}$) (**Table 5.2**). In some cases, small decreases in activity were observed at high cofactor concentrations, and the data were also fit using a version of Equation 5.3 with a cofactor inhibition term. However, this resulted in similar kinetic parameters and no significant reduction in the error estimates. Thus, all data were fit with Equation 5.3.

Initial rates were first collected for uncomplexed SpyCatcher-GGGS-AdhD at pH 8.8 and 7.75 mM NaCl (**Table 5.2**) to ensure the measured activity was comparable to previous reported kinetic parameters of AdhD [17, 25, 26]. The catalytic parameters were found to be similar to previous reports, suggesting that any change in catalytic efficiency upon being fused to sfGFP are solely due to the complexation of the sfGFP variants and not an effect of the SpyCatcher domain or the GGGS linker.

Table 5.2 Kinetic Parameters fit to Simplified Ordered Bi-Bi Rate Equation for complexes. Data fit to (Eq 5.3) for the Oxidation Reaction with 2,3-butanediol and NAD^+ for -30 sfGFP-AdhD and 0 sfGFP-AdhD Complexes

Protein	pH	Salt (mM)	k_{cat}/K_B (μM^{-1} s^{-1})	K_{ia} (μM)
SpyCatcher-GGGS-AdhD	8.8	7.75	$(8.5 \pm 0.8) \times 10^{-6}$ ‡	30 ± 10
-30 sfGFP- AdhD Complexes	7.8	7.75	$(2.3 \pm 0.2) \times 10^{-6}$*	35 ± 9
0 sfGFP- AdhD Complexes	7.8	7.75	$(1.5 \pm 0.2) \times 10^{-6}$*	21 ± 10
-30 sfGFP –AdhD Complexes	7.8	200	$(7.1 \pm 0.6) \times 10^{-6}$	110 ± 18
0 sfGFP –AdhD Complexes	7.8	200	$(3.7 \pm 0.8) \times 10^{-6}$	76 ± 39
-30 sfGFP –AdhD Complexes	8.8	7.75	$(1.3 \pm 0.09) \times 10^{-5}$‡	38 ± 9
0 sfGFP –AdhD Complexes	8.8	7.75	$(1.2 \pm 0.1) \times 10^{-5}$‡	47 ± 12
-30 sfGFP – AdhD Complexes	8.8	200	$(2.0 \pm 0.2) \times 10^{-5}$	56 ± 12*
0 sfGFP – AdhD Complexes	8.8	200	$(2.4 \pm 0.2) \times 10^{-5}$	83 ± 14*

Protein	pH	Salt (mM)	$(k_{cat}/K_B)/K_{ia}$ (μM^{-2} s^{-1})
SpyCatcher-GGGS-AdhD	8.8	7.75	$(2.8 \pm 1.0) \times 10^{-7}$
-30 sfGFP- AdhD Complexes	7.8	7.75	$(6.6 \pm 1.8) \times 10^{-8}$
0 sfGFP- AdhD Complexes	7.8	7.75	$(7.1 \pm 3.5) \times 10^{-8}$
-30 sfGFP –AdhD Complexes	7.8	200	$(6.5 \pm 1.2) \times 10^{-8}$
0 sfGFP –AdhD Complexes	7.8	200	$(4.9 \pm 2.7) \times 10^{-8}$
-30 sfGFP –AdhD Complexes	8.8	7.75	$(3.4 \pm 0.8) \times 10^{-7}$*
0 sfGFP –AdhD Complexes	8.8	7.75	$(2.6 \pm 0.7) \times 10^{-7}$*
-30 sfGFP – AdhD Complexes	8.8	200	$(3.6 \pm 0.8) \times 10^{-7}$*
0 sfGFP – AdhD Complexes	8.8	200	$(2.9 \pm 0.5) \times 10^{-7}$*

Data was collected in at least triplicate. Errors bars represent 95% confidence intervals.

‡ Indicates significant difference from SpyCatcher-GGGS-AdhD by Student's t-test

*Indicates significant difference between 0 sfGFP and -30sfGFP at the same salt and pH by Student's t-test

The activity of the complexes formed by the addition of the 0 and -30 sfGFP proteins can be compared to the unfused SpyCatcher-GGGS-AdhD protein at pH 8.8 and a salt concentration of 7.75 mM. The fusion of both sfGFP proteins led to significant increases in the apparent k_{cat} values and this was consistent with the previous observations made at the fixed substrate concentrations (**Figure 5.3**). NAD(H) is negatively charged, however the apparent K_M values were found to increase with both of the sfGFP fusions, independent of charge, although this did not reach statistical significance. The increases in the apparent k_{cat} and apparent K_M values for the sfGFP fusions led to apparent k_{cat}/K_M values that were statistically unchanged compared to the free SpyCatcher-GGGS-AdhD protein. However, the apparent k_{cat}/K_M for –30 sfGFP was significantly increased compared to the 0 sfGFP complex. This indicates that the addition of the sfGFP proteins affects the binding of the reactants and the formation of the catalytic transition states which cannot be captured by making measurements at a single reactant and cofactor concentration.

More complete kinetic measurements were made for 0 and the -30 GFP complexes with varying salt and pH concentrations. Overall, pH has a large impact on the catalytic efficiency of the enzyme. The catalytic efficiency of -30 sfGFP complex with 7.75 and 200 mM NaCl increased by 415% and 450% when the pH was increased from 7.8 to pH 8.8. For the 0 sfGFP complexes, the catalytic efficiency also increased at pH to 8.8 as compared to pH 7.8. In 7.75 mM NaCl, the activity increased 260% and at 200 mM NaCl the activity increased 500%.

To untangle the global effect of the charge addition from the impacts of pH and ionic strength on the kinetic parameters, an N-way ANOVA was performed with all of the kinetic parameters (**Table 5.2**). Overall, the apparent k_{cat} of the enzymes (k_{cat}/K_B) increased by an order of magnitude at pH 8.8 compared to pH 7.8. The N-way ANOVA revealed that the salt and pH

significant affect the apparent k_{cat} and the effect of the sfGFP charge was not significant (**Figure 5.4A** and **Figure 5.4D**). The higher the pH, the greater the apparent turnover rate of the enzyme. The addition of salt also increased the apparent turnover rate of the enzyme. Two-factor interactions indicate that the protein charge and pH interaction is significant as is the salt and pH interaction. Post-hoc analysis revealed that an increase in pH increased the apparent catalytic turnover regardless of the charge of the sfGFP. This can be observed in the increase by an order of magnitude of the turnover rate at both -30 and 0 sfGFP complexes. The different combinations of low salt and high salt at pH 7.8 and 8.8 are all significantly different. Therefore, it can be concluded that the increased pH and salt concentrations alone lead to increases in the apparent k_{cat} of the AdhD enzyme.

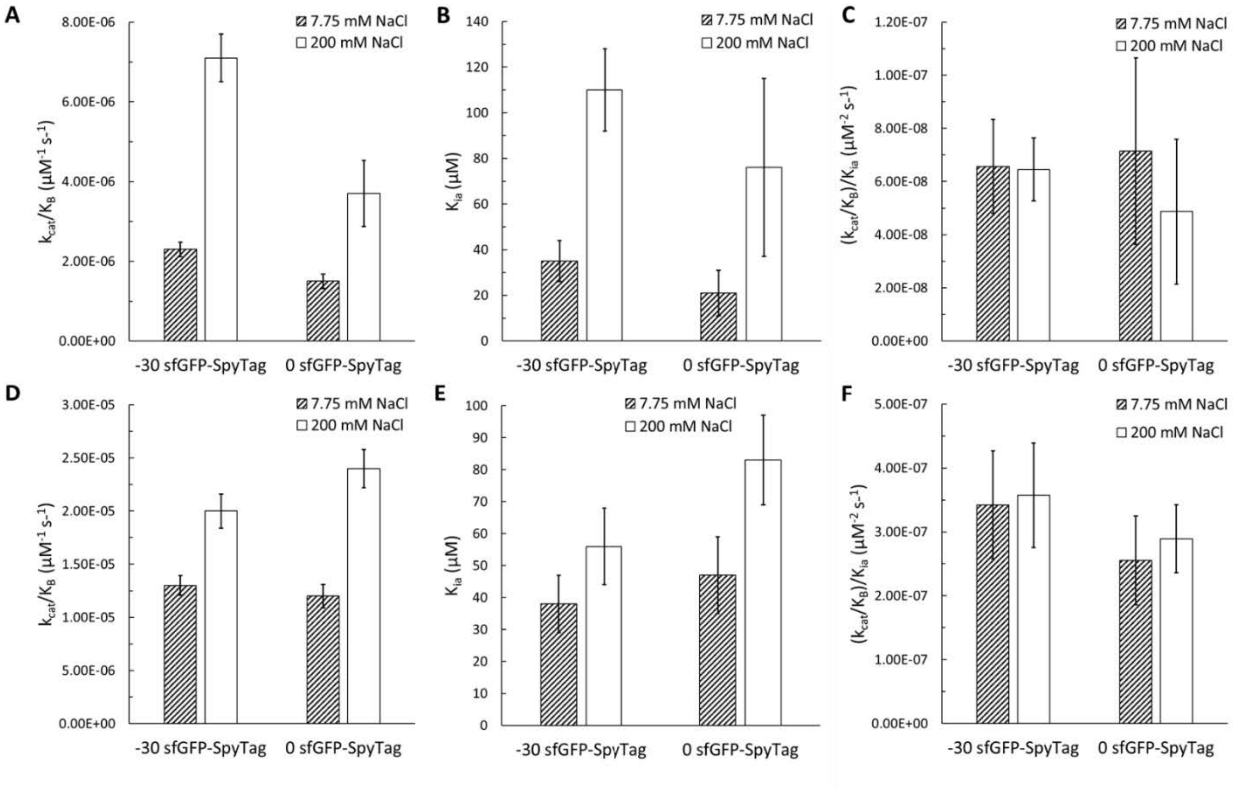

Figure 5.4 Kinetic parameters for oxidation reaction with 2,3-butanediol and NAD^+. Data fit to simplified ordered bi-bi rate equation (5.3) at (A-C) pH 7.8 and (D-F) pH 8.8. Error bars represent 95% confidence intervals. N-way ANOVA was used to explore the impact of pH, salt, and surface charge on the global data set as discussed in the text.

The apparent K_M, (K_{ia}), is the cofactor dissociation constant of the enzyme for the charged NAD^+ cofactor. N-way ANOVA over the entire data set revealed that this parameter is a function of the salt concentration (**Figure 5.4B and E**). This suggests that the addition of salt decreases the affinity of enzyme for the cofactor. The K_{ia} for -30 sfGFP at pH 7.8 increased by 215% upon the addition of salt (from 7.75 to 200 mM NaCl). The K_{ia} for 0 sfGFP increased by 260%. The changes at pH 8.8 were less drastic. For -30 sfGFP, the K_{ia} increased by 50% while it increased 75% for 0 sfGFP. Two-factor interactions revealed that salt and pH interactions are also significant. Interestingly, the effect of the charge of the sfGFP did not reach significance by N-way ANOVA. At low pH, the addition of the -30 sfGFP tended to increase the apparent K_M value and at the higher pH the addition of the -30 sfGFP tended to decrease the apparent K_M value, and this became significant by the Student's t-test only at 200 mM NaCl. Thus, the introduction of the charge can affect the binding of the charged cofactor, but the effect of pH and ionic strength are more dominant.

The apparent catalytic efficiency parameter, $((k_{cat}/K_B)/K_{ia})$, was found to be a function of pH and the charge of the sfGFP protein in complexation by N-way ANOVA (**Figure 5.4C and 4F**). The two factor interactions between sfGFP protein and pH and salt and pH were found to be significant. The post-hoc analysis revealed that at a given pH, the effect of the salt is not significant, suggesting that although it was significant in the turnover of the enzyme and the cofactor dissociation constant, the salt effects largely cancel out when comparing apparent catalytic efficiencies. However, the apparent catalytic efficiency is a function of fusion protein charge as -30 and 0 sfGFP-AdhD complexes at pH 8.8 were significantly more active than the complexes at pH 7.8. Furthermore, -30 sfGFP-AdhD is significantly more active than 0

sfGFP-AdhD at pH 8.8. This suggests that complexation of AdhD with -30 sfGFP affects the microenvironment differently than fusions to 0 sfGFP, thereby significantly increasing the apparent catalytic efficiency of AdhD.

5.4.7 Effect of sfGFP-SpyTag on Ground-State and Transition-State Binding Energies

The apparent k_{cat} and K_M values can be used to estimate the impact of the sfGFP charge (-30 versus 0) on the thermodynamic binding energies of the AdhD enzyme. The apparent K_M values can be used to explore the impact on the ground state binding energy, which shows the effect of the sfGFP charge on the formation of the enzyme/cofactor complexes (Equation 5.4). And the apparent catalytic efficiencies (k_{cat}/K_M) can be used to estimate the impact on the transition state binding energies, which shows the effect of the sfGFP charge on the formation of the enzyme/cofactor/substrate transition state complexes (Equation 5.5).

$$\Delta\Delta G_b = -RT \ln\left[(K_d)_{0\ sfGFP-SpyTag}/(K_d)_{-30\ sfGFP-SpyTag}\right] \tag{5.4}$$

$$\Delta\Delta G_b^{\neq} = RT \ln\left[\left(\frac{k_{cat}}{K_A}\right)_{0\ sfGFP-SpyTag}\Big/\left(\frac{k_{cat}}{K_A}\right)_{-30\ sfGFP-SpyTag}\right] \tag{5.5}$$

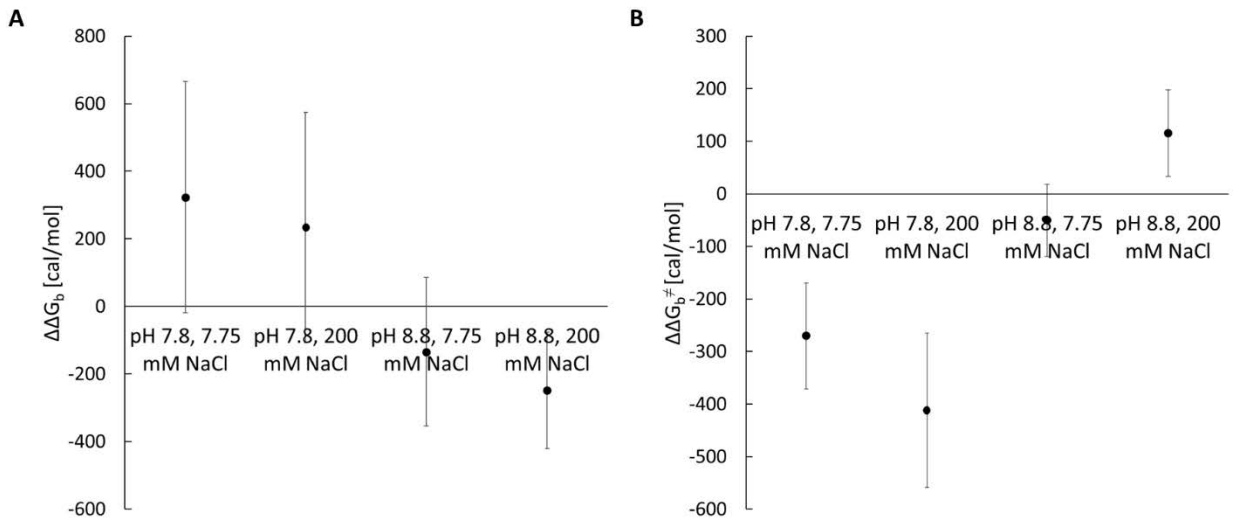

Figure 5.5 Change in (a) ground-state and (b) transition-state binding energies. Energies calculated with -30 and 0 sfGFP-SpyTag at pH 7.8 and 8.8 at 7.75 and 200 mM NaCl.

At low pH, the -30 charge leads to an increase in the transition-state binding energy, a decrease in the substrate binding energy, and the effect of salt is minor (**Figure 5.5**). At pH 8.8, the -30 charge on the sfGFP leads to an increase in the ground-state binding energy while the transition-state binding energy is reduced. At the higher pH, increased salt decreases the transition-state binding energy even further (**Figure 5.5**). The biggest synergistic impact happens at neutral pH and low salt, where the addition of -30 GFP leads to improvements in both the ground and transition state binding energies, thus improving the catalytic microenvironment.

Overall the effects of fusing supercharged sfGFP proteins to AdhD were unexpected. Prior research would suggest that the addition of charge near the active site should influence the local pH and the addition of the +36 sfGFP protein should increase the local pH while the addition of the -30 sfGFP protein should decrease the local pH. This was not observed; rather the tethering of -30 sfGFP leads to increases in activity while no significant effects were observed with the +36 sfGFP complexes. Further analysis of these results suggests that the addition of the -30 charges to

the sfGFP reduces affinity for cofactor but increases the stabilization of the catalytic transition state at low pH. At high pH and high salt, the reverse trend is seen where the addition of the -30 charges to the sfGFP increases the binding energy for the cofactor, but a transition state destabilization is observed. Interestingly, at the optimal pH of the enzyme (8.8) and most physiological salt concentration, the addition of the -30 negative charge on the sfGFP leads to both a stabilization of both the ground and transition states, leading to significant improvements in biocatalysis.

Nature uses charged patches on proteins to affect biocatalytic rates, termed electrostatic guidance, where the surface charge limits the diffusion of charged intermediates, thus preventing their equilibration with the bulk solution. There has been a good deal of interest in exploring this and other substrate channeling mechanisms in natural and engineered protein systems [63]. The surface charge effect have been observed in the metabolon complex formed with citrate synthase and malate dehydrogenase enzymes in the citric acid cycle [146]. To prove the importance of this channeling effect, a single site-directed mutation was made to disrupt the positively charged patch on the protein complexes and this lead to a measurable loss in the substrate channeling between the two active sites [64]. The results obtained in current work suggest that the charged patches observed near the active sites of many proteins may also affect the local microenvironment of the enzymes through in interplay of local pH and local ionic strength effects. This opens up the possibility of using supercharged protein domains to introduce electrostatic guidance capabilities to enzymes, which may increase enzymatic efficiencies.

5.5 Conclusion

In conclusion, the covalent complexation of -30 sfGFP to AdhD using the SpyCatcher/SpyTag fusion technology at pH 8.8 resulted in a protein that is significantly more active than the AdhD protein complexed with an uncharged sfGFP. And the covalent bond between the proteins was required as the mixing of the unfused domains did not introduce a kinetic benefit. Both salt and pH significantly affect the activity of AdhD and at low pH, the addition of the -30 sfGFP fusion appears to influence the local ionic strength more than the local pH. This leads to an improvement in both cofactor binding as well as the formation of the catalytic transition state. The appending of supercharged domains to proteins may be useful technique for modulating biocatalytic microenvironments and this may be especially valuable in *in vivo* applications as there is no need for chemical modification of the proteins.

5.6 Supporting Information

Ultramers to clone sfGFP with SpyTag at C-terminus into pET-28a(+)

-30 sfGFP-SpyTag

FWD: CGAGCTCCGTCGACAA ATGGGTGGCGCTAGCAAAGGTGAAGAGCTG

REV:
GTGCGGCCGCAAGCTTTACTTCGTCGGCTTGTAGGCGTCCACCATCACGATGTGGGC
CTTGTACAGCTCGTCCATTCCATGATCAATGCCTGCAG

0 sfGFP-SpyTag

FWD: CGAGCTCCGTCGACAAATGGGTGGCGCTAGCAAAGGTGAACGTCTG

Rev:
GTGCGGCCGCAAGCTTTACTTCGTCGGCTTGTAGGCGTCCACCATCACGATGTGGGC
CTTGTAGCGTTCGTCCATTCCGTGCGTAATGCCTG

+36 sfGFP-SpyTag

FWD: CGAGCTCCGTCGACAAATGGGTGGCGCTAGCAAAGGTGAACGTCTG

REV:
GTGCGGCCGCAAGCTTTACTTCGTCGGCTTGTAGGCGTCCACCATCACGATGTGGGC
CTTGTAGCGTTCGTCGCGTCCGTGCTTAAT

DNA Sequences

-30 sfGFP-SpyTag

```
ATGGGCAGCA GCCATCATCA TCATCATCAC AGCAGCGGCC TGGTGCCGCG CGGCAGCCAT 60
ATGGCTAGCA TGACTGGTGG ACAGCAAATG GGTCGCGGAT CCGAATTCGA GCTCCGTCGA 120
CAAATGGGTG GCGCTAGCAA AGGTGAAGAG CTGTTTGACG GTGTAGTACC GATCTTAGTG 180
GAATTAGACG GCGACGTGAA CGGTCACGAA TTTAGCGTGC GCGGCGAGGG CGAAGGTGAC 240
GCTACCGAGG GTGAATTGAC CCTGAAGTTT ATTTGCACAA CAGGCGAATT ACCCGTTCCG 300
TGGCCCACCT TAGTGACCAC CCTGACCTAT GGCGTTCAGT GCTTCAGTGA TTACCCAGAT 360
CATATGGATC AACACGATTT TTTCAAATCA GCCATGCCTG AAGGATATGT TCAAGAGCGT 420
ACAATCAGCT TCAAGGACGA TGGCACCTAT AAAACGCGTG CGGAAGTGAA ATTTGAAGGC 480
GACACATTAG TAAACCGTAT CGAACTGAAA GGTATCGACT TCAAAGAAGA CGGCAACATT 540
TTAGGCCATA AGCTGGAATA TAACTTTAAT TCTCATGACG TGTATATTAC GGCCGATAAA 600
CAGGAAAACG GTATCAAGGC AGAATTTGAA ATTCGCCATA ACGTGGAGGA CGGCAGCGTT 660
CAATTAGCGG ATCATTATCA ACAAAACACG CCGATTGGTG ATGGGCCTGT ACTGTTACCT 720
GACGATCACT ACCTGAGCAC GGAGTCAGCC CTGAGCAAAG ATCCGAACGA AGACCGCGAT 780
```

CACATGGTTC TGTTAGAATT CGTGACCGCT GCAGGCATTG ATCATGGAAT GGACGAGCTG 840
TACAAGGCCC ACATCGTGAT GGTGGACGCC TACAAGCCGA CGAAGTAA 888

0 sfGFP-SpyTag

ATGGGCAGCA GCCATCATCA TCATCATCAC AGCAGCGGCC TGGTGCCGCG CGGCAGCCAT 60
ATGGCTAGCA TGACTGGTGG ACAGCAAATG GGTCGCGGAT CCGAATTCGA GCTCCGTCGA 120
CAAATGGGTG GCGCTAGCAA AGGTGAACGT CTGTTTACTG GTGTAGTACC GATCTTAGTG 180
GAATTAGACG GCGACGTGAA CGGTCATAAA TTTAGCGTGC GCGGCGAGGG CGAAGGTGAC 240
GCTACCAATG GTAAATTGAC CCTGAAGTTT ATTTGCACAA CAGGCAAATT ACCCGTTCCG 300
TGGCCCACCT TAGTGACCAC CCTGACCTAT GGCGTTCAGT GCTTCAGTCG TTACCCTGAT 360
CATATGAAAC AACACGATTT TTTCAAATCA GCCATGCCTG AAGGATATGT TCAAGAGCGT 420
ACAATCAGCT TCAAGGACGA TGGCACCTAT AAAACGCGTG CGGAAGTGAA ATTTGAAGGC 480
GACACATTAG TAAATCGTAT CGAACTGAAA GGTCGTGACT TCAAAGAAGA CGGCAACATT 540
TTAGGCCATA AACTGGAATA TAACTTTAAT TCTCATAACG TGTATATTAC GGCCGATAAA 600
CAGAAGAATG GTATCAAGGC AAATTTCAAA ATTCGCCATA ACGTGGAGGA CGGCAGCGTT 660
CAATTAGCGG ATCATTATCA ACAAAACACG CCGATTGGTG ATGGGCCTGT ACTGTTACCT 720
CGCAACCACT ACCTGAGCAC CCAATCTGCC CTGAGCAAAG ATCCGAAAGA AAAACGCGAT 780
CACATGGTTC TGTTAGAATT CGTGACCGCT GCAGGCATTA CGCACGGAAT GGACGAACGC 840
TACAAGGCCC ACATCGTGAT GGTGGACGCC TACAAGCCGA CGAAGTAA 888

+36 sfGFP-SpyTag

ATGGGCAGCA GCCATCATCA TCATCATCAC AGCAGCGGCC TGGTGCCGCG CGGCAGCCAT 60
ATGGCTAGCA TGACTGGTGG ACAGCAAATG GGTCGCGGAT CCGAATTCGA GCTCCGTCGA 120
CAAATGGGTG GCGCTAGCAA AGGTGAACGT CTGTTTCGTG GTAAAGTACC GATCTTAGTG 180
GAATTAAAGG GCGACGTGAA CGGTCATAAA TTTAGCGTGC GCGGCAAAGG CAAAGGTGAC 240
GCTACCCGTG GTAAATTGAC CCTGAAGTTT ATTTGCACAA CAGGCAAATT ACCCGTTCCG 300
TGGCCCACCT TAGTGACCAC CCTGACCTAT GGCGTTCAGT GCTTCAGTCG TTACCCTAAA 360
CATATGAAAC GTCACGATTT TTTCAAATCA GCCATGCCTA AAGGATATGT TCAAGAGCGT 420
ACAATCAGCT TCAAGAAGGA TGGCAAATAT AAAACGCGTG CGGAAGTGAA ATTTGAAGGC 480
CGCACATTAG TAAATCGTAT CAAACTGAAA GGTCGTGACT TCAAAGAAAA AGGCAACATT 540
TTAGGCCATA AACTGCGTTA TAACTTTAAT TCTCATAAGG TGTATATTAC GGCCGATAAA 600
CGCAAGAATG GTATCAAGGC AAAATTCAAA ATTCGCCATA ACGTGAAAGA CGGCAGCGTT 660
CAATTAGCGG ATCATTATCA ACAAAACACG CCGATTGGTC GCGGGCCTGT ACTGTTACCT 720
CGCAACCACT ACCTGAGCAC CCGTTCTAAA CTGAGCAAAG ATCCGAAAGA AAAACGCGAT 780
CACATGGTTC TGTTAGAATT CGTGACCGCT GCAGGCATTA AGCACGGACG CGACGAACGC 840
TACAAGGCCC ACATCGTGAT GGTGGACGCC TACAAGCCGA CGAAGTAA 888

Amino Acid Sequences

-30 sfGFP-SpyTag:

MGSSHHHHHH SSGLVPRGSH MASMTGGQQM GRGSEFELRR QMGGASKGEE LFDGVVPILV 60
ELDGDVNGHE FSVRGEGEGD ATEGELTLKF ICTTGELPVP WPTLVTTLTY GVQCFSDYPD 120
HMDQHDFFKS AMPEGYVQER TISFKDDGTY KTRAEVKFEG DTLVNRIELK GIDFKEDGNI 180
LGHKLEYNFN SHDVYITADK QENGIKAEFE IRHNVEDGSV QLADHYQQNT PIGDGPVLLP 240
DDHYLSTESA LSKDPNEDRD HMVLLEFVTA AGIDHGMDEL YKAHIVMVDA YKPTK 295

0 sfGFP-SpyTag:

MGSSHHHHHH SSGLVPRGSH MASMTGGQQM GRGSEFELRR QMGGASKGER LFTGVVPILV 60
ELDGDVNGHK FSVRGEGEGD ATNGKLTLKF ICTTGKLPVP WPTLVTTLTY GVQCFSRYPD 120
HMKQHDFFKS AMPEGYVQER TISFKDDGTY KTRAEVKFEG DTLVNRIELK GRDFKEDGNI 180
LGHKLEYNFN SHNVYITADK QKNGIKANFK IRHNVEDGSV QLADHYQQNT PIGDGPVLLP 240
RNHYLSTQSA LSKDPKEKRD HMVLLEFVTA AGITHGMDER YKAHIVMVDA YKPTK 295

+36 sfGFP-SpyTag:

MGSSHHHHHH SSGLVPRGSH MASMTGGQQM GRGSEFELRR QMGGASKGER LFRGKVPILV 60
ELKGDVNGHK FSVRGKGKGD ATRGKLTLKF ICTTGKLPVP WPTLVTTLTY GVQCFSRYPK 120
HMKRHDFFKS AMPKGYVQER TISFKKDGKY KTRAEVKFEG RTLVNRIKLK GRDFKEKGNI 180
LGHKLRYNFN SHKVYITADK RKNGIKAKFK IRHNVKDGSV QLADHYQQNT PIGRGPVLLP 240
RNHYLSTRSK LSKDPKEKRD HMVLLEFVTA AGIKHGRDER YKAHIVMVDA YKPTK 295

Primers to clone AdhD into pET28a(+) at *NdeI*

FWD: CCGCGCGGCAGCCATATGGCAAAAAGGGTAAATGCATTCAACGACCTTAAGCGTA

REV: AGTCATGCTAGCCATTCACACACACCTCCTTGCCATCTCTCTATCCTC

Primers to linearize AdhD pET28a(+):

FWD: ATGGCAAAAAGGGTAAATG

REV: ATGGCTGCCGCGCGGCAC

Primers to clone SpyCatcher at N-terminus of AdhD pET28a(+):

FWD: TGGTGCCGCGCGGCAGCCATGGCGCCATGGTTGATACC

REV: GCATTTACCCTTTTTGCCATAATATGAGCGTCACCTTTAGTTGC

Primers to insert Glycine-Glycine-Glycine-Serine (GGGS) Linker between C-terminus SpyCatcher and N-terminus AdhD

FWD: GGAAGTATGGCAAAAAGGGTAAATG

REV: TCCTCCAATATGAGCGTCACCTTTAG

SpyCatcher-GGGS-AdhD DNA sequence:

ATGGGCAGCA GCCATCATCA TCATCATCAC AGCAGCGGCC TGGTGCCGCG CGGCAGCCAT 60
GGCGCCATGG TTGATACCTT ATCAGGTTTA TCAAGTGAGC AAGGTCAGTC CGGTGATATG 120
ACAATTGAAG AAGATAGTGC TACCCATATT AAATTCTCAA AACGTGATGA GGACGGCAAA 180

```
GAGTTAGCTG GTGCAACTAT GGAGTTGCGT GATTCATCTG GTAAAACTAT TAGTACATGG 240
ATTTCAGATG GACAAGTGAA AGATTTCTAC CTGTATCCAG GAAAATATAC ATTTGTCGAA 300
ACCGCAGCAC CAGACGGTTA TGAGGTAGCA ACTGCTATTA CCTTTACAGT TAATGAGCAA 360
GGTCAGGTTA CTGTAAATGG CAAAGCAACT AAAGGTGACG CTCATATTGG AGGAGGAAGT 420
ATGGCAAAAA GGGTAAATGC ATTCAACGAC CTTAAGCGTA TAGGAGATGA TAAGGTAACG 480
GCAATTGGAA TGGGAACATG GGGAATAGGA GGGAGAGAGA CCCCAGACTA TTCTAGGGAT 540
AAGGAAAGCA TAGAAGCAAT AAGATATGGA CTTGAATTAG GAATGAATTT AATCGACACA 600
GCGGAATTCT ATGGAGCTGG TCATGCTGAG GAAATAGTTG GAGAGGCCAT TAAAGAATTC 660
GAACGTGAGG ACATCTTCAT AGTGAGCAAG GTCTGGCCAA CTCACTTTGG GTATGAGGAA 720
GCAAAGAAGG CTGCTAGAGC AAGTGCTAAA AGGTTAGGAA CTTATATTGA CCTTTATTTG 780
TTGCACTGGC CCGTTGATGA CTTCAAGAAG ATAGAGGAGA CACTTCACGC TTTGGAAGAC 840
CTCGTAGATG AGGGAGTGAT AAGGTACATT GGAGTTAGCA ACTTCAATCT GGAACTTCTC 900
CAGCGCTCCC AGGAGGTCAT GAGGAAGTAT GAGATTGTAG CAAATCAAGT TAAATACTCA 960
GTGAAAGACC GCTGGCCCGA AACTACAGGA CTTCTCGACT ACATGAAGCG TGAAGGAATA 1020
GCATTAATGG CGTACACACC TCTAGAAAAG GGAACTCTTG CAAGGAATGA ATGTCTAGCT 1080
AAAATTGGAG AAAAATACGG AAAAACAGCT GCTCAAGTGG CTTTAAACTA CCTGATTTGG 1140
GAGGAAAATG TTGTAGCAAT TCCAAAAGCA AGCAACAAGG AACACCTCAA AGAAAACTTT 1200
GGAGCTATGG GATGGAGGCT TTCAGAGGAG GATAGAGAGA TGGCAAGGAG GTGTGTGTGA 1260
```

SpyCatcher-GGGS-AdhD amino acid sequence:

```
MGSSHHHHHH SSGLVPRGSH GAMVDTLSGL SSEQGQSGDM TIEEDSATHI KFSKRDEDGK 60
ELAGATMELR DSSGKTISTW ISDGQVKDFY LYPGKYTFVE TAAPDGYEVA TAITFTVNEQ 120
GQVTVNGKAT KGDAHIGGGS MAKRVNAFND LKRIGDDKVT AIGMGTWGIG GRETPDYSRD 180
KESIEAIRYG LELGMNLIDT AEFYGAGHAE EIVGEAIKEF EREDIFIVSK VWPTHFGYEE 240
AKKAARASAK RLGTYIDLYL LHWPVDDFKK IEETLHALED LVDEGVIRYI GVSNFNLELL 300
QRSQEVMRKY EIVANQVKYS VKDRWPETTG LLDYMKREGI ALMAYTPLEK GTLARNECLA 360
KIGEKYGKTA AQVALNYLIW EENVVAIPKA SNKEHLKENF GAMGWRLSEE DREMARRCV 419
```

- Catcher highlighted in blue
- Linker highlighted in red

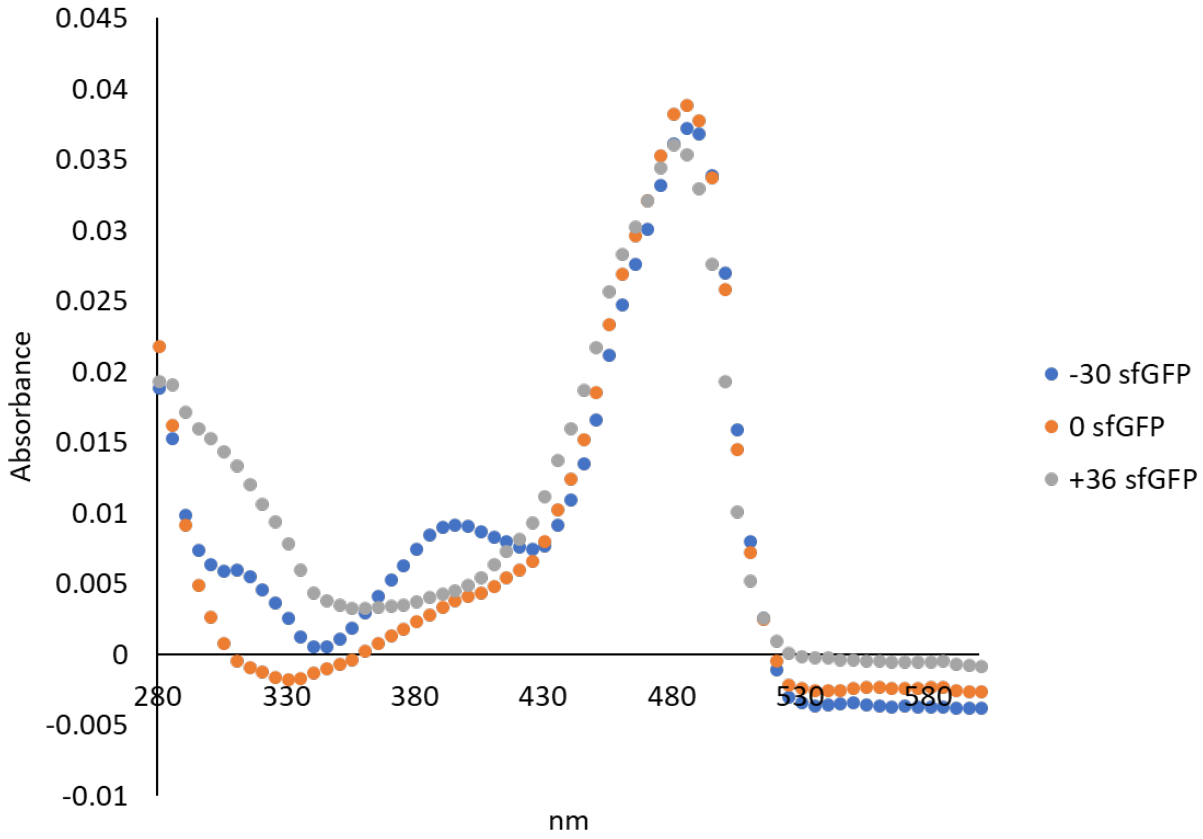

Figure 5.6 Spectral scans from 280 to 600 nm for sfGFP after normalizing sfGFP concentrations.

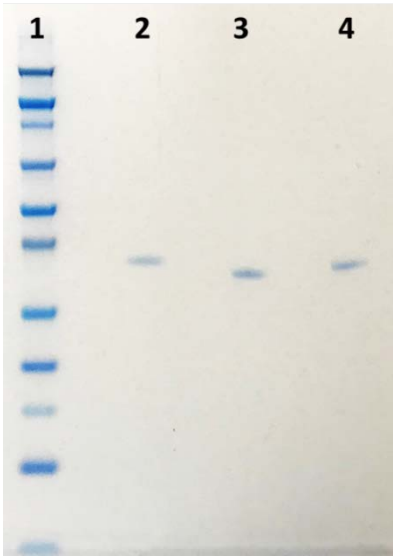

Figure 5.7 SDS-PAGE of sfGFP after normalizing at 485 nm. Lane 1: molecular weight marker, lane 2: -30 sfGFP, lane 3: 0 sfGFP, and lane 4: +36 sfGFP. A band at approximately 33 kDa is observed, consistent with the theoretical molecular masses.

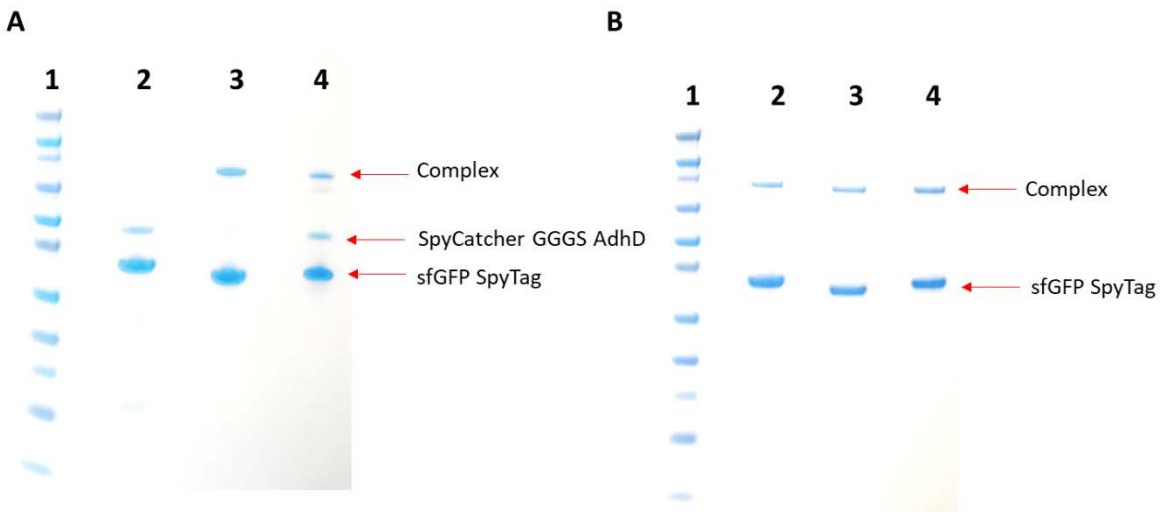

Figure 5.8 SDS-PAGE of sfGFP-SpyTag and SpyCatcher-GGGS-AdhD reaction. Lane 1: molecular weight maker, lane 2: -30 sfGFP-SpyTag + SpyCatcher-GGGS-AdhD, lane 3: 0 sfGFP-SpyTag + SpyCatcher-GGGS-AdhD, lane 4: +36 sfGFP-SpyTag + SpyCatcher-GGGS-AdhD in: (A) the absence of salt and (B) the presence of approximately 400 mM NaCl. A band at approximately 33 kDa is observed for sfGFP, 47 kDa for SpyCatcher-GGGS-AdhD, and 80 kDa for the complex between SpyTag and SpyCatcher, consistent with the theoretical molecular weights.

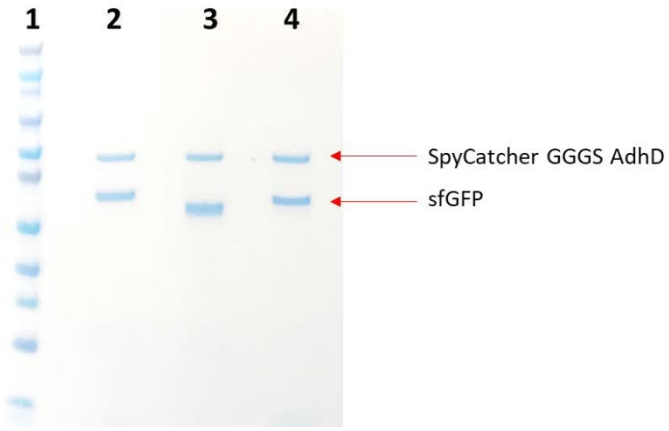

Figure 5.9 SDS-PAGE of reaction between sfGFP and SpyCatcher-GGGS-AdhD. Lane 1: molecular weight maker, lane 2: -30 sfGFP + SpyCatcher-GGGS-AdhD, lane 3: 0 sfGFP + SpyCatcher-GGGS-AdhD, and lane 4: +36 sfGFP + SpyCatcher-GGGS-AdhD. A band at approximately 33 kDa is observed for sfGFP and at 47 kDa for SpyCatcher-GGGS-AdhD, consistent with the theoretical molecular weights.

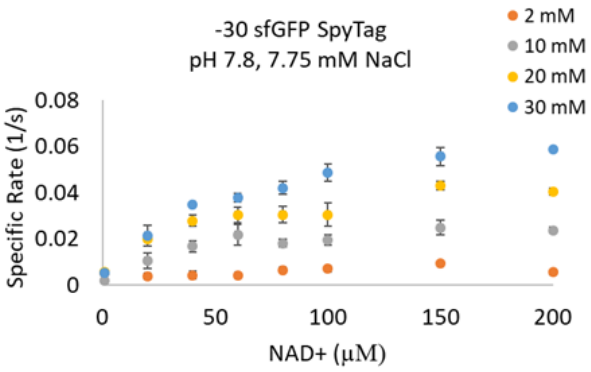
-30 sfGFP SpyTag
pH 7.8, 7.75 mM NaCl
2 mM
10 mM
20 mM
30 mM
Specific Rate (1/s)
0.08
0.06
0.04
0.02
0
0
50
100
150
200
NAD+ (µM)

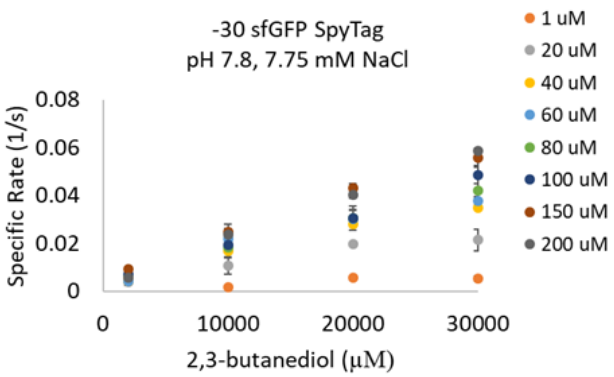
-30 sfGFP SpyTag
pH 7.8, 7.75 mM NaCl
1 uM
20 uM
40 uM
60 uM
80 uM
100 uM
150 uM
200 uM
Specific Rate (1/s)
0.08
0.06
0.04
0.02
0
0
10000
20000
30000
2,3-butanediol (µM)

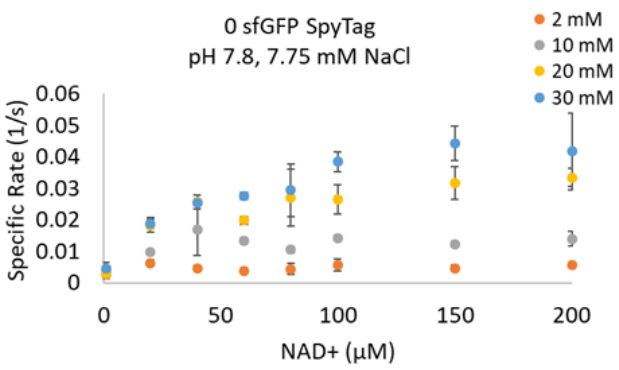
0 sfGFP SpyTag
pH 7.8, 7.75 mM NaCl
2 mM
10 mM
20 mM
30 mM
Specific Rate (1/s)
0.06
0.05
0.04
0.03
0.02
0.01
0
0
50
100
150
200
NAD+ (µM)

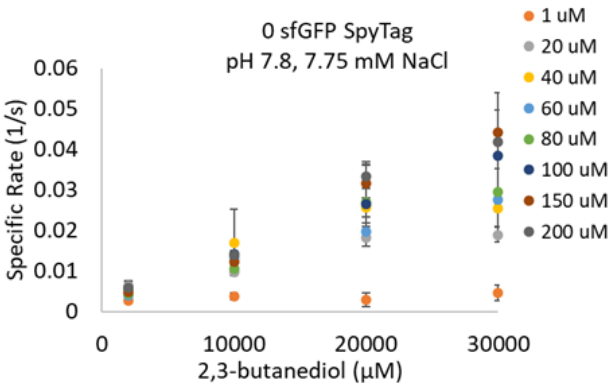
0 sfGFP SpyTag
pH 7.8, 7.75 mM NaCl
1 uM
20 uM
40 uM
60 uM
80 uM
100 uM
150 uM
200 uM
Specific Rate (1/s)
0.06
0.05
0.04
0.03
0.02
0.01
0
0
10000
20000
30000
2,3-butanediol (µM)

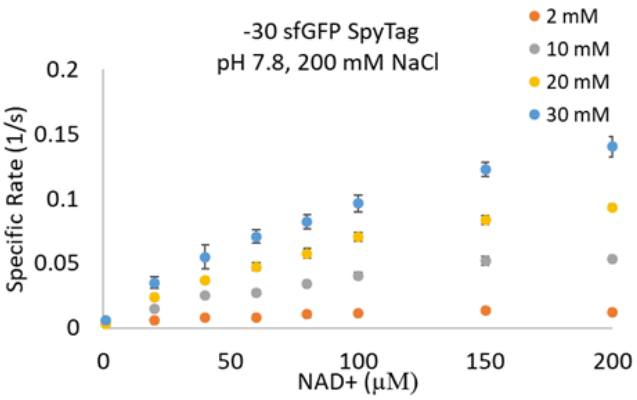
-30 sfGFP SpyTag
pH 7.8, 200 mM NaCl
2 mM
10 mM
20 mM
30 mM
Specific Rate (1/s)
0.2
0.15
0.1
0.05
0
0
50
100
150
200
NAD+ (µM)

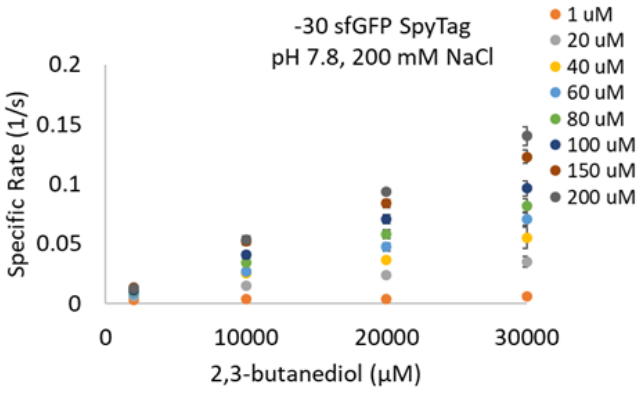
-30 sfGFP SpyTag
pH 7.8, 200 mM NaCl
1 uM
20 uM
40 uM
60 uM
80 uM
100 uM
150 uM
200 uM
Specific Rate (1/s)
0.2
0.15
0.1
0.05
0
0
10000
20000
30000
2,3-butanediol (µM)

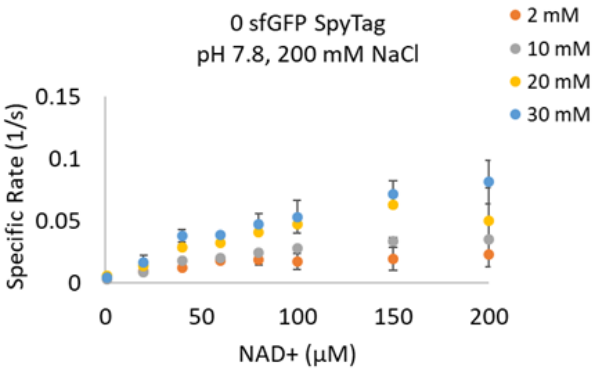
0 sfGFP SpyTag
pH 7.8, 200 mM NaCl
2 mM
10 mM
20 mM
30 mM
Specific Rate (1/s)
0.15
0.1
0.05
0
0
50
100
150
200
NAD+ (µM)

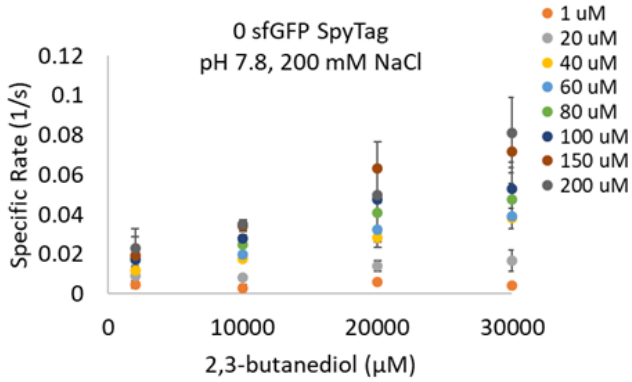
0 sfGFP SpyTag
pH 7.8, 200 mM NaCl
1 uM
20 uM
40 uM
60 uM
80 uM
100 uM
150 uM
200 uM
Specific Rate (1/s)
0.12
0.1
0.08
0.06
0.04
0.02
0
0
10000
20000
30000
2,3-butanediol (µM)

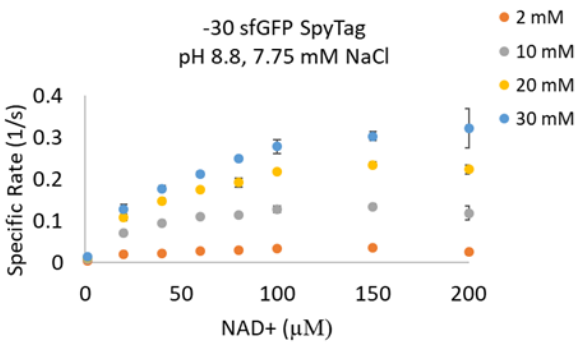
-30 sfGFP SpyTag
pH 8.8, 7.75 mM NaCl
2 mM
10 mM
20 mM
30 mM
Specific Rate (1/s)
0.4
0.3
0.2
0.1
0
0
50
100
150
200
NAD+ (µM)

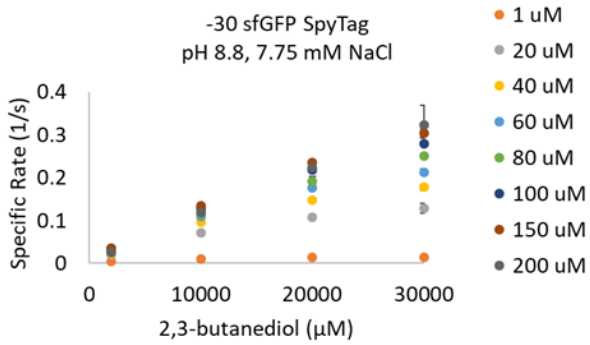
-30 sfGFP SpyTag
pH 8.8, 7.75 mM NaCl
1 uM
20 uM
40 uM
60 uM
80 uM
100 uM
150 uM
200 uM
Specific Rate (1/s)
0.4
0.3
0.2
0.1
0
0
10000
20000
30000
2,3-butanediol (µM)

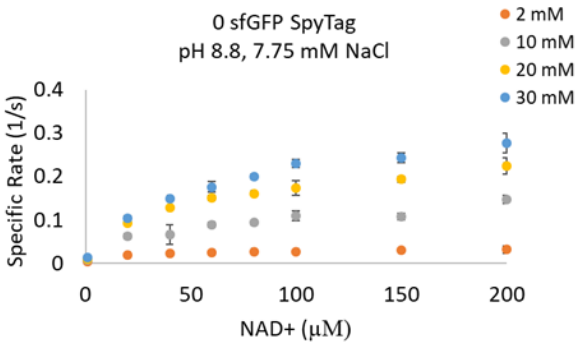
0 sfGFP SpyTag
pH 8.8, 7.75 mM NaCl
2 mM
10 mM
20 mM
30 mM
Specific Rate (1/s)
0.4
0.3
0.2
0.1
0
0
50
100
150
200
NAD+ (µM)

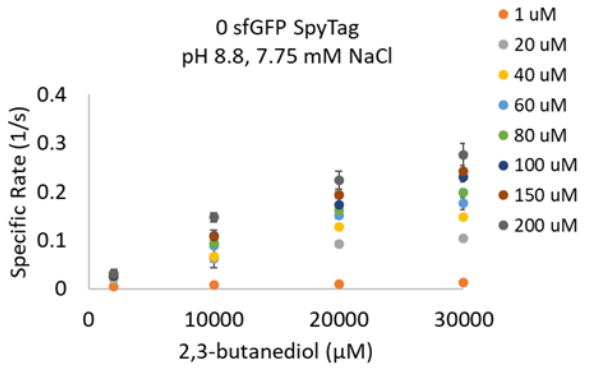
0 sfGFP SpyTag
pH 8.8, 7.75 mM NaCl
1 uM
20 uM
40 uM
60 uM
80 uM
100 uM
150 uM
200 uM
Specific Rate (1/s)
0.4
0.3
0.2
0.1
0
0
10000
20000
30000
2,3-butanediol (µM)

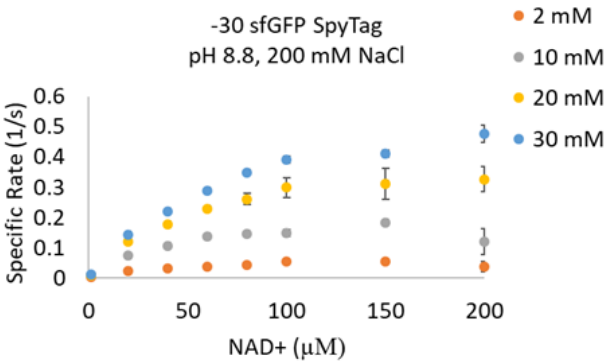
-30 sfGFP SpyTag
pH 8.8, 200 mM NaCl
2 mM
10 mM
20 mM
30 mM
Specific Rate (1/s)
0.6
0.5
0.4
0.3
0.2
0.1
0
0
50
100
150
200
NAD+ (µM)

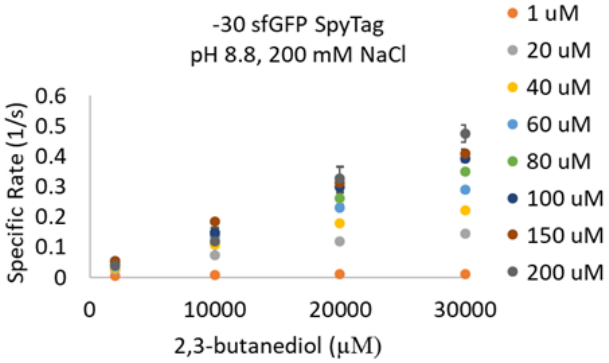
-30 sfGFP SpyTag
pH 8.8, 200 mM NaCl
1 uM
20 uM
40 uM
60 uM
80 uM
100 uM
150 uM
200 uM
Specific Rate (1/s)
0.6
0.5
0.4
0.3
0.2
0.1
0
0
10000
20000
30000
2,3-butanediol (µM)

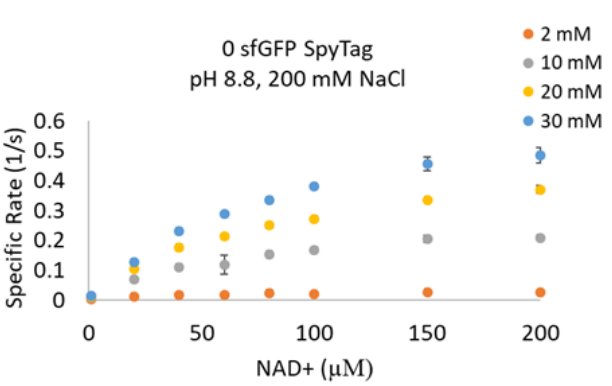
0 sfGFP SpyTag
pH 8.8, 200 mM NaCl
2 mM
10 mM
20 mM
30 mM
Specific Rate (1/s)
0.6
0.5
0.4
0.3
0.2
0.1
0
0
50
100
150
200
NAD+ (µM)

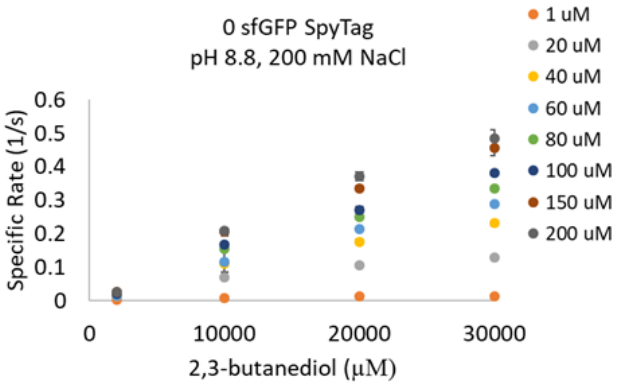
0 sfGFP SpyTag
pH 8.8, 200 mM NaCl
1 uM
20 uM
40 uM
60 uM
80 uM
100 uM
150 uM
200 uM
Specific Rate (1/s)
0.6
0.5
0.4
0.3
0.2
0.1
0
0
10000
20000
30000
2,3-butanediol (µM)

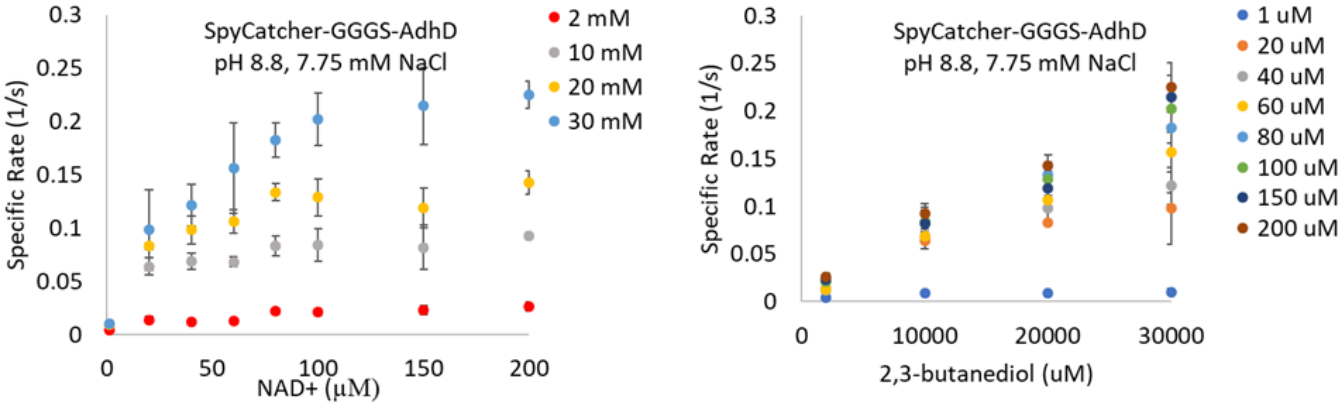

Figure 5.10 Specific rates as a function of 2,3-butanediol and NAD^+ concentration. Reactions performed with SpyCatcher-GGGS-AdhD, -30 and 0 sfGFP-SpyTag at pH 7.8 and 8.8 with 7.75 and 200 mM NaCl.

Table 5.3 Kinetic parameters for oxidation reaction with 2,3-butanediol and NAD^+ fit to simplified bi-bi rate equation (5.3) with three individual data sets.

Protein	pH	NaCl (mM)	k_{cat}/K_B (μM^{-1} s^{-1})	K_{ia} (μM)	$(k_{cat}/K_B)/K_{ia}$ (μM^{-2} s^{-1})
-30	7.8	7.75	2.10E-06 ± 3.30E-07	28 ± 16	7.50E-08 ± 4.44E-08
-30	7.8	7.75	2.20E-06 ± 2.60E-07	29 ± 12	7.59E-08 ± 3.26E-08
-30	7.8	7.75	2.40E-06 ± 3.40E-07	37 ± 17	6.49E-08 ± 3.12E-08
0	7.8	7.75	1.50E-06 ± 3.60E-07	27 ± 25	5.56E-08 ± 5.31E-08
0	7.8	7.75	1.70E-06 ± 3.60E-07	23 ± 20	7.39E-08 ± 6.62E-08
0	7.8	7.75	1.60E-06 ± 2.50E-07	21 ± 15	7.62E-08 ± 5.57E-08
-30	7.8	200	7.00E-06 ± 1.10E-06	120 ± 36	5.83E-08 ± 1.98E-08
-30	7.8	200	7.70E-06 ± 9.30E-07	117 ± 28	6.58E-08 ± 1.76E-08
-30	7.8	200	6.80E-06 ± 8.90E-07	94 ± 27	7.23E-08 ± 2.28E-08
0	7.8	200	3.70E-06 ± 1.70E-06	82 ± 86	4.51E-08 ± 5.17E-08
0	7.8	200	2.80E-06 ± 1.20E-06	49 ± 57	5.71E-08 ± 7.08E-08
0	7.8	200	6.10E-06 ± 1.50E-06	161 ± 70	3.79E-08 ± 1.89E-08
-30	8.8	7.75	1.20E-05 ± 1.70E-06	34 ± 16	3.53E-07 ± 1.73E-07
-30	8.8	7.75	1.30E-05 ± 1.40E-06	34 ± 12	3.82E-07 ± 1.41E-07
-30	8.8	7.75	1.50E-05 ± 1.70E-06	47 ± 16	3.19E-07 ± 1.15E-07
0	8.8	7.75	1.20E-05 ± 1.90E-06	48 ± 23	2.50E-07 ± 1.26E-07
0	8.8	7.75	1.10E-05 ± 1.80E-06	40 ± 20	2.75E-07 ± 1.45E-07
0	8.8	7.75	1.30E-05 ± 2.10E-06	53 ± 23	2.45E-07 ± 1.14E-07
-30	8.8	200	2.10E-05 ± 2.70E-06	61 ± 20	3.44E-07 ± 1.21E-07
-30	8.8	200	2.10E-05 ± 3.70E-06	58 ± 26	3.62E-07 ± 1.74E-07
-30	8.8	200	1.90E-05 ± 2.10E-06	48 ± 15	3.96E-07 ± 1.31E-07
0	8.8	200	2.30E-05 ± 3.00E-06	74 ± 23	3.11E-07 ± 1.05E-07
0	8.8	200	2.50E-05 ± 3.40E-06	81 ± 25	3.09E-07 ± 1.04E-07
0	8.8	200	2.60E-05 ± 3.10E-06	94 ± 24	2.77E-07 ± 7.79E-08

Table 5.4 Average kinetic parameters for oxidation reaction with 2,3-butanediol and NAD^+. Data fit to simplified bi-bi rate equation (5.3) for three individual data sets compared to global fit.

Protein	pH	Salt	k_{cat}/K_B (μM^{-1} s^{-1}) Averaged	Global Fit	K_{ia} (μM) Averaged	Global Fit	$(k_{cat}/K_B)/K_{ia}$ (μM^{-2} s^{-1}) Averaged	Global Fit
-30 sfGFP tag + GGGS	8.8	7.75	1.33E-05	1.30E-05	38	38	3.48E-07	3.42E-07
0 sfGFP tag + GGGS	8.8	7.75	1.20E-05	1.20E-05	47	47	2.55E-07	2.55E-07
-30 sfGFP tag + GGGS	8.8	200	2.03E-05	2.00E-05	56	56	3.65E-07	3.57E-07
0 sfGFP tag + GGGS	8.8	200	2.47E-05	2.40E-05	83	83	2.97E-07	2.89E-07
-30 sfGFP tag + GGGS	7.8	7.75	2.23E-06	2.30E-06	31	35	7.13E-08	6.57E-08
0 sfGFP tag + GGGS	7.8	7.75	1.60E-06	1.50E-06	24	21	6.76E-08	7.14E-08
-30 sfGFP tag + GGGS	7.8	200	7.17E-06	7.10E-06	110	110	6.50E-08	6.45E-08
0 sfGFP tag + GGGS	7.8	200	4.20E-06	3.70E-06	97	76	4.32E-08	4.87E-08

Table 5.5 Raw data to determine kinetic parameters for oxidation reaction with 2,3-butanediol and NAD^+. Data fit to simplified bi-bi rate equation (5.3).

0 sfGFP-SpyTag, pH 7.8, 7.75 mM NaCl

2,3-butanediol (μM)	NAD^+ (μM)	Specific Rate (1/s)
2000	1	0.00357
2000	1	0.00185
2000	1	0.00278
2000	20	0.00561
2000	20	0.00556
2000	20	0.00784
2000	40	0.00534
2000	40	0.00486
2000	40	0.00382
2000	60	0.00388
2000	60	0.00408
2000	60	0.00357
2000	80	0.00583
2000	80	0.00534
2000	80	0.00194
2000	100	0.00534
2000	100	0.00826
2000	100	0.00340
2000	150	0.00486
2000	150	0.00583
2000	150	0.00340
2000	200	0.00534
2000	200	0.00631
2000	200	0.00561
10000	1	0.00437
10000	1	0.00437
10000	1	0.00243
10000	20	0.0107
10000	20	0.00967
10000	20	0.00874
10000	40	0.0107
10000	40	0.0286
10000	40	0.0117
10000	60	0.0123
10000	60	0.0133
10000	60	0.0143
10000	80	0.0111
10000	80	0.0111
10000	80	0.00927

10000	100	0.0131
10000	100	0.0146
10000	100	0.0151
10000	150	0.0165
10000	150	0.0117
10000	150	0.00850
10000	200	0.0153
10000	200	0.0158
10000	200	0.0107
20000	1	0.00194
20000	1	0.00534
20000	1	0.00146
20000	20	0.0210
20000	20	0.0160
20000	20	0.0173
20000	40	0.0181
20000	40	0.0218
20000	40	0.0371
20000	60	0.0204
20000	60	0.0209
20000	60	0.0181
20000	80	0.0190
20000	80	0.0398
20000	80	0.0222
20000	100	0.0236
20000	100	0.0329
20000	100	0.0227
20000	150	0.0264
20000	150	0.0389
20000	150	0.0297
20000	200	0.0315
20000	200	0.0374
20000	200	0.0311
30000	1	0.00340
30000	1	0.00742
30000	1	0.00291
30000	20	0.0170
30000	20	0.0214
30000	20	0.0185
30000	40	0.0243
30000	40	0.0262
30000	40	0.0260
30000	60	0.0287
30000	60	0.0262
30000	60	0.0279

30000	80	0.0175
30000	80	0.0354
30000	80	0.0352
30000	100	0.0427
30000	100	0.0352
30000	100	0.0374
30000	150	0.0505
30000	150	0.0371
30000	150	0.0450
30000	200	0.0246
30000	200	0.0520
30000	200	0.0487

0 sfGFP-SpyTag, pH 7.8, 200 mM NaCl

2,3-butanediol (μM)	NAD^+ (μM)	Specific Rate (1/s)
2000	1	0.00534
2000	1	0.00243
2000	1	0.00637
2000	20	0.0102
2000	20	0.00816
2000	20	0.00918
2000	40	0.0136
2000	40	0.0121
2000	40	0.0102
2000	60	0.0199
2000	60	0.0160
2000	60	0.0180
2000	80	0.0250
2000	80	0.0151
2000	80	0.0158
2000	100	0.0209
2000	100	0.0227
2000	100	0.00850
2000	150	0.0296
2000	150	0.0214
2000	150	0.00742
2000	200	0.0301
2000	200	0.0296
2000	200	0.00918
10000	1	0.00510
10000	1	0.00204
10000	1	0.00161
10000	20	0.00923

10000	20	0.00825
10000	20	0.00777
10000	40	0.0185
10000	40	0.0180
10000	40	0.0165
10000	60	0.0194
10000	60	0.0199
10000	60	0.0204
10000	80	0.0243
10000	80	0.0257
10000	80	0.0238
10000	100	0.0283
10000	100	0.0297
10000	100	0.0255
10000	150	0.0315
10000	150	0.0371
10000	150	0.0334
10000	200	0.0325
10000	200	0.0384
10000	200	0.0338
20000	1	0.00612
20000	1	0.0061
20000	1	0.00612
20000	20	0.0107
20000	20	0.0136
20000	20	0.0175
20000	40	0.0255
20000	40	0.0291
20000	40	0.0306
20000	60	0.0315
20000	60	0.0324
20000	60	0.0335
20000	80	0.0403
20000	80	0.0408
20000	80	0.0423
20000	100	0.0468
20000	100	0.0496
20000	100	0.0459
20000	150	0.0630
20000	150	0.0640
20000	150	0.0621
20000	200	0.0695
20000	200	0.0122
20000	200	0.0681
30000	1	0.004370

30000	1	0.00388
30000	1	0.00437
30000	20	0.0223
30000	20	0.00973
30000	20	0.0185
30000	40	0.0329
30000	40	0.0452
30000	40	0.0359
30000	60	0.0399
30000	60	0.0371
30000	60	0.0398
30000	80	0.0440
30000	80	0.0399
30000	80	0.0589
30000	100	0.0352
30000	100	0.0579
30000	100	0.0663
30000	150	0.0686
30000	150	0.0607
30000	150	0.0862
30000	200	0.0695
30000	200	0.0681
30000	200	0.106

-30 sfGFP-SpyTag, pH 7.8, 7.75 mM NaCl

2,3-butanediol (μM)	NAD^+ (μM)	Specific Rate (1/s)
2000	1	0.00612
2000	1	0.00437
2000	1	0.00556
2000	20	0.00357
2000	20	0.00534
2000	20	0.00235
2000	40	0.00583
2000	40	0.00194
2000	40	0.00486
2000	60	0.00486
2000	60	0.00437
2000	60	0.00291
2000	80	0.00583
2000	80	0.00765
2000	80	0.00583
2000	100	0.00631

2000	100	0.00874
2000	100	0.00583
2000	150	0.00825
2000	150	0.00966
2000	150	0.00971
2000	200	0.00437
2000	200	0.00680
2000	200	0.00534
10000	1	0.00113
10000	1	0.00185
10000	1	0.00232
10000	20	0.00583
10000	20	0.0126
10000	20	0.0131
10000	40	0.0195
10000	40	0.0139
10000	40	0.0165
10000	60	0.0277
10000	60	0.0199
10000	60	0.0175
10000	80	0.0159
10000	80	0.0189
10000	80	0.0194
10000	100	0.0167
10000	100	0.0189
10000	100	0.0223
10000	150	0.0282
10000	150	0.0204
10000	150	0.0257
10000	200	0.0238
10000	200	0.0218
10000	200	0.0252
20000	1	0.00649
20000	1	0.00459
20000	1	0.00534
20000	20	0.0199
20000	20	0.0199
20000	20	0.0190
20000	40	0.0273
20000	40	0.0250
20000	40	0.0311
20000	60	0.0311
20000	60	0.0301
20000	60	0.0297
20000	80	0.0338

20000	80	0.0320
20000	80	0.0255
20000	100	0.0278
20000	100	0.0380
20000	100	0.0389
20000	150	0.0412
20000	150	0.0454
20000	150	0.0422
20000	200	0.0418
20000	200	0.0408
20000	200	0.0384
30000	1	0.00371
30000	1	0.00583
30000	1	0.00631
30000	20	0.0241
30000	20	0.0250
30000	20	0.0148
30000	40	0.0338
30000	40	0.0350
30000	40	0.0352
30000	60	0.0394
30000	60	0.0352
30000	60	0.0385
30000	80	0.0380
30000	80	0.0431
30000	80	0.0450
30000	100	0.0436
30000	100	0.0505
30000	100	0.0520
30000	150	0.0524
30000	150	0.0533
30000	150	0.0612
30000	200	0.0587
30000	200	0.0584
30000	200	0.0584

-30 sfGFP-SpyTag, pH 7.8, 200 mM NaCl

2,3-butanediol (μM)	NAD^+ (μM)	Specific Rate (1/s)
2000	1	0.00408
2000	1	0.00268
2000	1	0.00268
2000	20	0.00663
2000	20	0.00663

2000	20	0.00388
2000	40	0.00874
2000	40	0.00714
2000	40	0.00874
2000	60	0.00971
2000	60	0.00874
2000	60	0.00631
2000	80	0.0136
2000	80	0.00816
2000	80	0.00971
2000	100	0.0112
2000	100	0.0111
2000	100	0.0111
2000	150	0.0155
2000	150	0.0121
2000	150	0.0125
2000	200	0.0126
2000	200	0.0131
2000	200	0.0112
10000	1	0.00194
10000	1	0.00486
10000	1	0.00486
10000	20	0.0141
10000	20	0.0155
10000	20	0.0146
10000	40	0.0243
10000	40	0.0238
10000	40	0.0267
10000	60	0.0286
10000	60	0.0243
10000	60	0.0283
10000	80	0.0354
10000	80	0.0324
10000	80	0.0343
10000	100	0.0371
10000	100	0.0417
10000	100	0.0426
10000	150	0.0501
10000	150	0.0570
10000	150	0.0496
10000	200	0.0491
10000	200	0.0561
10000	200	0.0547
20000	1	0.00306
20000	1	0.00243

20000	1	0.00510
20000	20	0.0223
20000	20	0.0246
20000	20	0.0241
20000	40	0.0338
20000	40	0.0389
20000	40	0.0374
20000	60	0.0437
20000	60	0.0515
20000	60	0.0468
20000	80	0.0524
20000	80	0.0607
20000	80	0.0598
20000	100	0.0670
20000	100	0.0751
20000	100	0.0663
20000	150	0.0806
20000	150	0.0885
20000	150	0.0820
20000	200	0.0922
20000	200	0.0913
20000	200	0.0964
30000	1	0.00612
30000	1	0.00510
30000	1	0.00612
30000	20	0.0287
30000	20	0.0371
30000	20	0.0388
30000	40	0.0468
30000	40	0.0505
30000	40	0.0675
30000	60	0.0635
30000	60	0.0723
30000	60	0.0762
30000	80	0.0783
30000	80	0.0899
30000	80	0.0779
30000	100	0.0894
30000	100	0.105
30000	100	0.0945
30000	150	0.115
30000	150	0.127
30000	150	0.127
30000	200	0.129
30000	200	0.146

30000	200	0.145

0 sfGFP-SpyTag, pH 8.8, 7.75 mM NaCl

2,3-butanediol (μM)	NAD^+ (μM)	Specific Rate (1/s)
2000	1	0.00631
2000	1	0.00340
2000	1	0.00534
2000	20	0.0180
2000	20	0.0185
2000	20	0.0209
2000	40	0.0218
2000	40	0.0214
2000	40	0.0241
2000	60	0.0228
2000	60	0.0238
2000	60	0.0277
2000	80	0.0233
2000	80	0.0257
2000	80	0.0316
2000	100	0.0269
2000	100	0.0248
2000	100	0.0287
2000	150	0.0325
2000	150	0.0306
2000	150	0.0264
2000	200	0.0209
2000	200	0.0345
2000	200	0.0403
10000	1	0.0126
10000	1	0.00463
10000	1	0.00680
10000	20	0.0667
10000	20	0.0538
10000	20	0.0644
10000	40	0.0340
10000	40	0.0839
10000	40	0.0811
10000	60	0.0820
10000	60	0.0936
10000	60	0.0904
10000	80	0.0881
10000	80	0.0950

10000	80	0.0978
10000	100	0.0987
10000	100	0.103
10000	100	0.127
10000	150	0.102
10000	150	0.118
10000	150	0.101
10000	200	0.159
10000	200	0.147
10000	200	0.136
20000	1	0.0116
20000	1	0.00881
20000	1	0.0102
20000	20	0.0881
20000	20	0.0959
20000	20	0.0955
20000	40	0.126
20000	40	0.126
20000	40	0.131
20000	60	0.145
20000	60	0.159
20000	60	0.147
20000	80	0.160
20000	80	0.167
20000	80	0.156
20000	100	0.151
20000	100	0.184
20000	100	0.186
20000	150	0.185
20000	150	0.202
20000	150	0.193
20000	200	0.230
20000	200	0.199
20000	200	0.243
30000	1	0.0138
30000	1	0.00971
30000	1	0.0146
30000	20	0.111
30000	20	0.0955
30000	20	0.103
30000	40	0.146
30000	40	0.152
30000	40	0.147
30000	60	0.159
30000	60	0.185

30000	60	0.184
30000	80	0.205
30000	80	0.191
30000	80	0.201
30000	100	0.236
30000	100	0.216
30000	100	0.238
30000	150	0.254
30000	150	0.228
30000	150	0.246
30000	200	0.251
30000	200	0.272
30000	200	0.307

0 sfGFP-SpyTag, pH 8.8, 200 mM NaCl

2,3-butanediol (μM)	NAD^+ (μM)	Specific Rate (1/s)
2000	1	0.00728
2000	1	0.00194
2000	1	0.00291
2000	20	0.0117
2000	20	0.0131
2000	20	0.0141
2000	40	0.0158
2000	40	0.0180
2000	40	0.0155
2000	60	0.0214
2000	60	0.0167
2000	60	0.0107
2000	80	0.0228
2000	80	0.0218
2000	80	0.0287
2000	100	0.0222
2000	100	0.0180
2000	100	0.0199
2000	150	0.0255
2000	150	0.0278
2000	150	0.0278
2000	200	0.0273
2000	200	0.0252
2000	200	0.0228
10000	1	0.00971
10000	1	0.00881

10000	1	0.00825
10000	20	0.0746
10000	20	0.0667
10000	20	0.0700
10000	40	0.118
10000	40	0.110
10000	40	0.104
10000	60	0.141
10000	60	0.139
10000	60	0.0723
10000	80	0.148
10000	80	0.154
10000	80	0.159
10000	100	0.159
10000	100	0.176
10000	100	0.170
10000	150	0.193
10000	150	0.219
10000	150	0.204
10000	200	0.200
10000	200	0.208
10000	200	0.220
20000	1	0.0131
20000	1	0.0141
20000	1	0.0112
20000	20	0.103
20000	20	0.108
20000	20	0.105
20000	40	0.172
20000	40	0.185
20000	40	0.171
20000	60	0.209
20000	60	0.210
20000	60	0.219
20000	80	0.244
20000	80	0.261
20000	80	0.245
20000	100	0.260
20000	100	0.283
20000	100	0.272
20000	150	0.339
20000	150	0.342
20000	150	0.328
20000	200	0.377
20000	200	0.382

20000	200	0.354
30000	1	0.0126
30000	1	0.0141
30000	1	0.0162
30000	20	0.127
30000	20	0.126
30000	20	0.132
30000	40	0.224
30000	40	0.239
30000	40	0.231
30000	60	0.293
30000	60	0.282
30000	60	0.288
30000	80	0.336
30000	80	0.333
30000	80	0.339
30000	100	0.375
30000	100	0.390
30000	100	0.377
30000	150	0.425
30000	150	0.466
30000	150	0.477
30000	200	0.458
30000	200	0.478
30000	200	0.520

-30 sfGFP-SpyTag, pH 8.8, 7.75 mM NaCl

2,3-butanediol (μM)	NAD^+ (μM)	Specific Rate (1/s)
2000	1	0.00510
2000	1	0.00534
2000	1	0.00437
2000	20	0.0214
2000	20	0.0185
2000	20	0.0209
2000	40	0.0228
2000	40	0.0227
2000	40	0.0250
2000	60	0.0248
2000	60	0.0277
2000	60	0.0316
2000	80	0.0252
2000	80	0.0316

2000	80	0.0354
2000	100	0.0282
2000	100	0.0379
2000	100	0.0364
2000	150	0.0345
2000	150	0.0338
2000	150	0.0379
2000	200	0.0320
2000	200	0.0195
2000	200	0.0264
10000	1	0.00867
10000	1	0.00971
10000	1	0.0107
10000	20	0.0695
10000	20	0.0728
10000	20	0.0742
10000	40	0.0973
10000	40	0.0922
10000	40	0.0964
10000	60	0.111
10000	60	0.106
10000	60	0.112
10000	80	0.119
10000	80	0.109
10000	80	0.117
10000	100	0.134
10000	100	0.116
10000	100	0.133
10000	150	0.134
10000	150	0.130
10000	150	0.140
10000	200	0.0973
10000	200	0.137
10000	200	0.123
20000	1	0.0140
20000	1	0.0136
20000	1	0.0136
20000	20	0.101
20000	20	0.116
20000	20	0.106
20000	40	0.141
20000	40	0.153
20000	40	0.151
20000	60	0.174
20000	60	0.178

20000	60	0.175
20000	80	0.178
20000	80	0.202
20000	80	0.198
20000	100	0.218
20000	100	0.221
20000	100	0.217
20000	150	0.232
20000	150	0.244
20000	150	0.229
20000	200	0.210
20000	200	0.238
20000	200	0.223
30000	1	0.0136
30000	1	0.0126
30000	1	0.0151
30000	20	0.114
30000	20	0.142
30000	20	0.130
30000	40	0.168
30000	40	0.183
30000	40	0.182
30000	60	0.204
30000	60	0.219
30000	60	0.215
30000	80	0.246
30000	80	0.250
30000	80	0.256
30000	100	0.257
30000	100	0.285
30000	100	0.293
30000	150	0.298
30000	150	0.294
30000	150	0.318
30000	200	0.270
30000	200	0.313
30000	200	0.384

-30 sfGFP-SpyTag, pH 8.8, 200 mM NaCl

2,3-butanediol (μM)	NAD^+ (μM)	Specific Rate (1/s)
2000	1	0.00680
2000	1	0.00437
2000	1	0.00437
2000	20	0.0238
2000	20	0.0248
2000	20	0.0250
2000	40	0.0291
2000	40	0.0329
2000	40	0.0335
2000	60	0.0388
2000	60	0.0379
2000	60	0.0357
2000	80	0.0418
2000	80	0.0440
2000	80	0.0426
2000	100	0.0635
2000	100	0.0447
2000	100	0.0544
2000	150	0.0515
2000	150	0.0565
2000	150	0.0542
2000	200	0.0384
2000	200	0.0181
2000	200	0.0603
10000	1	0.00825
10000	1	0.00971
10000	1	0.00969
10000	20	0.0793
10000	20	0.0746
10000	20	0.0695
10000	40	0.111
10000	40	0.102
10000	40	0.109
10000	60	0.140
10000	60	0.141
10000	60	0.131
10000	80	0.148
10000	80	0.146
10000	80	0.146
10000	100	0.161

10000	100	0.136
10000	100	0.150
10000	150	0.181
10000	150	0.181
10000	150	0.190
10000	200	0.164
10000	200	0.0612
10000	200	0.137
20000	1	0.0102
20000	1	0.00971
20000	1	0.0107
20000	20	0.121
20000	20	0.116
20000	20	0.122
20000	40	0.171
20000	40	0.184
20000	40	0.178
20000	60	0.240
20000	60	0.224
20000	60	0.225
20000	80	0.279
20000	80	0.269
20000	80	0.236
20000	100	0.315
20000	100	0.330
20000	100	0.253
20000	150	0.307
20000	150	0.378
20000	150	0.250
20000	200	0.310
20000	200	0.383
20000	200	0.285
30000	1	0.0121
30000	1	0.0131
30000	1	0.0121
30000	20	0.147
30000	20	0.146
30000	20	0.140
30000	40	0.228
30000	40	0.216
30000	40	0.219
30000	60	0.278
30000	60	0.296
30000	60	0.294
30000	80	0.340

30000	80	0.351
30000	80	0.358
30000	100	0.377
30000	100	0.392
30000	100	0.404
30000	150	0.412
30000	150	0.424
30000	150	0.395
30000	200	0.514
30000	200	0.447
30000	200	0.467

SpyCatcher-GGGS-AdhD, pH 8.8, 7.75 mM NaCl

2,3-butanediol (μM)	NAD^+ (μM)	Specific Rate (1/s)
2000	1	0.00388
2000	1	0.00255
2000	1	0.00510
2000	20	0.0120
2000	20	0.0116
2000	20	0.0176
2000	40	0.0125
2000	40	0.0120
2000	40	0.0118
2000	60	0.0116
2000	60	0.0148
2000	60	0.0123
2000	80	0.0181
2000	80	0.0218
2000	80	0.0255
2000	100	0.0176
2000	100	0.0204
2000	100	0.0250
2000	150	0.0167
2000	150	0.0255
2000	150	0.0264
2000	200	0.0320
2000	200	0.0223
2000	200	0.0236
10000	1	0.00742
10000	1	0.0102
10000	1	0.00973
10000	20	0.0575
10000	20	0.0584

10000	20	0.0751
10000	40	0.0579
10000	40	0.0723
10000	40	0.0755
10000	60	0.0686
10000	60	0.0621
10000	60	0.0742
10000	80	0.0704
10000	80	0.0857
10000	80	0.0927
10000	100	0.0626
10000	100	0.0978
10000	100	0.0918
10000	150	0.0524
10000	150	0.0932
10000	150	0.100
10000	200	0.0955
10000	200	0.0950
10000	200	0.0881
20000	1	0.00927
20000	1	0.0107
20000	1	0.00834
20000	20	0.0797
20000	20	0.0871
20000	20	0.0820
20000	40	0.106
20000	40	0.109
20000	40	0.0793
20000	60	0.119
20000	60	0.108
20000	60	0.0922
20000	80	0.129
20000	80	0.127
20000	80	0.145
20000	100	0.132
20000	100	0.106
20000	100	0.148
20000	150	0.112
20000	150	0.100
20000	150	0.144
20000	200	0.153
20000	200	0.148
20000	200	0.127
30000	1	0.00534
30000	1	0.0134

30000	1	0.0122
30000	20	0.0473
30000	20	0.137
30000	20	0.110
30000	40	0.144
30000	40	0.0971
30000	40	0.123
30000	60	0.149
30000	60	0.212
30000	60	0.109
30000	80	0.202
30000	80	0.163
30000	80	0.184
30000	100	0.226
30000	100	0.169
30000	100	0.212
30000	150	0.261
30000	150	0.173
30000	150	0.210
30000	200	0.228
30000	200	0.208
30000	200	0.239

CHAPTER 6

ENGINEERED SUBSTRATE CHANNELING USING SUPERCHARGED SUPERFOLDER GFP SCAFFOLD

Project Collaborators: Walaa Abdallah and Scott Banta

6.1 Abstract

Substrate channeling can be used to increase efficiency in cascades by preventing the diffusion of intermediates into the bulk. In this work, we are engineering substrate channeling between recombinant human hexokinase II (HK2) and glucose-6-phosphate-dehydrogenase (G6PD) using a supercharged superfolder GFP (sfGFP) scaffold. Three different variants of sfGFP will be studied, -30, 0, and +36, as a means for electrostatic guidance. HK2 converts D-glucose and ATP to D-glucose-6-phosphate and ADP. G6PD converts D-glucose-6-phosphate and $NADP^+$ to 6-phospho-D-gluconate and NADPH. The channeling of the negative intermediate, D-glucose-6-phosphate, along the surface of sfGFP between HK2 and G6PD will be studied. It is presumed that it can be guided along the positive patch provided by +36 sfGFP, while -30 sfGFP should repel the intermediate preventing channeling. The efficiency of channeling through electrostatic guidance will be studied through detailed kinetics. Complexes were made with orthogonal tags including SpyTag/SpyCatcher and SnoopTag/SnoopCatcher, as well as through click chemistry between azides and alkynes.

6.2 Introduction

Substrate channeling occurs when an intermediate is transferred from one enzymatic active site to the next without diffusing or reaching equilibrium with the bulk environment. There has been a lot of misconceptions on how to achieve substrate channeling as a way to increase efficiency in cascades. A lot of focus has been on proximity being the source of channeling, which is incorrect once a distance of one nanometer has been exceeded [63]. Studies have shown that to achieve channeling, there must be some sort of bounded diffusion or sequestration. Channeling is desirable as it decreases the chance of side reactions, protects the cells from unstable or toxic intermediates, can increase local substrate concentrations, and increases overall yields and efficiency [63].

Methods of substrate channeling include intramolecular tunnels, chemical swings arms, and electrostatic guidance. An example of an intramolecular tunnel includes the hydrophobic tunnel that channels indole in tryptophan synthase [147]. Chemical swing arms are found in the pyruvate dehydrogenase complex where the intermediate acetyl group is transferred between enzymes [148]. Electrostatic guidance is found in the TCA cycle between malate dehydrogenase and citrate synthase. Previous work with these enzymes has shown that mutations in the positive patch connecting the two enzymes results in a decrease in substrate channeling. This suggested the guidance of the negative intermediate, oxaloacetate, along the positive patch through electrostatic guidance [64].

In this work, we are engineering substrate channeling using supercharged superfolder GFP (sfGFP). The GFP used here is from jellyfish *Aequorea Victoria* which consists of 11 β-strands wrapped around a central helix (PDB 1EMA) [56]. The cycle three mutations, enhanced GFP mutations, and six new mutations resulted in sfGFP (PDB 2B3P) [57, 60]. Mutations along the surface allowed charged variants to be developed and increased the stability of supercharged sfGFP [61].

sfGFP will be used to electrostatically guide the intermediate between recombinant human hexokinase II (HK2) and human glucose-6-phosphate dehydrogenase (G6PD). HK2 is responsible for catalyzing the first step of glycolysis. It converts D-glucose and ATP to D-glucose-6-phosphate and ADP [67]. There are four isomers of hexokinase, with class two being around 100 kDa. It consists of two halves that are both catalytic [67]. HK2 is a dimer (PDB 2NZT) and follows the random bi-bi rate equation [149]. Human glucose-6-phosphate dehydrogenase (G6PD) is responsible for catalyzing the first step of the pentose phosphate pathway [68]. Specifically, it converts glucose-6-phosphate and $NADP^+$, in the presence of magnesium chloride, to 6-phospho-

D-gluconate and NADPH. It is also known to have both a structural and catalytic $NADP^+$ binding site [69]. Its subunit is approximately 60 kDa, but is naturally a tetramer [150]. G6PD follows the random bi-bi rate equation [151].

The product of HK2, D-glucose-6-phosphate, is used by G6PD allowing for substrate channeling. As D-glucose-6-phosphate, the intermediate, is negatively charged, electrostatic guidance along a positively charged patch is possible (**Figure 6.1**). This will be demonstrated with superfolder GFP (sfGFP). Three different charges of sfGFP will be tested, -30, 0, and +36, where +36 is expected to provide substrate channeling, 0 is expected to allow for some channeling, while -30 sfGFP should direct the intermediate into the bulk.

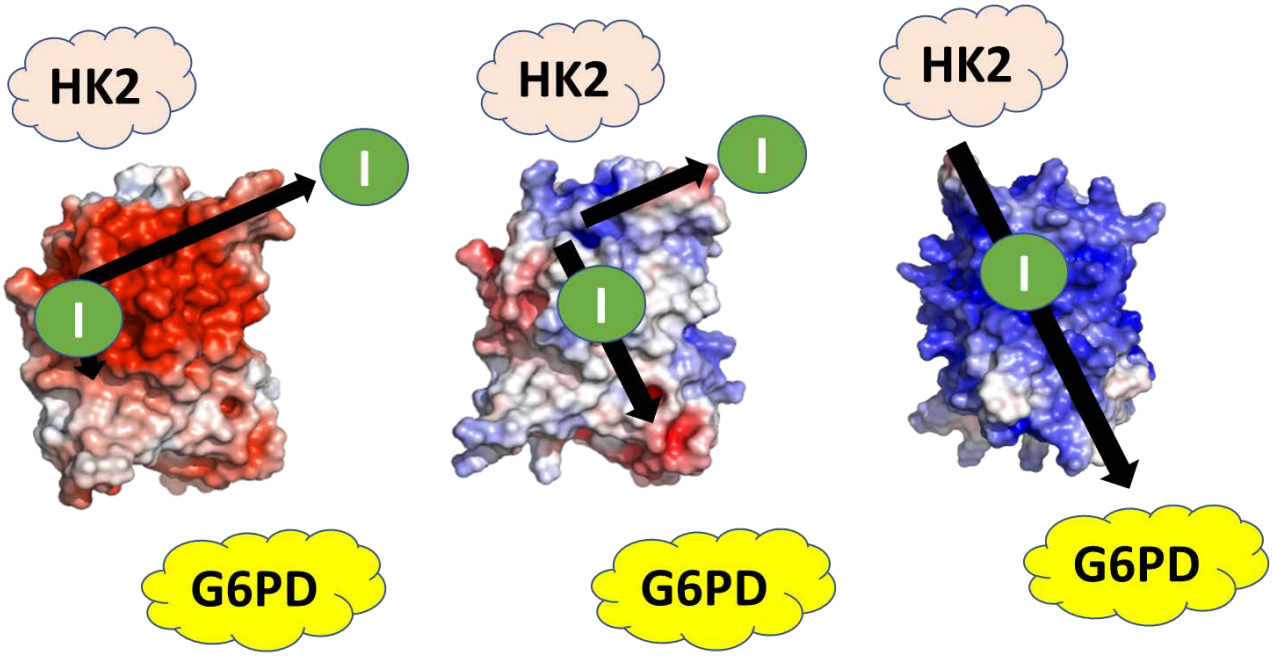

Figure 6.1 Schematic of engineered substrate channeling between HK2 and G6PD with sfGFP scaffold. -30 sfGFP is shown in red (left), 0 sfGFP is shown in white (middle), +36 sfGFP is shown in blue (right).

HK2 and G6PD will be complexed to sfGFP through two methods. The first involves HK2 and G6PD both being on top of the sfGFP barrel, as a result of the N and C-termini of sfGFP both

being on top of the barrel. This set-up will be accomplished through orthogonal tag systems SpyTag/SpyCatcher and SnoopTag/SnoopCatcher. The second method involves HK2 and G6PD on opposite sides of the sfGFP barrel through the previously mentioned tags, as well as through unnatural amino acid incorporation, allowing for click chemistry between azides and alkynes. These two set-ups will allow us to determine the effect of protein charge and enzyme location on the degree of substrate channeling in this three-enzyme system.

6.3 Materials and Methods

6.3.1 Materials

Oligonucleotides were purchased from Integrated DNA Technologies (Coralville, IA). Phusion high fidelity DNA polymerase and *E. coli* BL21(DE3) expression cells were from New England Biolabs (Ipswich, MA). NuPAGE SDS-PAGE gels, MOPS running buffer, and Novex sharp pre-stained protein standards were from Invitrogen (Carlsbad, CA). Histidine purification Nickel-NTA resin and TAMRA was purchased from ThermoFisher Scientific (Waltham, MA). Chromatography columns were from Bio-Rad (Hercules, CA). Molecular weight centrifugal filters were from EMD Millipore (Billerica, MA). Para-azidophenylalanine was from Bachem (Bubendorf, Switzerland) and O-propargyl-L-tyrosine was from Psyclo Peptide (Shanghai, China). All other chemicals, including kanamycin and spectinomycin, were from Sigma Aldrich (St. Louis, MO).

6.3.2 Cloning, Expression, Purification of SpyCatcher G6PD

The DNA sequence corresponding to human glucose-6-phosphate dehydrogenase (G6PD) was cloned into pET-28a(+) at *Nhe I*. The DNA sequence was obtained from Addgene (#41521). The resulting construct, G6PD-pET28, was used to clone SpyCatcher at the N-terminus at *Nde I*,

resulting in SpyCatcher G6PD. Final sequences were verified by DNA sequencing (see Supporting Information).

SpyCatcher G6PD was transformed into *E. coli* BL21(DE3) cells onto Luria Broth (LB) plates supplemented with 0.035 mg/ml kanamycin. Single colonies were inoculated at 37 ºC overnight in Luria Broth (LB) supplemented with 0.035 mg/ml kanamycin. Expression was performed the next day in the same media at 37 °C. When the cells reached on O.D. of approximately 0.60, induction was performed with 0.1 mM isopropyl β-D-1-thiogalactopyranoside (IPTG) and the cells were shaken at 200 rpm overnight at 37 °C.

The cells were harvested and resuspended in 20 mM sodium phosphate buffer with 500 mM NaCl, pH 7.4. They were then sonicated and centrifuged for 1 hour at 7000xg to remove cell debris. The clarified lysate was loaded onto chromatography columns containing Ni-NTA resin previously equilibrated with 20 mM sodium phosphate buffer with 500 mM NaCl, pH 7.4. The flow-through was collected and the column was washed with varying immidizole concentrations (75-500 mM immidizole) in 20 mM tris-HCl with 200 mM NaCl pH 7.4. Fractions were run on NuPAGE 4-12% Bis-tris gels in MES running buffer and protein bands at the expected molecular weight of approximately 75 kDa were observed. Fractions containing protein greater than 95% pure were pooled together and concentrated in 50 kDa MWCO centrifugal filters. They were then buffer exchanged into assay buffer 50 mM triethanolamine pH 7.6.

6.3.3 Cloning of sfGFP SpyTag, SnoopTag sfGFP SpyTag, and sfGFP SpyTag T50TAG

Different versions of sfGFP were made for different conjugation methods. sfGFP with SpyTag and SnoopTag will be used to attach HK2 and G6PD to the top of the sfGFP barrel. sfGFP

SpyTag with an amber stop codon will be used to attach HK2 and G6PD on opposite sides of the barrel. sfGFP SpyTag was used as the foundation for the constructs SnoopTag sfGFP SpyTag and sfGFP SpyTag T50TAG.

Cloning of sfGFP SpyTag plasmids was previously described in chapter 5. Briefly, sfGFP SpyTag was produced by cloning the PCR product of ultramers, containing the C-terminus sequence of sfGFP followed by the SpyTag sequence, into pET-28a(+) linearized with *Hind III* (see Supporting Information). This resulted in constructs -30 sfGFP SpyTag, 0 sfGFP SpyTag, and +36 sfGFP SpyTag. The genes were verified by DNA sequencing (complete sequencing can be found in Supporting Information). The final charges on the sfGFP mutants were increased by three upon addition of the poly-histidine purification tag and thrombin site, artifacts of the cloning, and the SpyTag sequence.

SnoopTag sfGFP SpyTag was cloned into pET28 after linearizing at *Hind III*. Ultramers with SnoopTag at the N-terminus were used to amplify SnoopTag sfGFP SpyTag from sfGFP SpyTag pET28 (see Supporting Information). The genes were verified by DNA sequencing (complete sequencing can be found in Supporting Information).

sfGFP SpyTag constructs were used to introduce an amber stop codon (TAG) at T50 to enable unnatural amino acid incorporation. The mutation was inserted using site-directed mutagenesis (see Supporting Information). The genes were verified by DNA sequencing (complete sequencing can be found in Supporting Information).

6.3.4 sfGFP SpyTag and SnoopTag sfGFP SpyTag Expression and Purification

sfGFP SpyTag and SnoopTag sfGFP SpyTag were transformed into *E. coli* BL21(DE3) cells onto Luria Broth (LB) plates supplemented with 0.035 mg/ml kanamycin for sfGFP. Single colonies were inoculated at 37 ºC overnight in Luria Broth (LB) supplemented with 0.035 mg/ml kanamycin. Expression was performed the next day in the same media at 37 °C. When the cells reached on O.D. of approximately 0.60, induction was performed with 0.5 mM isopropyl β-D-1-thiogalactopyranoside (IPTG). The cells were shaken at 200 rpm overnight at 25 °C.

The cells were harvested and resuspended in 10 mM tris with 1 M NaCl, pH 7.5. The lysate was sonicated and cell debris was removed by centrifuging at 7000xg for 1 hour. The clarified lysates were loaded onto chromatography columns containing Ni-NTA resin previously equilibrated with 10 mM tris with 1 M NaCl, pH 7.5. The column was washed with 20 mM immidizole and eluted with 500 mM immidizole. Fractions were run on NuPAGE 4-12% Bis-tris gels in MES running buffer and those containing protein greater than 95% pure were pooled together and briefly concentrated in 10 kDa MWCO filters. They were then dialyzed into 50 mM triethanolamine pH 7.6.

6.3.5 sfGFP SpyTag T50TAG Incorporation of para-azidophenylalanine and Purification

sfGFP SpyTag T50TAG and helper plasmid pULTRA were transformed into *E. coli* BL21(DE3) cells onto Luria Broth (LB) plates supplemented with 0.035 mg/ml kanamycin and 0.1 mg/ml spectinomycin. Single colonies were inoculated at 37 ºC overnight in Luria Broth (LB) supplemented with 0.035 mg/ml kanamycin and 0.1 mg/ml spectinomycin. Expression was

performed the next day in the same media at 37 °C. When the cells reached on O.D. of approximately 0.60, induction was performed with 0.5 mM isopropyl β-D-1-thiogalactopyranoside (IPTG). Cultures containing T50TAG were supplemented with para-azidophenylalanine (20 mg of unnatural amino acid per 50 mL expression) during induction. A negative control was also done where sfGFP SpyTag T50TAG was not supplemented with para-azidophenylalanine but was induced with IPTG. The cells were shaken at 200 rpm overnight at 25 °C.

The same method of lysis and purification previously described for sfGFP was used here. Protein fractions were run on NuPAGE 4-12% Bis-tris gels in MES running buffer. The clarified lysate of the negative control (sfGFP SpyTag without UAA) was also run on SDS-PAGE to ensure no wild-type protein was expressed through read-through expression. Fractions containing unnatural amino acid labeled protein greater than 95% pure were pooled together and briefly concentrated in 10 kDa MWCO filters. They were then dialyzed into 50 mM triethanolamine pH 7.6.

6.3.6 Cloning of HK2 D19TAG and HK2 SnoopCatcher

Two versions of HK2 were made – one with an amber stop codon for unnatural amino acid incorporation and the second with SnoopCatcher for conjugation to SnoopTag. HK2 containing unnatural amino acid can be used to click onto sfGFP SpyTag T50TAG resulting in HK2 and G6PD on opposite sides of the barrel. HK2 SnoopCatcher can be complexed with SnoopTag sfGFP SpyTag allowing HK2 and G6PD to attach through orthogonal tags on the top of the sfGFP barrel.

The DNA sequence corresponding to human hexokinase II (HK2) in pET-28a(+) was purchased from Addgene (#25529) and verified by DNA sequencing. To enable unnatural amino acid incorporation, D19 in HK2 was mutated to amber stop codon TAG (see supporting

information for primers), resulting in HK2 D19TAG. This can be clicked onto sfGFP SpyTag T50TAG resulting in HK2 and G6PD on opposite sides of the sfGFP barrel.

HK2 SnoopCatcher was made by restriction digesting HK2 pET28a with *Hind III* and ligating with amplified SnoopCatcher. Site-directed mutagenesis was then performed on the resulting construct to remove stop codons between HK2 and SnoopCatcher resulting in HK2 SnoopCatcher (see Supporting Information for primers). This can be covalently complexed with SnoopTag sfGFP SpyTag resulting in HK2 and G6PD on top of the sfGFP barrel.

HK2 D19TAG and HK2 SnoopCatcher were verified by DNA sequencing (see Supporting Information).

6.3.7 Expression and Purification of HK2 and HK2 SnoopCatcher

HK2 and HK2 SnoopCatcher were transformed into *E. coli* BL21(DE3) cells onto Luria Broth (LB) plates supplemented with 0.035 mg/ml kanamycin. Single colonies were inoculated at 37 ºC overnight in Luria Broth (LB) supplemented with 0.035 mg/ml kanamycin. Expression was performed the next day in the same media at 37 °C. When the cells reached on O.D. of approximately 0.60, induction was performed with 0.5 mM isopropyl β-D-1-thiogalactopyranoside (IPTG) and the cells were shaken at 200 rpm overnight at 18 °C.

The cells were harvested and resuspended in 20 mM sodium phosphate buffer with 500 mM NaCl, pH 7.4. They were then sonicated and centrifuged for 1 hour at 7000xg to remove cell debris. The clarified lysate was loaded onto chromatography columns containing Ni-NTA resin previously equilibrated with 20 mM sodium phosphate buffer with 500 mM NaCl, pH 7.4. The flow-through was collected and the column was washed with varying immidizole concentrations (75-500 mM immidizole) in 20 mM tris-HCl with 200 mM NaCl pH 7.4. Fractions were run on NuPAGE 4-

12% Bis-tris gels in MES running buffer and protein bands at the expected molecular weight of approximately 100 kDa were observed. Fractions containing protein greater than 95% pure were pooled together and concentrated in 50 kDa MWCO centrifugal filters. They were then buffer exchanged into 50 mM triethanolamine pH 7.6.

6.3.8 HK2 D19TAG Unnatural Amino Acid Incorporation and Purification

HK2 D19TAG and helper plasmid pULTRA were transformed into *E. coli* BL21(DE3) cells onto Luria Broth (LB) plates supplemented with 0.035 mg/ml kanamycin and 0.1 mg/ml spectinomycin. Single colonies were inoculated at 37 ºC overnight in Luria Broth (LB) supplemented with 0.035 mg/ml kanamycin and 0.1 mg/ml spectinomycin. Expression was performed the next day in the same media at 37 °C. When the cells reached on O.D. of approximately 0.60, induction was performed with 0.5 mM isopropyl β-D-1-thiogalactopyranoside (IPTG). Cultures containing D19TAG were supplemented with o-propargyl-tyrosine (20 mg of unnatural amino acid per 50 mL expression) during induction. A negative control was also done where HK2 D19TAG was not supplemented with o-propargyl-tyrosine but was induced with IPTG. The cells were shaken at 200 rpm overnight at 18 °C.

The same method of lysis and purification previously described for HK2 was used here. The clarified lysate of the negative control (HK2 without UAA) was run on SDS-PAGE to ensure no wild-type protein was expressed through read-through expression. Fractions containing the unnatural amino acid were run on NuPAGE 4-12% Bis-tris gels in MES running buffer and those containing protein greater than 95% pure were pooled together and briefly concentrated in 50 kDa MWCO filters. They were then dialyzed into 50 mM triethanolamine pH 7.6.

6.3.9 Determining Protein Concentrations

Concentrations of G6PD and HK2 as well as their modified variants were determined by reading the absorbances of the protein at 280 nm. The extinction coefficients of the monomers in M^{-1} cm^{-1} are as follows: G6PD 70290, SpyCatcher G6PD 81750, HK2 55360, and HK2 SnoopCatcher 65790. Spectral scans to normalize sfGFP concentrations were done as previously described in chapter 5 (**Figure 6.9**).

6.3.10 Kinetic Assays with HK2 and G6PD

To test the activity of SpyCatcher G6PD, 100 mM D-glucose-6-phosphate, 10 mM magnesium chloride, and 1 mM $NADP^+$ in 50 mM triethanolamine buffer (pH 7.6) were reacted in the presence of G6PD in a final volume of 250 µL. NADPH production was monitored at 340 nm.

To confirm HK2 can produce D-glucose-6-phosphate and that SpyCatcher G6PD uses it, the two enzymes were mixed in solution without supplying D-glucose-6-phosphate. HK2 and SpyCatcher G6PD were reacted with 216 mM D-glucose, 0.74 mM ATP, 10 mM $MgCl_2$, and 1 mM $NADP^+$ (final concentrations) in 50 mM triethanolamine buffer (pH 7.6). The final volume was 250 µL and the production of NADPH was monitored at 340 nm.

6.3.11 SpyTag/SpyCatcher and SnoopTag/SnoopCatcher Reactions

To test the ability of the SpyTag/SpyCatcher reaction, SpyCatcher G6PD was reacted with sfGFP SpyTag in 50 mM triethanolamine buffer (pH 7.6) in the presence of approximately 400 mM NaCl. The reaction was kept rotating overnight in 4 ºC. SDS-PAGE was run the next day to check for the presence of a covalent bond between SpyTag and SpyCatcher. The reaction with sfGFP SpyTag (with unnatural amino acid) will allow SpyCatcher G6PD and HK2 (with unnatural

amino acid) to attach on opposite sides of the barrel. The attachment of HK2 via click chemistry will be addressed in the next section.

To test the reaction between SnoopTag/SnoopCatcher, SnoopTag sfGFP SpyTag and HK2 SnoopCatcher were mixed together in the presence of NaCl at 4 °C overnight. SDS-PAGE was run the next day to check for the presence of a covalent bond between SnoopTag and SnoopCatcher. The reaction with SnoopTag sfGFP SpyTag will allow SpyCatcher G6PD and HK2 SnoopCatcher to attach on the top of the sfGFP barrel.

Mixing SnoopTag sfGFP SpyTag with SpyCatcher G6PD and HK2 SnoopCatcher to test the formation of a 3-enzyme complex was tested by mixing all three components overnight in 4 °C in the presence of NaCl. This reaction has yet to be optimized.

6.3.12 Click Chemistry Between sfGFP SpyTag T50TAG and HK2 D19TAG

To confirm the incorporation of the unnatural amino acid para-azidophenylalanine, sfGFP SpyTag T50TAG was clicked to alkyne TAMRA while sfGFP SpyTag without the UAA was tested as a negative control. Steps 3.1 to 3.3 and 5.1 to 5.4 from protocol number MP33368 from ThermoFisher and steps 1.1 to 2.7 from protocol number MP33370 were followed. The samples were run on NuPAGE 4-12% Bis-tris gels in MES running buffer and were observed under UV light prior to staining.

To confirm the incorporation of the unnatural amino acid o-propargyl-tyrosine in HK2 D19TAG, click chemistry was tested with TAMRA azide. A literature protocol for click chemistry was used, specifically steps 1a-1e, however, the reaction was allowed to proceed overnight in 4 ºC [51]. The samples were run on NuPAGE 4-12% Bis-tris gels in MES running buffer and were

observed under UV light prior to staining. The same protocol was used to test the ability to click sfGFP SpyTag T50TAG with azide and HK2 D19TAG with alkyne [51].

6.4 Results and Discussion

6.4.1 Cloning, Expression, and Purification of Proteins

The DNA sequence corresponding to glucose-6-phosphate dehydrogenase (G6PD) was cloned into pET-28a(+) followed by the insertion of SpyCatcher at the N-terminus, resulting in SpyCatcher G6PD. SpyCatcher G6PD was expressed in *E. coli* BL21(DE3) cells and was purified on a nickel column. It runs at approximately 75 kDa, consistent with its theoretical molecular weight (**Figure 6.8**).

sfGFP SpyTag and SnoopTag sfGFP SpyTag were cloned into pET-28a(+) and expressed in *E. coli* BL21(DE3) expression cells. The SnoopTag construct will be used to orthogonally attach G6PD and HK2 on top of the sfGFP barrel. sfGFP SpyTag T50TAG was treated similarly but supplied with the unnatural amino acid para-azidophenylalanine. sfGFP with the SpyTag and unnatural amino acid will be used to attach G6PD and HK2 on opposite sides of the barrel. All proteins were purified on a nickel column and run at approximately 35 kDa, consistent with their theoretical molecular weight (**Figure 6.9** and **Figure 6.10**).

HK2 pET-28a(+) was purchased from Addgene and was used to clone in SnoopCatcher at the C-terminus. HK2 and HK2 SnoopCatcher were expressed in *E. coli* BL21(DE3) expression cells. HK2 D19TAG was treated similarly but supplied with the unnatural amino acid o-propargyl-tyrosine. All proteins were purified on a nickel column. HK2 with and without the amber stop codon was purified on the nickel column and runs at 100 kDa, consistent with its theoretical

molecular weight (**Figure 6.11**). HK2 SnoopCatcher runs at approximately 115 kDa, consistent with its theoretical molecular weight (**Figure 6.12**).

6.4.2 Activity Assays with G6PD and HK2

To confirm G6PD and HK2 are active, activity assays were performed before setting up conjugation reactions. SpyCatcher G6PD activity was tested by reacting D-glucose-6-phosphate and $NADP^+$ (in the presence of magnesium chloride) and monitoring NADPH production at 340 nm. An increase in the slope was observed suggesting G6PD activity (**Figure 6.2**). Additionally, the rate doubled when the enzyme concentration doubled suggesting catalytic activity.

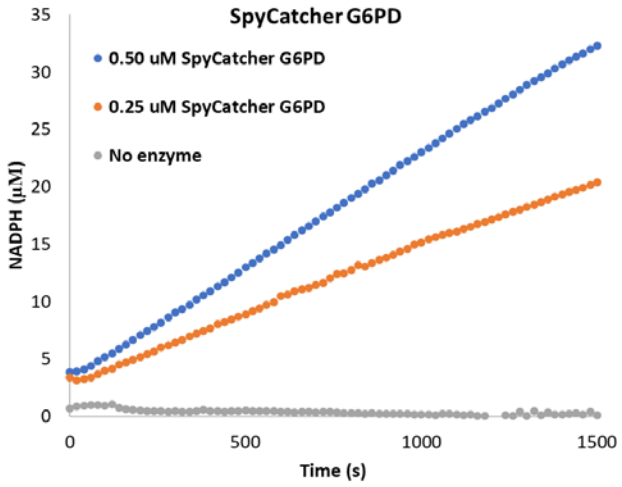

Figure 6.2 SpyCatcher G6PD activity assay. NADPH production was monitored at 340 nm upon reacting D-glucose-6-phosphate, $MgCl_2$, and $NADP^+$ in triethanolamine buffer (pH 7.6) with SpyCatcher G6PD.

To test the ability of SpyCatcher G6PD to use the product (D-glucose-6-phosphate) supplied by HK2, activity assays with all required substrates for HK2 and G6PD (except for D-glucose-6-

phosphate) were conducted (**Figure 6.3**). The ability of SpyCatcher G6PD to produce NADPH signifies that HK2 and SpyCatcher G6PD are active and that D-glucose-6-phopshate was produced by HK2 and consumed by SpyCatcher G6PD.

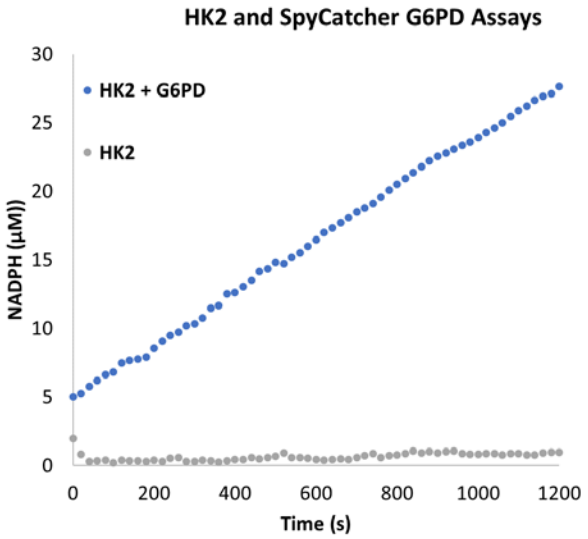

Figure 6.3 HK2 and SpyCatcher G6PD activity assay. HK2 with D-glucose and ATP was reacted with SpyCatcher G6PD with $MgCl_2$ and $NADP^+$ in triethanolamine buffer (pH 7.6) to monitor NADPH production.

6.4.3 SpyTag/SpyCatcher and SnoopTag/SnoopCatcher Reactions

Equimolar SpyCatcher G6PD was incubated with sfGFP SpyTag overnight in the presence of NaCl at 4 ºC. The formation of a higher molecular weight protein suggests the formation of a covalent bond resulting from the complex between sfGFP SpyTag and SpyCatcher G6PD (**Figure 6.4**).

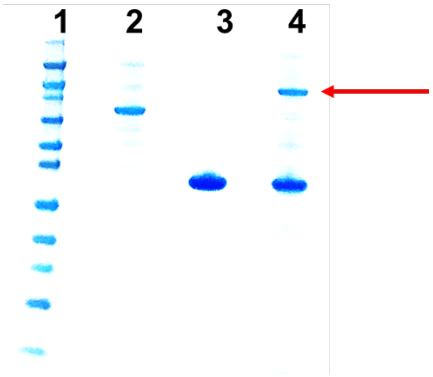

Figure 6.4 SDS-PAGE of sfGFP SpyTag - SpyCatcher G6PD complex. Lane 1: molecular weight marker, lane 2: SpyCatcher G6PD, lane 3: sfGFP SpyTag, and lane 4: sfGFP SpyTag-SpyCatcher G6PD complex. SpyCatcher G6PD runs at around 75 kDa, sfGFP runs at around 35 kDa, and the complex runs at around 110 kDa, consistent with the theoretical molecular weights.

The same reaction was repeated with SnoopTag sfGFP SpyTag and SpyCatcher G6PD and a similar complex was observed.

To test the ability of HK2 SnoopCatcher to attach onto SnoopTag sfGFP SpyTag, the two proteins were mixed together overnight in the presence of NaCl (**Figure 6.*5***). Reactions were set-up prior to HK2 SnoopCatcher purification optimization (**Figure 6.12**).

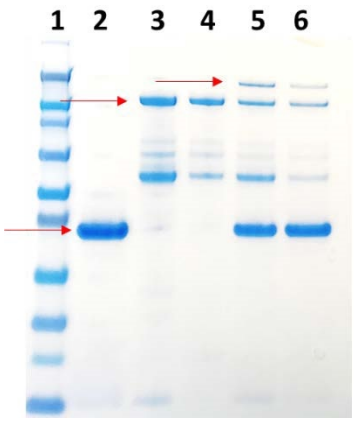

Figure 6.5 SDS-PAGE of SnoopTag sfGFP SpyTag-HK2 SnoopCatcher complex. Lane 1: molecular weight marker, lane 2: SnoopTag sfGFP SpyTag, lane 3: HK2 SnoopCatcher fraction A, lane 4: HK2 SnoopCatcher fraction B, lane 5: SnoopTag sfGFP SpyTag – HK2 SnoopCatcher A complex, and lane 6: SnoopTag sfGFP SpyTag – HK2 SnoopCatcher B complex. SnoopTag sfGFP SpyTag runs at approximately 35 kDa, HK2 SnoopCatcher runs at around 110 kDa, and the complex runs at approximately 150 kDa, consistent with their theoretical molecular weights.

Once again SnoopTag sfGFP SpyTag will be used to orthogonally attach SpyCatcher G6PD and HK2 SnoopCatcher on the top of the sfGFP barrel. To test the ability to form a 3-enzyme complex, all three proteins were mixed together in the presence of salt. A faint band at approximately 230 kDa corresponding the 3-enzyme complex was observed. However, the reaction has not been optimized and further work is required to separate unconjugated protein and impurities. Additionally, the formation of the complex cannot be confirmed until it is isolated and activity assays are performed.

6.4.4 sfGFP SpyTag T50TAG and HK2 D19TAG Click Reactions

To confirm unnatural amino acid incorporation in sfGFP SpyTag T50TAG and HK2 D19TAG, both were clicked with TAMRA, a small fluorescent molecule. sfGFP SpyTag was incorporated with azide para-azidophenylalanine and clicked with TAMRA alkyne in the presence of copper. Prior to staining, the SDS-PAGE gel was placed under UV light and a band at the

expected molecular weight was observed (**Figure 6.6**). No change in the molecular weight of sfGFP was expected as TAMRA is less than 1 kDa.

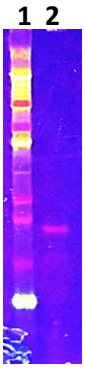

Figure 6.6 SDS-PAGE of sfGFP SpyTag T50TAG with para-azidophenylalanine clicked to TAMRA alkyne. Lane 1: molecular weight marker, 2: click chemistry product of sfGFP SpyTag with para-azidophenylalanine and TAMRA alkyne. Product observed at 35 kDa, consistent with the theoretical molecular weight of sfGFP SpyTag.

This suggests para-azidophenylalanine was successfully incorporated into sfGFP and the site is accessible. To test incorporation of alkyne o-propargyl-tyrosine in HK2, TAMRA azide was clicked on. Once again, a band at the expected molecular weight lit up, suggesting incorporation in HK2 was successful and the site is accessible (**Figure 6.7**).

Figure 6.7 SDS-PAGE of HK2 D19TAG with o-propargyl-tyrosine clicked to TAMRA azide. Lane 1: molecular weight marker, 2: click chemistry product of HK2 D19TAG with o-propargyl-tyrosine and TAMRA azide. Product observed at 100 kDa, consistent with the theoretical molecular weight.

Attempts to click sfGFP SpyTag T50TAG with para-azidophenylalanine and HK2 D19TAG with o-propargyl-tyrosine were unsuccessful. As a result, future work involves clicking sfGFP SpyTag T50TAG para-azidophenylalanine with synthesized SnoopTag-alkyne. This will then be reacted with SpyCatcher G6PD (reacts with SpyTag) and HK2 SnoopCatcher (reacts with SnoopTag). The final construct will have SpyCatcher G6PD and SnoopCatcher HK2 on opposite sides of the sfGFP barrel. The kinetics of this system will be compared to SnoopTag sfGFP SpyTag with SpyCatcher G6PD and HK2 SnoopCatcher on top of the barrel.

6.5 Conclusion/Future Work

The development of a three-enzyme complex should enable substrate channeling between HK2 and G6PD. Since the intermediate, D-glucose-6-phosphate, is negatively charged, electrostatic guidance should be possible along the surface of supercharged sfGFP scaffolds. Three different variants will be tested including -30, 0, and +36. Substrate channeling is expected with +36, repulsion is expected with -30, and 0 is expected to fall somewhere in between.

Two different set-ups of the complexes will be studied. In the first, HK2 and G6PD will be on top of the sfGFP barrel and will attach through orthogonal tagged systems, SpyTag/SpyCatcher and SnoopTag/SnoopCatcher. SDS-PAGE gels suggest the complex has been formed, but the yields are extremely low, and the unconjugated proteins are present in solution. As a result, the reaction needs to be optimized. Furthermore, isolating the three-enzyme complex will be required in order to test the efficiency of substrate channeling. In the second set-up, HK2 and G6PD will be on opposite sides of the sfGFP barrel and will attach through both the tagged systems as well as through click chemistry. Although incorporation of azides and alkynes has been successful in

sfGFP and HK2, the click reaction between the two has been unsuccessful. Therefore, future work includes clicking synthesized SnoopTag-alkyne onto sfGFP SpyTag T50TAG. This will allow HK2 to attach via SnoopCatcher. This method is being tested as we believe the click reaction might be unsuccessful due to the steric hindrance provided by the bulky sfGFP and HK2 proteins making the click sites between them inaccessible. Once this set-up is accomplished, HK2 and G6PD will be on opposite sides of the sfGFP barrel and the intermediate should be guided along the surface of sfGFP. Here HK2 and G6PD are not adjacent to one another, which is unlike the first set-up where there is a possibility that HK2 and G6PD are close enough to make sfGFP unnecessary.

Kinetics will be tested by saturating one of the substrates in both HK2 and G6PD to study Michalis-Menton type kinetics. The reaction with HK2 will proceed by saturating ATP and the reaction with G6PD will be performed by saturating $NADP^+$. This will allow the intermediate to be studied. Of course, the reactions will be performed with the different sfGFP variants as well as with the proteins mixed in solution and complexed together.

6.6 Supporting Information

Primers to clone G6PD into pET-28a(+) at *NheI*

FWD: GCGGCAGCCATATGGCTATGGCAGAGCAGGTGGCCCTGAGC

REV: CACCAGTCATGCTAGTCAGAGCTTGTGGGGGTTCACCCACTTGTAGGT

Primers to clone SpyCatcher at N-terminus of G6PD pET-28a(+) at *NdeI*

FWD: GCCGCGCGGCAGCCATGGCGCCATGGTTGATACCTTATCAGGTTTATCAAGTGAG

REV: TCTGCCATAGCCATACCAATATGAGCGTCACCTTTAGTTGCTTTGCCATTTACAGTAACC

SpyCatcher G6PD pET-28a(+) DNA Sequence

```
ATGGGCAGCA GCCATCATCA TCATCATCAC AGCAGCGGCC TGGTGCCGCG CGGCAGCCAT 60
GGCGCCATGG TTGATACCTT ATCAGGTTTA TCAAGTGAGC AAGGTCAGTC CGGTGATATG 120
ACAATTGAAG AAGATAGTGC TACCCATATT AAATTCTCAA AACGTGATGA GGACGGCAAA 180
GAGTTAGCTG GTGCAACTAT GGAGTTGCGT GATTCATCTG GTAAAACTAT TAGTACATGG 240
ATTTCAGATG GACAAGTGAA AGATTTCTAC CTGTATCCAG GAAAATATAC ATTTGTCGAA 300
ACCGCAGCAC CAGACGGTTA TGAGGTAGCA ACTGCTATTA CCTTTACAGT TAATGAGCAA 360
GGTCAGGTTA CTGTAAATGG CAAAGCAACT AAAGGTGACG CTCATATTGG TATGGCTATG 420
GCAGAGCAGG TGGCCCTGAG CCGGACCCAG GTGTGCGGGA TCCTGCGGGA AGAGCTTTTC 480
CAGGGCGATG CCTTCCATCA GTCGGATACA CACATATTCA TCATCATGGG TGCATCGGGT 540
GACCTGGCCA AGAAGAAGAT CTACCCCACC ATCTGGTGGC TGTTCCGGGA TGGCCTTCTG 600
CCCGAAAACA CCTTCATCGT GGGCTATGCC CGTTCCCGCC TCACAGTGGC TGACATCCGC 660
AAACAGAGTG AGCCCTTCTT CAAGGCCACC CCAGAGGAGA AGCTCAAGCT GGAGGACTTC 720
TTTGCCCGCA ACTCCTATGT GGCTGGCCAG TACGATGATG CAGCCTCCTA CCAGCGCCTC 780
AACAGCCACA TGAATGCCCT CCACCTGGGG TCACAGGCCA ACCGCCTCTT CTACCTGGCC 840
TTGCCCCCGA CCGTCTACGA GGCCGTCACC AAGAACATTC ACGAGTCCTG CATGAGCCAG 900
ATAGGCTGGA ACCGCATCAT CGTGGAGAAG CCCTTCGGGA GGGACCTGCA GAGCTCTGAC 960
CGGCTGTCCA ACCACATCTC CTCCCTGTTC CGTGAGGACC AGATCTACCG CATCGACCAC 1020
TACCTGGGCA AGGAGATGGT GCAGAACCTC ATGGTGCTGA GATTTGCCAA CAGGATCTTC 1080
GGCCCCATCT GGAACCGGGA CAACATCGCC TGCGTTATCC TCACCTTCAA GGAGCCCTTT 1140
GGCACTGAGG GTCGCGGGGG CTATTTCGAT GAATTTGGGA TCATCCGGGA CGTGATGCAG 1200
AACCACCTAC TGCAGATGCT GTGTCTGGTG GCCATGGAGA AGCCCGCCTC CACCAACTCA 1260
GATGACGTCC GTGATGAGAA GGTCAAGGTG TTGAAATGCA TCTCAGAGGT GCAGGCCAAC 1320
AATGTGGTCC TGGGCCAGTA CGTGGGGAAC CCCGATGGAG AGGGCGAGGC CACCAAAGGG 1380
TACCTGGACG ACCCCACGGT GCCCCGCGGG TCCACCACCG CCACTTTTGC AGCCGTCGTC 1440
CTCTATGTGG AGAATGAGAG GTGGGATGGG GTGCCCTTCA TCCTGCGCTG CGGCAAGGCC 1500
CTGAACGAGC GCAAGGCCGA GGTGAGGCTG CAGTTCCATG ATGTGGCCGG CGACATCTTC 1560
CACCAGCAGT GCAAGCGCAA CGAGCTGGTG ATCCGCGTGC AGCCCAACGA GGCCGTGTAC 1620
ACCAAGATGA TGACCAAGAA GCCGGGCATG TTCTTCAACC CCGAGGAGTC GGAGCTGGAC 1680
CTGACCTACG GCAACAGATA CAAGAACGTG AAGCTCCCTG ACGCCTATGA GCGCCTCATC 1740
CTGGACGTCT TCTGCGGGAG CCAGATGCAC TTCGTGCGCA GCGACGAGCT CCGTGAGGCC 1800
TGGCGTATTT TCACCCCACT GCTGCACCAG ATTGAGCTGG AGAAGCCCAA GCCCATCCCC 1860
TATATTTATG GCAGCCGAGG CCCCACGGAG GCAGACGAGC TGATGAAGAG AGTGGGTTTC 1920
CAGTATGAGG GCACCTACAA GTGGGTGAAC CCCCACAAGC TCTGA 1965
```

SpyCatcher G6PD Protein Sequence (SpyCatcher highlighted in blue)

```
MGSSHHHHHH SSGLVPRGSH GAMVDTLSGL SSEQGQSGDM TIEEDSATHI KFSKRDEDGK 60
ELAGATMELR DSSGKTISTW ISDGQVKDFY LYPGKYTFVE TAAPDGYEVA TAITFTVNEQ 120
GQVTVNGKAT KGDAHIGMAM AEQVALSRTQ VCGILREELF QGDAFHQSDT HIFIIMGASG 180
DLAKKKIYPT IWWLFRDGLL PENTFIVGYA RSRLTVADIR KQSEPFFKAT PEEKLKLEDF 240
FARNSYVAGQ YDDAASYQRL NSHMNALHLG SQANRLFYLA LPPTVYEAVT KNIHESCMSQ 300
IGWNRIIVEK PFGRDLQSSD RLSNHISSLF REDQIYRIDH YLGKEMVQNL MVLRFANRIF 360
GPIWNRDNIA CVILTFKEPF GTEGRGGYFD EFGIIRDVMQ NHLLQMLCLV AMEKPASTNS 420
DDVRDEKVKV LKCISEVQAN NVVLGQYVGN PDGEGEATKG YLDDPTVPRG STTATFAAVV 480
LYVENERWDG VPFILRCGKA LNERKAEVRL QFHDVAGDIF HQQCKRNELV IRVQPNEAVY 540
TKMMTKKPGM FFNPEESELD LTYGNRYKNV KLPDAYERLI LDVFCGSQMH FVRSDELREA 600
WRIFTPLLHQ IELEKPKPIP YIYGSRGPTE ADELMKRVGF QYEGTYKWVN PHKL 654
```

Ultramers to clone sfGFP with SpyTag at C-terminus into pET-28a(+)

-30 sfGFP SpyTag

FWD: CGAGCTCCGTCGACAA ATGGGTGGCGCTAGCAAAGGTGAAGAGCTG

REV:
GTGCGGCCGCAAGCTTTACTTCGTCGGCTTGTAGGCGTCCACCATCACGATGTGGGC
CTTGTACAGCTCGTCCATTCCATGATCAATGCCTGCAG

0 sfGFP SpyTag

FWD: CGAGCTCCGTCGACAAATGGGTGGCGCTAGCAAAGGTGAACGTCTG

REV:
GTGCGGCCGCAAGCTTTACTTCGTCGGCTTGTAGGCGTCCACCATCACGATGTGGGC
CTTGTAGCGTTCGTCCATTCCGTGCGTAATGCCTG

+36 sfGFP SpyTag

FWD: CGAGCTCCGTCGACAAATGGGTGGCGCTAGCAAAGGTGAACGTCTG

REV:
GTGCGGCCGCAAGCTTTACTTCGTCGGCTTGTAGGCGTCCACCATCACGATGTGGGC
CTTGTAGCGTTCGTCGCGTCCGTGCTTAAT

Primers for T50TAG in sfGFP-SpyTag for Unnatural Amino Acid Incorporation

-30 sfGFP:

FWD: CCGAGGGTGAATTGACCCTGAAGTTTATTTGCACATAGGGCGAATTACCCGTTCCGTGGC

REV: GCCACGGAACGGGTAATTCGCCCTATGTGCAAATAAACTTCAGGGTCAATTCACCCTCGG

0 sfGFP:

FWD: CCAATGGTAAATTGACCCTGAAGTTTATTTGCACATAGGGCAAATTACCCGTTCCGTGGC

REV: GCCACGGAACGGGTAATTTGCCCTATGTGCAAATAAACTTCAGGGTCAATTTACCATTGG

+36 sfGFP:

FWD: CGTGGTAAATTGACCCTGAAGTTTATTTGCACATAGGGCAAATTACCCGTTCCGTGGC

REV: GCCACGGAACGGGTAATTTGCCCTATGTGCAAATAAACTTCAGGGTCAATTTACCACG

Primers to add stop codon before SpyTag in sfGFP-SpyTag

-30 sfGFP:

FWD: TTGATCATGGAATGGACGAGCTGTACAAGTGACACATCGTGATGGTGGACGCCTACAAGC

REV: GCTTGTAGGCGTCCACCATCACGATGTGTCACTTGTACAGCTCGTCCATTCCATGATCAA

0 sfGFP:

FWD: ACGCACGGAATGGACGAACGCTACAAGTGACACATCGTGATGGTGGACGCCTACAAGC

REV: GCTTGTAGGCGTCCACCATCACGATGTGTCACTTGTAGCGTTCGTCCATTCCGTGCGT

+36 sfGFP:

FWD: CACGGACGCGACGAACGCTACAAGTGACACATCGTGATGGTGGACGCCTACAAGC

REV: GCTTGTAGGCGTCCACCATCACGATGTGTCACTTGTAGCGTTCGTCGCGTCCGTG

DNA Sequences

-30 sfGFP SpyTag

```
ATGGGCAGCA GCCATCATCA TCATCATCAC AGCAGCGGCC TGGTGCCGCG CGGCAGCCAT 60
ATGGCTAGCA TGACTGGTGG ACAGCAAATG GGTCGCGGAT CCGAATTCGA GCTCCGTCGA 120
CAAATGGGTG GCGCTAGCAA AGGTGAAGAG CTGTTTGACG GTGTAGTACC GATCTTAGTG 180
GAATTAGACG GCGACGTGAA CGGTCACGAA TTTAGCGTGC GCGGCGAGGG CGAAGGTGAC 240
GCTACCGAGG GTGAATTGAC CCTGAAGTTT ATTTGCACAA CAGGCGAATT ACCCGTTCCG 300
TGGCCCACCT TAGTGACCAC CCTGACCTAT GGCGTTCAGT GCTTCAGTGA TTACCCAGAT 360
CATATGGATC AACACGATTT TTTCAAATCA GCCATGCCTG AAGGATATGT TCAAGAGCGT 420
ACAATCAGCT TCAAGGACGA TGGCACCTAT AAAACGCGTG CGGAAGTGAA ATTTGAAGGC 480
GACACATTAG TAAACCGTAT CGAACTGAAA GGTATCGACT TCAAAGAAGA CGGCAACATT 540
TTAGGCCATA AGCTGGAATA TAACTTTAAT TCTCATGACG TGTATATTAC GGCCGATAAA 600
CAGGAAAACG GTATCAAGGC AGAATTTGAA ATTCGCCATA ACGTGGAGGA CGGCAGCGTT 660
CAATTAGCGG ATCATTATCA ACAAAACACG CCGATTGGTG ATGGGCCTGT ACTGTTACCT 720
GACGATCACT ACCTGAGCAC GGAGTCAGCC CTGAGCAAAG ATCCGAACGA AGACCGCGAT 780
CACATGGTTC TGTTAGAATT CGTGACCGCT GCAGGCATTG ATCATGGAAT GGACGAGCTG 840
TACAAGGCCC ACATCGTGAT GGTGGACGCC TACAAGCCGA CGAAGTAA 888
```

0 sfGFP SpyTag

```
ATGGGCAGCA GCCATCATCA TCATCATCAC AGCAGCGGCC TGGTGCCGCG CGGCAGCCAT 60
ATGGCTAGCA TGACTGGTGG ACAGCAAATG GGTCGCGGAT CCGAATTCGA GCTCCGTCGA 120
CAAATGGGTG GCGCTAGCAA AGGTGAACGT CTGTTTACTG GTGTAGTACC GATCTTAGTG 180
GAATTAGACG GCGACGTGAA CGGTCATAAA TTTAGCGTGC GCGGCGAGGG CGAAGGTGAC 240
GCTACCAATG GTAAATTGAC CCTGAAGTTT ATTTGCACAA CAGGCAAATT ACCCGTTCCG 300
TGGCCCACCT TAGTGACCAC CCTGACCTAT GGCGTTCAGT GCTTCAGTCG TTACCCTGAT 360
CATATGAAAC AACACGATTT TTTCAAATCA GCCATGCCTG AAGGATATGT TCAAGAGCGT 420
ACAATCAGCT TCAAGGACGA TGGCACCTAT AAAACGCGTG CGGAAGTGAA ATTTGAAGGC 480
GACACATTAG TAAATCGTAT CGAACTGAAA GGTCGTGACT TCAAAGAAGA CGGCAACATT 540
TTAGGCCATA AACTGGAATA TAACTTTAAT TCTCATAACG TGTATATTAC GGCCGATAAA 600
CAGAAGAATG GTATCAAGGC AAATTTCAAA ATTCGCCATA ACGTGGAGGA CGGCAGCGTT 660
CAATTAGCGG ATCATTATCA ACAAAACACG CCGATTGGTG ATGGGCCTGT ACTGTTACCT 720
CGCAACCACT ACCTGAGCAC CCAATCTGCC CTGAGCAAAG ATCCGAAAGA AAAACGCGAT 780
CACATGGTTC TGTTAGAATT CGTGACCGCT GCAGGCATTA CGCACGGAAT GGACGAACGC 840
TACAAGGCCC ACATCGTGAT GGTGGACGCC TACAAGCCGA CGAAGTAA 888
```

+36 sfGFP SpyTag

```
ATGGGCAGCA GCCATCATCA TCATCATCAC AGCAGCGGCC TGGTGCCGCG CGGCAGCCAT 60
ATGGCTAGCA TGACTGGTGG ACAGCAAATG GGTCGCGGAT CCGAATTCGA GCTCCGTCGA 120
CAAATGGGTG GCGCTAGCAA AGGTGAACGT CTGTTTCGTG GTAAAGTACC GATCTTAGTG 180
GAATTAAAGG GCGACGTGAA CGGTCATAAA TTTAGCGTGC GCGGCAAAGG CAAAGGTGAC 240
GCTACCCGTG GTAAATTGAC CCTGAAGTTT ATTTGCACAA CAGGCAAATT ACCCGTTCCG 300
TGGCCCACCT TAGTGACCAC CCTGACCTAT GGCGTTCAGT GCTTCAGTCG TTACCCTAAA 360
CATATGAAAC GTCACGATTT TTTCAAATCA GCCATGCCTA AAGGATATGT TCAAGAGCGT 420
ACAATCAGCT TCAAGAAGGA TGGCAAATAT AAAACGCGTG CGGAAGTGAA ATTTGAAGGC 480
```

```
CGCACATTAG TAAATCGTAT CAAACTGAAA GGTCGTGACT TCAAAGAAAA AGGCAACATT 540
TTAGGCCATA AACTGCGTTA TAACTTTAAT TCTCATAAGG TGTATATTAC GGCCGATAAA 600
CGCAAGAATG GTATCAAGGC AAAATTCAAA ATTCGCCATA ACGTGAAAGA CGGCAGCGTT 660
CAATTAGCGG ATCATTATCA ACAAAACACG CCGATTGGTC GCGGGCCTGT ACTGTTACCT 720
CGCAACCACT ACCTGAGCAC CCGTTCTAAA CTGAGCAAAG ATCCGAAAGA AAAACGCGAT 780
CACATGGTTC TGTTAGAATT CGTGACCGCT GCAGGCATTA AGCACGGACG CGACGAACGC 840
TACAAGGCCC ACATCGTGAT GGTGGACGCC TACAAGCCGA CGAAGTAA 888
```

Amino Acid Sequences

-30 sfGFP SpyTag:

```
MGSSHHHHHH SSGLVPRGSH MASMTGGQQM GRGSEFELRR QMGGASKGEE LFDGVVPILV 60
ELDGDVNGHE FSVRGEGEGD ATEGELTLKF ICTTGELPVP WPTLVTTLTY GVQCFSDYPD 120
HMDQHDFFKS AMPEGYVQER TISFKDDGTY KTRAEVKFEG DTLVNRIELK GIDFKEDGNI 180
LGHKLEYNFN SHDVYITADK QENGIKAEFE IRHNVEDGSV QLADHYQQNT PIGDGPVLLP 240
DDHYLSTESA LSKDPNEDRD HMVLLEFVTA AGIDHGMDEL YKAHIVMVDA YKPTK 295
```

0 sfGFP SpyTag:

```
MGSSHHHHHH SSGLVPRGSH MASMTGGQQM GRGSEFELRR QMGGASKGER LFTGVVPILV 60
ELDGDVNGHK FSVRGEGEGD ATNGKLTLKF ICTTGKLPVP WPTLVTTLTY GVQCFSRYPD 120
HMKQHDFFKS AMPEGYVQER TISFKDDGTY KTRAEVKFEG DTLVNRIELK GRDFKEDGNI 180
LGHKLEYNFN SHNVYITADK QKNGIKANFK IRHNVEDGSV QLADHYQQNT PIGDGPVLLP 240
RNHYLSTQSA LSKDPKEKRD HMVLLEFVTA AGITHGMDER YKAHIVMVDA YKPTK 295
```

+36 sfGFP SpyTag:

```
MGSSHHHHHH SSGLVPRGSH MASMTGGQQM GRGSEFELRR QMGGASKGER LFRGKVPILV 60
ELKGDVNGHK FSVRGKGKGD ATRGKLTLKF ICTTGKLPVP WPTLVTTLTY GVQCFSRYPK 120
HMKRHDFFKS AMPKGYVQER TISFKKDGKY KTRAEVKFEG RTLVNRIKLK GRDFKEKGNI 180
LGHKLRYNFN SHKVYITADK RKNGIKAKFK IRHNVKDGSV QLADHYQQNT PIGRGPVLLP 240
RNHYLSTRSK LSKDPKEKRD HMVLLEFVTA AGIKHGRDER YKAHIVMVDA YKPTK 295
```

(**Amino acid mutated to stop codon highlighted in red – to remove SpyTag)

(**Amino acid mutated to amber stop codon for unnatural amino acid incorporation highlighted in blue)

Ultramers to clone SnoopTag at the N-terminus of sfGFP-SpyTag pET-28a(+)

SnoopTag -30 sfGFP SpyTag

FWD:

CGAGCTCCGTCGACAAATGGGAAAACTGGGCGATATTGAATTTATTAAAGTGAACAAAGGTAGT
GGTGAAAGTGGTATGGGTCGCGGATCCGAATTCGAGCTC

REV:
GTGCGGCCGCAAGCTTTACTTCGTCGGCTTGTAGGCGTCCACCATCACGATGTGGGC
CTTGTAGCGTTCGTCGCGTCCGTGCTTAAT

SnoopTag 0 sfGFP SpyTag / SnoopTag +36 sfGFP SpyTag

FWD:
CGAGCTCCGTCGACAAATGGGAAAACTGGGCGATATTGAATTTATTAAAGTGAACAAAGGTAGT
GGTGAAAGTGGTATGGGTGGCGCTAGCAAAGGTGAACGTCTGTTT

REV: GTGCGGCCGCAAGCTTTACTTCGTCGGCTTGTAGGCGTCCACCATCAC

SnoopTag +36 sfGFP SpyTag DNA Sequence

```
ATGGGCAGCA GCCATCATCA TCATCATCAC AGCAGCGGCC TGGTGCCGCG CGGCAGCCAT 60
ATGGCTAGCA TGACTGGTGG ACAGCAAATG GGTCGCGGAT CCGAATTCGA GCTCCGTCGA 120
CAAATGGGAA AACTGGGCGA TATTGAATTT ATTAAAGTGA ACAAAGGTAG TGGTGAAAGT 180
GGTATGGGTG GCGCTAGCAA AGGTGAACGT CTGTTTCGTG GTAAAGTACC GATCTTAGTG 240
GAATTAAAGG GCGACGTGAA CGGTCATAAA TTTAGCGTGC GCGGCAAAGG CAAAGGTGAC 300
GCTACCCGTG GTAAATTGAC CCTGAAGTTT ATTTGCACAA CAGGCAAATT ACCCGTTCCG 360
TGGCCCACCT TAGTGACCAC CCTGACCTAT GGCGTTCAGT GCTTCAGTCG TTACCCTAAA 420
CATATGAAAC GTCACGATTT TTTCAAATCA GCCATGCCTA AAGGATATGT TCAAGAGCGT 480
ACAATCAGCT TCAAGAAGGA TGGCAAATAT AAAACGCGTG CGGAAGTGAA ATTTGAAGGC 540
CGCACATTAG TAAATCGTAT CAAACTGAAA GGTCGTGACT TCAAAGAAAA AGGCAACATT 600
TTAGGCCATA AACTGCGTTA TAACTTTAAT TCTCATAAGG TGTATATTAC GGCCGATAAA 660
CGCAAGAATG GTATCAAGGC AAAATTCAAA ATTCGCCATA ACGTGAAAGA CGGCAGCGTT 720
CAATTAGCGG ATCATTATCA ACAAAACACG CCGATTGGTC GCGGGCCTGT ACTGTTACCT 780
CGCAACCACT ACCTGAGCAC CCGTTCTAAA CTGAGCAAAG ATCCGAAAGA AAAACGCGAT 840
CACATGGTTC TGTTAGAATT CGTGACCGCT GCAGGCATTA AGCACGGACG CGACGAACGC 900
TACAAGGCCC ACATCGTGAT GGTGGACGCC TACAAGCCGA CGAAGTAA 948
```

SnoopTag +36 sfGFP SpyTag Protein Sequence (SnoopTag / sfGFP / SpyTag)

```
MGSSHHHHHH SSGLVPRGSH MASMTGGQQM GRGSEFELRR QMGKLGDIEF IKVNKGSGES 60
GMGGASKGER LFRGKVPILV ELKGDVNGHK FSVRGKGKGD ATRGKLTLKF ICTTGKLPVP 120
WPTLVTTLTY GVQCFSRYPK HMKRHDFFKS AMPKGYVQER TISFKKDGKY KTRAEVKFEG 180
RTLVNRIKLK GRDFKEKGNI LGHKLRYNFN SHKVYITADK RKNGIKAKFK IRHNVKDGSV 240
QLADHYQQNT PIGRGPVLLP RNHYLSTRSK LSKDPKEKRD HMVLLEFVTA AGIKHGRDER 300
YKAHIVMVDA YKPTK 315
```

Primers for Site-Directed Mutagenesis for D19TAG HK2 pET-28a(+)

FWD: GGCCTGGTTCCGCGTGGTAGT**TAG**CAAGTGCAGAAGGTTGACCAGTATCTCTACCACATG

REV: CATGTGGTAGAGATACTGGTCAACCTTCTGCACTTGCTAACTACCACGCGGAACCAGGCC

Primers to Clone SnoopCatcher at C-terminus of HK2 pET-28a(+) at *Hind III*

FWD: GGACAGTGATGACGAATGAAGCCGCTGCGTGGTGC

REV: GTGCGGCCGCAAGCTTCATTTCGGCGGTATCGGTTCATTGGTGATATAATGT

Primers to remove stop codon between HK2 and SnoopCatcher

FWD: CCGCATCCGTGAGGCTGGACAGTCATCACGAATGAAGCCGCTGCGTGGTG

REV: CACCACGCAGCGGCTTCATTCGTGATGACTGTCCAGCCTCACGGATGCGG

HK2-pET28a(+) SnoopCatcher DNA sequence

```
atgggcagca gccatcatca tcatcatcac agcagcggcc tggttccgcg tggtagtgac 60
caagtgcaga aggttgacca gtatctctac cacatgcgcc tctctgatga gaccctcttg 120
gagatctcta agcggttccg caaggagatg gagaaagggc ttggagccac cactcaccct 180
actgcagcag tgaagatgct gcccaccttt gtgaggtcca ctccagatgg gacagaacac 240
ggagagttcc tggctctgga tcttggaggg accaacttcc gtgtgctttg ggtgaaagta 300
acggacaatg ggctccagaa ggtggagatg gagaatcaga tctatgccat ccctgaggac 360
atcatgcgag gcagtggcac ccagctgttt gaccacattg ccgaatgcct ggctaacttc 420
atggataagc tacaaatcaa agacaagaag ctcccactgg gttttacctt ctcgttcccc 480
tgccaccaga ctaaactaga cgagagtttc ctggtctcat ggaccaaggg attcaagtcc 540
agtggagtgg aaggcagaga cgttgtggct ctgatccgga aggccatcca gaggagaggg 600
gactttgata tcgacattgt ggctgtggtg aatgacacag ttgggaccat gatgacctgt 660
ggttatgatg accacaactg tgagattggt ctcattgtgg gcacgggcag caacgcctgc 720
tacatggaag agatgcgcca catcgacatg gtggaaggcg atgaggggcg gatgtgtatc 780
aatatggagt ggggggcctt cggggacgat ggctcgctca acgacattcg cactgagttt 840
gaccaggaga ttgacatggg ctcactgaac ccgggaaagc aactgtttga gaagatgatc 900
agtgggatgt acatggggga gctggtgagg cttatcctgg tgaagatggc caaggaggag 960
ctgctctttg gggggaagct cagcccagag cttctcaaca ccggtcgctt tgagaccaaa 1020
gacatctcag acattgaagg ggagaaggat ggcatccgga aggcccgtga ggtcctgatg 1080
cggttgggcc tggacccgac tcaggaggac tgcgtggcca ctcaccggat ctgccagatc 1140
gtgtccacac gctccgccag cctgtgcgca gccaccctgg ccgccgtgct gcagcgcatc 1200
aaggagaaca aaggcgagga gcggctgcgc tctactattg gggtcgacgg ttccgtctac 1260
aagaaacacc cccattttgc caagcgtcta cataagaccg tgcggcggct ggtgcccggc 1320
tgcgatgtcc gcttcctccg ctccgaggat ggcagtggca aaggtgcagc catggtgaca 1380
gcagtggctt accggctggc cgatcaacac cgtgcccgcc agaagacatt agagcatctg 1440
cagctgagcc atgaccagct gctggaggtc aagaggagga tgaaggtaga aatggagcga 1500
ggtctgagca aggagactca tgccagtgcc cccgtcaaga tgctgcccac ctacgtgtgt 1560
gctaccccgg acggcacaga gaaaggggac ttcttggcct tggaccttgg aggaacaaat 1620
ttccgggtcc tgctggtccg tgttcggaat gggaagtggg gtggagtgga gatgcacaac 1680
aagatctacg ccatcccgca ggaggtcatg cacggcaccg gggacgagct ctttgaccac 1740
attgtccagt gcatcgcgga cttcctcgag tacatgggca tgaagggcgt gtccctgcct 1800
ctgggtttta ccttctcctt cccctgccag cagaacagcc tggacgagag catcctcctc 1860
aagtggacaa aaggcttcaa ggcatctggc tgcgagggcg aggacgtggt gaccctgctg 1920
aaggaagcga tccaccggcg agaggagttt gacctggatg tggttgctgt ggtgaacgac 1980
acagtcggaa ctatgatgac ctgtggcttt gaagaccctc actgtgaagt tggcctcatt 2040
```

gttggcacgg gcagcaatgc ctgctacatg gaggagatgc gcaacgtgga actggtggaa 2100
ggagaagagg ggcggatgtg tgtgaacatg gaatgggggg ccttcgggga caatggatgc 2160
ctagatgact tccgcacaga atttgatgtg gctgtggatg agctttcact caaccccggc 2220
aagcagaggt tcgagaaaat gatcagtgga atgtacctgg gtgagattgt ccgtaacatt 2280
ctcatcgatt tcaccaagcg tggactactc ttccgaggcc gcatctcaga gcggctcaag 2340
acaaggggca tctttgaaac caagttcttg tctcagattg agagtgactg cctggccctg 2400
ctgcaagtcc gagccatcct gcaacactta gggcttgaga gcacctgtga cgacagcatc 2460
attgttaagg aggtgtgcac tgtggtggcc cggcgggcag cccagctctg tggcgcaggc 2520
atggccgctg tggtggacag gatacgagaa aaccgtgggc tggacgctct caaagtgaca 2580
gtgggtgtgg atgggaccct ctacaagcta catcctcact ttgccaaagt catgcatgag 2640
acagtgaagg acctggctcc gaaatgtgat gtgtctttcc tgcagtcaga ggatggcagc 2700
gggaaggggg cggcgctcat cactgctgtg gcctgccgca tccgtgaggc tggacagtca 2760
tcacgaatga agccgctgcg tggtgccgtg tttagcctgc agaaacagca tcccgactat 2820
cccgatatct atggcgcgat tgatcagaat gggacctatc aaaatgtgcg taccggcgaa 2880
gatggtaaac tgacctttaa gaatctgagc gatggcaaat atcgcctgtt tgaaaatagc 2940
gaacccgctg gctataaacc ggtgcagaat aagccgattg tggcgtttca gattgtgaat 3000
ggcgaagtgc gtgatgtgac cagcattgtg ccgcaggata ttccggctac atatgaattt 3060
accaacggta aacattatat caccaatgaa ccgataccgc cgaaa 3105

HK2-pET28a(+) SnoopCatcher Protein Sequence (SnoopCatcher highlighted in red)

MGSSHHHHHH SSGLVPRGSD QVQKVDQYLY HMRLSDETLL EISKRFRKEM EKGLGATTHP 60
TAAVKMLPTF VRSTPDGTEH GEFLALDLGG TNFRVLWVKV TDNGLQKVEM ENQIYAIPED 120
IMRGSGTQLF DHIAECLANF MDKLQIKDKK LPLGFTFSFP CHQTKLDESF LVSWTKGFKS 180
SGVEGRDVVA LIRKAIQRRG DFDIDIVAVV NDTVGTMMTC GYDDHNCEIG LIVGTGSNAC 240
YMEEMRHIDM VEGDEGRMCI NMEWGAFGDD GSLNDIRTEF DQEIDMGSLN PGKQLFEKMI 300
SGMYMGELVR LILVKMAKEE LLFGGKLSPE LLNTGRFETK DISDIEGEKD GIRKAREVLM 360
RLGLDPTQED CVATHRICQI VSTRSASLCA ATLAAVLQRI KENKGEERLR STIGVDGSVY 420
KKHPHFAKRL HKTVRRLVPG CDVRFLRSED GSGKGAAMVT AVAYRLADQH RARQKTLEHL 480
QLSHDQLLEV KRRMKVEMER GLSKETHASA PVKMLPTYVC ATPDGTEKGD FLALDLGGTN 540
FRVLLVRVRN GKWGGVEMHN KIYAIPQEVM HGTGDELFDH IVQCIADFLE YMGMKGVSLP 600
LGFTFSFPCQ QNSLDESILL KWTKGFKASG CEGEDVVTLL KEAIHRREEF DLDVVAVVND 660
TVGTMMTCGF EDPHCEVGLI VGTGSNACYM EEMRNVELVE GEEGRMCVNM EWGAFGDNGC 720
LDDFRTEFDV AVDELSLNPG KQRFEKMISG MYLGEIVRNI LIDFTKRGLL FRGRISERLK 780
TRGIFETKFL SQIESDCLAL LQVRAILQHL GLESTCDDSI IVKEVCTVVA RRAAQLCGAG 840
MAAVVDRIRE NRGLDALKVT VGVDGTLYKL HPHFAKVMHE TVKDLAPKCD VSFLQSEDGS 900
GKGAALITAV ACRIREAGQS SRMKPLRGAV FSLQKQHPDY PDIYGAIDQN GTYQNVRTGE 960
DGKLTFKNLS DGKYRLFENS EPAGYKPVQN KPIVAFQIVN GEVRDVTSIV PQDIPATYEF 1020
TNGKHYITNE PIPPK 1035

** Amino acid mutated to amber stop codon to test unnatural amino acid incorporation highlighted in blue. Stop codon for HK2 D19TAG gene in pET-28a(+) would be where the current “S” is underlined (before SnoopCatcher was cloned in).

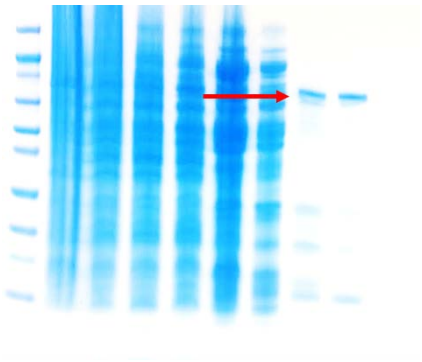

Figure 6.8 SDS-PAGE of SpyCatcher G6PD nickel column purification. A band at around 75 kDa is observed, consistent with the theoretical molecular weight.

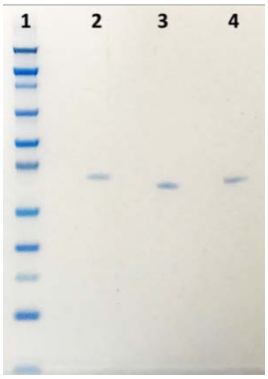

Figure 6.9 SDS-PAGE of sfGFP after normalizing at 485 nm. Lane 1: molecular weight marker, lane 2: -30 sfGFP, lane 3: 0 sfGFP, and lane 4: +36 sfGFP. A band at approximately 33 kDa is observed, consistent with the theoretical molecular masses.

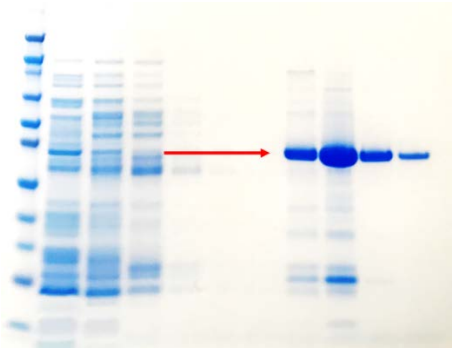

Figure 6.10 SDS-PAGE of SnoopTag sfGFP SpyTag purification on nickel column. Protein ladder followed by elution with varying immidizole concentrations. SnoopTag sfGFP SpyTag runs at approximately 36 kDa, consistent with its theoretical molecular weight.

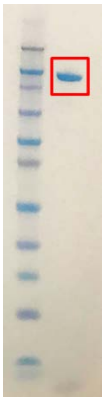

Figure 6.11 SDS-PAGE of HK2 and HK2 D19TAG. Protein runs at approximately 100 kDa, consistent with its theoretical molecular weight (band followed by molecular weight marker).

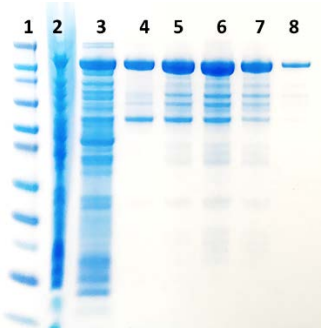

Figure 6.12 SDS-PAGE of HK2 SnoopCatcher. Lane 1: molecular weight marker, lane 2-8: HK2 SnoopCatcher with varying immidizole concentrations. Protein runs at approximately 115 kDa, consistent with its theoretical molecular weight.

CHAPTER 7

SUMMARY

In this thesis work, we extensively engineered thermostable alcohol dehydrogenase D, AdhD, from deep thermal sea vent archaea *Pyrococcus furiosus.* AdhD, our model enzyme, was used to develop engineering approaches to control activity and selectivity of enzymes for multi-step catalysis (chapters 2-6). AdhD was chosen as it is well studied in our lab, is monomeric, thermostable, and easy to engineer, all of which makes it a potentially relevant industrial catalyst. Through our various engineering approaches, we have developed an engineering toolbox that can be used to control activity and selectivity of enzymes to enable the development of biomimetic cascades. This should increase the throughput of multi-step systems and prevent the need for multiple recovery steps. Additionally, it should allow for effective substrate channeling to prevent loss of intermediates and increase catalysis.

Using point mutations or insertions in substrate loop B (chapter 2) and domain insertion in substrate loop A (chapter 3) of AdhD, we have controlled cofactor specificity. The difference lies in the external control of this selectivity provided by introducing an intrinsically disordered protein (chapter 3). To expand the substrate selectivity of AdhD, we broadened its functionality through site-specific unnatural amino acid incorporation. This allowed for the development of hybrids with an organic catalyst (TEMPO) to enable selective alcohol oxidation and to impart enzymatic selectivity onto organic catalysts both in solution and in hydrogels (chapter 4). Approaches that retain the structure of AdhD but increase catalysis through microenvironment engineering was also studied through fusions with sfGFP (chapter 5). The end goal was to combine the various approaches and tools developed through our work with AdhD and use what we learned to engineer substrate channeling in a three-enzyme system (chapter 6).

In chapter 2, we proved that a single mutation or insertion in substrate loop B of AdhD can control cofactor selectivity. Single point amino acid mutations or insertions on the back side of the

cofactor binding pocket resulted in a change in cofactor selectivity. This approach emphasizes that changes in substrate loops can affect cofactor selectivity and that substrate and cofactor selectivity are not exclusive. The reversal or broadening of cofactor selectivity affected the transition binding energies suggesting that point mutations can affect the stability of the ternary enzyme/cofactor/substrate complex. This approach should be modular, and a similar effect should be seen in other members of the aldo-keto (AKR) superfamily as they contain similar substrate loops. Therefore, potential future work can include testing the affect of these mutations in other aldo-keto reductases such as human aldose reductase, which has been engineered in the Banta Lab.

In chapter 3, additional work was done with AdhD to control cofactor selectivity, but changes were made in substrate loop A. A repeat-in-toxin domain from *Bordetella pertussis*, which is intrinsically disordered in the absence of calcium and folds into the β-roll secondary structure in the presence of calcium, was inserted into AdhD in a process called domain insertion. Both parts retained their function, namely the folding of the RTX domain was calcium-dependent while AdhD retained its activity with alcohols. The chimeric protein, β-AdhD, was reminiscent of a dimmer where, as calcium is titrated into the system, the cofactor selectivity switches from NAD^+ to $NADP^+$. This approach can be used to impart dynamic regulation of cofactor specificity to develop novel biocatalysts and biopathways for both *in vivo* and *in vitro* systems. This type of real-time external control can be used to develop multi-step cascades.

Future work involving β-AdhD includes inserting different enzymes after β-AdhD in a multi-step cascade. If enzymes with different cofactor selectivity (NADH versus NADPH) are utilized, the direction of the pathway can be controlled externally depending on the absence or presence of calcium. In the absence of calcium, β-AdhD utilizes NAD^+ and converts it to NADH whereas in the presence of calcium, $NADP^+$ is converted to NAPDH. Depending on the cofactor

preference of the proceeding enzymes, one route in the cascade will proceed while the other will not. These types of approaches are modular as AdhD is a member of the AKR superfamily which shares many characteristics including varying substrate loops, which was the insertion site used here.

In chapter 4, site-specific unnatural amino acid incorporation was used to introduce a new functional group into AdhD and expand its capabilities. A biological catalyst, AdhD, was modified with an azide-containing unnatural amino acid. This was clicked with an organic catalyst, TEMPO, containing an alkyne group. The result was an AdhD-TEMPO bio-organo hybrid. The development of various hybrids between TEMPO and different AdhD mutants with different sites containing the unnatural amino acid served multiple functions. As AdhD oxidizes secondary alcohols with medium carbon chain lengths and TEMPO oxidizes primary alcohols of any chain length, a hybrid of these two catalysts should be able to selectivity oxidize alcohols. Furthermore, since AdhD is cofactor dependent and since TEMPO must be regenerated, the reaction that proceeds can be externally controlled. In two of the hybrids (M1 AdhD/TEMPO and Y205 AdhD/TEMPO) selective oxidation of alcohols should result, with Y205 imparting steric hindrance as it is buried in the cofactor binding pocket. The third hybrid (Y64 AdhD/TEMPO) resulted in enzymatic selectivity being transferred to an organic catalyst. Future work that has already been started includes expanding the use of these hybrids by inserting them into hydrogels. This will allow for selective alcohol oxidation as well as hydrogel formation.

Furthermore, site-specific incorporation into AdhD containing substrate loops from another AKR member, human aldose reductase (hAR) has been completed. This chimeric protein has previously been shown to impart hAR cofactor and substrate selectivity onto AdhD. Developing a hybrid of this chimera with TEMPO will serve the purposes previously mentioned,

but this time with a different cofactor and substrate than those preferred by AdhD. This work can be expanded through residue-specific incorporation of unnatural amino acids onto AdhD to increase the number of TEMPO molecules attached to AdhD. The number of TEMPO molecules and its positions may affect activity in unanticipated ways.

In chapter 5, AdhD structure was retained while increasing its catalytic efficiency through microenvironment engineering. We developed a three-domain protein system consisting of AdhD, SpyTag/SpyCatcher, and supercharged superfolder GFP (sfGFP). It was determined that there is a complex interplay between salt, pH, and protein charge. Although the various effects and interactions are not completely understood, we have shown that using charged sfGFP can increase the catalytic efficiency of AdhD. It seems that negative sfGFP increases the apparent local ionic strength which accelerates rates in a certain pH range. Additionally, although salt and pH affected the kinetic parameters of AdhD-sfGFP fusions, the overall catalytic efficiency was a function of protein charge. This work can be expanded with other supercharged proteins to determine if this trend is consistent and if other changes, such as changes in local pH, play a role in catalysis.

In chapter 6, sfGFP was used to engineer substrate channeling between hexokinase II (HK2) and glucose-6-phosphate-dehydrogenase (G6PD). The previous tools and approaches that were studied with AdhD in chapters 2-5 were used to engineer substrate channeling in a three-enzyme system: HK2, G6PD, and sfGFP. HK2 converts D-glucose and ATP to D-glucose-6-phosphate and ADP. G6PD converts glucose-6-phosphate and $NADP^+$, in the presence of magnesium chloride, to 6-phospho-D-gluconate and NADPH. The intermediate, glucose-6-phosphate is negatively charged allowing for electrostatic guidance along a positively charged patch (such as +36 sfGFP). Channeling should decrease diffusion of the intermediate into the bulk thereby increasing the efficiency of the cascades. Preliminary work has shown the ability to

develop the cascades through orthogonal tagged systems. Additionally, the ability of having HK2 and G6PD work in tandem has been successful. Future work includes testing the difference in kinetics between HK2 and G6PD complexes with various supercharged sfGFP including -30, 0, and +36. Furthermore, different approaches will have to be looked into to determine the extent of substrate channeling.

REFERENCES

[1] Lancaster, L., Abdallah, W., Banta, S., Wheeldon, I., Engineering enzyme microenvironments for enhanced biocatalysis. *Chem. Soc. Rev.* 2018.

[2] Chica, R. A., Protein Engineering in the 21st Century. *Protein Sci.* 2015, *24*, 431-433.

[3] Case, F., *Chemistry World*, Royal Society of Chemistry 2016.

[4] Bundy, B. C., Swartz, J. R., Site-specific incorporation of p-propargyloxyphenylalanine in a cell-free environment for direct protein-protein click conjugation. *Bioconjugate Chem.* 2010, *21*, 255-263.

[5] Hess, G., Generic Biologics. *Chem. Eng. News* 2008, *86*, 34-35.

[6] Ali, M. E., Rahman, M. M., Sarkar, S. M., Hamid, S. B. A., Heterogeneous metal catalysts for oxidation reactions. *J. Nanomater* 2014, *2014*, 1-23.

[7] Abdellaoui, S., Hickey, D. P., Stephens, A. R., Minteer, S. D., Recombinant oxalate decarboxylase: enhancement of a hybrid catalytic cascade for the complete electro-oxidation of glycerol *Chem. Commun.* 2015, *51*, 14330-14333.

[8] Baker, K., Bleczinski, C., Lin, H., Salazar-Jimenez, G., *et al.*, Chemical complementation: A reaction-independent genetic assay for enzyme catalysis. *Proc. Natl. Acad. Sci.* 2002, *99*, 16537-16542.

[9] Zeymer, C., Hilvert, D., Directed evolution of protein catalysts. *Annu. Rev. Biochem.* 2018, *87*, 131-157.

[10] Bruggink, A., Schoevaart, R., Kieboom, T., Concepts of nature in organic synthesis: cascade catalysis and multistep conversions in concert. *Org. Process Res. Dev.* 2003, *7*, 622-640.

[11] Solanki, K., Abdallah, W., Banta, S., Extreme makeover: Engineering the activity of a thermostable alcohol dehydrogenase (AdhD) from Pyrococcus furiosus. *Biotechnol. J.* 2016, *11*, 1483-1497.

[12] Machielsen, R., Uria, A. R., Kengen, S. W. M., Oost, J. v. d., Production and characterization of a thermostable alcohol dehydrogenase that belongs to the aldo-keto reductase superfamily. *App. Environ. Microbiol.* 2006, *72*, 233-238.

[13] Hyndman, D., Bauman, D. R., Heredia, V. V., Penning, T. M., The aldo-keto reductase superfamily homepage. *Chem. Biol. Interact.* 2003, *143-144*, 621-631.

[14] Sanli, G., Blaber, M., Structural assembly of the active site in an aldo-keto reductase by NADPH cofactor. *J. Mol. Biol.* 2001, *309*, 1209-1218.

[15] Bohren, K. M., Grimshaw, C. E., Lai, C. J., Harrison, D. H., *et al.*, Tyrosine-48 is the proton donor and histidine-110 directs substrate stereochemical selectivity in the reduction reaction of human aldose reductase: enzyme kinetics and crystal structure of the Y48H mutant enzyme. *Biochemistry* 1994, *33*, 2021-2032.

[16] Ratnam, K., Ma, H., Penning, T. M., The arginine 276 anchor for NADP(H) dictates fluorescence kinetic transients in 3α-hydroxysteroid dehydrogenase, a representative aldo−keto reductase. *Biochemistry* 1999, *38*, 7856-7864.

[17] Campbell, E., Wheeldon, I. R., Banta, S., Broadening the cofactor specificity of a thermostable alcohol dehydrogenase using rational protein design introduces novel kinetic transient behavior. *Biotechnol. Bioeng.* 2010, *107*, 763 - 774.

[18] Wheeldon, I. R., Campbell, E., Banta, S., A chimeric fusion protein engineered with disparate functionalities-enzymatic activity and self-assembly. *J. Mol. Biol.* 2009, *392*, 129-142.

[19] Campbell, E., Chuang, S., Banta, S., Modular exchange of substrate-binding loops alters both substrate and cofactor specificity in a member of the aldo-keto reductase superfamily. *Protein Eng. Des. Sel.* 2013, *26*, 181-186.

[20] Campbell, E., Meredith, M., Minteer, S. D., Banta, S., Enzymatic biofuel cells utilizing a biomimetic cofactor. *Chem. Commun.* 2012, *48*, 1898-1900.

[21] Agledal, L., Niere, M., Ziegler, M., The phosphate makes a difference: cellular functions of NADP. *Redox Report* 2015, *15*, 2-10.

[22] Scrutton, N. S., Berry, A., Perham, R. N., Redesign of the coenzyme specificity of a dehydrogenase by protein engineering. *Nature* 1990, *343*, 38-43.

[23] Sanli, G., Dudley, J. I., Blaber, M., Structural biology of the aldo-keto reductase family of enzymes: catalysis and cofactor binding. *Cell Biochem. Biophys.* 2003, *38*, 79-101.

[24] Crowley, P. B., Golovin, A., Cation-pi interactions in protein-protein interfaces. *Proteins: Struct., Funct., Bioinf.* 2005, *59*, 231-239.

[25] Solanki, K., Abdallah, W., Banta, S., Engineering the cofactor specificity of an alcohol dehydrogenase via single mutations or insertions distal to the 2′-phosphate group of NADP(H). *Protein Eng. Des. Sel.* 2017, *30*, 373-380.

[26] Abdallah, W., Solanki, K., Banta, S., Insertion of a calcium-responsive β-roll domain into a thermostable alcohol dehydrogenase enables tunable control over cofactor selectivity. *ACS Catal.* 2018, *8*, 1602-1613.

[27] Link, A. J., Mock, M. L., Tirrell, D. A., Non-canonical amino acids in protein engineering. *Curr. Opin. Biotechnol.* 2003, *14*, 603-609.

[28] Stromgaard, A., Jensen, A. A., Stromgaard, K., Site-specific incorporation of unnatural amino acids into proteins. *ChemBioChem* 2004, *5*, 909-916.

[29] Lang, K., Chin, J. W., Cellular incorporation of unnatural amino acids and bioorthogonal labeling of proteins. *Chemical Reviews* 2014, *114*, 4764-4806.

[30] Chatterjee, A., Sun, S. B., Furman, J. L., Xiao, H., Schultz, P. G., A versatile platform for single- and multiple-unnatural amino acid mutagenesis in Escherichia coli. *Biochemistry* 2013, *52*, 1828-1837.

[31] Schultz, K., Supekova, L., Ryu, Y., Xie, J., *et al.*, A genetically encoded infrared probe. *J. Am. Chem. Soc.* 2006, *128*, 13984–13985.

[32] Miyake-Stoner, S., Miller, A., Hammill, J., Peeler, J., *et al.*, Probing protein folding using site-specifically encoded unnatural amino acids as FRET donors with tryptophan. *Biochemistry* 2009, *48*, 5953-5962.

[33] McMenimen, K. A., Petersson, E. J., Lester, H. A., Dougherty, D. A., Probing the Mg2+ blockade site of an N-methyl-D-aspartate (NMDA) receptor with unnatural amino acid mutagenesis. *ACS Chem. Biol.* 2006, *1*, 227-234.

[34] Srivastava, P., Yang, H., Ellis-Guardiola, K., Lewis, J. C., Engineering a dirhodium artificial metalloenzyme for selective olefin cyclopropanation. *Nat. Commun.* 2015, *6:7789*.

[35] Jackson, J. C., Hammill, J. T., Mehl, R. A., Site-specific incorporation of a (19)F-amino acid into proteins as an NMR probe for characterizing protein structure and reactivity. *J. Am. Chem. Soc.* 2007, *129*, 1160-1166.

[36] Caló, E., V.Khutoryanskiy, V., Biomedical applications of hydrogels: A review of patents and commercial products. *Eur. Polym. J.* 2015, *65*, 252-267.

[37] Wheeldon, I. R., Gallaway, J. W., Barton, S. C., Banta, S., Bioelectrocatalytic hydrogels from electronconducting metallopolypeptides coassembled with bifunctional enzymatic building blocks. *Proc. Natl. Acad. Sci.* 2008, *105*, 15275-15280.

[38] Lu, H. D., Wheeldon, I. R., Banta, S., Catalytic biomaterials: engineering organophosphate hydrolase to form self-assembling enzymatic hydrogels. *Protein Eng. Des. Sel.* 2010, *23*, 559-566.

[39] Wheeldon, I. R., Barton, S. C., Banta, S., Bioactive proteinaceous hydrogels from designed bifunctional building blocks. *Biomacromolecules* 2007, *8*, 2990-2994.

[40] Shen, W., Lammertink, R. G. H., Sakata, J. K., Kornfield, J. A., Tirrell, D. A., Assembly of an artificial protein hydrogel through leucine zipper aggregation and bisulfide bond formation. *Macromolecules* 2005, *38*, 3909-3916.

[41] Wheeldon, I., *Chemical Engineering*, Columbia University, New York, NY 2009, p. 195.

[42] Hoover, J. M., Stahl, S. S., Highly practical copper(I)/TEMPO catalyst system for chemoselective aerobic oxidation of primary alcohols. *J. Am. Chem. Soc.* 2011, *133*, 16901-16910.

[43] Badalyan, A., Stahl, S. S., Cooperative electrocatalytic alcohol oxidation with electron-proton-transfer mediators. *Nature* 2016, *535*, 406-410.

[44] Ciriminna, R., Palmisano, P. G., Pagliaro, D. M., Electrodes functionalized with the 2,2,6,6 Tetramethylpiperidinyloxy radical for waste-free oxidation of alcohols *ChemCatChem* 2018, 7, 552-558.

[45] Lancaster, L., Hickey, D. P., Sigman, M. S., Minteer, S. D., Wheeldon, I., Bioinspired design of a hybrid bifunctional enzymatic/organic electrocatalyst for site selective alcohol oxidation. *Chem. Commun.* 2018, *54*, 491-494.

[46] Astolfi, P., Brandi, P., Galli, C., Gentili, P., *et al.*, New mediators for the enzyme laccase: mechanistic features and selectivity in the oxidation of non-phenolic substrates. *New J. Chem.* 2005, *29*, 1308-1317.

[47] Sletten, E. M., Bertozzi, C. R., Bioorthogonal Chemistry: Fishing for Selectivity in a Sea of Functionality. *Angew. Chem. Int. Ed.* 2009, *48*, 6974-6998.

[48] Jin, L., Tolentino, D. R., Melaimi, M., Bertrand, G., Isolation of bis(copper) key intermediates in Cu-catalyzed azide-alkyne "click reaction". *Sci. Adv.* 2015, *1:e1500304*, 1-5.

[49] Hein, J. E., Fokin, V. V., Copper-catalyzed azide–alkyne cycloaddition (CuAAC) and beyond: new reactivity of copper(I) acetylides. *Chem. Soc. Rev.* 2010, *39*, 1302-1315.

[50] Uttamapinant, C., Tangpeerachaikul, A., Grecian, S., Clarke, S., *et al.*, Fast, cell-compatible click chemistry with copper-chelating azides for biomolecular labeling. *Angew. Chem. Int. Ed.* 2012, *51*, 5852-5856.

[51] Presolski, S. I., Hong, V. P., Finn, M. G., Copper-catalyzed azide-alkyne click chemistry for bioconjugation, *Current Protocols in Chemical Biology*, Wiley, Hoboken, NJ 2011, pp. 153-162.

[52] Chenoweth, K., Chenoweth, D., III, W. A. G., Cyclooctyne-based reagents for uncatalyzed click chemistry: A computational survey. *Org. Biomol. Chem.* 2009, *7*, 5255-5258.

[53] Li, L., Fierer, J. O., Rapoport, T. A., Howarth, M., Structural analysis and optimization of the covalent association between SpyCatcher and a peptide tag. *Journal of Molecular Biology* 2014, *426*, 309-317.

[54] Zakeri, B., Fierer, J. O., Celik, E., Chittock, E. C., *et al.*, Peptide tag forming a rapid covalent bond to a protein, through engineering a bacterial adhesin. *Proc. Natl. Acad. Sci.* 2012, *109*, 690-697.

[55] Veggiani, G., Nakamura, T., Brenner, M. D., Gayet, R. V., *et al.*, Programmable polyproteams built using twin peptide superglues. *Proc. Natl. Acad. Sci.* 2016, *113*, 1202-1207.

[56] Doi, N., Yanagawa, H., Design of generic biosensors based on green fluorescent proteins with allosteric sites by directed evolution. *FEBS Lett.* 1999, *453*, 305-307.

[57] Fukuda, H., Arai, M., Kuwajima, K., Folding of green fluorescent protein and the cycle3 mutant. *Biochemistry* 2000, *39*, 12025-12032.

[58] Tsien, R. Y., The Green Fluorescent Protein. *Annu. Rev. Biochem.* 1998, *67*, 509-544.

[59] Wang, L., Xie, J., Deniz, A. A., Schultz, P. G., Unnatural amino acid mutagenesis of green fluorescent protein. *J. Org. Chem.* 2003, *68*, 174-176.

[60] Pedelacq, J.-D., Cabantous, S., Tran, T., Terwilliger, T. C., Waldo, G. S., Engineering and characterization of a superfolder green fluorescent protein. *Nat. Biotechnol.* 2006, *24*, 79-88.

[61] Lawrence, M. S., Phillips, K. J., Liu, D. R., Supercharging proteins can impart unusual resilience. *J. Am. Chem. Soc.* 2007, *129*, 10110-10112.

[62] Stepanenko, O. V., Stepanenko, O. V., Kuznetsova, I. M., Verkhusha, V. V., Turoverov, K. K., Sensitivity of superfolder GFP to ionic agents. *PLoS One* 2014, *9*, e110750.

[63] Wheeldon, I., Minteer, S. D., Banta, S., Barton, S. C., *et al.*, Substrate channelling as an approach to cascade reactions. *Nat. Chem.* 2016, *8*, 299-309.

[64] Bulutoglu, B., Garcia, K. E., Wu, F., Minteer, S. D., Banta, S., Direct evidence for metabolon formation and substrate channeling in recombinant TCA cycle enzymes. *ACS Chem. Biol.* 2016, *11*, 2847-2853.

[65] Zhang, Y., Tsitkov, S., Hess, H., Proximity does not contribute to activity enhancement in the glucose oxidase–horseradish peroxidase cascade. *Nat. Commun.* 2016, *7:13982*.

[66] Spivey, H. O., Ova´di, J., Substrate Channeling. *Methods* 1999, *19*, 306-321.

[67] Jeong, E. J., Park, K., Yi, S. Y., Kang, H. J., *et al.*, Stress-governed expression and purification of human type II hexokinase in Escherichia coli. *J. Microbiol. Biotechnol.* 2007, *17*, 638-643.

[68] Gomez-Manzo, S., Terro´n-Herna´ndez, J., Mora, I. d. l. M.-d. l., Garcı´a-Torres, I., *et al.*, Cloning, expression, purification and characterization of his-tagged human glucose-6-phosphate dehydrogenase: a simplified method for protein yield. *Protein J* 2013, *32*, 585-592.

[69] Wang, X.-T., Engel, P. C., Clinical mutants of human glucose 6-phosphate dehydrogenase: Impairment of NADP+ binding affects both folding and stability. *Biochim. Biophys. Acta* 2009, *1792*, 804-809.

[70] Liu, Y., Hickey, D. P., Guo, J.-Y., Earl, E., *et al.*, Substrate channeling in an artificial metabolon: A molecular dynamics blueprint for an experimental peptide bridge. *ACS Catal.* 2017, *7*, 2486-2493.

[71] Penning, T. M., Molecular determinants of steroid recognition and catalysis in aldo-keto reductases. Lessons from 3a-hydroxysteroid dehydrogenase. *J. Steroid Biochem. Mol. Biol.* 1999, *69*, 211-225.

[72] Cooper, W. C., Jin, Y., Penning, T. M., Elucidation of a complete kinetic mechanism for a mammalian hydroxysteroid dehydrogenase (HSD) and identification of all enzyme forms on the reaction coordinate: the example of rat liver 3alpha-HSD (AKR1C9). *J. Biol. Chem.* 2007, *282*, 33484-33493.

[73] Kubiseski, T. J., Flynn, T. G., Studies on Human Aldose Reductase: Probing the role of arginine 268 by site-directed mutagenesis. *J. Biol. Chem.* 1995, *270*, 16911-16917.

[74] Ellis, E. M., Microbial aldo-keto reductases. *FEMS Microbiol. Lett.* 2002, *216*, 121-131.

[75] Medina, M., Luquita, A., Tejero, J. s., Hermoso, J., *et al.*, Probing the determinants of coenzyme specificity in ferredoxin-NADP+ reductase by site-directed mutagenesis. *J. Biol. Chem.* 2001, *276*, 11902-11912.

[76] Banta, S., Swanson, B. A., Wu, S., Jarnagin, A., Anderson, S., Optimizing an artificial metabolic pathway: engineering the cofactor specificity of corynebacterium 2,5-diketo-D-gluconic acid reductase for use in vitamin C biosynthesis. *Biochemistry* 2002, *41*, 6226-6236.

[77] Leitgeb, S., Petschacher, B., Wilson, D. K., Nidetzky, B., Fine tuning of coenzyme specificity in family 2 aldo-keto reductases revealed by crystal structures of the Lys-274 fi Arg mutant of Candida tenuis xylose reductase (AKR2B5) bound to NAD+ and NADP+. *FEBS Lett.* 2005, *579*, 763-767.

[78] Hsieh, J.-Y., Liu, G.-Y., Chang, G.-G., Hung, H.-C., Determinants of the dual cofactor specificity and substrate cooperativity of the human mitochondrial NAD(P)+-dependent malic enzyme: functional roles of glutamine 362. *J. Biol. Chem.* 2006, *281*, 23237–23245.

[79] Brinkmann-Chen, S., Flock, T., Cahn, J. K. B., Snow, C. D., *et al.*, General approach to reversing ketol-acid reductoisomerase cofactor dependence from NADPH to NADH. *Proc. Natl. Acad. Sci.* 2013, *110*, 10946-10951.

[80] Maddock, D. J., Patrick, W. M., Gerth, M. L., Substitutions at the cofactor phosphate-binding site of a clostridial alcohol dehydrogenase lead to unexpected changes in substrate specificity. *Protein Eng. Des. Sel.* 2015, *28*, 251-258.

[81] Sanli, G., Banta, S., Anderson, S., Blaber, M., Structural alteration of cofactor specificity in Corynebacterium 2,5-diketo-D-gluconic acid reductase. *Protein Sci.* 2004, *13*, 504-512.

[82] Khoury, G. A., Fazelinia, H., Chin, J. W., Pantazes, R. J., *et al.*, Computational design of Candida boidinii xylose reductase for altered cofactor specificity. *Protein Sci.* 2009, *18*, 2125-2138.

[83] Xia, X.-L., Cong, S., Weng, X.-R., Chen, J.-H., *et al.*, Molecular simulation to investigate the cofactor specificity for pichia stipitis Xylose reductase. *Med. Chem.* 2013, *9*, 958-992.

[84] Cui, D., Zhang, L., Jiang, S., Yao, Z., *et al.*, A computational strategy for altering an enzyme in its cofactor preference to NAD(H) and/or NADP(H). *FEBS* 2015, *282*, 2339-2351.

[85] Bastian, S., Liu, X., Meyerowitz, J. T., Snow, C. D., *et al.*, Engineered ketol-acid reductoisomerase and alcohol dehydrogenase enable anaerobic 2-methylpropan-1-ol production at theoretical yield in Escherichia coli. *Metab. Eng.* 2011, *13*, 345-352.

[86] Cahn, J. K. B., Baumschlager, A., Brinkmann-Chen, S., Arnold, F. H., Mutations in adenine-binding pockets enhance catalytic properties of NAD(P)H-dependent enzymes. *Protein Eng. Des. Sel.* 2016, *29*, 31-38.

[87] Guex, N., Peitsch, M. C., SWISS-MODEL and the Swiss-PdbViewer: An environment for comparative protein modeling. *Electrophoresis* 1997, *18*, 2714-2723.

[88] Segel, I., *Enzyme Kinetics Behavior and Analysis of Rapid Equilibrium and Steady State Enzyme Systems*, John Wiley & Sons, Hoboken, New Jersey 1993.

[89] Jackman, M. P., Parry, M. A. A., Hofsteenge, J., Stone, S. R., Intrinsic fluorescence changes and rapid kinetics of the reaction of thrombin with hirudin. *J. Biol. Chem.* 1992, *267*, 15375-15383.

[90] Fersht , A., *Enzyme Structure and Mechanism*, W.H. Freeman and Company, New York, NY 1985.

[91] Liu, X., Wang, C., Zhang, L., Yao, Z., *et al.*, Structural and mutational studies on an aldo-keto reductase AKR5C3 from Gluconobacter oxydans. *Protein Sci.* 2014, *23*, 1540-1549.

[92] Rosell, A., Valencia, E., Ochoa, W. F., Fita, I., *et al.*, Complete reversal of coenzyme specificity by concerted mutation of three consecutive residues in alcohol dehydrogenase. *J. Biol. Chem.* 2003, *278*, 40573-40580.

[93] Watanabe, S., Kodaki, T., Makino, K., Complete reversal of coenzyme specificity of xylitol dehydrogenase and increase of thermostability by the introduction of structural zinc. *J. Biol. Chem.* 2005, *280*, 10340-10349.

[94] Ehsani, M., Ferna´ndez, M. R., Biosca, J. A., Dequin, S., Reversal of coenzyme specificity of 2,3-butanediol dehydrogenase from Saccharomyces cerevisae and in vivo functional analysis. *Biotechnol. Bioeng.* 2009, *104*, 381-389.

[95] Wang, Y., San, K.-Y., Bennett, G. N., Cofactor engineering for advancing chemical biotechnology. *Curr. Opin. Biotechnol.* 2013, *24*, 994-999.

[96] Banta, S., A.Swanson, B., Wu, S., Jarnagin, A., Anderson, S., Alteration of the specificity of the cofactor-binding pocket of Corynebacterium 2,5-diketo-D-gluconic acid reductase A. *Protein Eng.* 2002, *15*, 131-140.

[97] Hoelsch, K., Sührer, I., Heusel, M., Weuster-Botz, D., Engineering of formate dehydrogenase: synergistic effect of mutations affecting cofactor specificity and chemical stability. *Appl. Microbiol. Biotechnol.* 2013, *97*, 2473-2481.

[98] Cahn, J. K. B., Werlang, C. A., Baumschlager, A., Brinkmann-Chen, S., *et al.*, A general tool for engineering the NAD/NADP cofactor preference of oxidoreductases. *ACS Synth. Biol.* 2017, *6*, 326-333.

[99] Brophy, J. A. N., Voigt, C. A., Principles of genetic circuit design. *Nature Methods* 2014, *11*, 508-520.

[100] Wright, P. E., Dyson, H. J., Intrinsically disordered proteins in cellular signalling and regulation. *Nat. Rev. Mol. Cell Biol.* 2015, *16*, 18-29.

[101] Felli, I., Pierattelli, R., Tompa, P., *NMR of Biomolecules: Towards Mechanistic Systems Biology*, Wiley, Hoboken, NJ 2012.

[102] Shur, O., Banta, S., Rearranging and concatenating a native RTX domain to understand sequence modularity. *Protein Eng. Des. Sel.* 2013, *26*, 171-180.

[103] Blenner, M. A., Shur, O., Szilvay, G. R., Cropek, D. M., Banta, S., Calcium-induced folding of a beta roll motif requires C-terminal entropic stabilization. *J. Mol. Biol.* 2010, *400*, 244-256.

[104] Szilvay, G. R., Blenner, M. A., Shur, O., Cropek, D. M., Banta, S., A FRET-based method for probing the conformational behavior of an intrinsically disordered repeat domain from Bordetella pertussis adenylate cyclase. *Biochemistry* 2009, *48*, 11273-11282.

[105] Shur, O., Wu, J., Cropek, D. M., Banta, S., Monitoring the conformational changes of an intrinsically disordered peptide using a quartz crystal microbalance. *Protein Sci.* 2011, *20*, 925-930.

[106] Dooley, K., Kim, Y. H., Lu, H. D., Tu, R., Banta, S., Engineering of an environmentally responsive beta roll peptide for use as a calcium-dependent cross-linking domain for peptide hydrogel formation. *Biomacromolecules* 2012, *13*, 1758-1764.

[107] Shur, O., Dooley, K., Blenner, M., Baltimore, M., Banta, S., A designed, phase changing RTX-based peptide for efficient bioseparations. *BioTechniques* 2013, *54*, 197-206.

[108] Dooley, K., Bulutoglu, B., Banta, S., Doubling the cross-linking interface of a rationally designed beta roll peptide for calcium-dependent proteinaceous hydrogel formation. *Biomacromolecules* 2014, *15*, 3617-3624.

[109] Bumba, L., Masin, J., Macek, P., Wald, T., *et al.*, Calcium-driven folding of RTX domain B-rolls ratchets translocation of RTX proteins through type I secretion ducts. *Mol. Cell* 2016, *62*, 47-62.

[110] Gasteiger, E., Hoogland, C., A, G., Duvaud, S., *et al.*, *The Proteomics Protocols HandbookThe Proteomics Protocols Handbook*, Human Press, New York, NY 2005.
[111] Splittgerber, A. G., Simplified treatment of two-substrate enzyme kinetics. *J. Chem. Edu.* 1983, *60*, 651-655.

[112] Guntas, G., Ostermeier, M., Creation of an allosteric enzyme by domain insertion. *J. Mol. Biol.* 2004, *336*, 263-273.

[113] Guntas, G., Mansell, T. J., Kim, J. R., Ostermeier, M., Directed evolution of protein switches and their application to the creation of ligand-binding proteins. *Proc. Natl. Acad. Sci.* 2005, *102*, 11224-11229.

[114] Ha, J.-H., Loh, S. N., Protein conformational switches: from nature to design. *Chem. Eur. J.* 2012, *18*, 7984-7999.

[115] Mills, B. M., Chong, L. T., Molecular simulations of mutually exclusive folding in a two-domain protein switch. *Biophys. J.* 2011, *100*, 756-764.

[116] Cutler, T. A., Mills, B. M., Lubin, D. J., Chong, L. T., Loh, S. N., Effect of interdomain linker length on an antagonistic folding-unfolding equilibrium between two protein domains. *J. Mol. Biol.* 2009, *386*, 854-868.

[117] Radley, T. L., Markowska, A. I., Bettinger, B. T., Ha, J.-H., Loh, S. N., Allosteric switching by mutually exclusive folding of protein domains. *J. Mol. Biol.* 2003, *332*, 529-536.

[118] Choi, J. H., Laurent, A. H., Hilser, V. J., Ostermeier, M., Design of protein switches based on an ensemble model of allostery. *Nat. Commun.* 2015, *6:6968*.

[119] Choi, J. H., Xiong, T., Ostermeier, M., The interplay between effector binding and allostery in an engineered protein switch. *Protein Sci.* 2016, *25*, 1605-1616.

[120] Jez, J. M., Penning, T. M., The aldo-keto reductase (AKR) superfamily: an update. *Chem. Biol. Interact* 2001, *130-132*, 499-525.

[121] Baldo, B. A., Chimeric fusion proteins used for therapy: indications, mechanisms, and safety. *Drug Saf.* 2015, *38*, 455-479.

[122] Uhlen, M., Forsberg, G., Moks, T., Hartmanis, M., Nilsson, B., Fusion proteins in biotechnology. *Curr. Opin. Biotechnol.* 1992, *2*, 569-575.

[123] Hoffman, A. S., Hydrogels for biomedical applications. *Adv. Drug Deliv. Rev.* 2012, *64*, 18-23.

[124] Kim, Y. H., Campbell, E., Yu, J., Minteer, S. D., Banta, S., Complete oxidation of methanol in biobattery devices using a hydrogel created from three modified dehydrogenases. *Angew. Chem. Int. Ed.* 2013, *52*, 1437-1440.

[125] Reddington, S. C., Baldwin, A. J., Thompson, R., Brancale, A., *et al.*, Directed evolution of GFP with non-natural amino acids identifies residues for augmenting and photoswitching fluorescence. *Chem. Sci.* 2015, *6*, 1159-1166.

[126] Peeler, J. C., Mehl, R. A., Site-specific incorporation of unnatural amino acids as probes for protein conformational changes, in: Pollegioni, L., Servi, S. (Eds.), *Unnatural Amino Acids: Methods and Protocols*, Humana Press, New York, New York 2012.

[127] Weltz, J. S., Schwartz, D. K., Kaar, J. L., Surface-mediated protein unfolding as a search process for denaturing sites. *ACS Nano* 2016, *10*, 730-738.

[128] Li, Y., Cirino, P. C., Recent advances in engineering proteins for biocatalysis. *Biotechnol Bioeng* 2014, *111*, 1273-1287.

[129] Bornscheuer, U. T., Huisman, G. W., Kazlauskas, R. J., Lutz, S., *et al.*, Engineering the third wave of biocatalysis. *Nature* 2012, *485*, 185-194.

[130] Lutz, S., Iamurri, S. M., Protein Engineering: Past, Present, and Future. *Methods Mol Biol* 2018, *1685*, 1-12.

[131] Singh, A., Glass, N., Tolba, M., Brovko, L., *et al.*, Immobilization of bacteriophages on gold surfaces for the specific capture of pathogens. *Biosensors and Bioelectronics* 2009, *24*, 3645-3651.

[132] Liese, A., Hilterhaus, L., Evaluation of immobilized enzymes for industrial applications. *Chemical Society Reviews* 2013, *42*, 6236-6249.

[133] Katchalski, E., Silman, I., Goldman, R., Effect of the microenvironment on the mode of action of immobilized enzymes. *Advances in enzymology and related areas of molecular biology* 1971, *34*, 445-536.

[134] Mateo, C., Palomo, J. M., Fernandez-Lorente, G., Guisan, J. M., Fernandez-Lafuente, R., Improvement of enzyme activity, stability and selectivity via immobilization techniques. *Enzyme Microb Technol.* 2007, *40*, 1451-1463.

[135] Solomon, B., Levin, Y., Studies on adsorption of amyloglucosidase on ion-exchange resins. *Biotechnol. Bioeng.* 1974, *16*, 1161-1177.

[136] Tomotani, E. J., Vitolo, M., Catalytic performance of invertase immobilized by adsorption on anionic exchange resin. *Process Biochem.* 2006, *41*, 1325-1331.

[137] Zhang, Y., Wang, Q., Hess, H., Increasing enzyme cascade throughput by pH-engineering the microenvironment of individual enzymes. *ACS Catal.* 2017, *7*, 2047-2051.

[138] Bulutoglu, B., Banta, S., Block V RTX domain of adenylate cyclase from Bordetella pertussis: a conformationally dynamic scaffold for protein engineering applications. *Toxins* 2017, *9*, 1-13.

[139] Gao, Y., Roberts, C. C., Zhu, J., Lin, J.-L., *et al.*, Tuning enzyme kinetics through designed intermolecular interactions far from the active site. *ACS Catal.* 2015, *5*, 2149-2153.

[140] Bulutoglu, B., Haghpanah, J., Campbell, E., Banta, S., Engineered biomolecular recognition of RDX by using a thermostable alcohol dehydrogenase as a protein scaffold. *ChemBioChem* 2018, *19*, 247-255.

[141] Zakeri, B., Fierer, J. O., Celik, E., Chittock, E. C., *et al.*, Peptide tag forming a rapid covalent bond to a protein, through engineering a bacterial adhesin. *Proc Natl Acad Sci U S A* 2012, *109*, E690-697.

[142] E., G., C., H., A., G., S., D., *et al.*, *Protein Identification and Analysis Tools on the ExPASy Server*, Humana Press, New York, NY 2005.

[143] Holder, A. N., Ellis, A. L., Zou, J., Chen, N., Yang, J. J., Facilitating chromophore formation of engineered Ca2+ binding green fluorescent proteins. *Arch. Biochem. Biophys.* 2009, *486*, 27-34.

[144] Der, B. S., Kluwe, C., Miklos, A. E., Jacak, R., *et al.*, Alternative computational protocols for supercharging protein surfaces for reversible unfolding and retention of stability. *PLoS One* 2013, *8*, 1-11.

[145] Goldstein, L., Microenvironmental effects on enzyme catalysis. Kinetic study of polyanionic and polycationic derivatives of chymotrypsin. *Biochemistry* 1972, *11*, 4072-4084.

[146] Wu, F., Minteer, S., Krebs cycle metabolon: structural evidence of substrate channeling revealed by cross-linking and mass spectrometry. *Angew Chem Int Ed Engl* 2015, *54*, 1851-1854.

[147] Hyde, C. C., Ahmed, S. A., Padlan, E. A., Miles, E. W., Davies, D. R., Three-dimensional structure of the tryptophan synthase alpha 2 beta 2 multienzyme complex from Salmonella typhimurium. *J. Biol. Chem.* 1988, *263*, 17857-17871.

[148] Zhou, Z. H., McCarthy, D. B., O'Connor, C. M., Reed, L. J., Stoops, J. K., The remarkable structural and functional organization of the eukaryotic pyruvate dehydrogenase complexes. *Proc. Natl. Acad. Sci.* 2001, *98*, 14802-14807.

[149] Wilson, J. E., Hexokinases. *Rev. Physiol. Biochem. Pharmacol.* 1995, *126*, 65-198.

[150] Au, S. W., Gover, S., Lam, V. M., Adams, M. J., Human glucose-6-phosphate dehydrogenase: the crystal structure reveals a structural NADP+ molecule and provides insights into enzyme deficiency. *Structure* 2000, *8*, 293-303.

[151] Wang, X.-T., Au, S. W. N., Lam, V. M. S., Engel, P. C., Recombinant human glucose-6-phosphate dehydrogenase Evidence for a rapid-equilibrium random-order mechanism. *European Journal of Biochemistry* 2002, *269*, 3417-3424.